CHARACTERIZING NEURAL TISSUES WITH MASS SPECTROMETRY IMAGING VIA ENHANCED COMPUTATIONAL APPROACHES

BY

TYLER ANDRE ZIMMERMAN

DISSERTATION

Submitted in partial fulfillment of the requirements
for the degree of Doctor of Philosophy in Chemistry
in the Graduate College of the
University of Illinois at Urbana-Champaign, 2010

Urbana, Illinois

Doctoral Committee:

Professor Jonathan V. Sweedler, Chair and Director of Research
Professor Neil Kelleher, Northwestern University
Professor Sandra Rodriguez-Zas
Professor Andrzej Wieckowski

ABSTRACT

Neuropeptides affect the activity of the myriad of neuronal circuits in the brain. They are under tight spatial and chemical control and the dynamics of their release and catabolism directly modify neuronal network activity. Understanding neuropeptide functioning requires approaches to determine their chemical and spatial heterogeneity within neural tissue, but most imaging techniques do not provide the complete information desired. To provide chemical information, most imaging techniques used to study the nervous system require preselection and labeling of the peptides of interest; however, mass spectrometry imaging (MSI) detects analytes across a broad mass range without the need to target a specific analyte. When used with matrix-assisted laser desorption/ionization (MALDI), MSI detects analytes in the mass range of neuropeptides. MALDI MSI simultaneously provides spatial and chemical information resulting in images that plot the spatial distributions of neuropeptides over the surface of a thin slice of neural tissue.

Here a variety of approaches for neuropeptide characterization are developed. Specifically, several computational approaches are combined with MALDI MSI to create improved approaches that provide spatial distributions and neuropeptide characterizations. After successfully validating these MALDI MSI protocols, the methods are applied to characterize both known and unidentified neuropeptides from neural tissues. The methods are further adapted from tissue analysis to be able to perform tandem MS (MS/MS) imaging on neuronal cultures to enable the study of network formation. In addition, MALDI MSI has been carried out over the timecourse of nervous system regeneration in planarian flatworms resulting in the discovery of two novel

neuropeptides that may be involved in planarian regeneration. In addition, several bioinformatic tools are developed to predict final neuropeptide structures and associated masses that can be compared to experimental MSI data in order to make assignments of neuropeptide identities. The integration of computational approaches into the experimental design of MALDI MSI has allowed improved instrument automation and enhanced data acquisition and analysis. These tools also make the methods versatile and adaptable to new sample types.

DEDICATION

This volume is dedicated to the memory of my
grandfather, the Rev. Dr. Marvin A. Johnson, Ed.D.,
a friendly Chicago native and a creative thinker,
and to the memory of my great-uncle, the Hon. Leroy
M. Zimmerman, former member of the Pennsylvania
House of Representatives from the 99th district.

ACKNOWLEDGMENTS

My decision to pursue chemistry as a career came in 1997, for which I have to thank the U.S. Naval Academy Merit Badge Jamboree “Jambo” in Annapolis, Maryland then sponsored by the National Eagle Scout Association of which I am a current member. More information on Jambo is in the cover story of the November-December 2001 edition of Scouting magazine. At the 1997 Jambo, I earned the chemistry merit badge and this program was run by midshipmen and by the inspiring Larry R. Sherman, Professor Emeritus of Chemistry at the University of Scranton. I thank Bill Minford, Ph.D. of Boy Scouts of America Troop 242 in Cherryville, PA for planning our participation in this event. Later, I took chemistry in high school and my teacher Louise Shive, Ed.D. is now an Assistant Professor in the Education Department at Muhlenberg College. I also acknowledge her husband, Donald W. Shive, Professor of Chemistry at Muhlenberg with whom I participated in the Muhlenberg Exploring Environmental Chemistry program.

I recognize my parents in Pennsylvania for providing constant support and who are about to celebrate their 30th wedding anniversary: my father, Gerald A. Zimmerman, Ph.D. a clinical psychologist and my mother, Karen E. Zimmerman. I recognize my siblings Jeremy, Kurt, and Jessamy. In downtown Chicago, my aunt’s family has provided a high degree of hospitality and chances to visit the city on many occasions. Specifically, I thank my aunt, Lisa Zimmerman, for picking me up at the airport and my uncle, David Ramsay Steele, Ph.D., the widely published author and publisher, for his gifts of books. I additionally acknowledge my cousins Emma, Allan, Ursula, and Duncan for playing string quartets with me upon my visits.

During my graduate school career, I enjoyed several musical diversions that include singing in the University of Illinois Chorale and the Allerton Barn Festival Chorus, for which I thank my friend Fred A. Stoltzfus, Professor and Chair of Choral Music. I acknowledge the CHORALE of the local Urbana-Champaign community for a free trip to Logan, Utah and Sun Valley, Idaho to sing on stage with the great singer/songwriter Peter Cetera, formerly of the rock band Chicago. I thank David R. Ziegler in Pennsylvania for covering transportation costs and for casting me in the lead role of Joseph in Andrew Lloyd Webber’s *Joseph and the Technicolor Dreamcoat* in two sold out amateur productions at the historic Roxy Theater in Northampton, PA.

My undergraduate research was done in the Laboratory for Chemometrics at the University of Delaware with the congenial Professor Steven D. Brown. I am also grateful to his graduate student at the time, Anthony J. Myles, Ph.D., who taught me much of what I currently know about research.

I thank my graduate research advisor at the University of Illinois, Professor Jonathan V. Sweedler, for the chance to work in the Beckman Institute and for his untiring effort and support. His vast knowledge and experience is useful to draw upon, like that of my other dissertation committee members: Professors Neil Kelleher, Sandra Rodriquez-Zas, and Andrzej Wieckowski. Within the Sweedler lab, I thank current and former coworkers including Andinet Amare, Stephanie Baker, Michael Ewing, Michael Heien, Eric Monroe, Tim Richmond, Elena Romanova, Stanislav Rubakhin, and Kevin Tucker. At the University of Illinois but outside of the Sweedler group, I thank C. Mark Bee, Jim Collins, Ji Eun Lee, Professor Phil Newmark, Scott J. Robinson, Juile Sides, Bruce Southey, and Leonid Zamdborg.

For my future postdoctoral job at the Université de Liège in Liège, Belgium, thanks go to Professor Edwin de Pauw for hiring me and to the Belgian government for funding my postdoctoral fellowship.

Of course, there are other people I could acknowledge – I could go on and on.

TABLE OF CONTENTS

CHAPTER 1

INTRODUCTION AND RESEARCH SUMMARY

1.1 Introduction

An organism's central nervous system requires complex intercellular signaling between neurons through either chemical or electrical synapses, which are critical connections between neurons used for cell-cell communication. Of the two types of synapses, electrical synapses that are also called gap junctions conduct signals more rapidly and are generally found in neural circuits where speed is needed[1] such as those for the initiation of reflexes. Communication takes place at electrical synapses through the flow of ions between neurons, ions such as K^+, Na^+, Ca^{2+}, and Cl^-. Chemical synapses, however, are more common and a variety of signaling molecules are transmitted between neurons through chemical synapses, including small molecule neurotransmitters like dopamine or larger neurotransmitters that take the form of peptides (chains of amino acids) called neuropeptides. Neuropeptides also communicate via receptors located not at synapses but on the surfaces of the neuron soma, dendrites, or axon, and also create, release, and modify the actions of many non-neural cells.[2] Neuropeptides are a diverse class of cell-cell signaling molecules in the nervous system that are built from an alphabet of 20 common amino acids, and they are created through enzymatic bond cleavages from larger prohormone sequences that may contain several copies of the same peptide with similar or slightly varied sequences.[3] Even more structural variety is added by posttranslational modifications (PTMs), which are chemical additions to the amino acids within the peptide chain after peptide synthesis. This variety of neuropeptide structures is used by the nervous system to represent motor, sensory, and cognitive information and to modulate such diverse processes as learning,[4] memory,[5] homeostasis,[6] feeding,[7, 8] reproduction,[9] analgesia/nociception,[2] reward,[10] and sleep-wake cycles.[11] In doing so, peptides act in a number of capacities such as being growth/trophic factors that are important in cell differentiation for tissue repair or cancer cell growth,[12] as hormones that regulate blood pressure,[13] and as modulators that regulate dynamic processes found in the immune system[14] or in learning and memory.[5] Of course, a single neuropeptide structure may have several functions, and often processes are controlled by multiple neuropeptides. In the presence of such dynamic processes and structural diversity, successful characterization of neuropeptides within the nervous system presents significant measurement challenges.

As the nervous system is spatially heterogeneous, often with differing chemical contents between neighboring cells, imaging techniques have become important approaches to provide critical information in the characterization of nervous tissue. Imaging techniques are applied at different scales including subcellular, cellular, tissue, system, and whole organisms. Some of these techniques are positron emission tomography (PET),[15] magnetic resonance imaging (MRI),[16] single photon emission computed tomography (SPECT),[17] optical imaging,[18] and fluorescence imaging.[19] Greater chemical information can be added through genomic techniques such as in-situ hybridization that maps the expression levels of mRNA transcripts. While these techniques are useful in research and medical diagnostics, one drawback is that they require fluorescent or radiochemical labeling of the specific analyte of interest. In contrast to genomics appraoches, after mRNA transcripts are endogenously translated into prohormones that are subsequently converted into neuropeptides, the peptides can be measured by proteomics techniques like immunohistochemistry[20, 21] or mass spectrometry imaging (MSI).[22, 23] As neuropeptides commonly undergo PTMs during their synthesis, a proteomic level analysis aids in their characterization of final bioactive forms. Mass spectrometry provides a powerful modality for chemical characterization of neuropeptides, as it is able to detect a variety of analytes over a broad mass range without the need for analyte labeling or preselection.[7, 24, 25]

Mass spectrometry is basically a molecular balance that can weigh analytes within complex biological matrices at the molecular level.[26] Mass spectrometry can be turned into an imaging technique by successively acquiring data from a grid of positions over the surface of a thin slice of neural tissue.[27] In this way, MSI provides chemical and spatial information simultaneously and is ideal for characterizing the interactions of neuropeptides and other signaling molecules.[28] More information on how MSI is applied to the imaging of thin tissue slices is provided in Chapter 2. Despite the advantages of MSI for the detection of neuropeptides, the nervous system still presents a number of analytical measurement challenges.

Characterizing neuropeptides using mass spectrometry imaging presents several measurement challenges, as nervous systems are: (1) chemically heterogeneous, (2) dynamic over short time scales, and (3) complex, with rare peptides some of which are below the limits of detection.

Analytical/bioanalytical chemistry[29-33] is the field concerned with advancing measurement science to overcome these challenges. Such advances can take place through improvements to initial sample preparation procedures, to instrumentation, and/or to data analysis steps.[34] This dissertation describes improvements for a particular type of MSI called MALDI-MSI,[27] where MALDI stands for matrix-assisted laser desorption/ionization. The MALDI ionization source uses a UV laser beam to irradiate the sample surface thereby desorbing analytes from a tissue surface for subsequent automated mass measurement. To prevent sample fragmentation caused by the laser beam, a matrix solution containing a dissolved UV-absorbing compound is sprayed, e.g. with an airbrush, over the tissue surface. However, in applying matrix there is a tradeoff in terms of the amount of matrix exposure, whereas more exposure of the surface to the matrix solution causes increased signal quality but at the same time causes hydrophilic small peptides to spread over the surface thus destroying spatial information. A significant effort has been to overcome such limitations while performing MSI of nervous system tissues.

The stretched sample method[35] was developed in the Sweedler lab to eliminate this tradeoff by placing a thin tissue slice onto a monolayer of ~40 µm glass beads embedded in a stretchable layer of Parafilm M. Upon manual stretching a 16-fold increase in area is obtained, and the beads separate the neurons from each other to create thousands of chemically isolated islands that can be analyzed individually. The hydrophobicity of the parafilm layer inhibits analyte migration upon extended periods of MALDI matrix application, thus eliminating the tradeoff in MALDI-MSI between signal and spatial resolution. Of course, stretching the samples destroys the original tissue configuration and there is also the necessity to acquire data from randomly located bead positions over the 2D surface. Thus, computational methods are developed to enable imaging of stretched samples.

1.2 Dissertation and research overview

As described above, Chapter 2 outlines approaches on how MSI is applied to the imaging of thin tissue slices, first by discussing the various instrumentation considerations, then focusing on aspects of sample preparation that can be tailored to the needs of the experiment. Information is also given on experimental design and how to analyze large MSI datasets.

Chapter 3 describes computational improvements and new software created to turn the stretched sample method into an MS imaging method,[36, 37] including automated data acquisition at the location of individual beads/cells, and image reconstruction to create 2D ion images that correspond to the original tissue configuration. The newly developed stretched imaging method is validated on a sample of peptide-coated beads of multiple colors embedded in Parafilm M. Angiotensin I peptide standard is coated onto clear color beads and angiotensin II peptide standard is coated onto colored beads. Validation was performed by visually comparing the reconstructed ion images to optical images of the sample taken before stretching where the two colors of beads are distinguishable. Results show a high degree of alignment for this sample of ~200 total beads, but improvements are then needed to be made in spatial accuracy of automated data acquisition to adapt the stretched imaging of larger area tissue samples that cover the surface area of several thousands of beads.

Chapter 4 describes a number of improvements to the stretched imaging method to enable its application to real tissue samples.[37] Among several improvements is a new way for automating data acquisition from stretched samples based on using laser melted holes in the parafilm as spatial calibration markers. The improved stretched imaging method is validated by comparing reconstructed ion images that map known neuropeptides in tissue slices taken from the invertebrate *Aplysia californica* (a sea slug) to previously obtained immunochemistry images. The stretched imaging results match well to previously obtained data, and the method is also used to obtain distribution information on putative peptides from other less well-characterized regions of the *Aplysia* central nervous system (CNS).

In Chapter 5, the new stretched imaging method rises to the challenge of reconstructing ion images from mammalian tissue from mouse pituitary.[38] While *Aplysia* neurons are large, up to several hundred microns in diameter, mouse pituitary neurons are smaller, averaging around 10 µm and so the challenges to spatial measurements are greater. The improved spatial resolution provided by the stretched imaging method is able to successfully produce high quality ion images from mouse pituitary. Chapter 5 is written in the form of a tutorial/protocol to aid other researchers who desire to use these protocols.

Chapter 6 shows another application of the stretched imaging method, not to neural tissues but this time to neuronal cultures attached to the stretchable bead/parafilm substrates. The high spatial resolution and improved signal afforded by the stretched imaging method will allow study of the process of neuronal network formation in dense neuronal cultures from a variety of different model organisms. In addition, the ability was added to perform tandem MS (or MS/MS) imaging. In tandem MS, from each bead position analytes are detected by a first round of MS, fragmented in a collision cell by collisions with inert gas molecules, and the resulting fragments are detected with a second round of MS. As opposed to the normal mode of having a single round of MS detection where only the mass of the intact parent ion is obtained, in the additional round of MS the way the analyte fragments can be used to determine amino acid sequence. The ability to do MS/MSI on stretched neuronal cultures creates a discovery tool[39] for the simultaneous mapping and identification of neuropeptides from these samples.

Chapter 7 describes the process of developing software created in-house as part of the stretched imaging method. This chapter makes references to the source code included in Appendix A of this dissertation that is written in the Java programming language. The main components of the software provide for automated data acquisition on stretched samples, and image reconstruction. As the stretched imaging method has been adapted to different measurement challenges, so also have the in-house created software and computational methods evolved along with it. This evolution of computational methods is described along with the potential for their further adaptation to a variety of different experimental designs and projects.

Chapter 8 describes an MSI study that does not involve sample stretching but that focuses on planarian regeneration. The *S. mediterranea* planarian flatworms show the ability to regenerate a new head upon head amputation, where the head also forms a new tail so that two complete organisms are produced from one. Studying peptides involved in CNS formation in the regenerating animal may give insights into regenerative medicine or give information on how to prevent helminth infections. To try to determine which peptides may be involved in planarian CNS regeneration, traditional MSI on thin tissue slices was used to see which analyte masses are detectable near the proliferating wound site. The amino acid sequences corresponding to these parent masses were obtained by subjecting extracts of whole animal planarians to liquid chromatography as a separation technique coupled to tandem MS (LC-MS/MS) using a collision cell to fragment the parent ions. Using this approach, 24 amino sequences were identified based on sequence similarity to sequences from other genomes. These may be involved in regeneration and include structural/metabolic proteins, several known planarian neuropeptides, and two planarian neuropeptide genes discovered during these studies. Future studies will characterize the functions of these peptides by knockout versus wild type experiments to see any differing consequences on the regeneration process.

The final chapter, Chapter 9, is a discussion of my contributions to NeuroPred software, a tool to predict cleavage sites in neuropeptide precursors and provide the masses of the resulting peptides. These predicted masses can be compared to mass spectrometry imaging data to aid in assigning an identity to an analyte. As mentioned previously, neuropeptides are created from larger prohormone sequences through the enzymatic cleavage of peptide bonds at certain mono-, di-, and tribasic amino acid sites. The neuropeptides then undergo posttranslational modifications. The occurrence of these processing steps at specific amino acid residues can be predicted to some extent based on the properties of combinations of surrounding amino acids. For instance, bond cleavage sometimes occurs at basic sites but only when proline is not an immediately adjacent amino acid and a number of other conditions are satisfied. This chapter also includes an update on how NeuroPred has been applied by users at the University of Illinois and other institutions to predict the final masses of neuropeptide products in various studies.

1.3 Conclusions

Analytical chemistry is focused on the ability to gain new information from new ways of measurement. Methodological innovations can be made in sample preparation, instrumentation, and data analysis and this dissertation describes improvements in all three areas. Besides the use of MALDI MSI in this research, other types of analytical chemistry instrumentation are used in conjunction with MSI. These include liquid chromatography (LC), direct MALDI MS, Fourier transform ion cyclotron resonance tandem mass spectrometry (FT-ICR-MS/MS), and environmental scanning electron microscopy (ESEM). In this dissertation, computation is combined with instrumentation to create new measurement tools, as in the stretched imaging method. Using these approaches, the methods presented here can be further developed and applied to characterize other neuronal samples with enhanced measurement results.

1.4 References

1. Hesketh, G. G.; Eyk, J. E. V.; Tomaselli, G. F. Mechanisms of gap junction traffic in health and disease. *J. Cardiovasc. Pharmacol.* **2009**, *54*, 263-272.

2. Li, W.; Chang, M.; Peng, Y.-L.; Gao, Y.-H.; Zhang, J.-n.; Han, R.-W.; Wang, R. Neuropeptide S produces antinociceptive effects at the supraspinal level in mice. *Regul. Pept.* **2009**, *156*, 90-95.

3. Turner, A. J. Neuropeptide processing enzymes. *Trends Neurosci.* **1984**, *7*, 258-260.

4. Ögren, S. O.; Kuteeva, E.; Elvander-Tottie, E.; Hökfelt, T. Neuropeptides in learning and memory processes with focus on galanin. *Eur. J. Pharamacol.* **2009**, *626*, 9-17.

5. Guelpinar, M. A.; Yegen, B. C. The physiology of learning and memory: role of peptides and stress. *Curr. Prot. Peptide Sci.* **2004**, *5*, 457-473.

6. Tsuneki, H.; Wada, T.; Sasaoka, T. Role of orexin in the regulation of glucose homeostasis. *Acta Physiologica* **2010**, *198*, 335-348.

7. Sweedler, J. V.; Li, L.; Rubakhin, S. S.; Alexeeva, V.; Dembrow, N. C.; Dowling, O.; Jing, J.; Weiss, K. R.; Vilim, F. S. Identification and characterization of the feeding circuit-activating peptides, a novel neuropeptide family of aplysia. *J. Neurosci.* **2002**, *22*, 7797-7808.

8. Kageyama, H.; Takenoya, F.; Shiba, K.; Shioda, S. Neuronal circuits involving ghrelin in the hypothalamus-mediated regulation of feeding. *Neuopeptides* **2010**, *44*, 133-138.

9. Tsutsui, K.; Bentley, G. E.; Kriegsfeld, L. J.; Osugi, T.; Seong, J. Y.; Vaudry, H. Discovery and evolutionary history of gonadotrophin-inhibitory hormone and kisspeptin: new key neuropeptides controlling reproduction. *J. Neuroendocrinol.* **2010**, *22*, 716-727.

10. Wu, C.-H.; Tao, P.-L.; Huang, E. Y.-K. Distribution of neuropeptide FF (NPFF) receptors in correlation with morphine-induced reward in the rat brain. *Peptides* **2010**, *31*, 1374-1382.

11. Piper, D. C.; Upton, N.; Smith, M. I.; Hunter, A. J. The novel brain neuropeptide, orexin-A, modulates the sleep-wake cycle of rats. *Eur. J. Neurosci.* **2000**, *12*, 726-730.

12. Gelato, M. C. Growth hormone-releasing hormone: clinical perspectives revisited. *Endocrinologist* **2005**, *15*, 159-164.

13. Paul, M.; Mehr, A. P.; Kreutz, R. Physiology of local renin-angiotensin systems. *Physiol. Rev.* **2006**, *86*, 747-803.

14. Jessop, D. S. Neuropeptides: modulators of immune responses in health and disease. *Int. Rev. Neurobiol.* **2002**, *52,* 67-91.

15. Cagnin, A.; Kassiou, M.; Meikle, S. R.; Banati, R. B. Positron emission tomography imaging of neuroinflammation. *Neurotherapeut.* **2007**, *4*, 443-452.

16. Ferris, C. F. Functional magnetic resonance imaging and the neurobiology of vasopressin and oxytocin. *Prog. Brain Res.* **2008**, *170*, 305-320.

17. Dietlein, M.; Pels, H.; Schulz, H.; Staak, O.; Borchmann, P.; Schomäcker, K.; Fischer, T.; Eschner, W.; Strandmann, E. P.; Schicha, H.; Engert, A.; Schnell, R. Imaging of central nervous system lymphomas with iodine-123 labeled rituximab. *Eur. J. Haematol.* **2005**, *74,* 348-352.

18. Dittman, J. Worm watching: imaging nervous system structure and function in Caenorhabditis elegans. *Adv. Genet.* **2009**, *65*, 39-78.

19. Tucker, K. L. In vivo imaging of the mammalian nervous system using fluorescent proteins. *Histochem. Cell Biol.* **2001**, *115*, 31-39.

20. Kamada, N.; Tano, K.; Oyabu, A.; Imura, Y.; Narita, N.; Tashiro, Y.; Uchida, A.; Komada, Y.; Narita, M. Immunohistochemical localization of manserin, a novel neuropeptide derived from secretogranin II, in rat adrenal gland, and its upregulation by physical stress. *Int. J. Pept. Res. Therapeut.* **2010**, *16*, 55-61.

21. Silva, A. B.; Aw, D.; Palmer, D. B. Neuropeptides and thymic hormones in the Xenopus thymus. *Front. Biosci.* **2009**, *14*, 1990-2003.

22. Chen, R.; Li, L. Mass spectral imaging and profiling of neuropeptides at the organ and cellular domains. *Anal. Bioanal. Chem.* **2010**, *397*, 3185-3193.

23. Monroe, E. B.; Annangudi, S. P.; Hatcher, N. G.; Gutstein, H. B.; Rubakhin, S. S.; Sweedler, J. V. SIMS and MALDI MS imaging of the spinal cord. *Proteomics* **2008**, *8*, 3746-3754.

24. Boonen, K.; Landuyt, B.; Baggerman, G.; Husson, S. J.; Huybrechts, J.; Schoofs, L. Peptidomics: The integrated approach of MS, hyphenated techniques and bioinformatics for neuropeptide analysis. *J. Sep. Sci.* **2008**, *31*, 427 – 445.

25. Hortin, G. L. The MALDI-TOF mass spectrometric view of the plasma proteome and peptidome. *Clin. Chem.* **2006**, *52*, 1223-1237.

26. Chace, D. H.; Sparkman, O. D., "What is mass spectrometry?: the importance of communicating the concept of mass spectrometry to professionals, media, and the consumer," presented at the American Society for Mass Spectrometry, http://www.asms.org/Portals/0/ASMS%20images/WhatIsMSPoster.pdf, 2005.

27. Rohner, T. C.; Staab, D.; Stoeckli, M. MALDI mass spectrometric imaging of biological tissue sections. *Mach. Age. Dev*. **2005.**, *126*, 177-185.

28. Zimmerman, T. A.; Monroe, E. B.; Tucker, K. R.; Rubakhin, S. S.; Sweedler, J. V. Chapter 13: imaging of cells and tissues with mass spectrometry: adding chemical information to imaging. *Methods Cell Biol.* **2008**, *89*, 361-390.

29. Kazuhiro, I. Bio-analytical chemistry and proteome analysis. *Chromatogr.* **2009**, *30, Suppl. 1*, 37-40.

30. Murray, R. W. Analytical chemistry: the science of chemical measurements. *Anal. Chem.* **2007**, *79*, 1765.

31. Laitinen, H. A. History of analytical chemistry in the U.S.A. *Tantala* **1989**, *36*, 1-9.

32. Murray, R. W. Teaching of analytical chemistry in the U.S. *Tantala* **1989**, *36*, 11-17.

33. Larive, C. K. Instruction in bioanalytical chemistry. *Anal. Bioanal. Chem.* **2005**, *382*, 855–856.

34. Schatzlein, D.; Volker, T. The chemical analysis process. *Spectroscopy* **2008**, *23*, 30-35.

35. Monroe, E. B.; Jurchen, J. C.; Koszczuk, B. A.; Losh, J. L.; Rubakhin, S. S.; Sweedler, J. V. Massively parallel sample preparation for the MALDI MS analyses of tissue. *Anal. Chem.* **2006**, *78*, 6826-6832.

36. Zimmerman, T. A.; Monroe, E. B.; Sweedler, J. V. Adapting the stretched sample method from tissue profiling to imaging. *Proteomics* **2008**, *8*, 3809–3815.

37. Zimmerman, T. A.; Rubakhin, S. S.; Romanova, E. V.; Tucker, K. R.; Sweedler, J. V. MALDI mass spectrometric imaging using the stretched sample method to reveal neuropeptide distributions in Aplysia nervous tissue. *Anal. Chem.* **2009**, *81*, 9402–9409.

38. Zimmerman, T. A.; Rubakhin, S. S.; Sweedler, J. V. Mass spectrometry imaging using the stretched sample approach. *Methods Mol. Biol.* **2010**, *656*, 465-479.

39. Svensson, M.; Sköld, K.; Svenningsson, P.; Andren, P. E. Peptidomics-based discovery of novel neuropeptides. *J. Proteome Res.* **2003**, *2*, 213–219.

CHAPTER 2

IMAGING OF CELLS AND TISSUES WITH MASS SPECTROMETRY: ADDING CHEMICAL INFORMATION TO IMAGING

2.1 Notes and Acknowledgements

This introductory chapter is adapted from the publication in the book series *Methods in Cell Biology*, **2008,** *89,* 361-390, and is reprinted with permissions from Elsevier. In this chapter, the topic of mass spectrometry imaging is introducted with a focus on the associated the experimental protocols. The co-authors for this chapter are Eric B. Monroe, Kevin R. Tucker, Stanislav S. Rubakhin, and Jonathan V. Sweedler. Funding for this work comes from the National Institute on Drug Abuse under Award No. P30DA018310 to the UIUC Center on Neuroproteomics on Cell to Cell Signaling and Award No. PHS 5 R01DA17940.

2.2 Abstract

Techniques that map the distribution of compounds in biological tissues can be invaluable in addressing a number of critical questions in biology and medicine. One of the newer methods, mass spectrometric imaging, has enabled investigation of spatial localization for a variety of compounds ranging from atomics to proteins. The ability of mass spectrometry to detect and differentiate a large number of unlabeled compounds makes the approach amenable to the study of complex biological tissues. This chapter focuses on recent advances in the instrumentation and sample preparation protocols that make mass spectrometric imaging of biological samples possible, including strategies for both tissue and single-cell imaging using the following mass spectrometric ionization

methods: matrix-assisted laser desorption/ionization, secondary ion, electrospray, and desorption electrospray.

2.3 Introduction

The intrinsic chemical and structural complexities of biological tissues and cells present significant analytical measurement challenges. Microscopy has long been considered one of the most powerful techniques to study the distribution of biologically relevant compounds in tissues. Chemical images of analyte distributions in biological specimens have been made possible via affinity labeling with antibodies or other chemical labels/stains in combination with optical microscopy. In fact, these imaging approaches have a several centuries-long history.

More recently, the last century has witnessed the development of the exceptionally effective chemical characterization approach known as mass spectrometry (MS). Using modern MS techniques, a small volume sample can be assayed and information on literally thousands of compounds observed. Can these two approaches—imaging and MS—be successfully combined to achieve even greater information content? As documented throughout this chapter, this combined imaging approach is now being used to examine a wide range of tissues and biological processes.

In general, MS imaging (MSI) techniques include a spatially-resolved ionization method to collect mass spectra from an array of positions across a sample. Following data acquisition, the intensities of selected signals from the mass spectra are each plotted to create a pixel array and hence, an ion image or distribution map for the individual signal/compound (Figure 2.1). The high level of spatial and chemical information afforded by MSI enables the distribution of many compounds to be imaged in a single experiment without the need for prior knowledge of the identity of the analyte(s) of interest.

At present, research efforts are actively directed towards furthering the development and application of MSI to study a broader range of compounds in tissues. Just as there are a number of optical techniques from which to choose for a particular application, different MS approaches are available for characterizing the varying types of analytes, with many of these methods adaptable to MSI. For example, secondary ion mass spectrometry (SIMS) imaging is often used to study the distribution of atoms and small molecules in tissues and even single cells at spatial resolutions below a micron. Matrix-assisted laser desorption/ionization (MALDI) MSI has become a popular imaging method for examining small molecules, peptides and proteins from a variety of tissue sections at a wide range of spatial resolutions and scales, including whole animal preparations.[1] Recently, imaging techniques using electrospray ionization (ESI) and desorption electrospray ionization (DESI) have been developed as alternative methods for the direct analysis of tissues at atmospheric pressure.[2]

Beyond higher resolution imaging, low resolution spatial profiling of tissues is also useful for understanding the localization of compounds in a tissue sample, particularly via MALDI MS. In all cases of MSI, the chemical information content is high but the data is at a lower spatial resolution than what is commonly afforded by optical microscopy. This chapter focuses on experimental strategies aimed at creating visual distribution maps of an analyte across a sample rather than profiling the sample at discrete points.

MSI relies on the desorption and ionization of biologically relevant compounds from structurally and biochemically heterogeneous samples. Many of the fixation approaches developed for optical and electron microscopy are not compatible with MSI and so new MS-specific protocols have been designed. As will be discussed in more detail later, care must be taken to ensure that analytes retain their native form and distribution within the samples. Mass spectra are obtained directly from the tissue surface (or in the case of MALDI MS, a thin coat of matrix on the tissue) such that the distribution of analytes resembles their *in vivo* state and the observed result is biologically relevant. The imaging approaches outlined in this chapter largely involve the *in situ* analyses of compounds from biological samples using the high vacuum instrumentation inherent to MS, although progress towards *in vivo* analyses has been made using the DESI scheme.[2]

In addition to MS-compatible preparation protocols, an overview of each of the various ionization techniques (MALDI, SIMS, ESI, DESI) is presented, with further details available elsewhere.[3] While it seems obvious that selecting the ideal MS ionization methodology is important, it is the significance of choosing the appropriate sample preparation protocol that is consistently cited as being the key to experimental success. The optimal protocol depends, to some extent, on the nature of the tissue sample.[4] In the following sections, we highlight the instruments and sample preparation processes associated with MSI experiments, and briefly discuss the strategies used to analyze and visualize the large datasets that are associated with these investigations.

2.4. Instrumentation

Although spatial analysis of biological tissues with MSI employs a vast range of mass spectrometers and associated instrumentation, each mass spectrometer is conceptually similar in that it contains an ionization source, a mass analyzer, and a detector. Here we describe the available mass spectrometer configurations and provide guidance in selecting the most appropriate set-up for a particular MSI experiment.

2.4.1 MALDI MS

Laser-desorption MS has been used to profile tissues since the 1970s. However, the largest molecules that could be ionized were typically less than 1000 Da. The refined method of MALDI MS, introduced by Karas and Hillenkamp,[5] and Tanaka[6] in the latter portion of the 1980s, can ionize higher molecular weight biomolecules, owing to the minimal analyte fragmentation induced during the desorption and ionization processes.

In this methodology, the sample is prepared by mixing it with a matrix. Although most MALDI applications use a solid organic matrix, a variety of liquid and solid matrices have been introduced, including glycerol and derivatives of benzoic and cinnamic acids. During the measurement process, the matrix absorbs nanoseconds-long ultraviolet (UV) or infrared (IR) laser pulses that resonantly excite the matrix, causing extremely rapid localized heating and subsequent ejection of neutral and charged analyte molecules, atoms, matrix molecules and analyte–matrix clusters. UV lasers are commonly used in MSI applications[7] although IR lasers have been applied.[8-10] Analyte ionization occurs after laser irradiation while the analyte is in the MALDI matrix crystals or in the expanding plume. Primarily, the result is singly-charged ions, either positive [M

$+ H]^+$ or negative $[M - H]^-$. The sample stage, laser, and mass analyzer are the key components in the MALDI instrument instrument.

2.4.1.1 Sample Stage

In MALDI MSI, images are acquired by moving, or rastering, the sample in a controlled manner under a fixed-position laser beam. The sample movement (on the stage) must be both precise and accurate at small length-scales. This is not often an issue as modern translation stages can move in submicron steps with high reproducibility. However, many imaging experiments are performed on MALDI instruments not designed for imaging and so their stage movements may not be as accurate or precise as desired. Often, ion images must be overlaid on an optical image of the sample to assist in matching chemical information to morphological features, which may exacerbate any discrepancies in stage motion. The introduction of an ion microscope, where specialized optics are used to create ion images of the whole sample at once, eliminates the need for sample movement.[11]

2.4.1.2 Laser

Selecting a laser and its operating parameters is important to the success of a MALDI MSI experiment. The laser beam diameter can limit the maximal spatial resolution of images to the beam spot-size. Both UV and IR lasers have been used for imaging with remarkable results. Whereas UV irradiation is certainly more common and provides a smaller beam diameter, IR lasers offer some additional advantages, one of which is the ability to use a different family of matrices that includes water/ice.

The two most common UV lasers for MALDI MSI include the nitrogen (337 nm) and the frequency-tripled Nd:YAG lasers (355 nm). Both lasers can be focused to spot sizes considerably below 50 µm. Although the range of 50–100 µm is the common spot size, the use of additional focusing elements can further reduce the size of the probed area.[12] To increase the spatial resolution of an imaging experiment, an alternative approach uses only a portion of the beam profile to ionize a sample by oversampling the raster pattern.[13] Briefly, this method involves completely ablating the MALDI matrix coat at each sample position before moving the sample to the next position. If the movement is smaller than the diameter of the laser beam, signals only originate from the portion of the laser beam profile that overlaps with the non-ablated portion of the sample surface. Using this method, images have been obtained at a spatial resolution of 15 µm with a 100 × 200 µm laser beam, as shown in Figure 2.2.[13]

Nitrogen lasers have been commonly used for MALDI MSI due, in part, to their relatively low cost and strong performance in providing quality mass spectra. In addition, a vast amount of research and development regarding sample preparation strategies has been performed with MS instruments equipped with a nitrogen laser. The low pulse rate (3–20 Hz) of the older N_2 lasers is a significant time constraint when tens to hundreds of thousands of laser shots are necessary to produce an image. Newer nitrogen lasers are able to operate faster, approaching the >200 Hz repetition rates of solid state lasers. The frequency-tripled Nd:YAG, a diode-pumped solid-state laser, is attractive for high-throughput applications, such as proteomics or imaging, for both its robustness (>10^9 shot lifetime) and high repetition rate.

Overall, the Nd:YAG laser's performance has been favorable; however, it produces results inferior to nitrogen lasers in some applications. For instance, with the MALDI matrix sinapinic acid, the results are not as good as with a comparable nitrogen laser, but similar results are obtained from both lasers when using α-cyano-4-hydroxycinnamic acid (CHCA) as the matrix. Lower laser powers and slightly defocused beams can reduce one negative aspect of the highly efficient Nd:YAG laser—fast sample consumption. Promising work to improve the performance of solid-state lasers for MALDI to that of a nitrogen laser has focused on structuring and modulating the Nd:YAG beam, with great success.[14]

While the use of UV lasers is nearly ubiquitous in MALDI MSI, other lasers have unique benefits and are worthy of consideration. For example, IR lasers such as Er:YAG (erbium-doped yttrium aluminum garnet) (2.94 μm) enable the use of matrices such as native frozen water[15] and frozen tissue, as well as glycerol,[16, 17] which is often employed as a preservative/stabilization compound during sample dissection and storage.[18] IR-MALDI also produces a low degree of metastable ion fragmentation and an analytical mass range similar to that of UV-MALDI; however, the long wavelength and difficulty in focusing the laser to a small spot-size present challenges for higher spatial resolution MSI experiments using traditional scanning microprobe analyses. Fiber optics,[12] near field operation,[19] or the mass microscope[11] help to alleviate these challenges and enable tissue imaging without the addition of acidic matrices that alter the physiological conditions of the sample.

2.4.1.3 Mass Analyzers

A large variety of mass analyzers are available for MS. Because of the pulsed nature of laser ionization, its high repetition rate, and the large mass range provided, MALDI MSI requirements are met by the analytical figures of merit of time-of-flight (ToF) instruments. MALDI MSI has also been adapted to several other mass analyzers including the ion trap, hybrid quadrupole ToF, and Fourier-transform (FT).[9] As we discuss each mass analyzer, special focus on their application to MSI experiments will be included.

In ToF mass measurements, ions are accelerated to a constant kinetic energy and move into a field-free region. The ions separate while traveling along the flight tube because smaller ions have a higher velocity than larger molecules. What limits the resolution obtainable? During formation, ions have a range of kinetic energies causing a spread of flight times. This effect is reduced and a higher resolution spectrum results when a reflectron is used in the instrument. Briefly, a reflectron, usually located at an end of the flight tube, uses electric fields to reflect ions back to the other end of the flight tube to an ion detector. The interaction of analyte ions with the reflectron's electric fields corrects for small differences in the ions initial kinetic energy such that ions of the same *m/z* reach the detector at the same time. Thus, the mass resolution of a reflectron instrument is higher. ToF instruments are commonly used in MSI because of their high sensitivity, mass range, and duty cycle.

The addition of fragmentation capabilities to a ToF instrument not only enhances the confidence of analyte identification, it enables the identification of unknown signals via *de novo* or database-guided sequencing of peptides or proteins. Sequential ToFs (sometimes known as ToF/ToFs), like other tandem methods, are becoming more common. Using fragment signals acquired across a sample in MSI can also assist in distinguishing compounds of similar mass. This is particularly beneficial for the study of small molecules such as drugs and their metabolites in specific tissues[20] and in the whole animal.[1]

Another mass analyzer used with MALDI is the ion trap, which confines ions to a specific region by applying a radio frequency potential to the trapping electrodes. To detect the ions, the radio frequency potential is ramped or a supplemental voltage is applied to the endcap electrodes to sequentially eject the ions from the trap. Ion traps are well suited for analyzing small to moderate molecular weight molecules with MALDI, but the reduced mass-to-charge ratio (*m/z*) range prevents the investigation of large proteins. In addition, the lower duty-cycle of ion traps increases image acquisition time, an important consideration when an image consists of tens of thousands individual mass spectra. However, unlike ToF instruments, ion traps enable multiple levels of analyte fragmentation (MS^n) to increase the amount of information available when identifying an unknown.[21, 22] Further, ion traps tend to be less expensive than other mass analyzers. These characteristics make them attractive for MSI experiments of compounds with masses below several kilodaltons.

Hybrid ion trap or quadrupole ToF mass spectrometers place a quadrupole mass filter or ion trap between the ion source and the flight tube. In this case, the ion trap is used to filter and store ions before sending them into the ToF portion of the analyzer for mass separation and analysis. These instruments tend to have higher mass accuracy than ToF-only instruments and have the added benefit of MS^n capabilities; multiple fragmentation cycles may occur in the ion trap with the resulting fragments being sent to the ToF for analysis.

The FT mass spectrometer is the highest performance mass analyzer discussed here. FT mass spectrometers separate and detect ions in an ion cyclotron in the presence of a large magnetic field. The motion of the ions in the cyclotron induces a periodic signal from the detection plates. Because this ion motion is a function of the *m/z*, the frequency of the induced signals may be deconvolved by applying a Fourier transform to produce a mass spectrum. The advantages of this approach include the high mass accuracy and precision obtainable. Why are not most imaging experiments performed using FT MS? FT mass spectrometers require a large superconducting magnet, resulting in higher instrument cost. In addition, the limited mass range for singly-charged analytes and the longer spectral acquisition time for ion accumulation/detection are considerations when using FT MS for imaging. Of course, the high mass resolution enables compounds with similar mass to be differentiated and imaged.[9]

Although the ToF has been the predominant mass analyzer used in MALDI MSI, the adaptation of multiple mass analyzers to imaging has expanded the range of applications amenable to MSI. Commercial MALDI mass spectrometers now commonly have imaging capabilities, and several instruments originally designed for other applications may be fitted with commercial MALDI sources. Each analyzer has specific benefits and shortcomings when applied to imaging applications; thus, instrument selection is based on the needs of the experiment.

Mass analyzers are often used in conjunction with other off-line, non-imaging strategies. For instance, serial sections adjacent to an imaged tissue section can be collected, homogenized, and analyzed with liquid chromatography (LC) MS in order to increase the quantity of analyte available for identification via MS/MS studies.[23]

2.4.2. SIMS

Among all of the ionization techniques used in MSI, SIMS may be the original approach, having been documented as early as 1910, with imaging of tissues reported in the 1960s [24]. In SIMS, the impact of a primary ion beam penetrates several nanometers into a sample, thereby causing the ejection, or sputtering, of material that may include atoms, clusters of atoms, and molecular fragments. The penetration depth and amount of ejected matter is determined largely by selection of the specific primary ion source,[25] and will be discussed further in this section. Unlike MALDI MS, this ionization mechanism tends to be rather harsh and has, until recently, somewhat limited SIMS imaging to the analysis of atoms and smaller molecular ions. However, recent advances in both sample preparation and instrumentation (notably improved primary ion sources) have greatly expanded the mass range and sensitivity of SIMS measurements.

2.4.2.1 Primary Ion Source

Just as in MALDI MS, the first stage of the experiment is the generation of ions. Because the characteristics of the primary ion beam often determine overall performance, selecting the appropriate source is important. A wide variety of primary ion sources have been developed over the years including Ar^+, Xe^+, O_2^+, Cs^+, In^+, Au^+, Ga^+, He_3^+, SF_6^+, CO_2^+, $C_2F_6^+$, Au_x^+ and Bi_x^+ cluster ions and C_{60}^+ (buckminsterfullerene). Of these sources, Ga^+, Au_x^+, Bi_x^+ and C_{60}^+ are most commonly used for biological studies. Recent developments and the availability of several of these cluster ion sources (e.g., Au_x^+, Bi_x^+, C_{60}^+) have greatly expanded the mass range and sensitivity of SIMS imaging experiments, making the imaging of molecular (e.g., M^+) and pseudo-molecular ions (e.g., $[M+H]^+$) from tissues and even isolated cells attractive. Nonetheless, the other ion sources still provide valuable tools to study the distribution of atomics or isotopically-labeled compounds.

Besides the identity of the primary ion sources, the size of the beam and the primary ion flux, which are typically interdependent, influence the spatial resolution and duration of an imaging experiment. Unlike the laser pulses used in MALDI MSI, the primary ion beam is readily focused to well below a micrometer in diameter for most sources, and is rastered across the sample rather than moving the sample under an ionizing beam. This both speeds analyses and reduces the impact of irregularities in sample stage movement, allowing high spatial resolution images to be obtained. Most imaging experiments are performed below the "static limit" such that the primary ion dosage is less than 10^{13} primary ion impacts/cm^2. This limit aims to prevent the gross sputtering of the sample by impacting only ~1% of the sample surface. Beyond the static limit, the surface of the sample begins to erode, which enables depth profiling of the sample. Although depth profiling is useful for hard materials, biological tissue depth profiling has been complicated by several issues including molecular fragmentation.[26] Even so, several examples have been reported, such as depth profiling of *Xenopus* oocytes with the C_{60} source.[27] As can be expected, approaching the static limit greatly benefits the sensitivity of analyses as it more completely samples the surface.

2.4.2.2 Mass Analyzers

Owing to the high repetition rates typically used for SIMS, only a few mass analyzers are appropriate for these imaging experiments. ToF mass spectrometers are most commonly used for molecular imaging, although dynamic SIMS instruments often include a sector mass analyzer, which employs an electric or magnetic field to filter ions on their flight towards a detector or array of detectors. The deflection magnitude depends on *m/z,* with lighter, faster moving ions being deflected more. If a single detector is used, the electric/magnetic field may be ramped or scanned to sequentially detect analytes. When investigating an individual analyte, the field is kept constant to continuously detect the analyte. Alternatively, in a selective-ion monitoring mode, a series of detectors may be used to monitor several ions at once. Sector mass spectrometers, often used for atomic analyses, have been applied to imaging human hair,[28] the distribution of boron neutron capture therapy drugs,[29] and human brain sections.[30]

The ToF instruments applied in SIMS imaging experiments operate on the same principles as discussed previously, with several utilizing a standard ToF arrangement for mass analysis. Alternatively, the TRIFT line of SIMS mass spectrometers from Physical Electronics employs a series of three electrostatic analyzers (ESAs) along the ion flight path to account for kinetic energy differences among the ions. To compensate for the small velocity differences of individual ions, three 90º turns in the ion path function much like the reflectron described earlier by causing ions of different kinetic energy, but with the same nominal *m/z*, to travel slightly longer or shorter paths before reaching the detector.[25, 31]

ESAs also enable stigmatic imaging experiments. Unlike the microprobe methodology of chemical imaging, the stigmatic imaging capabilities enable TRIFT spectrometers to serve as chemical microscopes. This is accomplished by desorbing ions from a relatively large region of a sample all at once, thus retaining the spatial distribution of the ions during mass separation, prior to their detection with a position-sensitive detector.[11] Recently adapted to MALDI MSI, this approach enables an entire sample to be imaged for each laser or ion pulse. Although the summation of multiple laser shots greatly increases the fidelity of images, this method is currently limited to the imaging of a single analyte signal rather than the collection of a complete mass spectrum [32-34].

2.4.2.3 Other Instrumentation Considerations

Recognizing that the mass analyzer and primary ion source are the two most important instrument components, charge-compensating devices and temperature controls also may be beneficial for individual imaging experiments. A low energy electron flood-gun is often used to reduce sample charging that may occur during the experiment, which can greatly degrade mass resolution and secondary ion yield.[35, 36] In addition, several sample preparation strategies have been developed to limit sample charging, and will be discussed later. The ability to control the temperature of the sample surface itself can also be of significant benefit. Cooled sample stages enable the use of frozen, hydrated samples and *in situ* freeze-fractured samples, both of which have shown great value in imaging experiments.[37] The frozen water acts as a matrix to enhance secondary ion yields while freeze-fracturing protocols facilitate imaging of internal structures that may not otherwise be available for study, particularly in single-cell analyses.

2.4.3 DESI and ESI

DESI and ESI ion sources are a relatively recent development for MSI, and are currently undergoing rapid advancement. Both DESI and ESI produce a constant flow of ions for analysis, with the ion trap mass analyzer being most commonly used for these MSI studies.

In DESI, perhaps the newest ionization approach applied to imaging, pneumatically assisted electrosprayed droplets of solvent are directed onto a sample surface that is analyzed at atmospheric conditions. The method requires minimal adaptation to existing mass spectrometers and unlike the previously discussed ionization methods, the DESI ionization source is relatively simple and may be readily constructed in house.[2] The basic set up is comprised of a pneumatically assisted micro-electrospray source, a positioning device, and often a sample holder/translation assembly for imaging purposes.[38] The ion source consists of a stainless steel t-junction that enables a high pressure sheath gas to exit the source supersonically and coaxially, along with the electrosprayed solvent, via several fused silica capillaries, delivering both gas and solvent to the sample surface.[39, 40] The sprayer should be mounted on a solid stage that enables its positioning in three dimensions and adjustment of the angle from the ion source to the surface. By placing the sample on its own translation stage, a continuous movement or raster/pixelation strategy may be used for MSI experiments. The various translational aspects facilitate the optimization of sprayer-to-mass spectrometer, sprayer-to-sample, and sample-to-mass spectrometer distances, as well as the angle from the sprayer-to-sample and sample-to-source, while also enabling compensation for surface height or profile variations. Commercialized ion sources (Prosolia, Indianapolis, IN) also use several charge coupled device (CCD) cameras for angle and sample visualization.[38]

Traditional ESI techniques have not been commonly used as ionization methodologies for MSI experiments, in part due to analyte collection concerns when using a liquid interface in a spatially distinct manner. Two methods have, however, been developed to accomplish these tasks. In the first, developed by Smith and coworkers[41], a brain slice was divided into an ordered array of samples that were individually digested in separate vials and analyzed. Because sample preparation is very important in this methodology, it will be discussed in further detail in the following sample preparation section.

In the second strategy, a sampling probe is used to apply small amounts of a liquid to a sample surface, then the liquid is pulled back through a central channel to an electrospray tip.[42] The probe consists of nested capillaries whereby the eluting solvent is applied through the larger, exterior capillary and then drawn from the tissue surface in a continuous manner via the central capillary. The application of a solvent (such as 1:1 methanol:water) dissolves the analyte from the surface in the area directly under the probe. By scanning the surface in two dimensions via a series of line scans, the probe selectively scans the sample in a manner that enables the creation of ion images.[43] In practice, the solvent is pushed through a 330-µm inner diameter capillary at 10–15 µL/min with a standard syringe pump and is collected back through a 127-µm inner diameter capillary (254-µm outer diameter). The analytes are then transferred towards an electrospray tip held at a high potential to induce electrospray. The probe is kept 20–50 μm above the sample surface. For imaging experiments, the sample may be moved under the probe at ~100 μm/sec to produce ~600 μm spatial resolution ion images (as defined by the sampling width of the probe).[43]

2.5. Sample Preparation for MSI

2.5.1. Sample Collection and Isolation

Traditionally, imaging experiments have focused on the analysis of thin tissue sections. In order to preserve tissue morphology as well as native distribution of analytes, tissues must be rapidly dissected following animal sacrifice and flash-frozen to inhibit enzymatic degradation and analyte redistribution. Immediately following dissection, the tissue is briefly (30–60 sec) submerged in a cryogenic liquid such as liquid nitrogen. Liquid nitrogen slushed–liquid propane is often used for its enhanced thermal conductivity and higher boiling point because it reduces freezing time. Alternatively, dry ice and ethanol may be used to freeze smaller tissues. The goal of these freezing protocols is to prevent enzymatic degradation as well as ice crystal formation. Sample cracking may be prevented by gently submerging the tissue and loosely wrapping it in aluminum foil to prevent it from adhering to the walls of a Dewar. Once frozen, tissues have been stored at –80 ^{o}C for more than a year with successful MSI after storage.[4]

Once sample preparation is complete, the frozen tissues are then sectioned and transferred to a substrate suitable for MSI experiments. The intact tissue is first affixed to the cryostat stage using either a droplet of water or a small amount of optimal cutting temperature (OCT) embedding media. Tissues should not be embedded in the OCT as its presence on the tissue sections, which can occur during sectioning, has been found to reduce ion formation and the quality of the mass spectra.[4] This effect may be eliminated by using only a small amount of OCT to affix the tissue to the stage, taking care to ensure that the OCT does not contact the cut tissue face or microtome blade during sectioning, as in Figure 2.3. Note also that often a small film of oil is applied to separate individual microtome blades during packaging and should be removed by rinsing the blade with acetone or methanol to prevent any chemical contamination.[44] If the tissue must be embedded to facilitate sectioning, a thin layer of water may be used to coat the sample in a thin layer of ice while the tissue is held at cutting temperatures, or embedded in agar to help preserve tissue morphology without degrading the quality of the mass spectra [45]. The sections, 5–50 μm thick, are collected at –5 °C to –25 °C using a cryomicrotome. The exact temperature is tissue-dependant but typically is within this range of values. Although thicker sections are easier to collect and manipulate, thinner sections have been shown to provide higher quality mass spectra.[46] During sectioning, tissue orientation should be considered in order to ensure the section contains the morphological features of interest.

After sectioning, tissues must be transferred to a suitable sample plate for MS analyses, using one of several available methodologies. Commonly, the tissue is transferred to a cold sample plate or conductive indium tin oxide (ITO)-coated glass slide using forceps for thicker sections or an artist's brush for thinner sections. Care should be taken during transfer as a thin tissue slice is easily deformed. The tissue section is then thaw-mounted to the cold sample plate by quickly warming them together. There are a number of ways to accomplish this. The easiest is by placing a finger or hand on the opposite side of the sample plate and using body heat to warm the sample and sample plate together. In another, the sample may be warmed in a desiccator, taking care to prevent condensation when moving from the cryotome to the desiccator. Finally, a sample plate that is at room temperature may be placed directly on a tissue section, which then thaws onto the plate. Although the transfer methods are similar in nature, the cold plate transfer produces superior mass spectra as the transfer is quantitative, whereas the warm plate transfer often leaves a small amount of ice on the cryostat cutting surface, which may retain analyte.[4] In the cold plate method, ice that contains water-soluble compounds is thawed on the sample plate so that these compounds remain with the tissue sample.

Although the majority of imaging experiments are performed using thin tissue sections, the sensitivity and resolution afforded by MSI experiments now enable the profiling and imaging of single, isolated or cultured cells. Isolation of single cells is useful when studying neural tissues, as individual cells often are chemically different from their immediate neighbors. As might be expected, the isolation of single cells from tissues is often non-trivial, but several protocols have been developed to assist with this process, including partial enzymatic digestion, glycerol stabilization, and fracturing methodologies for cell cultures.

In the case of larger, more physically stable cells, such as those found in the nervous system of several invertebrate neurobiological models, cells may be isolated after partial enzymatic digestion of the ganglionic sheath in a physiological solution containing 1% protease for 1–2.5 hours at 36 ºC. Following sheath removal, cells are isolated using sharp needles or via suction from small glass or plastic pipettes and then transferred to a glass slide or other suitable mass spectrometer target.[18] Although samples for MALDI MSI may also be fixed in a 4% paraformaldehyde solution, cross-linking of the cellular membrane during the paraformaldehyde fixation may be detrimental to SIMS studies of the lipid membrane.

In contrast to invertebrate cells, the isolation of mammalian neurons is somewhat more involved as the cells are typically smaller than invertebrate neurons. To isolate single pituitary cells from rats, Rubakhin and co-workers[47] used a physiological solution containing 30% glycerol to improve sample preparation and reduce the time required for isolation. A natural stabilizing agent, glycerol allows extracellular physiological solution to be removed without lysing the cells or significantly altering the biochemical profile of neurons.[48] Following glycerol stabilization, cells may be mechanically separated with fine glass pipettes using micromanipulators under an inverted microscope.

In addition to isolating cells directly from tissues, cell culturing may also be of great value in MSI experiments. Glycerol stabilization may be applied to cultures in the same manner as the cell isolates. Cultures may also be flash-frozen and freeze-fractured or analyzed in a frozen-hydrated state.[49] Although these freezing protocols require the sample to be maintained in a frozen state, frozen samples may also be freeze dried. Alternatively, 50 mM trehalose may be added to the culture solution prior to freeze drying to create a condition similar to a freeze-fracturing protocol, precluding the need for the sample to remain frozen over the course of preparation and analysis. [50]

2.5.2. Preparing the Sample for MSI

Each of the various MSI approaches (MALDI, SIMS, DESI, ESI) has different ionization methods, and each works best with specific types of analytes. Thus, it should not be surprising that sample preparation methods are also distinct for each. In this section, the more common sample treatments are described for each of these ionization approaches.

2.5.3 MALDI MSI

MALDI MS requires that analytes from a tissue be incorporated into a thin matrix layer. The extraction of analytes without fixation/cross-linking in the matrix often is accompanied by analyte migration. Thus, proper matrix application is one of the most important steps in the acquisition of high quality MALDI MSI from tissue. Of course, heterogeneities in ion yield across the sample can introduce significant experimental artifacts into the produced ion images.

Can we address these concerns by optimizing protocol parameters? Matrix deposition conditions, including matrix composition, concentration, method of application, and thickness of application, are important factors in developing a matrix application protocol. Choosing the right matrix often depends on the mass range of interest and the laser wavelength. For UV lasers, sinapinic acid (3,5-dimethoxy-4-hydroxycinnamic acid) performs well with higher mass analytes such as proteins, while CHCA performs well with compounds under ~3 kDa such as peptides. Due to a tendency to form large heterogeneous crystals, 2,5-dihydroxybenzoic acid (DHB) is less commonly used for imaging, with the exception of controlled spotting and crystallization in profiling experiments, which may be considered a low pixel count image.[51] The selected matrix is often dissolved in 1:1 acetonitrile:water or ethanol:water solutions, which is useful for a variety of thin tissue measurements and analytes of different solubilities.[4] Matrix concentration and amount affects signal quality, crystal coverage, and crystal size. Often higher matrix:solvent ratios lead to larger crystals on the surface of the tissue section.[51] Sinapinic acid matrix, for instance, has an optimal concentration of ~10–30 mg/mL; signal quality often increases with concentration, with a saturated solution of 30 mg/mL providing better results.[4] The other matrices tend to have an optimal concentration similar to that of the sinapinic acid.

Typically, other than ethanol washing, tissue processing is kept to a minimum. Washing increases the intensity of protein signal from 3- to 10-fold, depending on the specific sample. In ethanol washing, the target-affixed tissue is submerged in cold 70% HPLC grade ethanol for 30 s, followed by drying under a nitrogen stream. The precipitation of proteins from the solution increases their signal intensity and decreases the amount of protein delocalization that otherwise occurs while the sample is exposed to a liquid phase, thus preserving spatial resolution.[44] To further increase signal quality, a second washing step in 90% ethanol, 9% glacial acetic acid, and 1% deionized water may also be used to help remove salts and phospholipids.[44] However, the ethanol washing procedure may potentially remove desirable ethanol-soluble compounds from the tissue. Variations on this ethanol rinsing procedure include employing 0.3–1% trifluoroacetic acid (an ion-paring agent often added to MALDI matrix solutions) to further increase signal,[4] or applying a small amount of MALDI matrix to the ethanol wash to “seed” matrix crystallization on the tissue.[52]

The spatial resolution desired is an important factor in determining the method of matrix application. If relatively low-spatial resolution is acceptable, as when comparing diseased versus normal states, profiling experiments are often sufficient.[53] In profiling, small discrete matrix droplets are manually deposited onto areas of the tissue, reducing spatial resolution to the size and spacing of the droplets. As a benefit, such matrix droplets often extract more analyte from the tissue and thus result in higher signal intensities compared to traditional imaging protocols. When a higher spatial resolution is required to examine the spatial structure of small morphological features, matrix can be applied in a thin homogenous layer across the tissue to enable imaging.

Several application strategies are used to apply MALDI matrix to tissue sections. A large drop may be dragged across the tissue or the sample may be immersed in an organic solvent solution that has been saturated with the selected MALDI matrix. However, both of these methods increase the likelihood that some analyte redistribution will occur.[54] Higher spatial resolution experiments may be achieved by the application of a homogenous layer of matrix or small, evenly-distributed matrix droplets onto the tissue. Homogenous matrix application requires the use of a device to create a fine mist of matrix, sprayed in a series of even coats to the tissue. Typically, this consists of a glass spray nebulizer that is typically used to develop thin-layer chromatography (TLC) plates, an artist’s airbrush, or a similar home-built sprayer. Applying the matrix in a series of thin coats prevents the matrix layer from becoming too thick (which may result in multiple crystal layers and reduced ion yields) or the tissue section becoming too wet (which may induce analyte redistribution). Roughly ten passes, lasting 5–10 s each, with a drying period of 1–2 min between coats, limits the analyte migration that can occur when the tissue sample is wet and yields the most intense signals.[44] It is important to allow the tissue to nearly dry between coats but not become completely dry. This requires optimization of the protocol according to tissue and atmospheric conditions within the lab. Following matrix coating, samples may be coated with a thin layer of metal such as gold to increase ion yield from the tissue sections;[32] however, such treatment is often not necessary. Although samples may be stored at –80 ºC until needed, it is preferable to analyze samples shortly following preparation.

An alternative to spray nebulizers is electrospray deposition, which applies high voltage to a liquid in a glass or metal capillary to create a matrix spray of small droplets.[55] By controlling the spray needle with an X-Y translation stage, this methodology offers a high level of homogeneity.[44]

Recently, an acoustic printer has been used to deposit high density droplet patterns of matrix in an automated manner. Matrix is placed in a reservoir below the sample and an acoustic pulse ejects a small droplet of matrix onto the sample. The sample is mounted on a two-dimensional translation stage that enables the printing of spot arrays. Uniform droplets, ranging in size from 0.1 pL to 10 μL, may be applied by the acoustic ejection process at a spatial resolution of ~200 μm.[56] Unlike the homogenous coating methods where analyte redistribution is a problem, here such migration is limited to the diameter of the printed spot. Acoustic printing has recently been applied to the study of breast cancer,[57] toxicity in rat kidney,[58] and pharmacokinetics [1].

Before the application of matrix as outlined above, tissues may be seeded with matrix to allow greater crystal homogeneity across the sample, as shown in Figure 2.4. Matrix may be added to the ethanol washes, as mentioned previously, or to a solid matrix such as sinapinic acid, which may be mechanically ground into a fine powder and then spread across the tissue section. The subsequent application of liquid matrix then forms smaller, more homogenous crystals to create a more stable, uniform signal across the entire tissue section. Smaller matrix crystals also reduce the number of laser shots needed at each location, thus reducing the time needed to collect the mass spectra from the sample. Matrix seeding has only recently been applied to MALDI MSI of mouse brain tissue.[59]

Another deposition method combines both matrix seeding and high density microspotting to improve signal intensities for profiling/imaging experiments. In this two-step "spray-droplet" method, a sprayed low-concentration matrix seed layer is followed by microdroplet application via inkjet printing of a higher-concentration matrix solution.[60]

The previously outlined techniques have focused on analyzing intact, complete tissue sections. The Sweedler group[61] has developed a method, the "stretched sample" approach, to study tissue sections at approximately single cell spatial resolution that allows maximal matrix-analyte incorporation while inhibiting analyte redistribution. Briefly, a substrate is prepared by affixing a monolayer of glass beads (~38 μm diameter from MoSci Corp., Rolla, MO) to a Parafilm M membrane using pressure and heat. A tissue section is then placed on the substrate and adheres strongly to the glass beads. The substrate is manually stretched to fragment the tissue as the beads separate. Fragmentation occurs because the mechanical stability of the tissue section is less than that of both the tissue-bead and bead-Parafilm M adhesion. As the substrate may be stretched to four times its original size, individual beads are separated by ~100 μm from one another by the hydrophobic Parafilm M membrane, which inhibits analyte migration during matrix application. Additionally, water may be condensed onto the sample in small droplets to increase the time of analyte incorporation without fear of redistribution as long as the droplets do not form connections between adjacent beads. This slow extraction/crystal formation methodology has also been found to reduce the presence of alkali metal adducts by inducing mutually exclusive crystallization of the MALDI matrix and the salts from the tissue.[62]

2.5.4 SIMS Imaging

As mentioned previously, owing to a combination of decreased analyte redistribution and a smaller probe dimension, SIMS imaging provides higher spatial resolutions than MALDI MSI. This spatial resolution is routinely at the single micron to 100 nanometer range. Because SIMS uses primary ion impacts to desorb and ionize analytes from a sample, large molecules are ionized less effectively than in MALDI MS, in large part due to an increased level of fragmentation during the desorption/ionization process.[34] This increased fragmentation has traditionally limited SIMS to the analysis of atomics and relatively small molecules. Nonetheless, developments in sample preparation techniques, including cryogenic treatment of tissue, surface metallization, and matrix enhancement, as well as the “softer” primary ion sources discussed previously, make the imaging of ever-larger biomolecules in tissues more feasible. Sample preparation remains the principal challenge, particularly at high spatial resolutions. Differences in ionization efficiency caused by variations in the chemical and topological properties across a sample surface can complicate analyses and sample preparation strategies.[63] SIMS is a surface-sensitive ionization process, thus it is inherently attuned to the interaction of the ion beam with the surface. Fortunately, these surface effects can be largely controlled and/or overcome by choosing the appropriate sample preparation and data processing protocols.

Following isolation, samples for SIMS are often subject to cryogenic treatments such as flash freezing or freeze fracturing. Flash freezing fixes the sample by rapidly cooling it at a rate of ~5000 K/s in a coolant such as Freon 22 or liquid nitrogen-slushed propane.[64] The rapid cooling rate quenches the movement of even atomic ions such as sodium and potassium within a sample, which is indicative of the high level of preservation necessary for imaging at sub-micron spatial scales. Frozen samples may be transferred into the SIMS instrument using a cold transfer stage in a hydrated state[37] or freeze dried to preserve the sample, keeping in mind that the drying process may allow some analyte redistribution to occur. The alternative cryogenic treatment, freeze-fracture, was originally developed for electron microscopy, and is used to access subcellular features within a sample.[65] Often the sample is placed between two silicon shards prior to flash freezing. While under liquid nitrogen, the two pieces of silicon are then separated to fracture the frozen sample. This fracturing is beneficial for the study of single cells and may expose several different regions of the cell; for example, the outer membrane surface or the intracellular components, which may be identified on the basis of the spatial and chemical patterns that arise from the SIMS analyses.[65] This fracturing enables the interior of isolated cells to be examined that would not otherwise be available due to the surface-profiling nature of static SIMS. To limit analyte migration, the freeze-fractured cells are freeze dried at –90 °C or analyzed in a frozen hydrated state in which the water ice helps to reduce analyte fragmentation.[66] Phosphocholine was recently imaged in freeze-fractured cells from rat kidney tissue.[67] An analogous fracture method was developed for SIMS imaging by using 50 mM trehalose at room temperature, instead of freezing, to stabilize cell cultures.[50]

In SIMS, when charged particles impact the sample surface, notable surface charging and analyte fragmentation can occur. One of the most promising means by which to address these issues is to apply a thin layer of metal to the sample surface. Sample metallization may be performed in either of two manners. In the imprint-imaging method, the sample is prepared and then pressed onto a silver surface, resulting in the transfer of a thin layer of sample to the metal; the metallized sample is then imaged. This technique has been shown to reduce the fragmentation of moderate-weight analytes and sub-kDa peptides and has been used to image phosphatidylcholine and cholesterol in human blood cells.[68, 69] Higher secondary ion yields are obtained from the silver surface compared to the direct analysis of tissue, and this method may be applied easily to both tissue and isolated cells.

An alternative metallization technique completely covers the sample surface with a 1–5 nm thick layer of metal such as gold or silver applied with a conventional sputter coater. This methodology is consistent with strategies used for SEM preparations. The metal coating not only prevents charging but is also believed to help “soften” the initial impact of the primary ions by forming a protective shell over the sample surface. Surface metallization both increases sensitivity and greatly expands the mass range available for analyses (to ~5 kDa) while keeping the sample surface intact rather than transferring it to another surface. After using this silver coating technique, the cholesterol signal was found to be up to 600 times higher in rat kidney.[70] Gold metallization has been used for

ToF-SIMS imaging of cholesterol and other cell membrane components in rat brain.[32] Direct surface metallization has also been applied to detect large synthetic polymers such as polyalanine [35], but not as yet to *in situ* large biomolecules. Although the sample is coated in this preparative strategy, analytes are not incorporated into the metal layer but rather are maintained in their native locations under the thin metallic coating.

Organic MALDI matrices are also being used for the analysis of tissues in SIMS. In matrix enhanced-SIMS (ME-SIMS), small molecule organic matrices (typically traditional MALDI matrices such as CHCA) are used to coat tissues in a similar manner to those methods outlined for MALDI MSI. These approaches result in the incorporation of analyte into the matrix layer. ME-SIMS has shown promise for extending the mass range to the level required for proteomics experiments, particularly when linked with surface metallization strategies.[35] In addition to improving the upper end of the mass range for SIMS, matrix-enhancement also reduces the fragmentation of lower mass analytes, thus increasing sensitivity across the mass range.[63] Although SIMS images can be collected at sub-micrometer spatial resolutions, matrix crystal size often limits the experimental spatial resolution to ~2–3 microns. Proteins as large as a lysozyme, at 14 kDa,[71] have been detected using the ME-SIMS approach, but thus far, compounds this large have not been directly detected from biological tissues. However, ME-SIMS has been used to create ion images of small peptides from a section of the cerebral ganglion of the pond snail, *Lymnaea stagnalis*, at 2.5 μm spatial resolution.[34]

2.5.5 DESI and ESI

Although used less frequently, DESI and ESI imaging methods have some advantages in that they require less sample preparation and do not have the vacuum requirements of SIMS and most MALDI MS instruments. Specifically, DESI relies on a supersonic electrosprayed solvent mixture to desorb analytes directly from a surface.[2] Although the precise mechanism of this desorption is still under investigation, as little or no sample preparation is required, the desorption properties of DESI are rather well suited for the two-dimensional imaging of biological samples. DESI MSI has been successfully used in detection, directly from the skin, of the antihistamine drug, loratadine, *in vivo*.[2] Furthermore, DESI has shown promise for its ability to ionize small and nonpolar molecules,[72] and provide images of tissue sections from rat brain for lipid analysis,[73] as well as images of the distribution of other small molecules. While the spatial resolution of such experiments is still low (~400 µm), DESI is useful in defining gross morphological features, as shown in Figure 2.5.[74]

Efforts to apply traditional ESI to imaging are complicated by the fact that this method was not designed as a surface analysis technique. Several methodologies have, however, been developed that incorporate this approach. Smith and co-workers[41] have developed a technique whereby a thick (1 mm) tissue section is dissected into 1 mm^3 cubes and individually digested and analyzed with LC coupled to FT MS. In this example, over 250 different protein distributions were imaged in a mouse brain by mapping the normalized intensity of a peptide resulting from the tryptic digest of the parent protein. Although the presented images were of low spatial resolution (1 mm), improved sample handling procedures and increased throughput of sample analyses may increase both the resolution and speed of these experiments.

An alternative ESI methodology utilizes a surface probe to remove analyte from a sample with a suitable solvent and then delivers the eluent to the mass spectrometer. This method has not yet been applied to the imaging of biological materials but is similar to online dialysates or push-pull perfusion probes. Furthermore, it would most likely require some desalting because the ESI process can be sensitive to the presence of high salt concentrations. Nonetheless, the spatial distribution of a dye mixture has been successfully examined from the surface of a thin-layer chromatography plate using the probe-ESI methodology.[42, 43]

2.6. Image Acquisition and Data Analysis

Mass spectral images often contain 10^4 pixels and have been as large as 10^7 pixels,[75] depending on the size of the sample and the spatial resolution. Since a mass spectrum is taken at each pixel location, dataset sizes can rapidly approach and even exceed several gigabytes. This presents challenges in both data acquisition and analysis. Software that interacts with the instrument to make acquisition of these large datasets more efficient is readily available for most MALDI mass spectrometers in either commercial (from instrument manufacturers) or freely available forms (www.maldi-msi.org). Although the specifics vary with each instrument, in general these programs create a list of positions on the sample target and gather mass spectra in an automated manner. Once collected, the mass spectra are processed into a form that is more easily analyzed. The freely available tools produce an Analyze 7.5 dataset that may be read by several software packages, such as BioMap or Matlab, to produce images.[59, 76] In general, commercially available software is tailored to the specific instrument and/or integrated into the instrument control and data analysis programs and results largely in proprietary formats. Unlike MALDI MS, imaging is nearly inherent to static SIMS instruments as rastering of the primary ion beam is required to prevent the rapid ablation of the sample surface. Therefore, imaging is typically integrated directly into the instrument control and data analysis software.

The large number of mass spectra and surface variations across a sample may introduce some level of systematic error into an experiment but can often be compensated for in post-processing. For example, an uneven sample surface topology may introduce mass errors or shifts in ToF-MS instruments, as the mass measurement depends on the flight distance and extraction efficiency. By measuring the shift in time-of-flight of a particular *m/z* signal across the surface, a height map can be generated and used to correct the acquired mass spectra.[34] Other widely used methods to correct for systematic errors include baseline subtraction, noise estimation, normalization, and spectral realignment.[44, 77] Localized charging may also introduce similar errors. However, this variation in ionization efficiency may be addressed by normalizing the ion image for a selected compound with the image of a ubiquitous compound.[49, 78]

Collecting a complete mass spectrum for each pixel in a high density raster over a sample generates up to several gigabytes of raw data, and particularly in the case of MALDI MSI, consumes a fair amount of time (several hours). This process can result in a significant number of laser shots and extensive instrument usage. If the mass range of the compounds and specific tissue region of interest is known, the dataset may be vastly simplified. Often it is impractical to perform many MALDI MSI experiments and it is more advantageous to use profiling or low-density raster patterns prior to final, high-density imaging of a sample for optimization and reproducibility experiments. For example, serial sections of a tissue sample may be taken so that each has approximately the same chemical profile as one another. This enables parallel profiling and imaging experiments to be performed so that the profiling results may assist in driving the specifications of the imaging experiment.

Often experiments are designed to examine different physiological states in order to identify changes in protein expression patterns that may be correlated with a disease state or stimulus (pharmacological, conditioning, etc.). Comparisons between tissues of a different nature or physiological role are also of great interest. Uncovering such correlations from the entire raw dataset requires the use of statistical methods. Clustering methods, such as principal components analysis (PCA) combined with linear discriminants, have been used to identify pixels and spatial regions that are spectrally correlated in the MALDI MSI[79] and SIMS data[80]. The analysis of mass spectra from 28 bacterial strains followed by PCA enabled the differentiation of gram-positive from gram-negative bacteria and, in some cases, individual species.[81] The analysis of cancer biopsies also resulted in the differentiation of the various stages of cancer, predicting patient mortality with an accuracy similar to traditional histological approaches.[52, 57]

2.7 Specialized Methods

2.7.1 Combining MSI with Histological Staining

Histological staining may be used to associate mass spectral data to morphological structures in a tissue. This enables comparison of multiple tissue sections to each other, or to a tissue atlas. Combining optical microscopic and mass spectral images requires careful selection of stains. While cresyl violet and methylene blue have shown to be compatible with MALDI MSI experiments,[77] conventional hematoxylin and eosin dyes suppress mass spectral signals. Typically, following sectioning, the tissue is placed onto a conductive glass slide so that it may be examined by optical microscopy. Suitable slides should be optically transparent and conductive to prevent charging such as slides coated with indium-tin oxide. Several hundred microliters of a staining solution are then pipetted onto the tissue section. Any excess stain can be removed by submerging the tissue in ethanol, which as mentioned previously, also serves to fix proteins.[77] Combining MALDI MSI with histological examination has aided in the identification of several novel biomarkers in human brain tumors[82] and breast cancer samples.[44]

2.7.2 Three-dimensional MSI

The ability to combine three-dimensional analyses with other imaging techniques such as magnetic resonance imaging (MRI) enables the highest information content available to be gleaned from a sample. In three-dimensional MSI, serial sectioning is followed by the acquisition of two-dimensional images of each section; then the individual sections are combined to create the three dimensional image. One issue when combining three-dimensional imaging with MSI is the registration of adjacent serial tissue sections while creating the third dimension based on two-dimensional morphologies. One way to address this issue is with histological staining, which assists in identifying landmark features in the tissue to aid in registration between sections. In addition, prior to sectioning, registration marks may be added to aid in image reconstruction. The efficacy of three-dimensional image reconstruction has been demonstrated using a series of 20 μm-thick sections from a mouse brain.[83] Three-dimensional images allow the study of detailed proteomic or pharmacodynamic information by enabling the chemical reconstruction of entire organs in a structural visualization scheme.

2.7.3 Tandem MSI

Although many analytes may be putatively identified on the basis of accurate mass match to a known compound, fragmentation data assists in the identification of novel signals or the verification of a signal's identity. In addition, imaging the distribution of a fragment ion across a sample separates signals from different compounds with the same nominal molecular mass. Tandem MSI (MS/MS) has been used for the concurrent imaging and *de novo* sequencing of several insect neuropeptides.[84] Imaging of the distribution of small organic molecules can be achieved by plotting the intensity of a selected fragment ion from a parent compound of interest. Khatib-Shahidi and co-workers[1] have used the MS/MS transition from the parent to fragment ion to image the distribution of a drug and its metabolites in a complete saggital section of a mouse following oral drug dosing. Similarly, a pharmaceutical study has mapped the location of an active drug in multiple types of rat tissues using tandem MSI.[22] Intermediate pressures

(0.17 torr) with MALDI MS, along with an intermediate-pressure linear ion trap, reduce fragmentation of labile analytes such as lipids, while also allowing tandem MSI experiments to resolve species of similar mass.[12] Tandem MSI also been used to image the distribution of cerebroside lipids in nerve tissues.[21]

2.8. Summary and Future Directions

The ability to map the distribution of a wide range of compounds directly from tissues and isolated cells will greatly aid researchers in many fields. A significant advantage of MS-based approaches is that analyte preselection or labeling is not typically required and little, if any, prior knowledge of the imaged compounds is needed. An additional benefit is that compounds may be directly sampled from a tissue (or following minimal preparation such as matrix coating) to enable the visualization of the native distribution of a wide range of both known and unknown compounds in a single experiment. Because of the reduced sample preparation steps, the amount of analyte required for characterization is often less than for separation/MS (*e.g.*, LC-MS) approaches. Although the field of MSI is rapidly developing, sample preparation protocols still require optimization as most have not been fully standardized or validated. In fact, as discussed throughout this chapter, sampling protocols must be tailored not only to the various methodologies, but also according to the type of tissue being analyzed.

The design of a successful MSI experiment requires consideration of several factors, including the mass range, spatial resolution, and sensitivity desired or required. Through careful selection of the right methodology and sample preparation strategy, high quality mass spectra can be obtained at thousands of positions across a sample at a broad range of spatial resolutions, from sub-micron to hundreds of microns. As a result, tens to hundreds of compounds can be imaged in a single experiment. MS-based imaging has shown real promise in addressing several biological questions, but the full potential of the approach is just beginning to be realized. The recent and rapid application of MSI to drug development, disease prognosis, and fundamental biochemistry suggests that MSI will enable significant biological breakthroughs in the future.

2.9 Glossary of Terms

Adduct: An ion produced by the addition of a cation or anion to a molecular species or a fragment of a molecular species. Commonly adducts are observed during the analysis of crude biological samples.

DESI (Desorption Electrospray Ionization): An ionization technique that involves an electrospray source to create charged droplets to ionize compounds from a surface. DESI is useful in the low mass range including analytes such as small molecule, lipids, and short peptides.

ESI (Electrospray Ionization): An ionization technique where the solution containing the analyte is passed through a needle held at high potential leading to a mist where the analyte becomes ionized.

FT-MS: A mass analyzer and detector that functions based on the periodic cyclonic motion of ions placed in a magnetic field. The frequency of cyclonic motion can be deconvolved into a mass spectrum using a Fourier transform.

Ion Trap: A mass analyzer that captures ions in a region of space using magnetic or electric fields. The ions can be accumulated in this space prior to release for MS, MS^n, or transfer to another mass analyzer.

ITO (Indium tin oxide): A conductive coating composed of indium (III) and tin (IV) oxides that is often applied to glass slides to maintain a conductive yet transparent surface for MS experiments with tissue sections.

LC-MS (Liquid Chromatography Mass Spectrometry): A hyphenated technique that combines separation based on physical characteristics of analytes and detection that enables the mass of analyte to be determined. Following separation, the solution can either be spotted onto a MALDI plate or directly plumbed via ESI into the mass analyzer.

MALDI (Matrix Assisted Laser Ion Desorption): An ionization technique involving embedding the analytes of interest in a matrix and irradiating the sample with a laser beam to form ions. The laser beam is absorbed by the matrix thus limiting analyte fragmentation.

MALDI Matrix: A low molecular weight compound that absorbs in the UV or visible region forming a plume where cocrystalized analytes become ionized. Matrix can be applied in many ways including using a pipette tip, a microspotter, or an airbrush depending on the needs of the experiment.

MSI (Mass Spectrometric Imaging): The use of mass spectrometry to produce spatially resolved mass spectrums of a sample. MSI produces data that are used to produce ion images allowing the spatial distribution of analytes to be uncovered.

MS^n: Also called tandem MS. Analysis involving the separation of ions, the selection and fragmentation of an ion, followed by the separation of those fragmentation products. While most mass analyers only perform this series of actions a single time, use of an ion trap facilitates its repetition for many cycles.

Nd:YAG Laser (Neodymium-Doped Yttrium Aluminum Garnet): A solid state laser using a $Nd{:}Y_3Al_5O_{12}$ crystal capable of being operated in either continuous or pulsed fashions. Nd:YAG lasers natively lase in the IR region but are frequently frequency doubled or tripled using nonlinear optics to produce UV and visible light.

PCA (Principal Component Analysis): A statistical operation that characterizes the largest types of variation in spectral dataset within a series of uncorrelated (i.e. orthogonal) principal components. Samples with similar types of spectral variation tend to cluster together when plotted in principal components space, allowing unknown samples to be classified into different types or compared to samples of known class identity.

Pseudomolecular ion: An ion formed by the addition of a cation or anion to the molecular species. A molecular ion, however, is formed by the addition or loss of an electron from the molecular species.

Reflectron: A reflectron improves the mass resolution of a ToF mass analyzer. A reflectron consists of an electrostatic field that is in the flight path of the analyte ions and redirects (or reflects) the ions toward the detector. The interaction of analyte ions with the field is proportional to their kinetic energy, thereby reducing the random distribution of analyte ion kinetic energies.

SIMS (Secondary Ion Mass Spectrometry): An ionization technique where the sample surface is sputtered with ions from an ion gun producing a plume where secondary ions are formed.

ToF (Time of Flight): A mass analyzer that separates ions based on the time it takes an ion to reach the detector at the end of the flight tube. Due to all species having the same kinetic energy, the time of the flight is proportional to the mass to charge ratio.

2.10 Tables and Figures

Table 2.1. List of acronyms and their meanings as used in this chapter.

Acronym	Meaning
CCD	Charge-Coupled Device
CHCA	α-cyano-4-hydroxycinnamic acid
DESI	Desorption Electrospray Ionization
DHB	2,5-dihydroxybenzoic acid
ESA	Electrostatic Analyser
ESI	Electrospray Ionization
FT	Fourier Transform
HPLC	High Performance Liquid Chromatography
ITO	Indium Tin Oxide
LC-MS	Liquid Chromatography Mass Spectrometry
MALDI	Matrix Assisted Laser Desorption Ionization
ME-SIMS	Matrix Enhanced Secondary Ion Mass Spectrometry
MS	Mass Spectrometry
MSI	Mass Spectrometric Imaging
Nd:YAG	Neodymium-Doped Yttrium Aluminum Garnet
OCT	Optimal Cutting Temperature
PCA	Principal Component Analysis
SEM	Scanning Electron Microscopy
SIMS	Secondary Ion Mass Spectrometry
TLC	Thin Layer Chromatography
TOF	Time of Flight

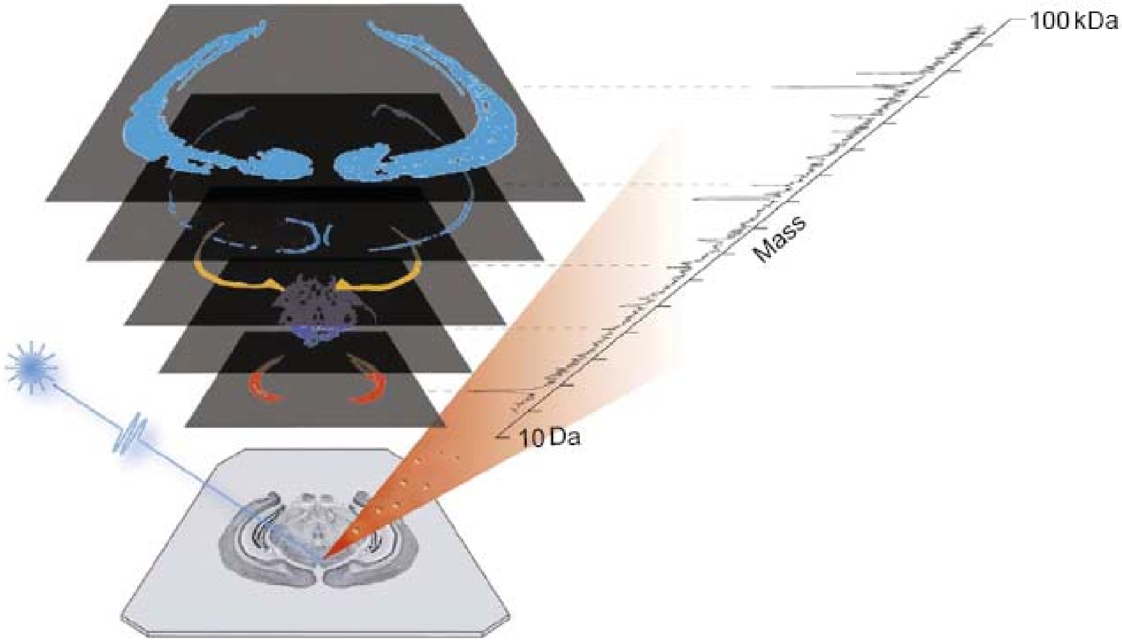

Figure 2.1 Overview of mass spectrometry imaging (MSI). A series of complete mass spectra are taken in an ordered array across the sample. The intensity of the signal for selected compounds of interest is then plotted following data acquisition to create a series of ion images. (Reprinted with permission from Elsevier).[7]

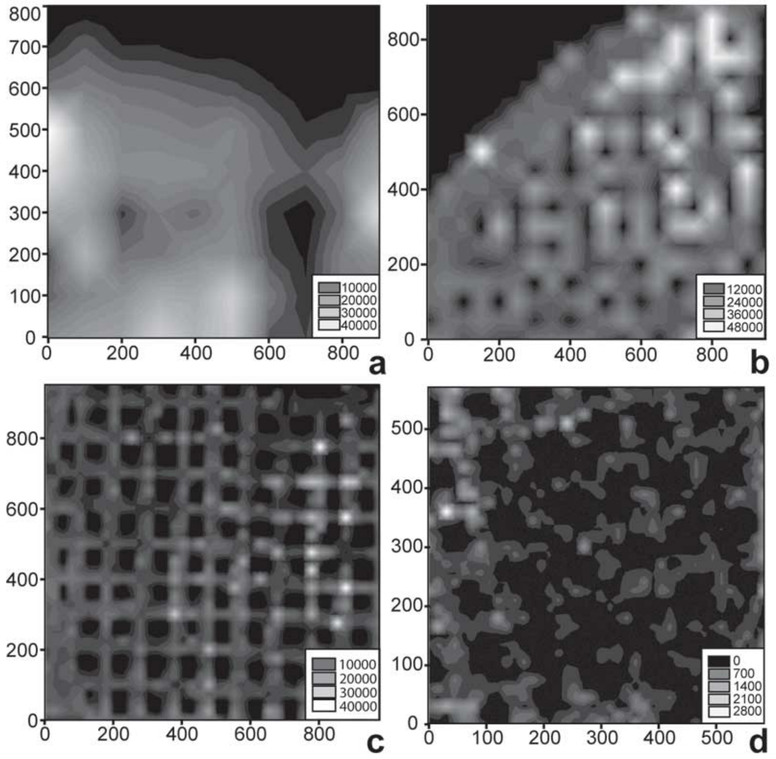

Figure 2.2 Matrix-assisted laser desorption/ionization-mass spectrometry images of the peptide angiotensin I (*m/z* 1297) on electron microscopy calibration grids (100 μm hole-to-hole spacing), obtained using an oversampling technique at raster sizes of (**a**) 100 μm, (**b**) 50 μm, (**c**) 25 μm, and (**d**) 15 μm, illustrate the utility of oversampling to resolve small features in the sample. (Reprinted with permission from Elsevier).[13]

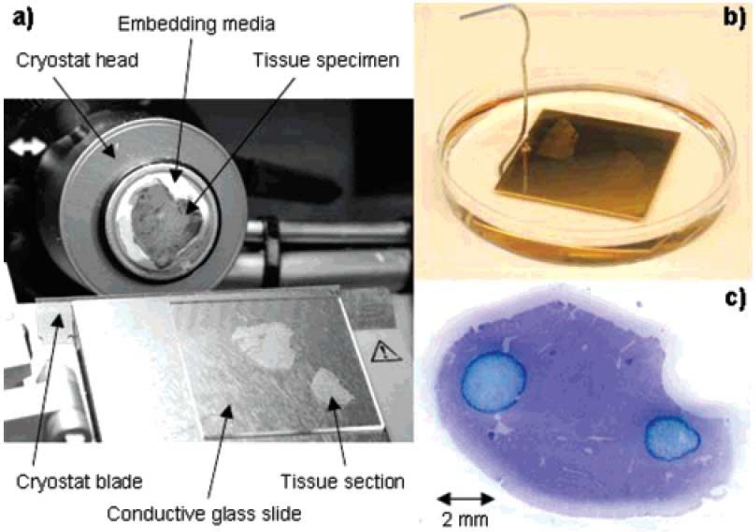

Figure 2.3 Tissue processing. (a) Tissue oriented on a cryostat, prior to sectioning. (b) Sectioned tissues are then rinsed with ethanol and often (c) stained for histology (microphotograph of stained tissue is presented). (Reprinted with permission from Elsevier and the American Chemical Society).[44]

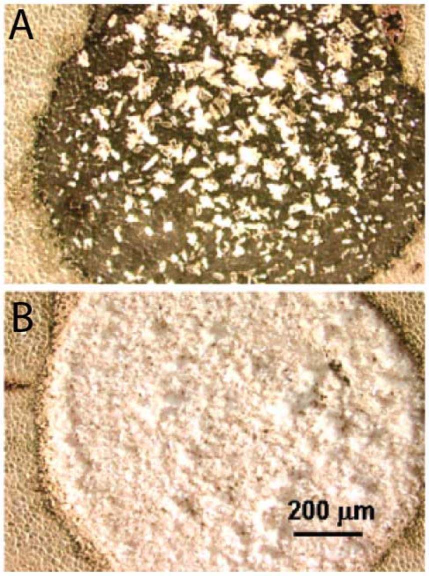

Figure 2.4 MALDI matrix applied to (A) unseeded rat liver tissue and (B) matrix-seeded tissue. Greater crystal homogeneity is observed in tissues that have been previously seeded with ground matrix. (Reprinted with permission from Elsevier and the American Chemical Society).[56]

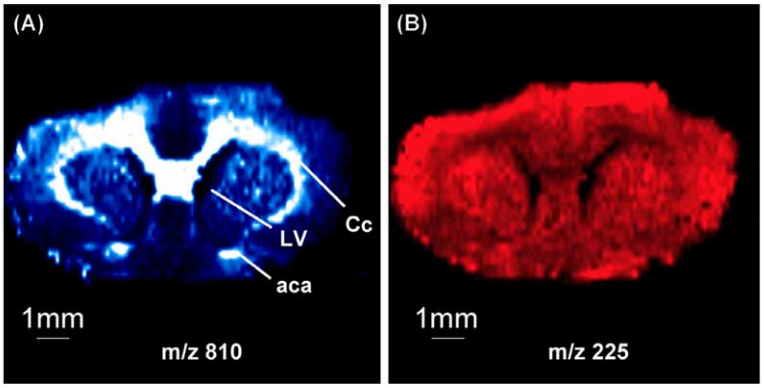

Figure 2.5 Negative ion DESI MS images of (A) *m/z* 810 and (B) *m/z* 255 from a 4 µm coronal section of rat brain tissue illustrate the utility of the method to resolve morphological features in tissues. LV, lateral ventricle; Cc, corpus callosum; aca, anterior commissure anterior part. (Reprinted with permission from Elsevier).[74]

2.11 References

1. Khatib-Shahidi, S., Andersson, M., Herman, J. L., Gillespie, T. A., and Caprioli, R. M. Direct molecular analysis of whole-body animal tissue sections by imaging MALDI mass spectrometry. *Anal. Chem.* **2006,** *78*, 6448-6456.

2. Takats, Z., Wiseman, J. M., Gologan, B., and Cooks, R. G. Mass spectrometry sampling under ambient conditions with desorption electrospray ionization. *Science* **2004,** *306*, 471-473.

3. Gross, M. L. and Caprioli, R. M., eds., *The encyclopedia of mass spectrometry: Ionization methods* (Elsevier, Oxford; San Diego, 2007).

4. Schwartz, S. A., Reyzer, M. L., and Caprioli, R. M. Direct tissue analysis using matrix-assisted laser desorption/ionization mass spectrometry: Practical aspects of sample preparation. *J. Mass Spectrom.* **2003,** *38*, 699-708.

5. Karas, M. and Hillenkamp, F. Laser desorption ionization of proteins with molecular masses exceeding 10,000 daltons. *Anal. Chem.* **1988,** *60*, 2299-2301.

6. Tanaka, K., Waki, H., Ido, Y., Akita, S., Yoshida, Y., Yoshida, T., and Matsuo, T. Protein and polymer analyses up to m/z 100.000 by laser ionization time-of-flight mass spectrometry. *Rapid Commun. Mass Spectrom.* **1988,** *2*, 151-153.

7. Rohner, T. C., Staab, D., and Stoeckli, M. MALDI mass spectrometric imaging of biological tissue sections. *Mech. Ageing Dev.* **2005,** *126*, 177-185.

8. Li, Y., Shrestha, B., and Vertes, A. Atmospheric pressure molecular imaging by infrared MALDI mass spectrometry. *Anal. Chem.* **2007,** *79*, 523-532.

9. Taban, I. M., Altelaar, A. F., van der Burgt, Y. E., McDonnell, L. A., Heeren, R. M., Fuchser, J., and Baykut, G. Imaging of peptides in the rat brain using MALDI-fticr mass spectrometry. *J. Am. Soc. Mass Spectrom.* **2007,** *18*, 145-151.

10. Luxembourg, S. L., McDonnell, L. A., Mize, T. H., and Heeren, R. M. Infrared mass spectrometric imaging below the diffraction limit. *J. Proteome Res.* **2005,** *4*, 671-673.

11. Luxembourg, S. L., Mize, T. H., McDonnell, L. A., and Heeren, R. M. High-spatial resolution mass spectrometric imaging of peptide and protein distributions on a surface. *Anal. Chem.* **2004,** *76*, 5339-5344.

12. Garrett, T. J., Prieto-Conaway, M. C., Kovtoun, V., Bui, H., Izgarian, N., Stafford, G., and Yost, R. A. Imaging of small molecules in tissue sections with a new intermediate-pressure MALDI linear ion trap mass spectrometer. *Int. J. Mass Spectrom.* **2007,** *260*, 166-176.

13. Jurchen, J. C., Rubakhin, S. S., and Sweedler, J. V. MALDI-MS imaging of features smaller than the size of the laser beam. *J. Am. Soc. Mass Spectrom.* **2005,** *16*, 1654-1659.

14. Holle, A., Haase, A., Kayser, M., and Hohndorf, J. Optimizing uv laser focus profiles for improved MALDI performance. *J. Mass Spectrom.* **2006,** *41*, 705-716.

15. Berkenkamp, S., Karas, M., and Hillenkamp, F. Ice as a matrix for ir-matrix-assisted laser desorption/ionization: Mass spectra from a protein single crystal. *Proc. Natl. Acad. Sci. U.S.A.* **1996,** *93*, 7003-7007.

16. Leisner, A., Rohlfing, A., Berkenkamp, S., Hillenkamp, F., and Dreisewerd, K. Infrared laser post-ionization of large biomolecules from an IR-MALD(I) plume. *J. Am. Soc. Mass Spectrom.* **2004,** *15*, 934-941.

17. Menzel, C., Dreisewerd, K., Berkenkamp, S., and Hillenkamp, F. The role of the laser pulse duration in infrared matrix-assisted laser desorption/ionization mass spectrometry. *J. Am. Soc. Mass Spectrom.* **2002,** *13*, 975-984.

18. Rubakhin, S. S., Greenough, W. T., and Sweedler, J. V. Spatial profiling with MALDI MS: Distribution of neuropeptides within single neurons. *Anal. Chem.* **2003,** *75*, 5374-5380.

19. Spengler, B. and Hubert, M. Scanning microprobe matrix-assisted laser desorption ionization (SMALDI) mass spectrometry: Instrumentation for sub-micrometer resolved LDI and MALDI surface analysis. *J. Am. Soc. Mass Spectrom.* **2002,** *13*, 735-748.

20. Hsieh, Y., Casale, R., Fukuda, E., Chen, J., Knemeyer, I., Wingate, J., Morrison, R., and Korfmacher, W. Matrix-assisted laser desorption/ionization imaging mass spectrometry for direct measurement of clozapine in rat brain tissue. *Rapid Commun. Mass Spectrom.* **2006,** *20*, 965-972.

21. Cha, S. and Yeung, E. S. Colloidal graphite-assisted laser desorption/ionization mass spectrometry and msn of small molecules. 1. Imaging of cerebrosides directly from rat brain tissue. *Anal. Chem.* **2007,** *79*, 2373-2385.

22. Drexler, D. M., Garrett, T. J., Cantone, J. L., Diters, R. W., Mitroka, J. G., Prieto Conaway, M. C., Adams, S. P., Yost, R. A., and Sanders, M. Utility of imaging mass spectrometry (ims) by matrix-assisted laser desorption ionization (MALDI) on an ion trap mass spectrometer in the analysis of drugs and metabolites in biological tissues. *J. Pharmacol. Toxicol. Methods* **2007,** *55*, 279-288.

23. Han, J. and Schey, K. L. MALDI tissue imaging of ocular lens alpha-crystallin. *Invest. Ophthalmol. Vis. Sci.* **2006,** *47*, 2990-2996.

24. Honig, R. E. The development of secondary ion mass spectrometry (SIMS): A retrospective. *Int. J. Mass Spectrom.* **1985,** *66*, 31-54.

25. Szakal, C., Kozole, J., and Winograd, N. Fundamental studies of the cluster ion bombardment of water ice. *Appl. Surf. Sci.* **2006,** *252*, 6526-6528.

26. Debois, D., Brunelle, A., and Laprevote, O. Attempts for molecular depth profiling directly on a rat brain tissue section using fullerene and bismuth cluster ion beams. *Int. J. Mass Spectrom.* **2007,** *260*, 115-120.

27. Fletcher, J. S., Lockyer, N. P., Vaidyanathan, S., and Vickerman, J. C. TOF-SIMS 3D biomolecular imaging of *xenopus laevis* oocytes using buckminsterfullerene (c60) primary ions. *Anal. Chem.* **2007,** *79*, 2199-2206.

28. Gillen, G., Roberson, S., Ng, C., and Stranick, M. Elemental and molecular imaging of human hair using secondary ion mass spectrometry. *Scanning* **1999,** *21*, 173-181.

29. Lorey, D. R., 2nd, Morrison, G. H., and Chandra, S. Dynamic secondary ion mass spectrometry analysis of boron from boron neutron capture therapy drugs in co-cultures: Single-cell imaging of two different cell types within the same ion microscopy field of imaging. *Anal. Chem.* **2001,** *73*, 3947-3953.

30. Candy, J. M., Oakley, A. E., Mountfort, S. A., Taylor, G. A., Morris, C. M., Bishop, H. E., and Edwardson, J. A. The imaging and quantification of aluminium in the human brain using dynamic secondary ion mass spectrometry (SIMS). *Biol. Cell* **1992,** *74*, 109-118.

31. Schueler, B., Sander, P., and Reed, D. A. A time-of-flight secondary ion microscope. *Vacuum* **1990,** *41*, 1661-1664.

32. Altelaar, A. F., Klinkert, I., Jalink, K., de Lange, R. P., Adan, R. A., Heeren, R. M., and Piersma, S. R. Gold-enhanced biomolecular surface imaging of cells and tissue by SIMS and MALDI mass spectrometry. *Anal. Chem.* **2006,** *78*, 734-742.

33. Altelaar, A. F. M., Taban, I. M., McDonnell, L. A., Verhaert, P. D. E. M., de Lange, R. P. J., Adan, R. A. H., Mooi, W. J., Heeren, R. M. A., and Piersma, S. R. High-resolution MALDI imaging mass spectrometry allows localization of peptide distributions at cellular length scales in pituitary tissue sections. *Int. J. Mass Spectrom.* **2007,** *260*, 203-211.

34. McDonnell, L. A., Piersma, S. R., MaartenAltelaar, A. F., Mize, T. H., Luxembourg, S. L., Verhaert, P. D., van Minnen, J., and Heeren, R. M. Subcellular imaging mass spectrometry of brain tissue. *J. Mass Spectrom.* **2005,** *40*, 160-168.

35. Delcorte, A., Bour, J., Aubriet, F., Muller, J. F., and Bertrand, P. Sample metallization for performance improvement in desorption/ionization of kilodalton molecules: Quantitative evaluation, imaging secondary ion MS, and laser ablation. *Anal. Chem.* **2003,** *75*, 6875-6885.

36. Wittig, A., Wiemann, M., Fartmann, M., Kriegeskotte, C., Arlinghaus, H. F., Zierold, K., and Sauerwein, W. Preparation of cells cultured on silicon wafers for mass spectrometry analysis. *Microsc. Res. Tech.* **2005,** *66*, 248-258.

37. Roddy, T. P., Cannon, D. M., Jr., Meserole, C. A., Winograd, N., and Ewing, A. G. Imaging of freeze-fractured cells with *in situ* fluorescence and time-of-flight secondary ion mass spectrometry. *Anal. Chem.* **2002,** *74*, 4011-4019.

38. Takats, Z., Wiseman, J. M., and Cooks, R. G. Ambient mass spectrometry using desorption electrospray ionization (DESI): Instrumentation, mechanisms and applications in forensics, chemistry, and biology. *J. Mass Spectrom.* **2005,** *40*, 1261-1275.

39. Takats, Z., Nanita, S. C., Cooks, R. G., Schlosser, G., and Vekey, K. Amino acid clusters formed by sonic spray ionization. *Anal. Chem.* **2003,** *75*, 1514-1523.

40. Takats, Z., Wiseman, J. M., Gologan, B., and Cooks, R. G. Electrosonic spray ionization. A gentle technique for generating folded proteins and protein complexes in the gas phase and for studying ion-molecule reactions at atmospheric pressure. *Anal. Chem.* **2004,** *76*, 4050-4058.

41. Petyuk, V. A., Qian, W. J., Chin, M. H., Wang, H., Livesay, E. A., Monroe, M. E., Adkins, J. N., Jaitly, N., Anderson, D. J., Camp, D. G., 2nd, Smith, D. J., and Smith, R. D. Spatial mapping of protein abundances in the mouse brain by voxelation integrated with high-throughput liquid chromatography-mass spectrometry. *Genome Res.* **2007,** *17*, 328-336.

42. Ford, M. J. and Van Berkel, G. J. An improved thin-layer chromatography/mass spectrometry coupling using a surface sampling probe electrospray ion trap system. *Rapid Commun. Mass Spectrom.* **2004,** *18*, 1303-1309.

43. Ford, M. J., Kertesz, V., and Van Berkel, G. J. Thin-layer chromatography/electrospray ionization triple-quadrupole linear ion trap mass spectrometry system: Analysis of rhodamine dyes separated on reversed-phase c8 plates. *J. Mass Spectrom.* **2005,** *40*, 866-875.

44. Chaurand, P., Norris, J. L., Cornett, D. S., Mobley, J. A., and Caprioli, R. M. New developments in profiling and imaging of proteins from tissue sections by MALDI mass spectrometry. *J. Proteome Res.* **2006,** *5*, 2889-2900.

45. Borner, K., Malmberg, P., Mansson, J.-E., and Nygren, H. Molecular imaging of lipids in cells and tissues. *Int. J. Mass Spectrom.* **2007,** *260*, 128-136.

46. Lemaire, R., Wisztorski, M., Desmons, A., Tabet, J. C., Day, R., Salzet, M., and Fournier, I. MALDI-MS direct tissue analysis of proteins: Improving signal sensitivity using organic treatments. *Anal. Chem.* **2006,** *78*, 7145-7153.

47. Rubakhin, S. S., Churchill, J. D., Greenough, W. T., and Sweedler, J. V. Profiling signaling peptides in single mammalian cells using mass spectrometry. *Anal. Chem.* **2006,** *78*, 7267-7272.

48. Miao, H., Rubakhin, S. S., and Sweedler, J. V. Subcellular analysis of d-aspartate. *Anal. Chem.* **2005,** *77*, 7190-7194.

49. Ostrowski, S. G., Van Bell, C. T., Winograd, N., and Ewing, A. G. Mass spectrometric imaging of highly curved membranes during *tetrahymena* mating. *Science* **2004,** *305*, 71-73.

50. Parry, S. and Winograd, N. High-resolution TOF-SIMS imaging of eukaryotic cells preserved in a trehalose matrix. *Anal. Chem.* **2005,** *77*, 7950-7957.

51. Lemaire, R., Tabet, J. C., Ducoroy, P., Hendra, J. B., Salzet, M., and Fournier, I. Solid ionic matrixes for direct tissue analysis and MALDI imaging. *Anal. Chem.* **2006,** *78*, 809-819.

52. Chaurand, P., Schwartz, S. A., Reyzer, M. L., and Caprioli, R. M. Imaging mass spectrometry: Principles and potentials. *Toxicol. Pathol.* **2005,** *33*, 92-101.

53. Caldwell, R. L. and Caprioli, R. M. Tissue profiling by mass spectrometry: A review of methodology and applications. *Mol. Cell. Proteomics* **2005,** *4*, 394-401.

54. Stoeckli, M., Chaurand, P., Hallahan, D. E., and Caprioli, R. M. Imaging mass spectrometry: A new technology for the analysis of protein expression in mammalian tissues. *Nat. Med.* **2001,** *7*, 493-496.

55. Kruse, R. and Sweedler, J. V. Spatial profiling invertebrate ganglia using MALDI MS. *J. Am. Soc. Mass Spectrom.* **2003,** *14*, 752-759.

56. Aerni, H. R., Cornett, D. S., and Caprioli, R. M. Automated acoustic matrix deposition for MALDI sample preparation. *Anal. Chem.* **2006,** *78*, 827-834.

57. Cornett, D. S., Mobley, J. A., Dias, E. C., Andersson, M., Arteaga, C. L., Sanders, M. E., and Caprioli, R. M. A novel histology-directed strategy for MALDI-MS tissue profiling that improves throughput and cellular specificity in human breast cancer. *Mol. Cell. Proteomics* **2006,** *5*, 1975-1983.

58. Meistermann, H., Norris, J. L., Aerni, H. R., Cornett, D. S., Friedlein, A., Erskine, A. R., Augustin, A., De Vera Mudry, M. C., Ruepp, S., Suter, L., Langen, H., Caprioli, R. M., and Ducret, A. Biomarker discovery by imaging mass spectrometry: Transthyretin is a biomarker for gentamicin-induced nephrotoxicity in rat. *Mol. Cell. Proteomics* **2006,** *5*, 1876-1886.

59. Clerens, S., Ceuppens, R., and Arckens, L. Createtarget and analyze this!: New software assisting imaging mass spectrometry on bruker reflex IV and Ultraflex II instruments. *Rapid Commun. Mass Spectrom.* **2006,** *20*, 3061-3066.

60. Sugiura, Y., Shimma, S., and Setou, M. Two-step matrix application technique to improve ionization efficiency for matrix-assisted laser desorption/ionization in imaging mass spectrometry. *Anal. Chem.* **2006,** *78*, 8227-8235.

61. Monroe, E. B., Jurchen, J. C., Koszczuk, B. A., Losh, J. L., Rubakhin, S. S., and Sweedler, J. V. Massively parallel sample preparation for the MALDI MS analyses of tissues. *Anal. Chem.* **2006,** *78*, 6826-6832.

62. Monroe, E. B., Koszczuk, B. A., Losh, J. L., Jurchen, J. C., and Sweedler, J. V. Measuring salty samples without adducts with MALDI MS. *Int. J. Mass Spectrom.* **2007,** *260*, 237-242.

63. Delcorte, A. Matrix-enhanced secondary ion mass spectrometry: The alchemist's solution? *Appl. Surf. Sci.* **2006,** *252*, 6582-6587.

64. Chandra, S. and Morrison, G. H. Sample preparation of animal tissues and cell cultures for secondary ion mass spectrometry (SIMS) microscopy. *Biol. Cell* **1992,** *74*, 31-42.

65. Roddy, T. P., Cannon, D. M., Jr., Ostrowski, S. G., Winograd, N., and Ewing, A. G. Identification of cellular sections with imaging mass spectrometry following freeze fracture. *Anal. Chem.* **2002,** *74*, 4020-4026.

66. Roddy, T. P., Cannon, D. M., Jr., Ostrowski, S. G., Ewing, A. G., and Winograd, N. Proton transfer in time-of-flight secondary ion mass spectrometry studies of frozen-hydrated dipalmitoylphosphatidylcholine. *Anal. Chem.* **2003,** *75*, 4087-4094.

67. Nygren, H., Borner, K., Malmberg, P., Tallarek, E., and Hagenhoff, B. Imaging TOF-SIMS of rat kidney prepared by high-pressure freezing. *Microsc. Res. Tech.* **2005,** *68*, 329-334.

68. Nygren, H., Eriksson, C., Malmberg, P., Sahlin, H., Carlsson, L., Lausmaa, J., and Sjovall, P. A cell preparation method allowing subcellular localization of cholesterol and phosphocholine with imaging TOF-SIMS. *Colloids Surf. B Biointerfaces* **2003,** *30*, 87-92.

69. Sjovall, P., Lausmaa, J., Nygren, H., Carlsson, L., and Malmberg, P. Imaging of membrane lipids in single cells by imprint-imaging time-of-flight secondary ion mass spectrometry. *Anal. Chem.* **2003,** *75*, 3429-3434.

70. Nygren, H., Johansson, B. R., and Malmberg, P. Bioimaging TOF-SIMS of tissues by gold ion bombardment of a silver-coated thin section. *Microsc. Res. Tech.* **2004,** *65*, 282-286.

71. Wu, K. J. and Odom, R. W. Matrix-enhanced secondary ion mass spectrometry: A method for molecular analysis of solid surfaces. *Anal. Chem.* **1996,** *68*, 873-882.

72. Van Berkel, G. J., Ford, M. J., and Deibel, M. A. Thin-layer chromatography and mass spectrometry coupled using desorption electrospray ionization. *Anal. Chem.* **2005,** *77*, 1207-1215.

73. Wiseman, J. M., Ifa, D. R., Song, Q., and Cooks, R. G. Tissue imaging at atmospheric pressure using desorption electrospray ionization (DESI) mass spectrometry. *Angew Chem. Int. Ed. Engl.* **2006,** *45*, 7188-7192.

74. Ifa, D. R., Wiseman, J. M., Song, Q., and Cooks, R. G. Development of capabilities for imaging mass spectrometry under ambient conditions with desorption electrospray ionization (DESI). *Int. J. Mass Spectrom.* **2007,** *259*, 8-15.

75. Amaya, K. R., Monroe, E. B., Sweedler, J. V., and Clayton, D. F. Lipid imaging in the zebra finch brain with secondary ion mass spectrometry. *Int. J. Mass Spectrom.* **2007,** *260*, 121-127.

76. Stoeckli, M., Staab, D., Staufenbiel, M., Wiederhold, K. H., and Signor, L. Molecular imaging of amyloid beta peptides in mouse brain sections using mass spectrometry. *Anal. Biochem.* **2002,** *311*, 33-39.

77. Chaurand, P., Schwartz, S. A., Billheimer, D., Xu, B. J., Crecelius, A., and Caprioli, R. M. Integrating histology and imaging mass spectrometry. *Anal. Chem.* **2004,** *76*, 1145-1155.

78. Monroe, E. B., Jurchen, J. C., Lee, J., Rubakhin, S. S., and Sweedler, J. V. Vitamin e imaging and localization in the neuronal membrane. *J. Am. Chem. Soc.* **2005,** *127*, 12152-12153.

79. McCombie, G., Staab, D., Stoeckli, M., and Knochenmuss, R. Spatial and spectral correlations in MALDI mass spectrometry images by clustering and multivariate analysis. *Anal. Chem.* **2005,** *77*, 6118-6124.

80. Tyler, B. J., Rayal, G., and Castner, D. G. Multivariate analysis strategies for processing tof-SIMS images of biomaterials. *Biomaterials* **2007,** *28*, 2412-2423.

81. Ingram, J. C., Bauer, W. F., Lehman, R. M., O'Connell, S. P., and Shaw, A. D. Detection of fatty acids from intact microorganisms by molecular beam static secondary ion mass spectrometry. *J. Microbiol. Methods* **2003,** *53*, 295-307.

82. Johnson, M. D., Floyd, J. L., and Caprioli, R. M. Proteomics in diagnostic neuropathology. *J. Neuropathol. Exp. Neurol.* **2006,** *65*, 837-845.

83. Crecelius, A. C., Cornett, D. S., Caprioli, R. M., Williams, B., Dawant, B. M., and Bodenheimer, B. Three-dimensional visualization of protein expression in mouse brain structures using imaging mass spectrometry. *J. Am. Soc. Mass Spectrom.* **2005,** *16*, 1093-1099.

84. Verhaert, P. D., Conaway, M. C. P., Pekar, T. M., and Miller, K. Neuropeptide imaging on an LTQ with vMALDI source: The complete `all-in-one' peptidome analysis. *Int. J. Mass Spectrom.* **2007,** *260*, 177-184.

CHAPTER 3

ADAPTING THE STRETCHED SAMPLE METHOD FROM TISSUE PROFILING TO IMAGING

3.1 Notes and Acknowledgements

This chapter is reproduced from a publication in *Proteomics*, **2008**, *8*, 3809-3815 with permissions from Wiley-VCH Verlag GmbH & Co. KgaA, copyright 2008. The co-authors on this paper are Eric B. Monroe and Jonathan V. Sweedler. Support comes from the National Institutes of Health under Award No. DE018866, and the National Institute on Drug Abuse under Award No. DA017940 and No. DA018310 to the UIUC Neuroproteomics Center on Cell-Cell Signaling. Dr. Michael L. Heien and Kevin R. Tucker are acknowledged for valuable discussion and assistance.

3.2 Abstract

The characterization and localization of peptides and proteins in tissues provides information that aids in understanding function and in characterizing disease states. Over the past decades, the use of mass spectrometry for the profiling and imaging of biological compounds from tissues has evolved into a powerful modality to accomplish these studies. One recently described sampling approach, the stretched sample method,[1] places a tissue section onto an array of glass beads embedded on a Parafilm M membrane. When the membrane is stretched, it separates the tissue section into thousands of cell-sized pieces for tissue profiling by MALDI MS. The physical separation between beads eliminates analyte redistribution during matrix application and allows long analyte extraction periods without loss of spatial resolution. Here we enhance this sampling

approach by introducing algorithms that enable the reconstruction of ion images from these stretched samples. As the first step, a sample-tailored data acquisition method is devised to obtain mass spectra exclusively from the beads, thereby reducing the time, instrument resources, and data handling required for such MS imaging experiments. Next, an image reconstruction algorithm matches data acquired from the stretched sample to the initial bead locations. The efficacy of this method is demonstrated using peptide-coated beads with known peptide distributions and appears well-suited to the MS imaging of heterogeneous tissue samples.

3.3 Introduction

Mass spectrometry imaging (MSI) is a technique that collects hundreds to thousands of mass spectra to not only identify biochemicals in a tissue sample, but also the spatial distribution of these compounds across the tissue. MALDI MSI has been utilized in studies of the interactions of signaling molecules in neural tissue,[2-4] the effects and distribution of pharmacological agents within tissue sections,[5-8] and disease and cancer-related biomarkers.[9-11] MALDI MS is tailored for the study of biological compounds ranging from small molecules and peptides to proteins directly from tissues.[12] However, the extraction of analytes with the MALDI matrix contributes to analyte redistribution and often limits the spatial resolution of resulting ion images. Several recent studies have improved the spatial resolution of MALDI MSI by reducing the effective laser beam diameter[13, 14] and enhancing focusing optics.[15, 16] Other studies have focused on reducing analyte migration by applying the MALDI matrix via a nebulized spray coating,[17] automated acoustic deposition,[18] electrospray deposition,[19] or matrix seeding.[20] Often, a balance must be struck between sensitivity and spatial resolution—increased analyte extraction periods result in improved signals but lead to analyte redistribution and a reduction of spatial resolution.

To address this issue, our group developed the stretched sample method,[1] successfully decoupling extraction/matrix incorporation from the spatial resolution of an imaging experiment. Briefly, a tissue section is adhered to an array of glass beads that have been embedded onto a Parafilm M membrane. Upon manual stretching, the tissue is rapidly separated into thousands of cell-sized fragments for study with MALDI MS. The physical separation between the beads, combined with the hydrophobic nature of the Parafilm M surface, eliminates analyte spreading during matrix application, even following extended periods of matrix extraction. Longer extraction periods also reduce the presence of cationic salt adducts.[21] Although this method is well-suited to the mass spectral profiling of tissue sections, sample stretching is inherently a non-uniform process and complicates the production of ion images. Here we describe computational methods to obtain mass spectra solely from the individual bead substrates, rather than from a predefined raster pattern, and reconstruct ion images from samples following stretching.

In traditional MALDI MSI experiments, mass spectra are obtained in a regular raster pattern of evenly spaced locations across the tissue via the creation of a virtual target plate.[22] However, with the ~100-μm, yet uneven, separation between samples in the stretched sample method, a raster pattern generates extraneous data and instrument usage by also sampling the empty Parafilm M substrate. In this new approach, we take optical images of the membrane both before and after stretching and automatically determine the location of each bead. Using the data obtained, we create geometry files for input into the mass spectrometer as a sample-specific data acquisition strategy for imaging the stretched samples.

The effort to evenly stretch the membrane spreads the beads out in the x and y dimensions roughly uniformly. However, because Parafilm M stretching is not exact and distortions occur, a one-to-one mapping of the initial and final bead positions is made difficult. Yet, in order to adapt the stretched sample methodology to imaging, the final bead positions must be related to their corresponding initial positions. This is accomplished using a simple free transform mechanism[23, 24] that closely mimics the actual stretching process, wherein the height, width, rotation, and position of an image are altered. Computational methods are also needed to calculate how the free transform process affects the positions of individual bead samples and to produce selected ion images. Using these algorithms, the image reconstruction methodology relates the MS spectra to their corresponding initial bead locations. We demonstrate this technique by using a sample of peptide-coated beads of known chemical distribution to mimic cells in a tissue sample.

3.4 Materials and Methods

3.4.1 Preparing Peptide-Coated Bead Substrates

Separate 115-µL solutions of 300 µM of angiotensin I or angiotensin II (both from Sigma-Aldrich, St. Louis, MO) were prepared in deionized water. The angiotensin I solution was added to approximately 100 mg of ~40-µm diameter clear glass beads (Mo-Sci Corporation, Rolla, MO) and the angiotensin II solution was added to a similar amount of ~40-µm diameter colored beads (Mo-Sci Corporation). The samples were shaken for 30 min and allowed to incubate overnight before removing the liquid by vacuum drying to ensure the adsorption of the peptides to the beads.

The beads were affixed to the Parafilm M (Pechiney, Neenah, WI) substrate similar to the means previously reported.[1] To isolate a small sample area, however, a 5-mm diameter mask was used during bead application, with this smaller area used to simplify the validation process. The mask was then removed and the beads affixed to the Parafilm M via the application of vertical pressure to glass slides placed over the substrate.[1]

3.4.2 Locating Bead Positions

On an initial transmission mode optical microscopic image of the sample, the coordinates of the bead positions were identified by using a color thresholding plugin[25] (http://www.dentistry.bham.ac.uk/landinig/software/software.html) for ImageJ, version 1.38 (developed at the U.S. National Institutes of Health and available on the Internet at http://rsb.info.nih.gov/ij/). This threshold allows for elimination of non-specific highlights of the background Parafilm M substrate, while selecting only bead regions. The “analyze particles” command was then used to report the x-y coordinates of the beads, with a circularity parameter of 0.6 to further exclude non-bead artifacts.

Next, the Parafilm M substrate was stretched, the stretched sample affixed to a glass slide, and a second transmission optical image taken. Often, the size of the stretched sample exceeded the available field of the microscope; in such cases, several overlapping images were stitched together using the Photomerge function of Photoshop CS, version

8.0 (Adobe Systems Inc., San Jose, CA). Thresholding and bead identification for the final stretched sample image was performed in the same manner as for the initial image.

3.4.3 Creating Custom Geometry Files

In order to selectively acquire mass spectra from individual beads in an automated manner, sample-tailored geometry files (for the mass spectrometer software controlling MS image acquisition) were created from the final bead locations, collected as described above. Optical images were calibrated by imaging a 1-mm calibration bar at the same magnification as the stretched sample image to calculate the pixel spacing of the sample image. This spacing was used to calculate the fractional distance (fraction of the distance from the origin at the center of the glass slide to the edge of the slide)[22] used by the Bruker (Bruker Daltonics, Billerica, MA) geometry file format (1 fractional distance ~ 50.8 mm).

A custom computer code was written in the Java programming language, version JDK 1.6.0 (http://java.sun.com), to perform the conversion of pixel x-y bead coordinates into the fractional distance coordinate system and to create new .xeo Bruker geometry files. This code accounts for differences in rotation angle between the stretched sample image and the orientation of the glass slide in the slide adapter, and is available at http://neuroproteomics.scs.uiuc.edu/imaging.html.

The code uses the manual linking of known points between the sample as it is observed within the instrument control software and the pixel coordinates of the optical image. These points of reference serve to connect the two coordinate systems. The use of several (2–4) calibration points greatly improves the fidelity of the created target file.

This matching procedure was performed prior to MALDI matrix application and special care was taken to ensure that the slide was in a constant position during the geometry file creation process. Following matrix application, the slide must be placed in the same position within the slide adapter.

3.4.4 MALDI MS Preparation and Analysis

Subsequent to creation of the geometry file, the sample was coated with a matrix solution of 30 mg/mL of 2,5-dihydroxybenzoic acid (Sigma-Aldrich, St. Louis, MO) in 75/25 acetone:water by use of a commercial airbrush (Badger, Franklin Park, IL) at a distance of ~15 cm. Following matrix application, recondensation procedures were applied as previously described to further increase analyte incorporation into the MALDI matrix.[1]

Mass spectra were collected in positive ion mode on an Ultraflex II ToF-ToF MS (Bruker Daltonics) with a solid-state UV laser and an accelerating voltage of +25 kV. Using the AutoXecute function in FlexControl 3.0 (Bruker Daltonics), the sample-tailored geometry file was read and mass spectra accumulated from each bead location from 100 laser shots at 50 Hz. It takes approximately 8 min to acquire data from 100 beads.

Collected mass spectra were converted into text files for reading by the in-house image reconstruction code using the batch conversion command in CompassXport (Bruker Daltonics) to produce mzXML files that were further converted into text files using MATLAB, version 7.2 (R2006a) (The MathWorks, Natick, MA) with the mzxmlread.m function from the Bioinformatics Toolbox 3.0, along with an in-house-written batch conversion wrapper code. The MATLAB wrapper code is freely available at http://neuroproteomics.scs.uiuc.edu/imaging.html.

3.4.5 Image Reconstruction

To perform image reconstruction, the Free Transform command in Photoshop CS is used to adjust the translation, height, width, and rotation of the image of the initial bead locations. Both the initial and stretched sample images are loaded as separate layers into a blank Photoshop CS file. By aligning the initial position image on top of the stretched sample image, the initial position image layer is manually transformed to match the dimensions of the stretched sample image layer. The Info palette reports the changes in the free transform parameters of the initial image, which are used as inputs to calculate the effect of the free transform on the position of each bead. By overlaying the two images in the same plane, the bead positions between the stretched sample image and transformed initial image can be matched based on closest spatial proximity with the Cartesian distance formula using the custom written code. To reduce matching errors during image reconstruction, if more than one stretched position is matched to a single initial position, the algorithm reassigns one of the positions to the next-nearest initial position in an iterative fashion.

The image reconstruction is validated by determining the number of bead position matches that are correct between the initial and final configurations. First, an array of true matches is manually created for each bead with the aid of a custom macro in ImageJ. Then the classification rate is generated by comparing this array of “true” matches to the array of matches created by the image reconstruction algorithm.

3.5 Results and Discussion

3.5.1 Sample-Tailored Data Acquisition

After preparing the bead substrate, the subsequent workflow for the stretched sample imaging method is outlined in Figure 3.1. Optical images of the sample before and after stretching are taken in a transmission mode, wherein the beads appear brighter than the Parafilm M substrate. The color thresholding plugin is used with ImageJ, which allows for greater control of thresholding parameters than the original ImageJ thresholding algorithm, to exclusively find the bead positions (see the initial sample image in Figure 3.2).

Following thresholding and bead location identification, the coordinates from the sample images are used to create sample-tailored geometry files. By manually directing the sample stage to a position on the slide that is located within the area of the sample, that position and its fractional distance coordinates can be recorded and matched with the pixel coordinates of the same position in the stretched sample image. To create a sample-tailored geometry file, the translation between these common points and the scaling between the two coordinate systems are used to calculate the coordinates of the individual beads. After the geometry file is created, selected sample positions are checked in FlexControl to ensure that the probe has located the position of each bead at a point that is within its 40-μm diameter region. In practice, the geometry files show a high level of accuracy in locating the beads. Automatically acquired mass spectra produced appreciable peptide signals from each bead without any apparent collection of mass spectra from the Parafilm M substrate.

Acquiring data in a sample-tailored fashion from the stretched samples saves time and instrument resources, and eases data handling. In the traditional method of obtaining imaging data via a regular raster, the total analysis time depends on the number of locations interrogated, the laser repetition rate, and the number of laser shots acquired at each spot. For example, a 1-mm^2 area of intact tissue requires ~600 beads and after stretching ~4-fold in each direction, results in a 16-mm^2 area. To collect mass spectra from the stretched sample, and assuming a 4-sec collection period (100 shots @ 50 Hz and 2 sec for stage motion, *etc.*) at each spot, a 50-μm raster to ensure that each bead location is interrogated would require 6400 spots, or >7 hours to collect. In contrast, using the sample-tailored acquisition strategy to interrogate the same stretched sample, requires only 600 spots and is completed in ~1 hour. The time savings does not scale linearly with the reduction in the number of spots due, in large part, to the increased distance the sample stage must move between consecutive collections. Regardless, not only are 580,000 laser shots saved over the course of the data acquisition process, but data handling is greatly simplified by eliminating the collection of extraneous information produced by collecting mass spectra from the Parafilm M substrate alone or from only a portion of a bead that might fall on the edge of the laser beam profile when sampled in a raster pattern.

3.5.2 Image Reconstruction

As described in the materials and methods section, during the reconstruction process an image of the initial bead positions is transformed and overlaid on top of the stretched sample image. Each bead makes a circular indentation in the membrane that is enlarged during the stretching process; thus, compared to the initial microphotograph, the free transformation procedure increases the apparent size of the beads in the initial sample image, complicating the overlay process (see part C of Figure 3.1). Following the bead position identification process, an image containing the small marks at the initial bead positions is created by our in-house written Java code. The bead indentations in the stretched sample image serve as guides and margins of error during the alignment process; the small bead markers align randomly within the indentation regions as shown in Figure 3.3. The position, height, width, and rotation angle of the initial positions image is recorded before and after alignment.

The Java code performs image reconstruction using the free transform parameters as inputs to link the bead locations, and handles the mass spectra for the creation of ion images. During image reconstruction, the positions are translated between the difference in the starting and final position of the initial positions image. Next, the predicted positions in the free transformed image are calculated using the trigonometric rotation functions. The individual positions are rotated by angle of rotation of the transformed image using Eq. 3.1.

$$\begin{aligned} x' &= x\cos\theta - y\sin\theta \\ y' &= x\sin\theta + y\cos\theta \end{aligned} \tag{3.1}$$

As the changes in height and width must be applied along the axis of rotation, the coordinate system is rotated to match this rotation using Eq. 2.

$$\begin{aligned} x' &= x\cos\theta + y\sin\theta \\ y' &= -x\sin\theta + y\cos\theta \end{aligned} \tag{3.2}$$

The rotation of the coordinate system allows the dimensions to be changed with a simple multiplication operation. Hence, the x-coordinate of each position is multiplied by the fractional change in width of the image. Likewise, the y-coordinate is multiplied by the fractional change in height. The final bead coordinates must then be rotated to match the axes of the coordinate system defined on the MALDI target by rotating the rotated coordinate system to match the x and y axes of the target plate at zero degrees using Eq. 3.2. This gives the calculated free transformed coordinates which, if plotted for verification purposes, should overlap with the transformed initial positions image. Each stretched sample position and its associated mass spectrum are matched to the transformed position that is closest in distance. Matching error occurs when two stretched sample positions are matched to the same transformed initial position. To reduce error, of the two stretched positions, the one that is nearer to the closest previously unassigned transformed initial position is reassigned to that unassigned position. Finally, the transformed initial positions are associated with mass spectra taken from the nearest stretched positions and are replaced with the corresponding initial positions.

To create ion images, the intensity of a selected signal, defined as the local maximum within a selected *m/z* range of the selected value, is plotted for each individual bead location in a false color scale corresponding to the signal intensity. In addition, when prompted, the classification rate of the automated reconstruction is calculated when a manual validation array of image reconstruction matches is present. This image reconstruction code is freely available at:

http://neuroproteomics.scs.uiuc.edu/imaging.html.

Although robust in terms of locating bead locations for a range of stretched samples, it is useful to perform the image reconstruction with the optical sample images prior to data acquisition in order to ensure that successful image reconstruction is possible. Generally, the free transform process is successful and rapid. Complications signify a problem in the stretching or substrate preparation such as large deviations from linear stretching, beads missing in a region, or a torn membrane. These samples are discarded prior to matrix application and mass spectra acquisition. The alignment process may be aided by the addition of a small percentage of colored beads to the substrate such that the resulting visual patterns can help to identify the rotational orientation of the sample before and after stretching.

The reproducibility and efficacy of the reconstruction methodology was investigated using the validation strategy detailed below. Six samples, containing between 129–139 beads each, were correctly classified at a 84.1 ± 6.4% rate. Most of the misclassifications resulted from nearest-neighbor or near-neighbor misassignments. The presence of multiple beads within a region of Parafilm M that was originally presumed to be an individual bead and localized "clumping" of 2–3 beads at the junction between several circular indentations results in the majority of the misclassification events. Because these are not common and only cause nearest-neighbor misassignments, these do not adversely affect the analyses as a whole.

3.5.3 Imaging a Stretched Sample of Peptide Standards

Reconstructed ion images of the angiotensin-coated bead sample containing 230 total beads are shown in Figure 3.4. Clear glass beads were coated with angiotensin I (Figure 3.4A), and the colored beads with angiotensin II (Figure 3.4B). The ion images closely correspond to the observed initial arrangement of the beads, as shown in Figure 3.2A. Owing to the desire to restrict the sample size for this trial illustration, the sample substrate is not entirely comprised of closest-packed beads, although such packing is otherwise readily achievable for larger substrates as would be used for tissue experiments. The large physical separation between beads in the stretched sample allows for single bead resolution and the production of ion images with a high degree of uniformity. In relation to tissue section analyses, this bead separation allows for the detection of rare signals that may arise from a single or small number of cells to be more accurately located when localized to a single or small number of individual beads. The spatial resolution in these images approximates 40 µm, the diameter of the individual beads. Although this value is appropriate for most tissue imaging applications, higher spatial resolution can be obtained by using smaller diameter beads.

3.6 Conclusion

Through the development of sample-tailored data acquisition and image reconstruction algorithms, the stretched sample method has been adapted from profiling to allow imaging as well. Using sample-tailored data acquisition significantly reduces analysis time by reducing the number of mass spectra that must be obtained, thus greatly easing data handling. The advantages of the stretched imaging method are particularly well-suited to the study of small and heterogeneous structures present throughout the nervous system. In addition, the parallel detection of isolated bead-sized samples may enable the detection of rare-cellular events or processes, where the origin of rare signals is isolated to the location of individual beads. Future work will both validate these approaches using thin tissue sections and compare the stretched sample approach to more traditional direct tissue mass spectrometric imaging.

3.7 Figures

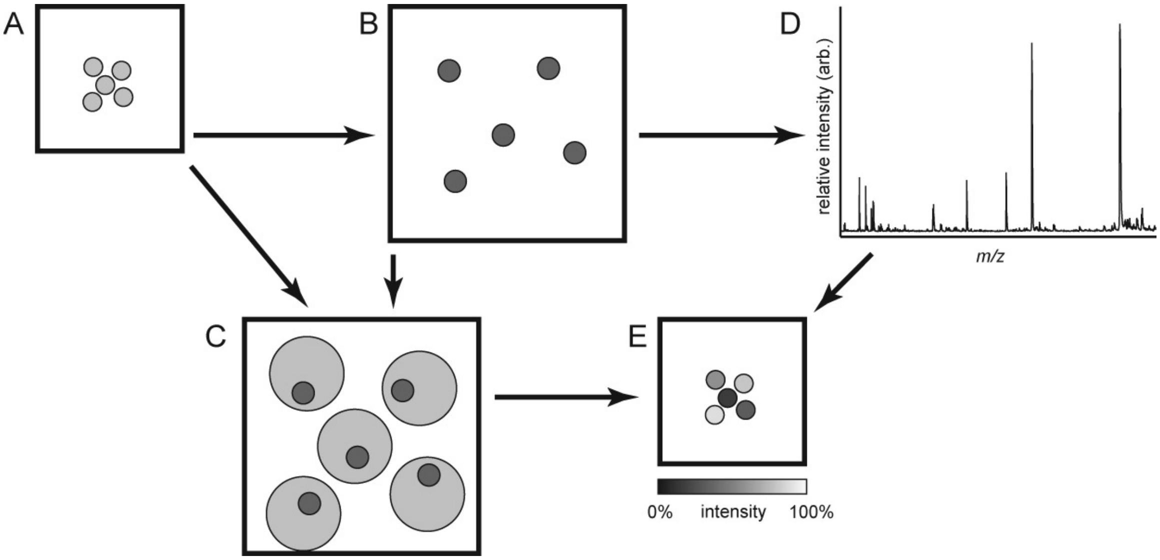

Figure 3.1. Schematic of the image reconstruction process. (A) Substrates are prepared and an optical image is taken prior to (B) stretching, after which another image is collected. Bead positions are identified from both images and a sample-specific geometry file is created from the stretched sample image. (C) Bead positions from each image are linked though a free transformation and computational algorithm. (D) Mass spectra are collected from each bead position from the stretched sample and combined with the linked bead position information to (E) create ion images by plotting selected signals from the mass spectra in false color at the initial bead locations.

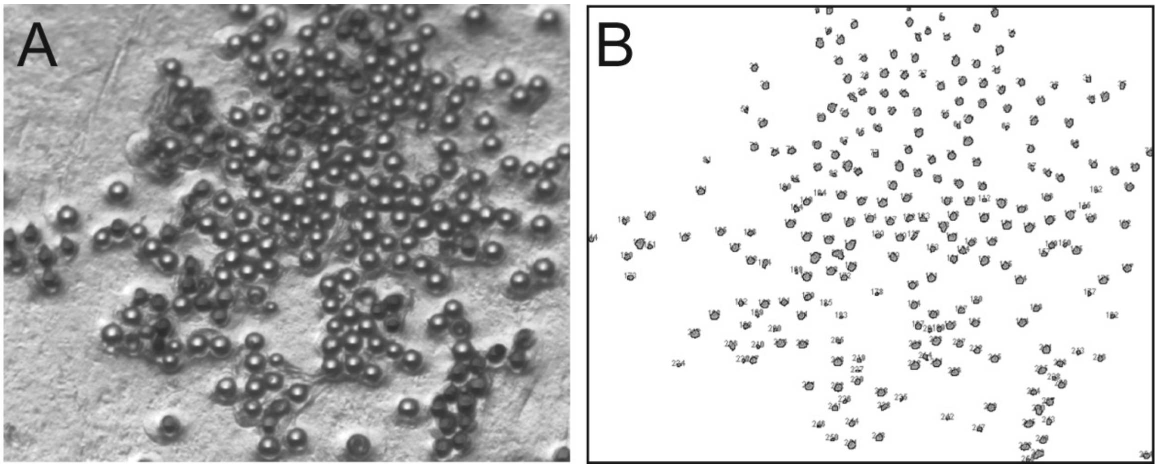

Figure 3.2. Automated bead identification. (A) A microphotograph of the prepared substrate is used to (B) automatically determine the bead locations. The automated process outputs a list of positions as well as an image that numbers and marks each bead position.

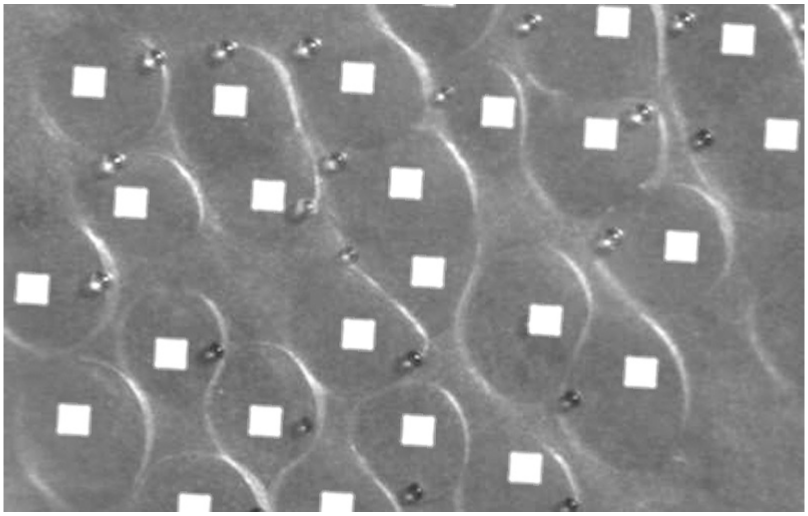

Figure 3.3. Overlay of free-transformed initial positions (white squares) with an optical image of the stretched sample. The indentations due to the partial embedding of the beads into the Parafilm M surface are visible and greatly aid in the alignment process. As individual beads may end up anywhere within the indented regions, the free transform aims to place positions in the middle of the deformed regions.

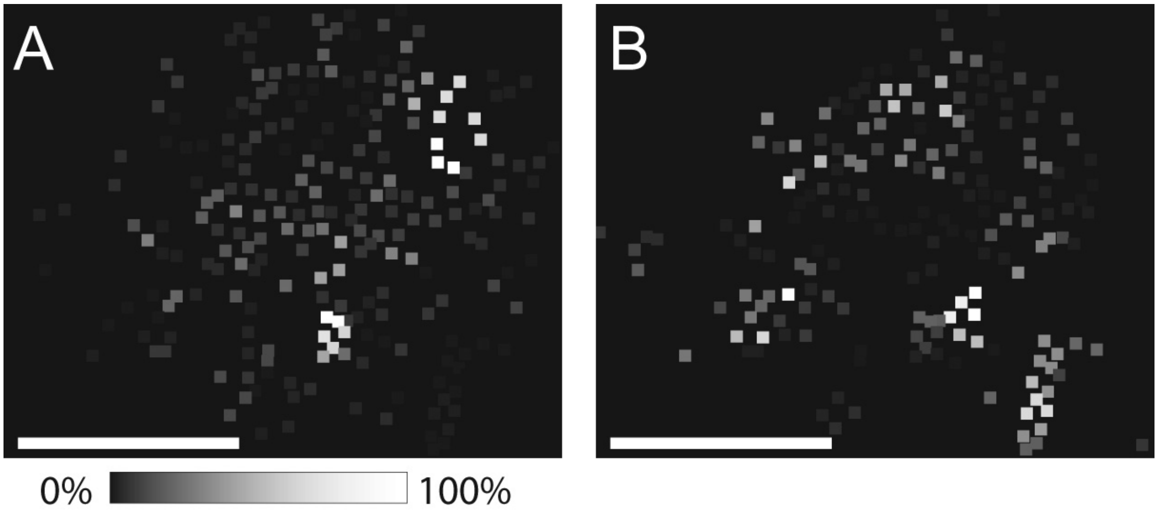

Figure 3.4. Reconstructed ion images from labeled bead substrates. Ion images for (A) angiotensin I and (B) angiotensin II correspond well with the expected results as clear beads were labeled with angiotensin I while angiotensin II was adsorbed to colored beads. Scale bars = 500 μm.

3.8 References

1. Monroe, E. B., Jurchen, J. C., Koszczuk, B. A., Losh, J. L., Rubakhin, S. S., and Sweedler, J. V. Massively parallel sample preparation for the MALDI MS analyses of tissues. *Anal. Chem.* **2006,** *78*, 6826-6832.

2. Rubakhin, S. S., Hatcher, N. G., Monroe, E. B., Heien, M. L., and Sweedler, J. V. Mass spectrometric imaging of the nervous system. *Curr. Pharma. Design* **2007,** *13*, 3325-3334.

3. DeKeyser, S. S., Kutz-Naber, K. K., Schmidt, J. J., Barrett-Wilt, G. A., and Li, L. Imaging mass spectrometry of neuropeptides in decapod crustacean neuronal tissues. *J. Proteome Res.* **2007,** *6*, 1782-1791.

4. Stoeckli, M., Staab, D., Staufenbiel, M., Wiederhold, K. H., and Signor, L. Molecular imaging of amyloid beta peptides in mouse brain sections using mass spectrometry. *Anal. Biochem.* **2002,** *311*, 33-39.

5. Hsieh, Y., Casale, R., Fukuda, E., Chen, J., Knemeyer, I., Wingate, J., Morrison, R., and Korfmacher, W. Matrix-assisted laser desorption/ionization imaging mass spectrometry for direct measurement of clozapine in rate brain tissue. *Rapid Commun. Mass Spectrom.* **2006,** *20*, 965-972.

6. Meistermann, H., Norris, J. L., Aerni, H. R., Cornett, D. S., Friedlein, A., Erskine, A. R., Augustin, A., De Vera Mudry, M. C., Ruepp, S., Suter, L., Langen, H., Caprioli, R. M., and Ducret, A. Biomarker discovery by imaging mass spectrometry: Transthyretin is a biomarker for gentamicin-induced nephrotoxicity in rat. *Mol. Cell.* **2006,** *5*, 1876-1886.

7. Khatib-Shahidi, S., Andersson, M., Herman, J. L., Gillespie, T. A., and Caprioli, R. M. Direct molecular analysis of whole-body animal tissue sections by imaging MALDI mass spectrometry. *Anal. Chem.* **2006,** *78*, 6448-6456.

8. Hsieh, Y., Chen, J., and Korfmacher, W. A. Mapping pharmaceuticals in tissues using MALDI imaging mass spectrometry. *Pharmacol. Toxicol. Methods* **2007,** *55*, 193-200.

9. Lemaire, R., Menguellet, S. A., Stauber, J., Marchaudon, V., Lucot, J.-P., Collinet, P., Farine, M.-O., Vinatier, D., Day, R., Ducoroy, P., Salzet, M., and Fournier, I. Specific MALDI imaging and profiling for biomarker hunting and validation: Fragment of the 11s proteasome activator complex, reg alpha fragment, is a new potential ovary cancer biomarker. *J. Proteome Res.* **2007,** *6*, 4127-4134.

10. Johnson, M. D., Floyd, J. L., and Caprioli, R. M. Proteomics in diagnostic neuropathology. *J. Neuropathol. Exp. Neurol.* **2006,** *65*, 837-845.

11. Stauber, J., Lemaire, R., Franck, J., Bonnel, D., Croix, D., Day, R., Wisztorski, M., Fournier, I., and Salzet, M. MALDI imaging of formalin-fixed paraffin-embedded tissues: Application to model animals of parkinson disease for biomarker hunting. *J. Proteome Res.* **2008,** *7*, 969-978.

12. Rubakhin, S. S., Jurchen, J. C., Monroe, E. B., and Sweedler, J. V. Imaging mass spectrometry: Fundamentals and applications to drug discovery. *Drug Discov. Today* **2005,** *10*, 823-837.

13. Jurchen, J. C., Rubakhin, S. S., and Sweedler, J. V. MALDI-MS imaging of features smaller than the size of the laser beam. *J. Am. Soc. Mass Spectrom.* **2005,** *16*, 1654-1659.

14. Spengler, B. and Hubert, M. Scanning microprobe matrix-assisted laser desorption ionization (SMALDI) mass spectrometry: Instrumentation for sub-micrometer resolved LDI and MALDI surface analysis. *J. Am. Soc. Mass Spectrom.* **2002,** *13*, 735-748.

15. Luxembourg, S. L., Mize, T. H., McDonnell, L. A., and Heeren, R. M. High-spatial resolution mass spectrometric imaging of peptide and protein distributions on a surface. *Anal. Chem.* **2004,** *76*, 5339-5344.

16. Luxembourg, S. L., Vaezaddeh, A. R., Amstalden, E. R., Zimmermann-Ivol, C. G., Hochstrasser, D. F., and Heeren, R. M. A. The molecular scanner in microscope mode. *Rapid Commun. Mass Spectrom.* **2006,** *20*, 3435-3442.

17. Chaurand, P., Norris, J. L., Cornett, D. S., Mobley, J. A., and Caprioli, R. M. New developments in profiling and imaging of proteins from tissue sections by MALDI mass spectrometry. *J. Proteome Res.* **2006,** *5*, 2889-2900.

18. Aerni, H. R., Cornett, D. S., and Caprioli, R. M. Automated acoustic matrix deposition for MALDI sample preparation. *Anal. Chem.* **2006,** *78*, 827-834.

19. Kruse, R. and Sweedler, J. V. Spatial profiling invertebrate ganglia using MALDI MS. *Am. Soc. Mass Spectrom.* **2003,** *14*, 752-759.

20. Chaurand, P., Schwartz, S. A., Reyzer, M. L., and Caprioli, R. M. Imaging mass spectrometry: Principles and potentials. *Toxicol. Pathol.* **2005,** *33*, 92-101.

21. Monroe, E. B., Koszczuk, B. A., Losh, J. L., Jurchen, J. C., and Sweedler, J. V. Measuring salty samples without adducts with MALDI MS. *Int. J. Mass Spectrom.* **2007,** *260*, 237-242.

22. Clerens, S., Ceuppens, R., and Arckens, L. Createtarget and analyze this!: New software assisting imaging mass spectrometry on bruker reflex IV and Ultraflex II instruments. *Rapid Commun. Mass Spectrom.* **2006,** *20*, 3061-3066.

23. Decker, J. D. Image editing. *Am. J. Orthod. Dentofacial Orthop.* **2004,** *125*, 215-219.

24. Hackel, R. E. and Saine, P. J. Creating retinal fundus maps. *J. Opthalmic Photog.* **2005,** *27*, 10-18.

25. Papadopulous, F., Spinelli, M., Valente, S., Foroni, L., Orrico, C., Alviano, F., and Pasquinelli, G. Common tasks in microscopic and ultrastructural image analysis in imagej. *Ultrastruct. Pathol.* **2007,** *31*, 401-407.

CHAPTER 4

MALDI MASS SPECTROMETRIC IMAGING USING THE STRETCHED SAMPLE METHOD TO REVEAL NEUROPEPTIDE DISTRIBUTIONS IN *APLYSIA* NERVOUS TISSUE

4.1 Notes and Acknowledgements

This chapter is reproduced from *Anal. Chem.*, **2009,** *81,* 9402-9409 with permissions from the American Chemical Society, copyright 2009. The co-authors on this paper are Stanislav S. Rubakhin, Elena V. Romanova, Kevin R. Tucker, and Jonathan V. Sweedler. The authors would like to thank Scott J. Robinson and Eric B. Monroe for valuable discussions and assistance. The project described was supported by Award No. DE018866 from the National Institute of Dental and Craniofacial Research (NIDCR) and the Office of Director, National Institutes of Health (NIH), and the National Institute on Drug Abuse under Award Nos. DA017940 and P30DA018310.

4.2 Abstract

Neuropeptides are a diverse set of complex cell-cell signaling molecules that modulate behavior, learning and memory. Their spatially heterogeneous distributions, large number of post-translational modifications, and wide range of physiologically active concentrations make their characterization challenging. Matrix-assisted laser desorption/ionization (MALDI) mass spectrometric imaging is well-suited to characterizing and mapping neuropeptides in the central nervous system. Because matrix application can cause peptide migration within tissue samples, application parameters for MALDI typically represent a compromise between attaining the highest signal quality

and preserving native spatial distributions. The stretched sample approach minimizes this tradeoff by fragmenting the tissue section into thousands of spatially isolated islands, each ~40 microns in size. This inhibits analyte migration between the pieces and, at the same time, reduces analyte-salt adduct formation. Here we present methodological improvements that enable the imaging of stretched tissues and reveal neuropeptide distributions in nervous tissue from *Aplysia californica*. The distributions of known neuropeptides are shown to correspond with previous immunohistochemical results, demonstrating that the stretched imaging method is well-suited for working with easily redistributed molecules and heterogeneous tissues, and reduces adducts from physiological salts.

4.3 Introduction

In contrast to many imaging methods, using mass spectrometry (MS) to image thin tissue sections allows acquisition of both chemical and spatial information without the need to preselect the analyte of interest. Matrix-assisted laser desorption/ionization (MALDI), a soft ionization technique, is suitable for mass spectrometric imaging (MSI) due to its high sensitivity and ease of interpretation; most peptides and proteins are ionized as intact molecular ions. Although tandem MS may be used to discover the sequences of unknown analytes, the high specificity of MS is often sufficient to identify analytes directly by mass matching in specific tissues where the identities of many analytes have already been determined.[1, 2] MALDI-MSI has been used to identify and map analytes in neuronal samples[3] containing diverse classes of lipids,[4] signaling peptides,[5] hormones,[6] and alternatively spliced forms of proteins.[7] Recently, such studies have revealed the distinct localizations of several neuropeptides in the white and gray matter of rat spinal cord,[8] allowed classification of tumorous gastric tissue from human patients,[9] and produced two- and three-dimensional molecular ion maps of neuropeptide distributions in the Jonah crab brain.[10]

Compared to their mammalian counterparts, invertebrate models such as *Aplysia californica* have morphologically simpler nervous systems, enabling a more refined focus on the mechanisms of neural plasticity underlying learning, memory, and complex behaviors.[11, 12] In addition, the peptide content of many of the large, reliably identifiable *Aplysia* neurons has been characterized,[2, 13, 14] facilitating validation of the results of MSI experiments. Nonetheless, despite the relative structural simplicity as compared to the mammalian central nervous system (CNS), *Aplysia* CNS tissue samples are biochemically complex and present a number of analytical measurement challenges. For example, the abdominal ganglion has numerous areas where adjacent peptidergic neurons contain unique sets of peptides expressed in varying amounts.[14, 15] Furthermore, the low amounts of some neuropeptides and/or peptides expressed only in a few neurons can be difficult to measure by MS for large tissue areas or for a whole tissue homogenate, especially in the presence of more abundant peptides.[16] Thus, MSI of neuronal samples requires both low detection limits and high spatial resolution.

It is during the matrix application step in traditional MALDI-MSI experiments that meeting these two prerequisites often involves a compromise. Although longer exposure of the sample to MALDI matrix improves peptide signals by allowing better analyte extraction and incorporation into the matrix, it reduces the quality of the resulting MS imaging by allowing analyte redistribution in tissue wetted by the matrix solution.[15,

[17] The formation of large matrix crystals over the area containing multiple cells also occurs, preventing more detailed localization than the size of individual matrix crystals. While spatial resolution can be improved by instrumentation advances such as enhanced ion optics, the improvement is often limited to smaller sample areas.[18] Furthermore, limitations resulting from sample preparation and matrix application are not addressed by enhancements to instrumentation. Several approaches that add matrix to tissues using sprayers and droplet generators can address several of these issues,[19-21] but the compromises mentioned above still remain.

With the stretched sample method,[15, 22] we have eliminated the signal and spatial resolution tradeoff issue in imaging experiments. A thin tissue slice is placed on a monolayer of beads embedded in a stretchable membrane. The membrane is then stretched, fragmenting the tissue into thousands of nearly single cell-sized pieces that strongly adhere to each bead. After stretching, the spatial separation of the beads/tissue pieces by the intervening hydrophobic membrane allows longer matrix application periods, thereby preventing analyte redistribution between beads. Providing additional benefit, multiple slow solvent condensation and recrystallization steps reduce relative signal intensities of inorganic ion adducts in the resulting spectra, even in the presence of high physiological salts.[23] Recent findings[24, 25] demonstrate that use of the Parafilm M membrane in MALDI-MS experiments as a surface for analyte deposition and detection can result in increased sensitivity of neuropeptide detection while appropriate membrane treatments significantly increase membrane stretchability.

However, the stretched sample approach can be hampered by nonuniform stretching of the membrane, so that reconstruction of ion images at the original bead positions is not a straightforward process. Thus, prior reports have focused on tissue profiling and the imaging capabilities of this sample preparation approach have yet to be validated. In contrast to standard tissue imaging, the bead locations are not in an ordered array. To achieve tissue imaging, the stretched sample approach has recently been adapted to include computational methods that realign the positions of the molecular ion signals acquired from stretched samples with their locations in the original intact tissue sections.[22] These reconstructed ion images from stretched samples can then be co-registered with the original sample morphology. Also, a recent enhancement in image acquisition speed is accomplished via automated data acquisition—at the individual bead locations—using sample-tailored geometry files to determine at what locations to acquire spectra. This suite of computational methods[22] has been applied to profile small numbers of peptide-coated beads.

Here we further refine and optimize the stretched imaging method to enable MALDI-MSI of thin tissue sections from the *Aplysia* CNS. Several computational and experimental improvements are made that now allow imaging of stretched biological tissues. We have developed new protocols and applied them to MS imaging of the *Aplysia* ganglia. Importantly, the peptide content of numerous cell populations in the abdominal ganglion has been characterized by traditional molecular biology and immunohistochemical approaches, providing validation of the MS imaging results. Although two other ganglia used in this study, the pleural and pedal, are widely used neurobiological models for studying neural plasticity,[26, 27] they are less well-characterized biochemically, and thus present an opportunity for MALDI-MSI analysis of neuropeptide diversity and localization.

4.4 Experimental

4.4.1 Parafilm M Substrate Preparation.

Hexagonally closest packed bead monolayer substrates on Parafilm M (Pechiney, Neenah, WI) were prepared containing both blue and clear beads as previously reported.[22] Creating substrates that are appropriate for work with *Aplysia* ganglia sections requires ~10 mg of 40-μm diameter glass beads for a ~1 cm diameter monolayer. An optical image of the entire bead substrate is then taken using a light microscope (Leica Microsystems, Bannockburn, IL). The positions of the beads in the initial (before stretching) sample image are determined via light thresholding as described previously[22] using ImageJ (version 1.38, http://rsb.info.gov/ij) with the Colour Thresholding plugin.

4.4.2 Tissue Preparation.

Aplysia californica were obtained from Charles Hollahan (Santa Barbara, CA), kept in an aquarium until use, and anesthetized with an injection of isotonic $MgCl_2$ solution equal to 50% of the animal's body weight.[15, 28] The abdominal ganglion, with the attached pleural-abdominal connectives and the pleural-pedal ganglia, were isolated and stored in artificial sea water (ASW) containing (in mM): 460 NaCl, 10 KCl, 10 $CaCl_2$, 22 $MgCl_2$, 6 $MgSO_4$, and 10 N-2-hydroxyethylpiperazine-N'-2-ethanesulfonic acid (HEPES) (pH 7.8).[15]

Before sectioning, a solid block of agarose gel was created by pouring a heated saturated solution of agarose IV (Sigma-Aldrich, St. Louis, MO) into a Petri dish where it solidified. The agarose block was freeze-mounted with a few drops of water added onto an HM 550 Ultramicrotome (Microm International, Walldorf, Germany) sample stage, and a smooth surface aligned to the cutting plane was created with the ultramicrotome by sectioning through the top layers of agarose. The abdominal ganglion was oriented on top of the newly created surface by holding and moving the pleural-abdominal connectives with forceps. A small amount of deionized water was added to the sample to improve freeze-mounting. Tissue sections of 10 μm thickness were cut at –20°C using the ultramicrotome. A Parafilm M bead substrate at room temperature was placed above the tissue slice positioned on the metal ultramicrotome section stage surface and manual pressure was applied using the wooden handle end of an artist's brush. The relative orientation of the sample on the bead substrate, in comparison to the orientation of the ganglia on the cutting stage, and the perimeter of the sample edges are marked with a marker on the back side of the Parafilm M layer. To allow maximal analyte extraction while the sample is still partially wet and to reduce bead clumping, the samples were immediately manually stretched and placed onto conductive indium tin-oxide (ITO)-coated glass slides. The excess Parafilm M was manually torn off the glass slide edges, followed immediately by coating with MALDI matrix. In addition, adjacent intact serial tissue slices were placed on a glass slide and optical images were taken.

4.4.3 MALDI Matrix Application, Condensation, and Metal Coating.

Samples were coated with 30 mg/mL of 2,5-dihydroxybenzoic acid (DHB) (Sigma-Aldrich) matrix solution in 50:50 acetone:water. Coating was done with an artist's spray brush (Thayer & Chandler, Kenosha, WI) at a distance of ~30 cm in eight brief (~1 s) passes followed by drying for 1–2 min. The extent of drying and matrix accumulation was visually monitored during drying periods using light microscopy. Total matrix application time was about 15 min per sample. The samples were then rehydrated using a laboratory constructed humidity-controlled chamber equipped for automated thermal cycling of the sample adapted from our previously reported protocol.[15] The new system consisted of a Peltier device (Ferrotec, Bedford, NH), a temperature controller with a panel interface (Ferrotec), a thermistor (Ferrotec), a water-cooled heat sink (D-Tek Customs, Mission Viejo, CA), and a DC power supply. The Peltier device was controlled to follow a temperature cycle program via the FTC1000 software package (Ferrotec). The relative humidity of the chamber was adjusted to 85–95% with the sample placed on top of the Peltier device. The thermal cycling program was then initiated: the sample was cooled over 60 s to 14°C and then held at 14°C for 90 s, then warmed over 60 s to 28°C and then held at 28°C for 150 s. This cycling was repeated 3 times (~18 min) and then the temperature was held at 28°C until the sample was completely dry. Throughout this process the sample could be visualized in real time using a CCD camera (DFW-X700, Sony, Tokyo, Japan) attached to a 7× zoom microscope (Edmund Optics, Barrington, NJ) to ensure that water pooling did not occur. After condensation, to increase signal obtained from the tissue and to reduce surface charging during imaging, the stretched sample surface was sputter-coated with a mixture of gold and paladium[29, 30] for 15 s with a DESK II TSC turbo sputter coater (Denton, Moorestown, NJ).

4.4.4 Geometry File Creation for Automated Data Acquisition.

In contrast to the previous method,[22] which used a 1 mm calibration bar to calibrate pixel spacing, the new method described here uses laser-melted holes in the membrane to create a spatial calibration grid. The MALDI laser repetition rate was increased to 200 Hz at maximal laser power to melt beam-sized holes in the membrane at a regular array of positions, as specified in the MTP Slide Adapter II geometry file, included in the Bruker FlexControl 3.0 software (Bruker Daltonics, Billerica, MA). Subsequent to matrix application and melting of holes in the membrane, optical images were taken of the stretched sample and the bead positions were located via light thresholding using ImageJ and the Colour Threshold plugin, as described previously.[22]

With a new in-house written Java code (available at http://www.neuroproteomics.scs.uiuc.edu/imaging.html), the pixel coordinates of the beads in the stretched sample image are converted directly into the fractional distance coordinates that are used in the Bruker geometry file format. The distance between each melted hole in the regular array is 0.0870 fractional distance units, as determined from the Bruker MTP Slide Adapter II geometry file, and the scaling is determined by dividing this value by the average distance in pixels, as measured in ImageJ, between the melted holes of the array in the stretched sample image (Eq. 4.1). The scaling is multiplied by the X and Y pixel coordinates corresponding to each bead to give the bead location in fractional distance coordinates (Eq. 4.2).

$$\frac{0.0870_{frac.dist.}}{\langle array\_spacing \rangle_{pixels}} = scaling_{\frac{frac.dist.}{pixels}} \tag{4.1}$$

$$scaling_{\frac{frac.dist.}{pixels}} \times XYcoordinate_{pixels} = XYcoordinate_{frac.dist.} \tag{4.2}$$

Besides scaling, the origin must be matched between the two coordinate systems by taking screen images in FlexControl of the melted holes and matching these visually with the holes in the stretched sample image to determine their pixel coordinates. It should be noted that the spatial accuracy of the geometry file alignment with bead positions decreases with the distance from the origin of the geometry file; this is due to the imprecision of coordinate system scaling. Therefore, multiple origins, called anchor points, are used to create four coordinate origins spaced throughout the sample. Bead positions in the geometry file are then calculated from their nearest anchor point.

Automated data acquisition is done at the locations of the individual bead positions using the sample-tailored geometry files with the AutoXecute function of FlexControl on an Ultraflex II TOF-TOF mass spectrometer (Bruker Daltonics) equipped with a solid-state UV laser and operated in positive ion mode. The laser repetition rate was set at 50 Hz with 100 repetitions at each bead location. Mass calibration was done in FlexControl with the aid of diluted Peptide Calibration Standard II (Bruker Daltonics) spotted onto the Parafilm M surface and mixed with MALDI matrix before the start of the imaging run. The total acquisition time for imaging the stretched abdominal ganglion sample containing 1839 beads was 2.3 h, and 5.4 h for the pleural-pedal ganglia sample of 4277 beads. The area of the imaged beads that contains tissue is smaller than the area of the total number of beads used in each experiment.

4.4.5 Image Reconstruction.

Before image reconstruction, the data is processed and converted into a text file format, which is read by the in-house written Java code used to produce reconstructed ion images. Raw Bruker fid spectrum files from the imaging run were converted into text files as previously reported.[22] The in house-written MATLAB, version 7.2, R2006a (The MathWorks, Natick, MA), wrapper code for batch conversion of mzXML files into text files was modified to include baseline subtraction of each spectrum with the msbackadj.m function[31] from the Bioinformatics Toolbox 3.0, and to smooth each spectrum with the mslowess.m function, using the default processing parameters. The msbackadj.m function estimates the baseline through a moving window of 200 data points in width followed by regressing the baseline to the estimates with a spline approximation. The mslowess.m function smoothes spectra through a locally weighted linear regression with a linear polynomial fitting with a moving window of 10 data points in size.

Image reconstruction using a free transform process and plotting of ion images is done as described previously[22] with the aid of an in-house written Java code (www.neuroproteomics.scs.uiuc.edu/imaging.html). Resulting ion images present two-dimensional plots of the distribution and intensity of the analytes of interest, determined by taking the maximum signal intensity value selected from each analyzed mass spectrum within a 2 Da window surrounding the targeted *m/z* value. For the resulting reconstructed abdominal ganglion images, a rotation of five degrees is necessary so that the signals originating from the left upper quadrant, specifically the LUQIN peptide (*m/z* 1200), used here as a marker peptide, are aligned with the expected biological location. This ensures that the ion image is co-registered with the orientation of the optical image of the adjacent serial tissue slice.

4.4.6 Methods for Traditional MS Imaging.

A traditional MALDI-MSI experiment, without tissue fragmentation using Parafilm M substrate, was performed on a 10-μm thick slice of abdominal ganglion placed onto an ITO-coated glass slide. Before matrix application, to reduce analyte migration, a fixative 20 mg/mL nitrocellulose solution in 2:1 acetone:water was applied in successive coatings over a 20 min period using the ImagePrep apparatus (Bruker Daltonics). A MALDI matrix of 20 mg/mL of DHB in 50:50 methanol:water was then applied in successive coatings over 1.5 h using the ImagePrep. The sample was subsequently imaged with the Ultraflex II using FlexImaging 3.0 software (Bruker Daltonics) in a regular array raster pattern of 120-μm spacing for a total of 545 spots, with the acquisition parameters set to 100 shots at 50 Hz at each spot.

4.5 Results and Discussion

To enable tissue section imaging, several improvements to the stretched imaging approach are described, including modified matrix application, methods for tracking tissue orientation, and a more accurate geometry file creation process. Sampling optimization includes the use of solid agarose surfaces aligned to the sectioning plane for tissue positioning and sectioning, and metal coating of samples to reduce surface charging. Lastly, a method for spectra batch processing facilitates peak picking in low quality spectra. These improved MSI protocols are then validated by comparing MS images of neuropeptide distributions in the *Aplysia* nervous system with previously published neuropeptide distributions maps.

The first step is to form the bead monolayer on the stretchable membrane substrate, which is placed between the surface of two glass slides to spread the beads over the membrane. To more effectively create a hexagonally packed bead monolayer on the Parafilm M layer, slight manual pressure is created against the membrane using an index finger moving in a circular motion. Too great a force results in formation of bi- or trilayers of beads and deformation of the Parafilm M sheet. Excess beads on top of the bead monolayer are removed with a stream of nitrogen gas, followed by another application of more intense manual pressure to embed the beads, ensuring a stronger mechanical contact between beads and the Parafilm M.

Improved results are achieved if the tissue section is stretched immediately after it is loaded onto the bead array surface while the tissue is still wet. Immediate stretching of an elastic wet tissue sample enhances fragmentation[15] and reduces tissue/bead clumping that can occur in dried *Aplysia* ganglion sections (see Figure 4.1). Uniform tissue fragmentation, without bead clumping, is necessary for successful image reconstruction. In addition, immediate application of MALDI matrix after the tissue sectioning and fragmentation steps, while the tissue is partially wet, improves the quality of molecular ion signals. This may be due to increased analyte extraction efficiency from wet tissues. The shorter the timeframe between sample preparation and placing it on the membrane, stretching and matrix application, the greater the likelihood of generating high quality images. Therefore, we take the required optical image of the bead-loaded, pre-stretched membrane before the tissue is applied to the bead surface, rather than after.

Continuous tracking of tissue orientation inside the ultramicrotome cryochamber while sectioning, during transfer to the bead substrate, and during stretching, maintains the tissue alignment. This alignment allows comparison of the resulting ion images with the morphological features in the optical images of adjacent tissue sections. Previously,[15] we embedded the sample onto a piece of *Aplysia* buccal muscle for more repeatable sectioning of unfixed tissues. Unfortunately, this approach was slow and limited our ability to perform quick positioning and orienting of the tissue in the desired sectioning plane. We now create an agarose surface aligned with the plane and place tissues on top of this surface. Pressing the bead substrate onto the tissue slice located on the cold ultramicrotome sample stage, instead of the original approach of transferring the tissue to the bead substrate with an artist's brush,[17] allows the sample orientation to be tracked and marked on the membrane. A room temperature bead substrate that is warmer than the tissue facilitates complete transfer of the sample onto the bead array. Labeling of the sample orientation and its perimeter with a marker on the back of the membrane is followed immediately by sample stretching. The perimeter markings aid in placing the appropriate section of the stretched Parafilm M membrane containing the sample onto the glass slide after stretching.

During matrix application, the use of a light microscope to observe both the quality of MALDI matrix crystal coverage and the drying process in between successive spray coatings effectively guides the matrix application process. A further increase in relative intensity of analyte signal can be achieved by assuring that the sample is conductive, thus eliminating buildup of electrical charge on the sample surface. This is done either by placing the stretched sample onto ITO glass slides or coating the sample with a thin layer of metal.[29] Samples that used both treatments, the conductive ITO slide and metal coating, were found to result in only slightly better analyte signal than either approach alone, and so the ITO-coated slides alone were used here. Using both steps may still be helpful if the Parafilm M membrane has poor contact with the conductive ITO slide surface.

After melting the guide markers in the Parafilm M surface and MALDI matrix application, and before creation of geometry files, a transmission mode optical image is taken of the stretched sample. Taking the bead image in grazing angle incident light helps to illuminate the bead positions for more effective light thresholding in ImageJ. However, bright light also makes the melted Parafilm M markers that serve as anchor points less visible. A separate image of the sample at lower exposure levels was often used to aid in visualizing the holes (Figure 4.1A).

This new geometry file creation method improves the spatial accuracy of determining the individual bead locations. In our previous method,[22] the value of the pixel scaling had a precision of several pixels over several millimeters, but had greater errors over longer distances so that the accuracy of indicating bead positions decreased for larger samples. Here the conversion is calculated by directly converting pixel coordinates into fractional distance coordinates using the laser-melted holes in the stretched sample image as the spatial calibration points. The value of the scaling is more accurately determined, making the geometry file more accurate over larger areas. Besides determination of scaling, the melted markers are also used as anchor points between the stretched sample optical image and the Ultraflex II coordinate system. Even with larger area samples such as in the ~4000 bead pleural-pedal sample described below, use of several melted anchor points allow the creation of an accurate geometry file covering the entire sample; here each bead position in fractional distance coordinates is calculated using the corresponding nearest melted anchor point as the origin.

Data processing is used to improve the quality of the reconstructed molecular ion images. The quality of analyte signal from each spot depends on many parameters, including the presence of signal suppression from highly abundant species, the degree of co-crystallization of analyte and MALDI matrix, and the presence of high concentrations of inorganic salts. It is not surprising that the peptide signals acquired from tissue fragments located on some beads have lower intensities and appear in spectra with a range of background chemical and/or digitization noise. Therefore,. The *mslowess* function in MATLAB is a function that provides local weighted scatter plot smoothing,[32] a linear local regression smoothing operation with a moving window that effectively reduces noise. The resulting smoothed signals allow more accurate peak picking by an in-house written Java code. Also, baseline subtraction over separate windows of 200 *m/z* with the *msbackadj* function[31] helps to reduce any influence of varying mass spectra quality on the quality of the final molecular ion image. Background subtraction is important in MSI experiments, otherwise a varying background may add noise or even false positive analyte detection to ion distribution images. These processing steps can allow peptides to be detected from spectra that would have appeared to only contain noise.

An important aspect of tissue imaging is matrix application. The Bruker ImagePrep[33, 34] has been reported to be more reproducible in matrix application than manual airbrush-assisted MALDI matrix application for traditional MS imaging. Figure 4.2 shows raw spectra acquired during traditional and stretched imaging experiments investigating peptide distribution in slices of *Aplysia* abdominal ganglion. Both approaches for MALDI matrix application produce uniform and high intensity analyte signals. The poorer reproducibility of airbrush-assisted matrix application for MSI, in part, relates to difficulties in controlling analyte redistribution in the wet matrix layer during the procedure. The stretched sample approach helps to reduce or even eliminate such effects. As mentioned previously, a recondensation procedure reduces extraneous signals from physiological salt adducts from intact tissue sections.[23] This is now confirmed with the new stretched imaging protocols (Figure 4.2). Because roughly the same laser spot size was used to procude both spectra, the lower signal intensity in the stretched sample spectrum results from the smaller smount of tissue corresponding to a single bead that is interrogated compared to traditional imaging. However, the nearly-single cell sample sizes provided by the stretched imaging approach may remove signal supression from more abundant peptides and enable the detection of rare signals that are originate from one or a few cells.

How well do these protocols work for the determination of peptide localization within tissue sections using MALDI-MSI? Because most peptides have yet to be MS imaged at cellular resolution, we use the *Aplysia* CNS to validate our approach. The abdominal ganglion, located in the animal's visceral body cavity, innervates the peripheral organs of the animal. This ganglion is a part of the CNS that also contains a group of the head ganglia. The branchial nerve extending from the abdominal ganglion can be seen in the lower right portion of the optical image of a serial tissue section in Figure 4.3A and can be used as a morphological reference point. Of the three different *Aplysia* ganglia imaged here, the abdominal ganglion has been the most thoroughly investigated by physiological,[35] molecular biological,[36] and chemical techniques.[37-39] The peptide content of numerous abdominal ganglion cells and cell populations has been reported, including prohormone expression and its post-translational processing.

Validation of the ion images produced by the stretched imaging method can therefore be performed via comparison to previously reported *in situ* and immunostaining results. For example, neuropeptide Y (NPY) is known to stimulate and regulate food intake in *Aplysia*, and has homologous peptides in vertebrates that are associated with stress.[40, 41] MALDI profiling has previously shown localization of NPY to the lower right quadrant on the ventral side of the abdominal ganglion and possibly to the RG cluster.[42] The distribution of ions match the *m/z* ratios of NPY in Figure 4.3B and C-flanking peptide of neuropeptide Y (CPON) in Figure 4.3C, indicating that both peptides are colocalized to the bottom-central region of the tissue slice, likely occupied by a portion of the RG cluster where NPY and related peptides were previously reported.[42] In addition, one of the R3-14 prohormone-related peptides that mediates cardiac output[43] is detected in the upper portion of the ganglion (Figure 4.3D). Signals corresponding by molecular mass to other R3-14 related peptides are detected in various other locations in the ganglion (data not shown). This is expected as R3-14 peptides are known to be transported throughout this ganglion.[44] Another example involves the R15 peptides that are encoded by an alternatively spliced R15 peptide gene,[45] which are thought to have broad regulatory functions, including excitatory effects on heart muscle and coordination of autonomic neural regulation with escape locomotion.[7, 46] R15 peptides are known to be located in the R15 giant neuron, in the heart exciter neuron RB_{HE}, and in the L9G gill motoneurons, as well as in the deeply located L40 cell, all of which have extensive projections throughout this ganglion.[7] Accordingly, a distribution of ions with *m/z* values corresponding to those of the R15-prohormone related peptides are shown in Figure 4.3E,F. These analytes are colocalized in the bottom and central regions of the ganglion slice image that correspond to the location of the R15-peptide expressing neurons. Egg-laying hormone (ELH) originates from bag cell clusters located at the rostrolateral part of the ganglion.[47] ELH, when injected into an animal, is sufficient to cause egg laying. The distribution of ions in the slice ion image, mass matching an ELH-related peptide called delta bag cell peptide, is shown in Figure 4.3G. The signal, located at the top of the MS image near the area occupied by bag cell clusters, as well as in other regions of the image, may result from the presence of these peptides in bag cell neuron projections to the neuropil, a dense tangle of neuronal processes in the center of the ganglion.[48]

Figure 4.4 shows a different set of ion images from the abdominal ganglion; panels A–C show the MSI results that fit previous published maps of mRNA expression or immunoreactivity for several known *Aplysia* prohormones (or for prohormone-related peptides) that are shown in panels D–F. Pedal peptide is widely expressed throughout the *Aplysia* nervous system.[49] In the immunostaining results shown in panel D, the dotted circles represent cells with high immunoreactivity for pedal peptide, matching the distribution of mass-matched ions from panel A. However, the filled circles in panel D indicate several cells labeled via the prior immunostaining where we did not detect the peptide with MSI, perhaps caused by sectioning of the tissue at an angle that did not appreciably intersect these cell somata. LUQIN peptide, a peptide that triggers the closing of the renal pore, is located in the left upper quadrant cells,[50, 51] and the ion image of mass matched LUQIN peptide in panel B correlates to the immunostaining map in panel E. We recently reported the existence and localization of the feeding circuit-activating peptides (FCAPs),[52] which initiate motor activity related to feeding behaviors. These peptide distributions, studied by *in situ* hybridization and immunohistochemistry, are shown to localize in the center of the ganglion on its dorsal side and in the bag cells,[52] as seen in panel F. Ions corresponding to one of the FCAPs were detected in areas of the tissue slice that correspond to the bag cells but not in the center of the slice (Panel C). This may be a result of sectioning the ganglion at a layer that did not intersect with those specific positive cells, or perhaps the concentration of the analytes was below their limits of detection in those cells.

While the abdominal ganglion provided validation of the stretched imaging method to detect and properly reconstruct ion images, the pleural-pedal ganglia, which are not as well-characterized, offer the opportunity to gain new information on the localization of known and putative peptides using the ion distribution maps obtained with our optimized stretched sample imaging protocol.

Figure 4.5A shows an optical image of a serial section of the left pleural-pedal ganglia sectioned near the dorsal surface. Figure 4.5B,C shows the distribution of ions *m/z* 1545 and *m/z* 1680 that correspond to calculated molecular ion masses of monoprotonated peptides from the recently reported novel *Aplysia* prohormone pleurin (GenBank accession number AY833131). These two images show two possible amidated peptide products from the pleurin prohormone that closely colocalize, although the distribution of the analyte with *m/z* 1545 extends slightly more into the pedal ganglion, panel B. The ion images in panels D–F show unknown ions at *m/z* 1990 and *m/z* 1970 in panels D and E that colocalize in the pleural ganglion and in the center of the pedal ganglion and an unknown at *m/z* 1599 in panel F that is localized only to the pedal ganglion.

Figure 4.6A,B shows ion images of peptide distributions matched with previously reported immunoreactivity maps of known peptides of the corresponding *m/z* in panels C,D. Pedal peptide exhibits a ribbon pattern of immunoreactivity on the dorsal surface of the pedal ganglion as shown in panel C, which matches the ion image for an analyte with the same mass in panel A. The small cardioactive peptides (SCPs) are involved in increasing heart rate, respiration, and synaptogenesis;[53-55] SCP_B has been found in pleural and pedal ganglia at locations similar to ones revealed by immunostaining shown in panel D, which are similar to those in the ion image of a mass matched ion, as plotted in panel B. Further work will compare additional known and unknown peptides for identifying unique chemical forms and localizations.

4.6 Conclusions

A set of improved protocols for the stretched sample method have been demonstrated that enable the imaging of neuropeptides in tissue sections. The analyte distribution images from ganglia of *Aplysia californica* correspond to those produced using other approaches. The stretched imaging approach offers several advantages compared to traditional MS imaging, such as the reduction of inorganic ion adducts and analyte redistribution during sample preparation and the ability to detect and spatially localize low abundant or sparse analytes. The optimization protocols are easily implemented for imaging tissue sections. Tissue stretching and profiling has been deomonstrated on mammalian spine and other tissues,[8, 56] and so, the imaging protocols are suitable for a variety of tissue types besides the *Aplysia* ganglia used here. Stretched imaging has applications in MS imaging of morphologically and chemically heterogeneous structures in the nervous system where changes in neuropeptide expression and transport caused by activity dependent changes, drugs of abuse, or progressive disease states[57] can be spatially localized. Another exciting application complements peptidomics studies from mewly characterized aminal models after a number of new prohormones are discovered;[14, 58, 59] the stretched sample imaging method can be used in a global fashion to develop specific antibodies for literally dozens of new prohormones and hudred of new neuropeptides.

4.7 Figures

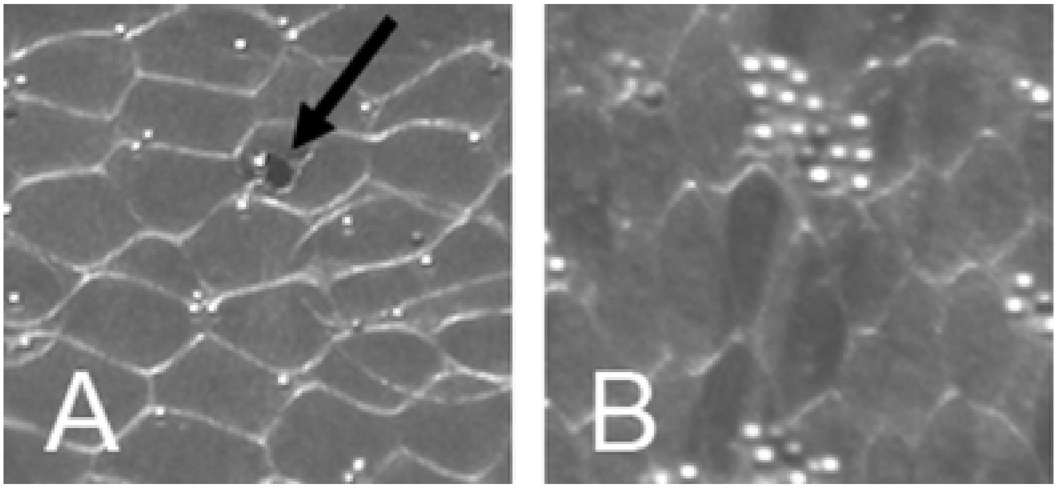

Figure 4.1. Quality of dividing of tissue sections into relatively uniform small pieces depends on tissue properties. **(A)** Stretching the thin CNS section immediately after it is sectioned, while the tissue is still hydrated, results in improved tissue fragmentation. A marker hole formed in the Parafilm M membrane using the TOF mass spectrometer laser is labeled by the arrow. The marker holes match the beam profile of the laser and are used as spatial calibration and anchor points during the creation of sample-tailored geometry files for automated data acquisition. **(B)** If the sample stretching is done after the tissue dries, tissue/bead clumping is observed.

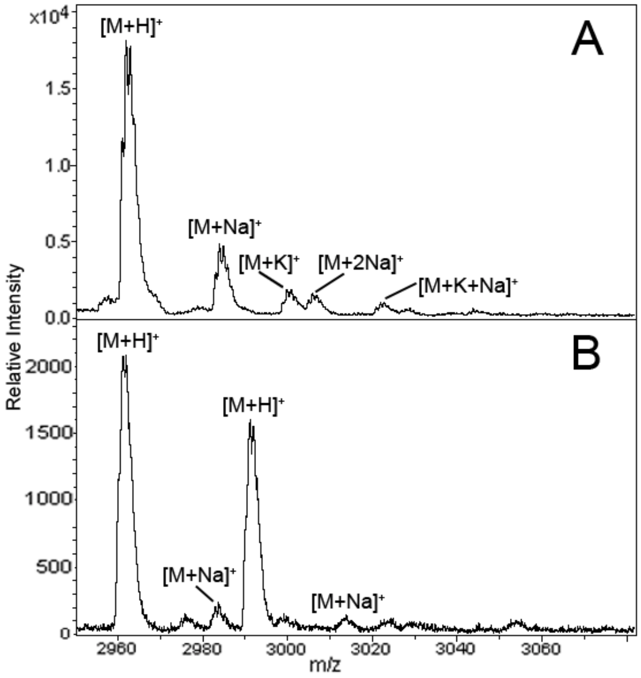

Figure 4.2. Representative mass spectra acquired from thin sections of *Aplysia* abdominal ganglia prepared using **(A)** traditional approaches when MALDI matrix is applied to the original (unfragmented) sample using the ImagePrep and **(B)** the stretched imaging approach using matrix spray-coating. Salt adducts are less visible in the mass spectrum acquired from the stretched sample, with relative intensities of the adduct signals further reduced by using multiple solvent (re)condensation cycles. When the inorganic ion adduct peaks are reduced, lower-level intensity peptide signals are sometimes detected.

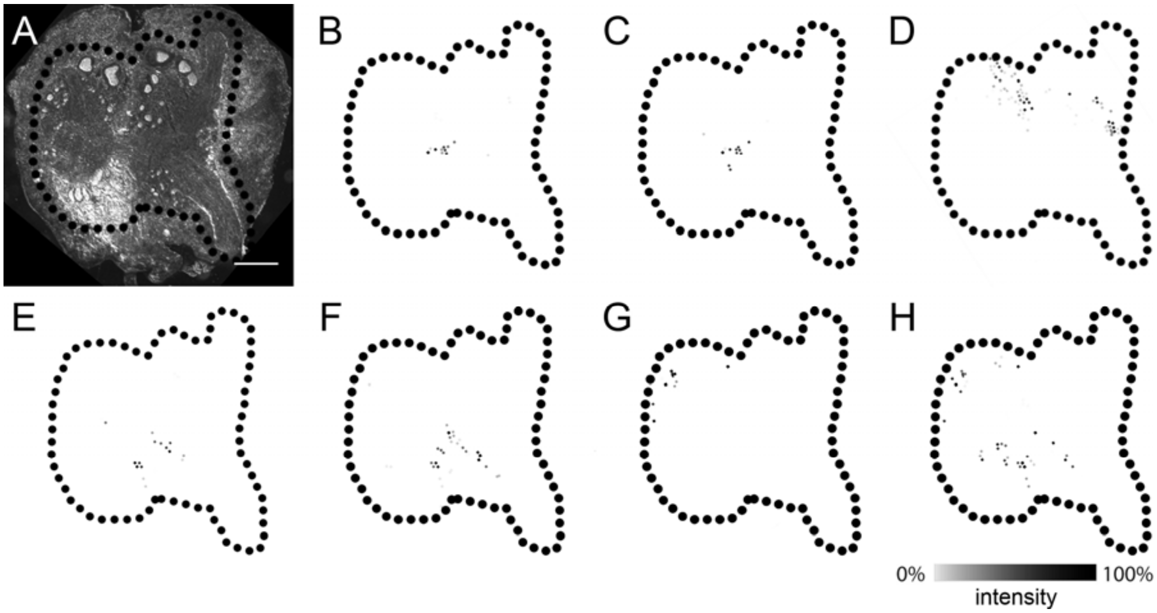

Figure 4.3. Images of peptide distribution in the abdominal ganglion obtained after the image reconstruction procedure agree with previously published data on localization of the analytes obtained using a variety of approaches. **(A)** Optical image of a 10-μm thick abdominal ganglion section cut close to the dorsal surface. Scale bar = 1 mm. Reconstructed ion images of **(B)** neuropeptide Y at *m/z* 4688, **(C)** and C-flanking peptide of neuropeptide Y at *m/z* 2567, colocalize in the center of the sample near the RG cluster.[42] **(D)** R3-14 peptide at *m/z* 1381 is known to localize to the R cluster of giant neurons in the right upper quadrant of the dorsal side of the ganglion.[44] **(E,F)** Pyroglutaminated-R15-α peptide at *m/z* 3981 and R15-β peptide, *m/z* 2860, colocalize in the center of the ganglion, near the location of the R15 cell and RB_{HE} cells, where it is known to be expressed.[7] As expected, **(G)** egg-laying hormone is seen near the location of the bag cells at the top of the ganglion. **(H)** Delta bag cell peptide appears both near the location of the bag cells and in the middle areas of the ganglion.

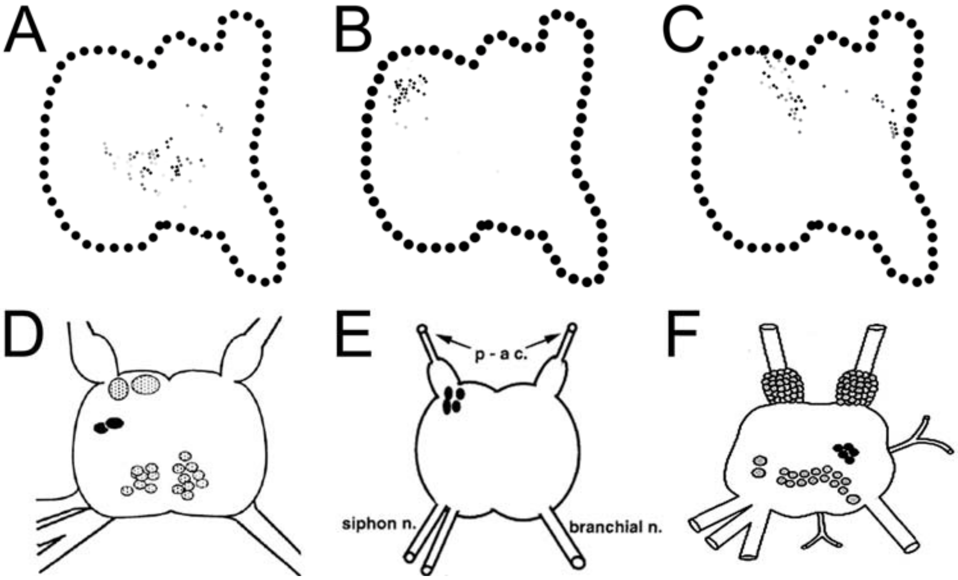

Figure 4.4. (A–C) Peptide distributions observed from a 10-μm section of the abdominal ganglion prepared using the stretched sample approach are similar to **(D–F)** observations from immunohistochemical data from antibodies raised to the same prohormones. **(A)** Distribution of pedal peptide at *m/z* 1540 matches the distributions using immunostaining **(D)**,[49] as does **(B,E)** left-upper quadrant peptide at *m/z* 1200[28] and **(C,F)** feeding-circuit activating peptide, FCAP, at m/z 1369.[52] The FCAP-related peptide shown in panel C was detected in areas occupied mostly by the bag cells where presence of the FCAP prohormone has been shown previously by combined immunoreactivity and *in situ* hybridization. (Panels D and F are adapted with permission from the Journal of Neuroscience from references 49 and 52, respectively. Society for Neuroscience. Panel E is adapted with permission from Wiley-Blackwell from reference 28).

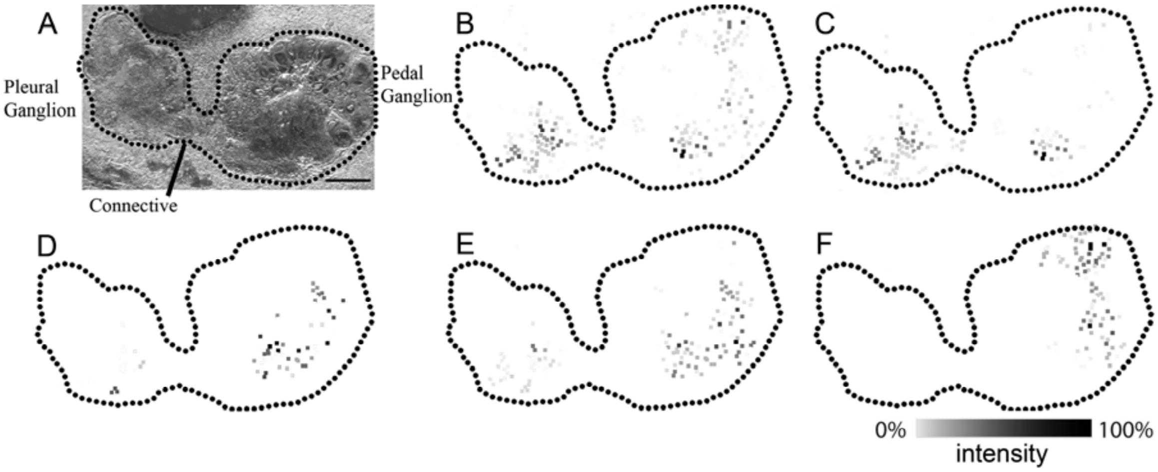

Figure 4.5. (A) Optical image of a 10-μm section from close to the dorsal surface of the left pleural-pedal ganglia. Scale bar = 0.5 mm. **(B–F)** Ion images of different peptide localizations in the tissue. **(B)** Pleurin peptide signals at *m/z* 1545 and **(C)** *m/z* 1680 colocalize in both ganglia. Localizations of putative novel neuropeptides at **(D)** *m/z* 1990, **(E)** *m/z* 1970, and **(F)** *m/z* 1599 do not match distributions of known peptides.

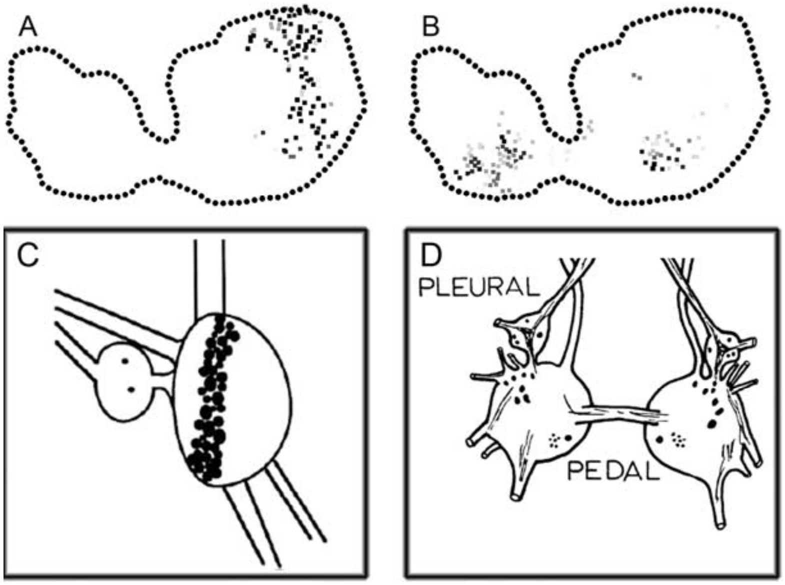

Figure 4.6. (A,B) Ion images of a thin section of the pleural-pedal ganglia are visually similar to **(C,D)** previously published drawings of distributions of these peptides obtained via immunostaining. **(A)** Data on pedal peptide at *m/z* 1540 and its localization matches well with the **(C)** immunostaining results[49] as a clear band of peptide can be seen across the pedal ganglion. **(B,D)** Data on SCP_B at *m/z* 1141 also matches the immunostaining results.[3] (Panels C and D are adapted with permission from the Journal of Neuroscience from references 49 and 55, respectively).

4.8 References

1. DeKeyser, S. S., Kutz-Naber, K. K., Schmidt, J. J., Barrett-Wilt, G. A., and Li, L. Imaging mass spectrometry of neuropeptides in decapod crustacean neuronal tissues. *J. Proteome Res.* **2007,** 1782-1791.

2. Li, L. and Sweedler, J. V. Peptides in our brain: Mass spectrometric-based measurement approaches and challenges. *Annual Reviews Analytical Chemistry* **2008,** *1*, 451-483.

3. Wisztorski, M., Croix, D., Macagno, E., Fournier, I., and Salzet, M. Molecular MALDI imaging: An emerging technology for neuroscience studies. *Dev. Neurobiol.* **2008,** *68*, 845-858.

4. Trim, P. J., Atkinson, S. J., Princivalle, A. P., Marshall, P. S., West, A., and Clench, M. R. Matrix-assisted laser desorption/ionisation mass spectrometry imaging of lipids in rat brain tissue with integrated unsupervised and supervised multivariant statistical analysis. *Rapid Commun. Mass Spectrom.* **2008,** *22*, 1503–1509.

5. Rubakhin, S. S., Churchill, J. D., Greenough, W. T., and Sweedler, J. V. Profiling signaling peptides in single mammalian cells using mass spectrometry. *Anal. Chem.* **2006,** *78*, 7267–7272.

6. Caprioli, R. M., Farmer, T. B., and Gile, J. Molecular imaging of biological samples: Localization of peptides and proteins using MALDI-TOF MS. *Anal. Chem.* **1997,** *69*, 4751-4760.

7. Romanova, E. V., McKay, N., Weiss, K. R., Sweedler, J. V., and Koester, J. Autonomic control network active in Aplysia during locomotion includes neurons that express splice variants of R15-neuropeptides. *J. Neurophysiol.* **2007,** *97*, 481–491.

8. Monroe, E. B., Annangudi, S. P., Hatcher, N. G., Gutstein, H. B., Rubakhin, S. S., and Sweedler, J. V. SIMS and MALDI MS imaging of the spinal cord. *Proteomics* **2008,** *8*, 3746–3754.

9. Deininger, S.-O., Matthias P. Ebert, Arne Fütterer, Marc Gerhard, and Röcken, C. MALDI imaging combined with hierarchical clustering as a new tool for the interpretation of complex human cancers. *J. Proteome Res.* **2008,** *7*, 5230–5236.

10. Chen, R., Hui, L., Sturm, R. M., and Li, L. Three dimensional mapping of neuropeptides and lipids in crustacean brain by mass spectral imaging. *J. Am. Soc. Mass Spectrom.* **2009,** *20*, 1068–1077.

11. Bailey, C. H. and Chen, M. Morphological basis of long-term habituation and sensitization in Aplysia. *Science* **1983,** *220*, 91-93.

12. Gingrich, K. J. and Byrne, J. H. Simulation of synaptic depression, posttetanic potentiation, and presynaptic facilitation of synaptic potentials from sensory neurons mediating gill-withdrawal reflex in Aplysia. *J. Neurophysiol.* **1985,** *53*, 652-669.

13. Kruse, R. and Sweedler, J. V. Spatial profiling invertebrate ganglia using MALDI MS. *J. Am. Soc. Mass Spectrom.* **2003,** *14*, 752–759.

14. Hummon, A. B., Amare, A., and Sweedler, J. V. Discovering new invertebrate neuropeptides using mass spectrometry. *Mass Spectrom. Rev.* **2006,** *25*, 77–98.

15. Monroe, E. B., Jurchen, J. C., Koszczuk, B. A., Losh, J. L., Rubakhin, S. S., and Sweedler, J. V. Massively parallel sample preparation for the MALDI MS analyses of tissues. *Anal. Chem.* **2006,** *78*, 6826–6832.

16. Li, L., Romanova, E. V., Rubakhin, S. S., Alexeeva, V., Weiss, K. R., Vilim, F. S., and Sweedler, J. V. Peptide profiling of cells with multiple gene products: Combining immunochemistry and MALDI mass spectrometry with on-plate microextraction. *Anal Chem* **2000,** *72*, 3867-3874.

17. Zimmerman, T. A., Monroe, E. B., Tucker, K. R., Rubakhin, S. S., and Sweedler, J. V., "Imaging of cells and tissues with mass spectrometry: Adding chemical information to imaging," in *Biophysical tools for biologists, volume two: In vivo techniques*, J. J. Correia and H. W. Detrich, eds. (Elsevier, San Diego, 2008), pp. 361–390.

18. Altelaar, A. F. M., Taban, I. M., McDonnell, L. A., Verhaert, P. D. E. M., Lange, R. P. J. d., Adanc, R. A. H., Mooid, W. J., Heeren, R. M. A., and Piersma, S. R. High-resolution MALDI imaging mass spectrometry allows localization of peptide distributions at cellular length scales in pituitary tissue sections. *Int. J. Mass Spectrom.* **2007,** *260*, 203–211.

19. Baluya, D. L., Garrett, T. J., and Yost, R. A. Automated MALDI matrix deposition method with inkjet printing for imaging mass spectrometry. *Anal. Chem.* **2007,** *79*, 6862-6867.

20. Chen, Y., Allegood, J., Liu, Y., Wang, E., Cachón-González, B., Cox, T. M., Merrill, A. H., and Sullards, M. C. Imaging MALDI mass spectrometry using an oscillating capillary nebulizer matrix coating system and its application to analysis of lipids in brain from a mouse model of Tay-Sachs/Sandhoff disease. *Anal. Chem.* **2008,** *80*, 2780-2788.

21. Aerni, H.-R., Cornett, D. S., and Caprioli, R. M. Automated acoustic matrix deposition for MALDI sample preparation. *Anal. Chem.* **2006,** *78*, 827-834.

22. Zimmerman, T. A., Monroe, E. B., and Sweedler, J. V. Adapting the stretched sample method from tissue profiling to imaging. *Proteomics* **2008,** *8*, 3809–3815.

23. Monroe, E. B., Koszczuk, B. A., Losh, J. L., Jurchen, J. C., and Sweedler, J. V. Measuring salty samples without adducts with MALDI MS. *Int. J. Mass Spectrom.* **2007,** *260*, 237–242.

24. Ma, M., Wang, J., Chen, R., and Li, L. Expanding the crustacean neuropeptidome using a multifaceted mass spectrometric approach. *J Proteome Res* **2009,** *8*, 2426-2437.

25. Wang, J., Chen, R., Ma, M., and Li, L. MALDI MS sample preparation by using paraffin wax film: Systematic study and application for peptide analysis. *Anal Chem* **2008,** *80*, 491-500.

26. Marinesco, S., Duran, K. L., and Wright, W. G. Evolution of learning in three aplysiid species: Differences in heterosynaptic plasticity contrast with conservation in serotonergic pathways. *J. Physiol.* **2003,** *550*, 241–253.

27. Stuart, D. K. and Strumwasser, F. Neuronal sites of action of a neurosecretory peptide, egg-laying hormone, in Aplysia californica. *J. Neurophysiol.* **1980,** *43*, 499-519.

28. Giardino, N. D., Aloyz, R. S., Zollinger, M., Miller, M. W., and Desgroseillers, L. L5-67 and LUQ-1 peptide precursors of apysia californica: Distribution and localization of immunoreactivity in the central nervous system and in peripheral tissues *J. Comp. Neurol.* **1996,** *374*, 230-245.

29. Altelaar, A. F. M., Klinkert, I., Jalink, K., Lange, R. P. J. d., Adan, R. A. H., Heeren, R. M. A., and Piersma, S. R. Gold-enhanced biomolecular surface imaging of cells and tissue by SIMS and MALDI mass spectrometry. *Anal. Chem.* **2006,** *78*, 734–742.

30. McCombie, G., Staab, D., Stoeckli, M., and Knochenmuss, R. Spatial and spectral correlations in MALDI mass spectrometry images by clustering and multivariate analysis. *Anal. Chem.* **2005,** *77*, 6118–6124.

31. McDonald, R. A., Skipp, P., Bennell, J., Potts, C., Thomas, L., and O'Connor, C. D. Mining whole-sample mass spectrometry proteomics data for biomarkers – an overview. *Expert Syst. Appl.* **2009,** *36*, 5333–5340.

32. Cho, H., Smalley, D. M., Theodorescu, D., Ley, K., and Lee, J. K. Statistical identification of differentially labeled peptides from liquid chromatography tandem mass spectrometry. *Proteomics* **2007,** *7*, 3681–3692.

33. Gustafsson, J. O. R., McColl, S. R., and Hoffmann, P. Imaging mass spectrometry and its methodological application to murine tissue. *J. Proteomics Bioinf.* **2008,** *1*, 458-463.

34. McDonnell, L. A., van Remoortere, A., van Zeijl, R. J., and Deelder, A. M. Mass spectrometry image correlation: Quantifying colocalization. *J Proteome Res* **2008,** *7*, 3619-3627.

35. Hatcher, N. G. and Sweedler, J. V. Aplysia bag cells function as a distributed neurosecretory network. *J. Neurophysiol.* **2008,** *99*, 333–343.

36. Song, Y. and Liu, Y.-M. Quantitation of cardioexcitatory Asn-D-Trp-Phe-NH2 diastereomers in aplysia's central nervous system by nanoscale liquid chromatography-tandem mass spectrometry. *J. Mass Spectrom.* **2008,** *43*, 1285–1290.

37. Ewing, M. A., Wang, J., Sheeley, S. A., and Sweedler, J. V. Detecting d-amino acid-containing neuropeptides using selective enzymatic digestion. *Anal. Chem.* **2008,** *80*, 2874-2880.

38. Jung, L. J. and Scheller, R. H. Peptide processing and targeting in the neuronal secretory pathway. *Science* **1991,** *251*, 1330-1335.

39. Li, L., Garden, R. W., and Sweedler, J. V. Single-cell MALDI: A new tool for direct peptide profiling. *Trends Biotechnol.* **2000,** *18*, 151-160.

40. Jing, J., Vilim, F. S., Horn, C. C., Alexeeva, V., Hatcher, N. G., Sasaki, K., Yashina, I., Zhurov, Y., Kupfermann, I., Sweedler, J. V., and Weiss, K. R. From hunger to satiety: Reconfiguration of a feeding network by Aplysia neuropeptide y. *J. Neurosci.* **2007,** *27*, 3490 –3502.

41. Husum, H. and Mathé, A. A. Early life stress changes concentrations of neuropeptide y and corticotropin-releasing hormone in adult rat brain. Lithium treatment modifies these changes. *Neuropsychopharmacol.* **2002,** *27*, 756–764.

42. Garden, R. W., Shippy, S. A., Li, L., Moroz, T. P., and Sweedler, J. V. Proteolytic processing of the Aplysia egg-laying hormone prohormone. *Proc. Natl. Acad. Sci. USA* **1998,** *95*, 3972–3977.

43. Newcomb, R. and Scheller, R. H. Proteolytic processing of the Aplysia R3-14 neuropeptide precursors and egg-laying hormone. *J. Neurosci.* **1987,** *7*, 854-863.

44. Kreiner, T., Sossin, W., and Scheller, R. H. Localization of Aplysia neurosecretory peptides to multiple populations of dense core vesicles. *J. Cell Biol.* **1986,** *102*, 769-782.

45. Alevizos, A., Karagogeos, D., Weiss, K. R., Buck, L., and Koester, J. R15 alpha-1 and R15 alpha-2 peptides from Aplysia: Comparison of bioactivity, distribution, and function of two peptides generated by alternative splicing. *J. Neurobiol.* **1991,** *22*, 405-417.

46. Skelton, M. E. and Koester, J. The morphology, innervation and neural control of the anterior arterial system of Aplysia californica. *J. Comp. Physiol. A* **1992,** *171*, 141-155.

47. Branton, W. D., Arch, S., Smock, T., and Mayeri, E. Evidence for mediation of a neuronal interaction by a behaviorally active peptide. *Proc. Natl. Acad. Sci. USA* **1978,** *75*, 5732-5736.

48. Conn, P. J. and Kaczmarek, L. K. Immunostaining for peptides of the egg-laying hormone/bag cell peptide precursor protein in the head ganglia of Aplysia. *Neurosci.* **1989,** *27*, 363-371.

49. Pearson, W. L. and Lloyd, P. E. Immunocytological localization of pedal peptide nervous system and periphery of Aplysia. *J. Neurosci.* **1989,** *9*, 318-325.

50. Koester, J. and Koch, U. T. Neural control of the circulatory system of Aplysia. *Experientia* **1987,** *43*, 972-980.

51. Koester, J. and Alevizosi, A. Innervation of the kidney of Aplysia by LIO, the LUQ cells, and an identified peripheral motoneuron. *J. Neurosci.* **1989,** *9*, 4078-4088.

52. Sweedler, J. V., Li, L., Rubakhin, S. S., Alexeeva, V., Dembrow, N. C., Dowling, O., Jing, J., Weiss, K. R., and Vilim, F. S. Identification and characterization of the feeding circuit-activating peptides, a novel neuropeptide family of Aplysia. *J. Neurosci.* **2002,** *22*, 7797–7808.

53. Lloyd, P. E., Schacher, S., Kupfermann, I., and Weiss, K. R. Release of neuropeptides during intracellular stimulation of single identified Aplysia neurons in culture. *Proc. Natl. Acad. Sci. USA* **1986,** *83*, 9794-9798.

54. Alevizos, A., Weiss, K. R., and Koesteri, J. SCP-containing R20 neurons modulate respiratory pumping in Aplysia. *J. Neurosci.* **1989,** *9*, 3058-3071.

55. Lloyd, P. E., Mahon, A. C., Kupfermann, I., Cohen, J. L., Scheller, R. H., and Weiss, K. R. Biochemical and immunocytological localization of molluscan small

cardioactive peptides in the nervous system of Aplysia californica. *J. Neurosci.* **1985,** *5*, 1851-1861.

56. Zimmerman, T. A., Rubakhin, S. S., and Sweedler, J. V., "Mass spectrometry imaging using the stretched sample approach," in *Mass spectrometric imaging: Principles and protocols*, S. S. Rubakhin and J. V. Sweedler, eds. (Springer, 2010), pp. 465-479.

57. Romanova, E. V., Hatcher, N. G., Rubakhin, S. S., and Sweedler, J. V. Characterizing intercellular signaling peptides in drug addiction. *Neuropharmacology* **2009,** *56 Suppl 1*, 196-204.

58. Consortium, T. B. G. S. a. A. The genome sequence of taurine cattle: A window to ruminant biology and evolution. *Science* **2009,** *324*, 522-528.

59. Amare, A. and Sweedler, J. V. Neuropeptide precursors in tribolium castaneum. *Peptides* **2007,** *28*, 1282-1290.

CHAPTER 5

THE STRETCHED SAMPLE METHOD AS APPLIED TO THE MASS SPECTROMETRIC IMAGING OF MOUSE PITUITARY

5.1 Notes and Acknowledgements

This chapter is in the form of a tutorial/protocol to aid other researchers who desire to use these protocols. This chapter is reproduced from a publication of the title "Mass spectrometry imaging using the stretched sample approach" from the book series: *Methods in Molecular Biology*, **2010**, 656, 465-479 with kind permissions from Springer Science+Business Media. Co-authors for this book chapter are Stanislav S. Rubakhin and Jonathan V. Sweedler. We thank Georgina M. Aldridge, University of Illinois at Urbana-Champaign, for providing the animals. The project described was supported by Award Number P30DA018310 from the National Institute On Drug Abuse and Award No. 5RO1DE018866 from the National Institute of Dental and Craniofacial Research (NIDCR) and the Office of Director (OD), National Institutes of Health (NIH).

5.2 Abstract

Matrix-assisted laser desorption/ionization (MALDI) mass spectrometry imaging (MSI) can determine tissue localization for a variety of analytes with high sensitivity, chemical specificity, and spatial resolution. MS image quality typically depends on the MALDI matrix application method used, particularly when the matrix solution or powder is applied directly to the tissue surface. Improper matrix application results in spatial redistribution of analytes and reduced MS signal quality. Here we present a stretched sample imaging protocol that removes the dependence of MS image quality on the matrix

application process and improves analyte extraction and sample desalting. First, the tissue sample is placed on a monolayer of solid support beads that are embedded in a hydrophobic membrane. Stretching the membrane fragments the tissue into thousands of nearly single-cell sized islands, with the pieces physically isolated from each other by the membrane. This spatial isolation prevents analyte transfer between beads, allowing for longer exposure of the tissue fragments to the MALDI matrix, thereby improving detectability of small analyte quantities without sacrificing spatial resolution. When using this method to reconstruct chemical images, complications result from non-uniform stretching of the supporting membrane. Addressing this concern, several computational tools enable automated data acquisition at individual bead locations and allow reconstruction of ion images corresponding to the original spatial conformation of the tissue section. Using mouse pituitary, we demonstrate the utility of this stretched imaging technique for characterizing peptide distributions in heterogeneous tissues at nearly single-cell resolution.

5.3 Introduction

Both invertebrate and mammalian nervous systems exhibit high levels of biochemical and morphological heterogeneity. Neighboring neurons often possess different sets of intercellular signaling peptides, with several prohormones encoding multiple peptides that are expressed differently among individual neurons. Investigation of the mammalian nervous system, where neurons number in the billions, presents a significant challenge when using classical labeling approaches to examine one or more cell-to-cell signaling molecules at a time. In contrast to other bioimaging techniques, mass spectrometry imaging (MSI) can uncover the distribution of a variety of analytes within tissues while simultaneously determining their chemical identities, without the need for specific labeling or immunostaining.[1-5] MSI has broad applications in academic, clinical, and industrial research, having had significant impact on cancer studies,[6-9] the search for new pharmaceuticals,[10] and investigations of the nervous system.[11] A variety of MSI approaches targeting different types of analytes have been developed over the years. MALDI MSI has become one of most successful technologies for investigation of peptide and protein distributions in fixed and freshly prepared tissues. The analyte desorption and ionization processes occurring during exposure of the MALDI matrix/analyte layer to UV or IR laser light allows detection of intact/unfragmented analytes. Not only is the entire sequence of ion desorption, formation, separation, and detection fast, the laser beam can be focused to sub-micrometer diameters. However, because the amount of proteins and peptides present decrease concomitantly with the size of the area being probed, the smallest laser diameters are not commonly used. Obviously, larger laser spot sizes allow desorption of increased amounts of analyte. Typical chemical images are generated with 25-50 μm spatial resolution.

In MALDI MSI, a liquid or powder matrix is deposited on top of the sample, incorporating the analyte into the matrix crystals. When illuminated with the laser, the matrix and analyte are vaporized and ionized. Although longer exposure of the sample to matrix facilitates extraction of the analyte of interest from the tissue, it can also delocalize the analyte. Shorter extraction times ameliorate this problem, but result in poorer signal. This issue is particularly problematic when investigating small hydrophilic substances that diffuse during matrix application. Recent advances in MALDI matrix solution application approaches have helped to create uniform MALDI matrix layers; these include spray coating,[12] electrospray deposition,[13] and automated acoustic deposition.[14] Using these techniques, the imaging of fine analyte spatial distributions has been achieved. However, each type of sample and even class of analytes requires individualized optimization of the MALDI matrix exposure duration and drying time.

The stretched sample protocol resolves these issues by eliminating redistribution of analytes during the matrix application stage. A tissue slice is placed on top of a monolayer comprised of ~40-µm diameter glass beads, which has been partially embedded into a layer of Parafilm M.[15] As the Parafilm M layer is manually stretched to a ~16-fold increase in area, the beads separate from each other and the tissue, which adheres to the beads, is fragmented into thousands of islands. Because each bead contains only one or a few cells, chemically and spatially separated by areas of hydrophobic membrane, the sample can be exposed to the MALDI matrix solution for a longer period of time without sacrificing spatial resolution. The spatial isolation of tissue fragments allows rare signals from small cellular clusters, single cells, and even subcellular regions to be better detected and spatially distinguished. Furthermore, multiple MALDI matrix wetting/recrystallization cycles can be accomplished via temperature-dependent condensation of solvents onto the stretched sample, which allows for increased incorporation of the analyte into the matrix, contributing to further signal enhancement.

Effective MS imaging of stretched samples demands new methods of data acquisition, along with image reconstruction protocols, to register the spectral data with the corresponding conformation of the tissue before stretching. Although classical MSI experiments collect data in a regular raster pattern over the sample,[16] the small tissue/cell islands in the stretched sample occur in irregular spatial patterns on the Parafilm M membrane. Incorporating a step to identify bead positions from optical images of the sample via light thresholding allows automated MS data acquisition from the individual bead positions. Image reconstruction is done *in silico* with a free transform process that mimics the actual stretching process.[17] During stretching, the beads tear sizable craters partially through the layer of Parafilm M, visible in an optical image of the stretched sample. Image reconstruction is performed by aligning an image of the initial positions of the embedded beads with an image of the tissue sample after stretching. The spectral data taken from the stretched sample are assigned to the nearest corresponding initial bead positions to reconstruct an ion image of the tissue in its original conformation. This novel stretched imaging method shows increased potential for identifying rare signals from heterogeneous tissue samples.[18]

5.4 Materials

5.4.1 Preparation of Parafilm M Substrate

1. Parafilm M (Pechiney, Neenah, WI).
2. Glass slides, 25 × 75 × 1.1 mm, (Delta Technologies, Stillwater MN).
3. At least 100 mg of ~40-um diameter clear glass beads (Mo-Sci Corp., Rolla, MO). Blue beads are optional, and are used as markers to aid image reconstruction. Beads of other types and sizes including liquid chromatography solid phase materials can be also used.
4. A heated aluminum block.

5.4.2 Tissue Preparation and Sample Stretching

1. Four month-old B6 mice obtained from an in-house colony bred by the Greenough group, University of Illinois at Urbana-Champaign, were used. Animals of similar strains can be purchased for research purposes from the Jackson (http://www.jax.org) or Harlan laboratories (http://www.harlan.com). A variety of tissues from different animals can be investigated using the protocol presented here.
2. SPECTRA-SONIC (or similar) solution, pH 7 (Spectrum Surgical Instruments Corp., Stow, OH) for surgical instrument clean up.
3. Modified Gey's balanced salt solution (mGBSS): 1.5 mM $CaCl_2$, 4.9 mM KCl, 0.2 mM KH_2PO_4, 11 mM $MgCl_2$, 0.3 mM $MgSO_4$, 138 mM NaCl, 27.7 mM $NaHCO_3$, 0.8 mM Na_2HPO_4, 25 mM HEPES and 10 mM glucose, pH 7.2 adjusted with NaOH.
4. Dissection tools including forceps, scissors (available online from Fine Science Tools http://www.finescience.com or World Precision Instruments - http://www.wpiinc.com), and a properly sharpened guillotine.
3. Cryostat capable of keeping the specimen temperature at –15 to –20^{o}C and of cutting 10- μm sections, e.g., Microm HM550 (Thermo Scientific, Waltham, MA).
4. Indium tin oxide (ITO)-coated glass slides, 25 × 75 × 1.1 mm, (Delta Technologies, Stillwater MN).
5. A piece of firm paper.
6. Liquid nitrogen and dry ice.

7. Vials for specimen storage.
8. Protective lab coat, gloves and goggles.

5.4.3 MALDI Matrix Application

1. MALDI matrix solution: 300 mg of 2,5-dihydroxybenzoic acid (Sigma-Aldrich, St. Louis, MO) in 10 mL of 75:25 acetone:water.
2. Artist's spray brush (Badger, Franklin Park, IL).
3. In-house built condensation chamber consisting of a Peltier device (Melcor, Trenton, NJ) connected to a cooling basin of water, and a thermocouple connected to a CN77000 temperature controller (Omega, Stamford, CT).
4. Acetone.

5.4.4 Mass Spectrometry and Automated Imaging

1. Optical stereomicroscope.
2. Inverted transmission light microscope with 2.5 - 10× magnification and equipped with a digital camera (e.g., AxioCam MRc camera controlled by the AxioVision digital image processing software package, Carl Zeiss, Bernreid, Germany; AxioVision LE is free and a sample version of the full package is available at http://www.zeiss.com/).
3. Ultraflex II MALDI-TOF mass spectrometer (Bruker Daltonics, Billerica, MA) with a solid-state UV laser.
4. MTP slide adapter (Bruker Daltonics) for insertion of slides into the MS instrument.

5. ImageJ, version 1.38 (National Institutes of Health, http://rsb.info.nih.gov/ij/).
6. Java SDK, version 1.6.0 (Sun Microsystems, http://java.sun.com).
7. FlexControl 3.0 (Bruker Daltonics).
8. Bead geometry application (free at http://neuroproteomics.scs.uiuc.edu/imaging.html).

5.4.5 Data Conversion

1. Software tool: CompassXport (Bruker Daltonics, free at http://www.brukerdaltonics.com; for more information see: http://www.ionsource.com/functional_reviews/CompassXport/CompassXport.htm).
2. Software package: MATLAB R2006a, version 7.2, and the Bioinformatics Toolbox 3.0 (The MathWorks, Natick, MA).
3. Batch conversion MATLAB code (free at http://neuroproteomics.scs.uiuc.edu/imaging.html).

5.4.6 Image Reconstruction

1. Photoshop CS, version 8.0 (Adobe Systems).
2. Java-based code to create image of dots at the initial bead positions (free at http://neuroproteomics.scs.uiuc.edu/imaging.html).
3. MSIReconstructor application (free at http://neuroproteomics.scs.uiuc.edu/imaging.html).

5.5 Methods

5.5.1. Preparation of Parafilm M Substrate

1. Parafilm M is cut into a square measuring approximately 5 cm × 5 cm and placed on top of a glass slide (*see* **Note 1**). In this step, the slide is used as a clean solid support and so does not require a conductive ITO-coated slide.
2. Approximately 100 mg of beads are transferred to the Parafilm M surface. Another glass slide is placed on top of the beads and vertical pressure is manually applied to partially embed the beads into the Parafilm M layer.
3. Application of a nitrogen stream to the substrate removes loose beads, ensuring an even monolayer is attached to the Parafilm M surface.
4. Placing the substrate between two glass slides and heating it on top of an aluminum block at ~60 ^{o}C for 10 - 15 s with downward manual pressure allows the beads to become more strongly and uniformly attached to the Parafilm M. Care must be taken to ensure that peripheral parts of the Parafilm M section, which might touch the metal block, do not melt onto it. A small separate piece of Parafilm M can be used to test if the temperature is such that the Parafilm M might be melted by the metal block.
5. An optical image of the initial bead/Parafilm M substrate is taken in transmission mode (see **Note 2**).

5.5.2 Tissue Preparation and Sample Stretching

1. Experimental animals are selected and prepared for sacrifice. Importantly, work performed on animals should comply with local and federal rules and regulations for the humane care and treatment of animals.
2. Surgical/dissection instruments are cleaned and sterilized by ultrasonic treatment in SPECTRA-SONIC (or similar) solution for 5 - 10 min, followed by autoclaving according to the manufacturer's manual.
3. Vials and paper are prepared; protective lab coat, gloves, and goggles are worn.
4. The animal is decapitated using a sharp guillotine.
5. The cranium is exposed by pushing the skin in a rostral direction using a piece of firm paper.
6. The cranial bones in the frontal plane are cut using long, thin scissors.
7. The brain is carefully lifted and discarded after removal of the previously cut dorsal part of the cranium. The pituitary typically remains in the scull, held in place by connective tissue.
8. The connective tissue surrounding the pituitary should be removed first; the pituitary is quickly removed using fine forceps.
9. The pituitary is briefly washed in ice cold mGBSS. The tissue is quickly frozen in liquid nitrogen and stored in a vial over dry ice for transport to the cryostat environment.
10. The pituitary is placed on a cooled (to –20^{o}C) sample stage inside of the cryostat, without addition of embedding solution (see **Note 3**).
11. Tissue sections are made (10-μm thick).

12. Within the cryostat, the room temperature bead substrate is positioned onto the tissue section and briefly pressed using an index finger or an artist's brush handle. This ensures transfer of the tissue from the cryostat surface onto the substrate surface. Using a magic marker, the orientation and perimeter of the tissue section within the bead substrate are marked on the back of the Parafilm M substrate.

13. An ITO-coated glass slide is mounted onto a tall, thin vertical support (the slide box cover works well) with tape, conductive side facing upwards (**Fig. 5.1A**). A digital multimeter can be used to determine which side is conductive. The glass slide box cover is the appropriate shape to support the slide as the stretched substrate is pushed onto the slide. This vertical support enables stretching without having to also hold the glass slide and can be stabilized by placing it between two holders such as large books, as illustrated in **Fig. 5.1A**.

14. The sample is stretched by hand and attached to the ITO-coated slide (**Fig. 5.1B - D**), and the excess Parafilm M is manually torn off of the sides of the slide (*see* **Note 4**). To ease the subsequent process of image reconstruction, the sample should be stretched with the maximum directional uniformity possible. The magic marker label along the perimeter (described above) helps when visually inspecting the sample to ensure it retains gross shape after the stretching process (see **Fig. 5.1**).

5.5.3 MALDI Matrix Application

1. MALDI matrix is applied using the artist's spray brush at an ~25 cm distance from the sample (*see* **Note 5**). The spray brush is washed with pure acetone after use.
2. Water is condensed onto the sample with the condensation chamber at 14°C for 60 s and the sample evaporated at 28°C for 90 s. This cycle is repeated three times for increased analyte extraction, followed by returning the sample to room temperature (*see* **Note 6**).
3. The specimen is loaded into the mass spectrometer. Mass spectral profiling[15] is used to assess the quality of peptide signal received from the specimen before MS imaging of the sample.

5.5.4 Mass Spectrometry and Automated Imaging

1. The glass slide with the stretched sample is loaded into the mass spectrometer. Although a calibration bar is typically used,[18] we determined that regularly-spaced laser-melted holes in the Parafilm M serve as more accurate spatial calibration markers. Provided that the sample is stretched to sufficient thinness, the mass spectrometer's UV laser beam is used to melt several ~100-micrometer diameter holes through the Parafilm M surface at several of the ordered positions found in the "MTP Slide Adapter II" geometry file included in the Bruker FlexControl software. The location of these points should be chosen so that they span the area of the tissue sample; depending on the size of the sample, 3 - 4 points is sufficient.

2. The specimen is unloaded from the mass spectrometer and a transmission mode optical image is taken with a digital camera coupled to an optical microscope. If several optical images are needed to cover the entire area of the sample, the Photomerge function in Photoshop can be used to stitch multiple images together.
3. ImageJ, along with the color threshold plugin, is used to automatically report the pixel coordinates of the beads (*see* **Note 7**). The computational steps for bead identification by thresholding are summarized in **Fig. 5.2A**. The Analyze-->Set Scale function is used to specify the units of the coordinates as pixels. The results of the threshold are viewed by selecting Analyze-->Analyze Particles-->Show Outlines. The circularity and size parameters can be adjusted and the process repeated until the outputted outlines image appears not to be highlighting non-bead regions and irregular shapes.
4. In ImageJ, the pixel coordinates of the center of the melted calibration regions are recorded and the distances between them are calculated using the Cartesian distance formula (*see* **Note 8**). If several equivalent distances can be calculated between the various calibration points, the variations in these distances are averaged (*see* **Note 9**).
5. The coordinates of the calibration points and stretched sample bead positions are entered into an in-house written Java-based application available on the web (*see* **Note 10**). The steps for geometry file creation are summarized in **Fig. 5.2B**.
6. The resulting geometry file is placed in the FlexControl software's geometry files root folder and can be easily found and automatically loaded by the software.

7. The sample is loaded into the mass spectrometer and mass calibration is performed using peptide standards.
8. An AutoXecute sequence is created using the geometry file, specifying an appropriate maximum laser intensity, a value of 100 laser shots per spot, and a 50 Hz repetition rate before starting the MS imaging run.
9. The region of interest is imaged using MALDI-TOF MS.

5.5.5 Data Conversion

1. The data must be converted from the Bruker fid file format to the more general mzXML format. The CompassXport software is run along with the –multiName tag at an MS-DOS prompt to create a file called new.mzXML within each spectrum directory.
2. MATLAB is used along with the bioinformatics toolbox and the batch conversion wrapper code available online (*see* **Note 10)** to convert mzXML files into spectra-containing text files. During this step, the data may be processed by baseline subtraction and smoothing with the Bioinformatics Toolbox functions in MATLAB to eliminate noise and create more uniform ion images.

5.5.6 Image Reconstruction

1. The coordinates of the initial bead positions are found in the same manner as for the stretched sample image, as outlined above in Section 2.4 step 3 (*see* **Note 11**).
2. A simple code (*see* **Note 10**) is compiled in Java and used to create a separate image that places small dots at the initial positions. These dots are easier to see

and aid the free transform process. The computational steps for image reconstruction are summarized in **Fig. 5.2C**.

3. The small dots image and the stretched sample optical images are opened into Photoshop. The free transform command (Ctrl + T) is used to report the centroid coordinates of each of the two images from the options bar. A duplicate background layer is created, and the black background is removed from the small dots image to create a transparent image using the Magic Wand tool in Photoshop. A new blank Photoshop image file is created, large enough (in the range of 5000 pixels × 5000 pixels) to hold both images when placed side-by-side in separate layers, allowing adequate work space to manipulate the images when aligning on top of each other. The small dots image must be placed in a layer above the stretched image layer. The new centroid positions of each image in the blank image file are recorded from the options bar. The free transform command is used to translate, rotate, and resize the small dots image until it is appropriately aligned on top of the stretched sample image. The small dots should each align within one of the bead-torn regions of the stretched sample image.
4. Before applying the transformation to the transformed images in Photoshop, the final width, height, and rotation angle are recorded into a text file from the Info palette, along with the final centroid position of each image.
5. The text files of the initial positions and the image reconstruction parameters, recorded both before and after the free transformation, are inputted into another in-house Java program (*see* **Note 10**) to create reconstructed ion images at select

m/z ratios of interest as seen in **Fig. 5.3** (*see* **Note 12**). The example shown in **Fig. 5.3** is with a thin tissue section from mouse pituitary.

5.6 Notes

1. Optionally, Parafilm M may be soaked for 1 h in either acetic acid (100%) or ammonium hydroxide solution (28.8 %) to soften the film.[19] After drying, this treatment allows the film to be stretched by a greater degree into a ~7-fold increase in each dimension. Use of the more elastic film results in formation of small, concentrated droplets of solution upon matrix application with less spatial spreading. In addition, soaking can reduce polymer signals resulting from the Parafilm M.
2. If only performing mass spectral profiling without imaging on stretched samples, as described in reference,[15] this step and the steps related to image reconstruction and geometry file creation can be omitted.
3. Most embedding media interferes with obtaining good signals in mass spectrometry investigations. One exception to this is embedding of tissues in low melting point agarose gel blocks or gelatin. It was found that a block of solidified saturated agarose solution that is freeze-mounted onto the dissection stage, followed by sectioning through the top layers of the gel, creates a flat surface for better freeze-mounting and orienting of the tissue.
4. For mass spectrometry imaging, it is important to prevent the tissue from completely drying as this will cause bead clumping and may reduce incorporation of analyte into the MALDI matrix crystals. Excess sample drying is prevented by

immediately applying MALDI matrix after stretching while the tissue is still partially wet. Thus, if more than one section is to be taken from the tissue, these sections are sectioned with the microtome after immediately applying MALDI matrix to the preceding stretched section.

5. A larger sprayer-to-sample distance helps in not over-wetting the sample, as larger (~0.5 mm) droplets can cause spreading, even in a stretched sample. A light microscope can be used to monitor the drying process, so that the sample is completely dry before the next spray application. The light microscope also helps to visually monitor the amount of matrix applied. Generally, several spraying-drying cycles over 10 - 20 min is sufficient. Alternatively, matrix application can be done by capillary deposition to control the size of the matrix spots and prevent the spatial redistribution of analytes.[19]
6. The solvent condensation/MALDI matrix recrystallization procedure has shown the ability to improve mass spectra quality by reducing the number and intensity of inorganic salt ion adducts typical for traditional MS imaging sample preparations. This reduction in potassium and sodium salt adducts creates less complex mass spectra.[20]
7. The success rate of the bead position identification depends on the quality of the optical images. Transmission-mode images are easier to threshold for bead positions as they appear brighter than the background Parafilm M.
8. As the FlexControl “MTP Slide Adapter II” geometry file uses a fractional distance coordinate system where the distance between each point in the regular

array is separated by exactly 0.086957 units, a new geometry file can be created in this coordinate system to acquire data at the bead positions.

9. Variations in the distances between calibration points that are larger than bead diameter signify inaccuracies in the optical image of the stretched sample such that the resulting geometry file may not accurately represent the bead positions. Inaccuracies sometimes occur because of errors in stitching of images by Photoshop and can be prevented by taking well-focused images with sufficient spatial overlap.
10. All in-house written Java software is available online, along with an example dataset with step-by-step instructions, at http://neuroproteomics.scs.uiuc.edu/imaging.html.
11. Alternatively, image reconstruction can be done before geometry file creation so that some time is saved in the rare event that image reconstruction is not successful, upon which the sample is discarded. Any difficulties with image reconstruction using the free transform approach arise from highly non-uniform stretching of the Parafilm M that can be prevented by visually adjusting for shape of the marked perimeter of the sample while stretching. Overall, image reconstruction is fairly reproducible, as a set of six samples resulted in a classification rate of 84.1% for bead position matching between the stretched and initial samples, with the remaining portion being only near-neighbor mismatches.[18]
12. The success of image reconstruction can be verified using an in-house written code (http://neuroproteomics.scs.uiuc.edu/imaging.html) that plots an image of

the calculated transformed initial positions. This image can be checked against the transformed image in Photoshop to verify for any calculation or positional errors.

5.7 Figures

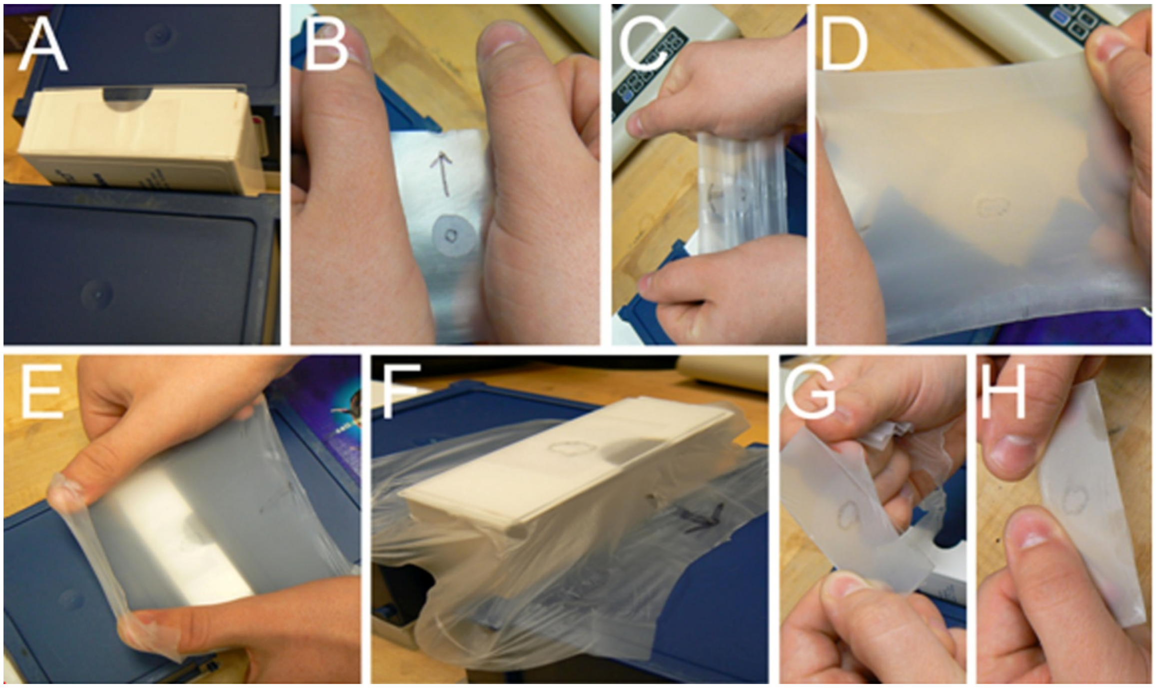

Figure 5.1. Manual stretching of the sample. (A) An apparatus holds the sample, so that both hands can be used during stretching; here this device consists of the glass slide (arrow) taped to the thin side of the slide box cover, laterally stabilized by heavy objects. (B) The bead substrate, with the location and orientation of the tissue marked, is manually stretched along one axis, (C) rotated 90 degrees and stretched, and (D) rotated and stretched again. (E) The stretched membrane is placed so that the marked sample area is on the glass slide. Use of thumbs provides a last bit of stretching before the sample is applied to the surface. (F) The arrow marking the orientation of the sample is clearly visible after stretching and can be marked again on the area of the glass slide if necessary. (G) The excess Parafilm M is removed from the edges of the glass slide. (H) A finished alide ready for matrix coating.

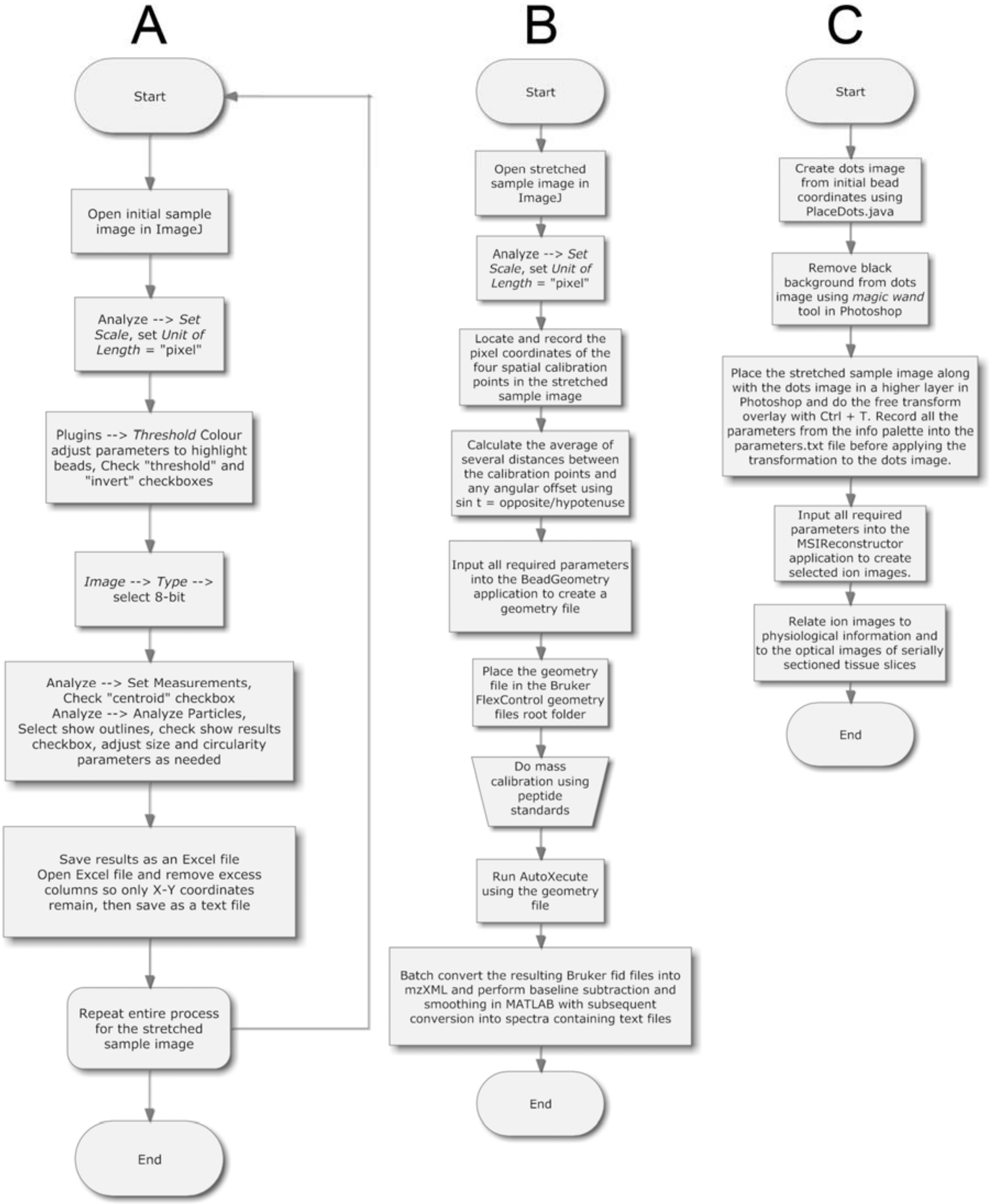

Figure 5.2. Flow chart for the computational steps in the stretched imaging method, including the process of (A) bead identification by light thresholding, (B) geometry file creation, and (C) image reconstruction. The custom software routines can be found online at http://neuroproteomics.scs.uiuc.edu/imaging.html.

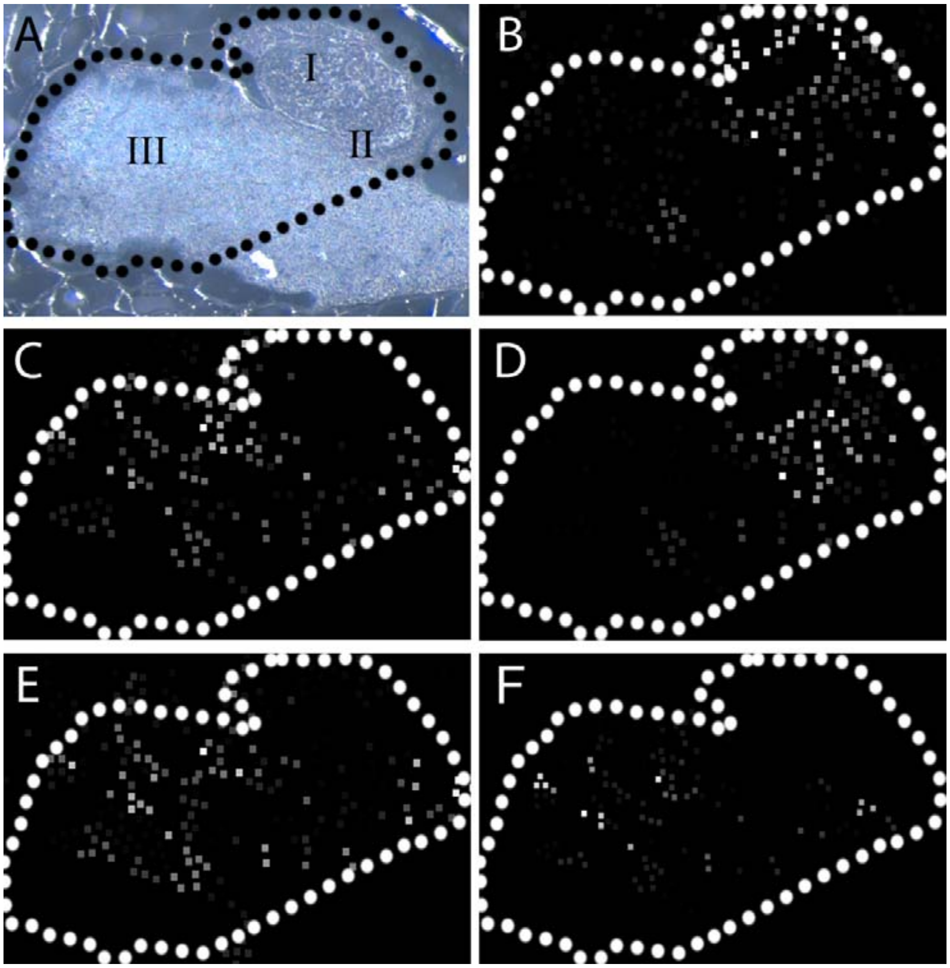

Figure 5.3. Reconstructed MALDI-MSI ion images from a 10-μm section of mouse pituitary prepared with the stretched sample method. (A) Optical photomicrograph of the pituitary section showing (I) the posterior lobe, (II) a darker band corresponding to the intermediate lobe, and (III) the anterior lobe. Only the outlined region tissue was imaged. Reconstructed ion images correspond to the outlined tissue area showing: (B) oxytocin, 1007 *m/z*; (C) di-Ac-α-MSH, 1707 *m/z*; (D) vasopressin, 1083 *m/z*; (E) POMC J-peptide, 1883 *m/z*; and (F) Arg-CLIP [1-22], 2505 *m/z*. The intermediate lobe is a small band that is highlighted by signals from the di-acetylated-α-MSH and J-peptide ion images.

5.8 References

1. Seeley, E. H. and Caprioli, R. M. Molecular imaging of proteins in tissues by mass spectrometry. *Proc. Natl. Acad. Sci. USA* **2008,** *105*, 18126-18131.
2. McDonnell, L. A. and Heeren, R. M. Imaging mass spectrometry. *Mass Spectrom. Rev.* **2007,** *26*, 606-643.
3. Pacholski, M. L. and Winograd, N. Imaging with mass spectrometry. *Chem. Rev.* **1999,** *99*, 2977-3006.
4. Rubakhin, S. S., Jurchen, J. C., Monroe, E. B., and Sweedler, J. V. Imaging mass spectrometry: Fundamentals and applications to drug discovery. *Drug Discov. Today* **2005,** *10*, 823-837.
5. Becker, J. S., *Inorganic mass spectrometry: Principles and applications* (John Wiley & Sons, Chichester, England ; Hoboken, NJ, 2007), p. 496.
6. Lemaire, R., Menguellet, S. A., Stauber, J., Marchaudon, V., Lucot, J.-P., Collinet, P., Farine, M.-O., Vinatier, D., Day, R., Ducoroy, P., Salzet, M., and Fournier, I. Specific MALDI imaging and profiling for biomarker hunting and validation: Fragment of the 11s proteasome activator complex, reg alpha fragment, is a new potential ovary cancer biomarker. *J. Proteome Res.* **2007,** *6*, 4127-4134.
7. Chandra, S., Tjarks, W., Lorey, D. R., 2nd, and Barth, R. F. Quantitative subcellular imaging of boron compounds in individual mitotic and interphase human glioblastoma cells with imaging secondary ion mass spectrometry (SIMS). *J. Microsc.* **2008,** *229*, 92-103.
8. Chaurand, P., Norris, J. L., Cornett, D. S., Mobley, J. A., and Caprioli, R. M. New developments in profiling and imaging of proteins from tissue sections by MALDI mass spectrometry. *J. Proteome Res.* **2006,** *5*, 2889-2900.
9. Chaurand, P., Rahman, M. A., Hunt, T., Mobley, J. A., Gu, G., Latham, J. C., Caprioli, R. M., and Kasper, S. Monitoring mouse prostate development by profiling and imaging mass spectrometry. *Mol. Cell. Proteomics* **2008,** *7*, 411-423.
10. Hsieh, Y., Chen, J., and Korfmacher, W. A. Mapping pharmaceuticals in tissues using MALDI imaging mass spectrometry. *Pharmacol. Toxicol. Methods* **2007,** *55*, 193-200.
11. Rubakhin, S. S., Hatcher, N. G., Monroe, E. B., Heien, M. L., and Sweedler, J. V. Mass spectrometric imaging of the nervous system. *Curr. Pharma. Des.* **2007,** *13*, 3325-3334.

12. Chaurand, P., Norris, J. L., Cornett, D. S., Mobley, J. A., and Caprioli, R. M. New developments in profiling and imaging of proteins from tissue sections by MALDI mass spectrometry. *J. Proteome Res.* **2006,** *5*, 2889-2900.

13. Kruse, R. and Sweedler, J. V. Spatial profiling invertebrate ganglia using MALDI MS. *Am. Soc. Mass Spectrom.* **2003,** *14*, 752-759.

14. Aerni, H. R., Cornett, D. S., and Caprioli, R. M. Automated acoustic matrix deposition for MALDI sample preparation. *Anal. Chem.* **2006,** *78*, 827-834.

15. Monroe, E. B., Jurchen, J. C., Koszczuk, B. A., Losh, J. L., Rubakhin, S. S., and Sweedler, J. V. Massively parallel sample preparation for the MALDI MS analyses of tissues. *Anal. Chem.* **2006,** *78*, 6826-6832.

16. Clerens, S., Ceuppens, R., and Arckens, L. Createtarget and analyze this!: New software assisting imaging mass spectrometry on bruker reflex IV and Ultraflex II instruments *Rapid Commun. Mass Spectrom.* **2006,** *20*, 3061-3066.

17. Decker, J. D. Image editing. *Am. J. Orthod. Dentofacial Orthop.* **2004,** *125*, 215-219.

18. Zimmerman, T. A., Monroe, E. B., and Sweedler, J. V. Adapting the stretched sample method from tissue profiling to imaging. *Proteomics* **2008,** *8*, 3809-3815.

19. Wang, J., Chen, R., Ma, M., and Li, L. MALDI MS sample preparation by using paraffin wax film: Systematic study and application for peptide analysis. *Anal. Chem.* **2008,** *80*, 491-500.

20. Monroe, E. B., Koszczuk, B. A., Losh, J. L., Jurchen, J. C., and Sweedler, J. V. Measuring salty samples without adducts with MALDI MS. *Int. J. Mass Spectrom.* **2007,** *260*, 237-242.

CHAPTER 6

MALDI MASS SPECTROMETRIC IMAGING OF NEURONAL CELL CULTURES

6.1 Notes and Acknowledgements.

The co-authors on this chapter are Stanislav S. Rubakhin and Jonathan V. Sweedler. The authors thank C. Mark Bee, Sergei Dikler, Scott J. Robinson, and Kevin R. Tucker for discussions and experimental assistance. The project described was supported by Award No. P30 DA018310 and Award No. 5RO1DA017940 from the National Institute On Drug Abuse and Award No. 5RO1DE018866 from the National Institute of Dental and Craniofacial Research (NIDCR) and the Office of Director (OD), National Institutes of Health (NIH).

6.2 Abstract

Mass spectrometry imaging (MSI) provides both chemical and spatial information for a broad range of analytes from a variety of sample types. Here, matrix-assisted laser desorption/ionization (MALDI) MSI using the stretched imaging method allows characterization of cultures of *Aplysia californica* neurons grown on an array of glass beads embedded in a stretchable layer of parafilm M. After growth, the membrane containing the cultured neurons is stretched to physically isolate the beads/neurons. The sample stretching procedure provides several advantages compared to direct imaging including increased analyte signal and MALDI matrix extraction time without analyte spreading between the physically separated beads. MALDI MS/MS imaging of using the stretched imaging method maps both parent and fragment ions of *A. californica* pedal

peptide from cultured neurons, thereby simultaneously obtaining information on its location and identity. Both optimized protocols and improved software for image reconstruction enable targeted MSI studies over a wide range of cells types and culture conditions.

6.3 Introduction

Cell cultures are widely used in fundamental,[1,2] applied,[3, 4] and clinical/diagnostic [5-7] sciences. Detection of known and unknown endogenous analytes and determination of their levels at the cellular and subcellular resolution aid many experiments involving cell cultures. As with biological tissues, analyte detection in cell cultures includes a variety of targeted approaches such as immunocytochemistry[8] and molecular information-rich spectroscopic approaches such as infrared spectroscopy[9,10] and mass spectrometry (MS).[11, 12] Each of these approaches has its own benefits and drawbacks. Some, e.g. immunochemistry, require preselection of analytes of interest. In contrast, MS allows analyte identification for a range of analytes but does not provide spatial/localization information. However, spatial information can be obtained from cell cultures by combining mass spectrometry with imaging.

Mass spectrometry imaging (MSI) has emerged as a powerful tool for investigation of biological specimens as it simultaneously provides chemical and spatial distribution information on many analytes without the need for preselection of an analyte of interest[13-18] Perhaps the first MSI technique to be used to analyze cultured cells was secondary ion mass spectrometry (SIMS) imaging.[19] SIMS imaging is capable of investigating chemically complex surfaces such as tissue slices or cell cultures with submicron spatial resolution.[20-28] Unfortunately, the mass range of SIMS limits its ability to detect peptides and proteins. Matrix-assisted laser desorption/ionization MSI (MALDI MSI) extends the mass range and is well positioned for localizing larger analytes from cultured cells,[29-32] as are several other laser desorption approaches.[33, 34] Adding spatial information, MALDI MSI has also been used for imaging cultured cells.[35, 36] In MALDI MSI, data acquisition is often done using an ordered array of positions to add spatial information and to allow the creation of 2D ion distribution maps,[37] although other data acquisition approaches are possible.[38-40]

Issues for obtaining single cell resolution from MALDI MSI investigations of peptides include the biochemical complexity of cell cultures, the close and random proximity of adjacent cells, significant differences in peptide content among neighboring cells, and the possibility of mechanical damage to cells during removal of extracellular media. We address several of these challenges by using the a sample preparation technique called the stretched imaging method,[41-43] which has been applied to characterize peptide distributions in tissue slices. In this approach, a thin tissue slice is placed onto a hexagonally packed monolayer beads embedded in a stretchable layer of Parafilm M. The substrate is stretched and, as the beads separate from each other, the tissue is fragmented into thousands of spatially and chemically isolated bead islands that contain one or a few cells.[42] This separation of the cells allows small, chemically isolated samples to be characterized while at the same time allowing increased analyte extraction from the tissue using more MALDI matrix contact time, therefore providing enhanced analyte signals. The hydrophobic nature of the intervening membrane after stretching between bead/cell positions prevents analyte migration upon the application of MALDI matrix with extended extraction periods.[37] The stretched imaging protocol thus reduces several challenges outlined above for MALDI MSI experiments.

Here we create MSI images from cultured neurons. The *Aplysia* neurons used here have well characterized peptide contents[41, 44, 45] and allow protocol validation; obviously, future applications will involve less well-characterized samples. Besides the abilities of MSI to generate chemical and spatial information from analytes in cell cultures, adding the ability to do tandem MS (MS/MS) *de novo* sequencing. In MALDI MSI, it is sometimes difficult to generate enough peptide signal for a peak in MS mode from a single cell[46] so that the peptide fragments in MS/MS mode have sufficient intensity to allow *de novo* amino acid sequencing. The stretched imaging protocol allows greater extraction of analyte signal and sufficient signal was observed using this approach to allow MS/MS sequencing. So, the stretched imaging method is further adapted here to provide both MS and MS/MS reconstructed ion images of high quality from *Aplysia* neuronal cultures. The ability to provide chemical, spatial, and amino acid sequence information from an automated image acquisition makes the newly adapted stretched imaging method well suited for the study of cell cultures from a variety of model organisms.

6.4 Experimental

6.4.1 Substrate Creation and Cell Isolation

Substrates that contain a hexagonally-packed layer of glass beads embedded in a Parafilm M layer (Pechiney, Neenah, WI) were created as in a previous manner,[42] but the ~40 µm glass beads (Mo-Sci Corp., Rolla, MO) were made from borosilicate instead barium/titanium as used previously. The borosilicate beads on the substrate were coated with poly-L- or poly-D-lysine. Individual neurons were isolated from the *Aplysia* central nervous system after enzymatic treatment and placed onto the bead substrate. The cell culture was allowed to develop overnight at 14^{o}C in artificial sea water (ASW) containing (in mM): 460 NaCl, 10 KCl, 10 $CaCl_2$, 22 $MgCl_2$, 6 $MgSO_4$, and 10 *N*-2-hydroxyethylpiperazine-*N′*−2-ethanesulfonic acid (HEPES) (pH 7.8)[42] supplemented with antibiotics: 100 units/mL penicillin G, 100 μg/mL streptomycin, and 100 μg/mL gentamicin and a saturated concentration of amphotericin B. Reagents used in the study were from Sigma-Aldrich, St. Louis, MO except where specifically noted.

6.4.2 Sample Preparation for Scanning Electron Microscopy

Although we attempted to study our cell cultures using light microscopy, difficulties of visualizing small features of neurons cultured on bead arrays hampered such efforts. Thus, environmental scanning electron microscopy (ESEM) was employed to image cultured cells on the bead array. For ESEM, cell cultures were fixed using 4 h treatment with a mixture of 2.5% glutaraldehyde and 2% paraformaldehyde in 0.1 M sodium cocadilate buffer. The samples were then washed for 15 min in 0.1 M sodium cocadilate buffer and dehydrated in a series of 37%, 67%, 95%, 100% ethanol solutions. A Samdri-PVT-3D critical point dryer (Tousimis Research Corp., Rockville, MD) was employed for ethanol removal from the samples. During this process the cool valve was opened and the samples were cooled to 0 ^{o}C followed by purging of ethanol and replacement with liquid CO_2. The heat was turned on and the sample was heated to above the critical temperature at 31 ^{o}C and pressure at 1072 psi for CO_2. The pressure was purged slowly over 9 min to 351 psi, followed by further release of pressure until equilibration with atmospheric pressure. The samples were removed and placed onto two sided tape (3M Corporation, St. Paul, MN) and this was mounted onto a sample stage. A Desk II Turbo Sputter Coater (Denton Vacuum, Moorestown, NJ) was used to coat the samples with Au/Pd for 65 s. The samples were then placed in a desiccator overnight. Environmental scanning electron microscopy (ESEM) images were taken with an XL30-ESEM-FEG (FEI, Hillsboro, OR) scanning electron microscope that includes a field-emission electron gun.

6.4.3 Sample Preparation for Mass Spectrometry Imaging

The cell cultures on bead substrates were stabilized for 10-20 min by replacement of ASW with 33% glycerol: 67% ASW solution, followed by removal of this extracellular media. A small amount of the glycerol/ASW solution remained on the sample which is acceptable for MALDI MS detection of peptides. The directional orientation of the sample before stretching was marked with a magic marker. Optical images of the sample were taken (Leica Microsystems, Bannockburn, IL) and followed by manual stretching of the samples and placing it onto conductive indium tin-oxide (ITO)-coated glass slides as previously reported.[41] These glass slides were inserted into a Bruker MTP Slide Adapter (Bruker Daltonics, Billerica, MA). For the samples used for acquiring MS/MS images, these samples were instead stretched and placed onto a metal TLC MALDI plate (Bruker Daltonics).

Application of the MALDI matrix solution immediately followed. The MALDI matrix of 30 mg/mL of 2,5-dihydroxybenzoic acid (DHB) (Sigma-Aldrich, St. Louis, MO) in 50:50 methanol/water was applied to the surface of the stretched samples using an artist's spray brush (Thayer & Chandler, Kenosha, WI) at a distance of ~30 cm as in a manner previously reported.[47] In the case where samples were placed on ITO slides, after matrix application a blade is used to remove Parafilm M from the surface near the edges of the glass slide to improve electrical contact to the metal MTP Slide Adapter (Bruker Daltonics). Optical images were taken of all samples after stretching. In the case of multiple images being needed for capture of the entire sample area, these subsidiary images were stitched together using Photoshop CS2 software (Adobe Systems, San Jose, CA).

6.4.4 Mass Spectrometry Imaging of Stretched Samples

The bead positions after sample stretching were automatically found as in a previous manner by light thresholding.[41] In the case of samples on ITO slides, the in-house written Java-based (http://java.sun.com) geometry file creation code as previously described was used to create sample-tailored geometry files. This bead geometry file creation code was then altered to make geometry files that correspond to the Bruker TLC Plate metal target geometry. This adapted code was then used to create appropriate geometry files for samples that had been placed on the Bruker TLC Plate target. The original and modified source codes are freely available at http://neuroproteomics.scs.illinois.edu/imaging.html.

Mass spectrometry was automated using the geometry files loaded into the AutoXecute feature of FlexControl 3.0 software (Bruker Daltonics) on an UltrafleXtreme MALDI TOF-TOF MS instrument (Bruker Daltonics). For samples on ITO glass slides, at each position 100 spectra accumulated at 1000 Hz using a mass range of 600-4000 Da.

For samples on the solid metal target, 100 spectra accumulated at each point and 400 spectra accumulated in Bruker LIFT mode (MS/MS) at 1000 Hz at points for which peaks were automatically selected by the software for MS/MS acquisition. Parent ion peaks were automatically selected by the software for acquisition of MS/MS spectra in LIFT mode using the parameters of a FlexAnalysis (Bruker Daltonics) method loaded into AutoXecute in the Bruker FlexControl 3.0 software. These thresholds were set at an intensity of greater than 400 counts and a signal/noise of better than 10. Mass calibration was done with Peptide Calibration Standard II (Bruker Daltonics). For the sample on the glass slide presented here, the entire area of the sample that included about 1,200 in total beads was imaged and this took about 40 min. For the sample on the metal target, the bead positions both before after stretching were not found by light thresholding, but instead the positions of the cells were manually located and their pixel coordinates recorded. Thus, the time to acquire MS and MS/MS spectra from a total of 28 positions was 6 min.

The spectra in Bruker fid files were baseline subtracted, smoothed, and converted into spectra-containing text files using a batch conversion script written in FlexAnalysis 3.3 software (Bruker Daltonics). The spectra-containing text files are then able to be read by the in-house written image reconstruction Java-based software.[41] For all samples, the image reconstruction code as previously described[41] was used to create selected MS ion images based on the *m/z* ratio of the analyte of interest. For the samples on the metal target, this image reconstruction code was modified to produce MS/MS ion images based on both *m/z* ratios of the parent ion and the fragment ion of interest. The image reconstruction portion of the code was unaltered but the portion that creates ion images was adapted to produce reconstructed MS/MS ion images. This code is freely available at http://neuroproteomics.scs.illinois.edu/imaging.html.

Results of tandem MS for the peptide parent ion at *m/z* 1540 were analyzed by BioTools 3.0 (Bruker Daltonics) where the assignment of the amino acid sequence was automatically generated and searched against a peptide database using Mascot software (Matrix Science Inc., Boston, MA) revealing the identity of the peptide.

6.5 Results and Discussion

Using, MALDI MSI, different types experiments can be devised where neuronal cultures of neurons from different regions of the CNS can form networks. Then, the ability of MALDI-MSI with the stretched imaging method to investigate stretched samples of neuronal cell cultures at cellular, and eventually at the subcellular, level will provide details on peptide distributions and their changes during the formation of networks. Such results will shed light onto network formation and repair, as well as changes in the distributions of peptides.[30, 48, 49] However, to enable such stretched imaging experiments, several protocol enhancements are necessary such as the use of lysine-coated borosilicate beads so that the cells attach properly to the substrate, the use of a metal MALDI target to reduce charging and enable MS/MS imaging, the verification of cell-bead attachment for cultured neurons, and the improved software for automated runs of MS and MS/MS imaging. The improvements are first described below followed by an application of the stretched imaging method to a stretched sample of cultured *Aplysia* neurons to create reconstructed ion images showing distributions of peptides and fragment peptides.

The use of a borosilicate glass bead substrate coated with poly-L- or D-lysine placed onto a Parafilm M layer provides an improved substrate for neuronal growth. In creating the bead substrate, we find that *Aplysia* neurons detach shortly after plating from the barium/titanium glass beads previously used with the stretched sample method with ~20-µm-thick tissue sections.[41, 42] However, the cultured neurons remain attached to substrates made with poly-L- and poly-D-lysine coated ~40 µm borosilicate glass beads, an expected result given the use of borosilicate[50-52] and lysine coating[53, 54] for neuronal cell culture. Besides the composition of the substrate, the relatively uniform three-dimensional surface of the bead monolayer with patterned topography is ideal the cells to attach and grow. The extending processes of cultured neurons respond favorably to topographic cues[55-57] and so the effects of growing on beads is expected to enhance neuronal growth. It was necessary to verify that the cultured cells are attaching to the beads when using this new type of bead substrate.

The attachment of cells to the beads allows successful fragmentation of either tissue samples or neuronal cultures upon stretching of the underlying support membrane. We found it difficult to visualize the attachment of individual neurons and their processes to beads using optical microscopy; thus, here environmental scanning electron microscopy (ESEM) is employed. ESEM can reveal small features such as neurites and growth cones in such cultures. ESEM investigation shows that the curved topography of the lysine-coated borosilicate bead monolayer provides a suitable substrate along which cultured *Aplysia* neurons extend their processes (see Fig. 6.1). In Fig. 6.1A, the neuron and its neurites are well attached to the beads. There are extending zones of adhesion atop the beads including a growth cone-like structure terminating the neurites. The neurites oftentimes cover multiple beads with many smaller extensions (filopodia), with some forming fine submicrometer bridges to neighboring beads. Intriguingly, the neurites that span the gaps between beads do so at positions where the beads were not touching, indicating these outgrowths likely "jumped" from bead to bead. Small ~2 μm enlargements in the processes, often termed varicosites[58] (putatively containing secretory vesicles) have been detected along the smallest branches that stem off from the main processes (Fig. 6.1B). Manual sample stretching separates adjacent beads and cells, and may also separate the neurite and the varicosities from the cell body during the stretch. While single cell measurements are possible as no more than a single cell appears on a most beads, subcellular MALDI MSI measurements may also be possible from these samples.

For the application of the stretched imaging method to MALDI MSI, here *Aplysia* neurons from pedal and cerebral ganglia were cultured onto bead arrays. An optical image was taken of the substrate and cell cultures before stretching (Fig. 6.2A). Several spherical cell bodies are visible in the image with some neurons located in close proximity to each other. Fig. 6.2B,C overlays the reconstructed ion images onto the initial sample image, and shows minimal analyte migration and that the ion signals are confined to the area of cell somas. Extended signal localization can be explained by cellular outgrowth to neighboring beads and seldom by bead clumping (where several beads stay adjacent after stretching).

How are peptide identifications made? Observed MS peaks of peptides from the MSI image can be identified using tandem MS after they have been tentatively assigned based on their *m/z* compared to lists of known peptides and from colocalization with other signals known to colocalize such as multiple peptides derived from the same prohormone. An MS spectrum taken from a stretched sample of cultured neurons is shown in Fig. 6.3. The culturing media contains high salt levels, and so analyte-salt adducts can be observed; if desired, these can be minimized via a condensation chamber that slowly condenses water onto the sample surface causing physiological salts to crystallize separately from analyte and reducing salt adducts in the mass spectra.[59] Not surprisingly given the source of the neurons, a high intensity peak corresponding to the *m/z* of pedal peptide[60] is observed (see Fig 6.3).

The ability to identify peptides by tandem MS sequencing allows peak assignments to be confirmed.[61-63] Several adjustments in the method enable MALDI-MS/MSI sequencing from stretched samples of cultured neurons, such as the use of a metal MALDI target and adapting the stretched imaging software to enable automated MS/MS imaging runs. Use of a metal MALDI target had previously been unnecessary, as the stretched imaging method to tissue sections used glass slides with a conductive indium tin-oxide coating.[41] The ITO slides even allowed peptide signals to be detected from stretched neuronal cultures (Fig. 6.2). However, these supports were found to be less efficient for the automated acquisition of tandem MS spectra. Attempts to acquire MS/MS spectra from stretched samples on ITO slides reproducibly led a large instability in the accuracy of parent ion *m/z* measurements. Shifts of up to 30 Da of the *m/z* ratio were observed, even after increasing the sample conductivity with a thin metal coating, thus preventing automated ion fragmentation. By placing the stretched sample onto a solid metal Bruker TLC MALDI plate, these issues were eliminated, possibly because of increased electrical conductivity and improved heat dissipation of the solid metal target.

The geometry file creation and image reconstruction software, as previously used for imaging of stretched thin tissue sections,[41] has been adapted for MS/MS imaging of stretched samples containing cultured neurons. Before adapting the software, light thresholding is used with optical images to automatically determine X-Y coordinates of beads, with this information used to create a geometry file that determines the location where spectra are collected.[41] The metal MALDI plate used for MS/MS imaging of samples prevents optical imaging of the stretched samples in transmission mode, however light thresholding for the creation of geometry files is possible using reflection-based optical images. In adjustment of the software, the geometry file creation software was modified from its previous application with glass slides and the Slide Adapter to the new geometry of the solid metal Bruker TLC plate. The software has been designed to be adapted to a range of other geometries. In addition, acquisition of MS/MS spectra from the specified locations precedes image reconstruction with the free transform process.[41] However, the image reconstruction code also had to be altered for the reconstruction of MS/MS ion images and to be able to read data effectively from MS/MS spectra from the Bruker in LIFT mode. This software is freely available online at: http://neuroproteomics.scs.illinois.edu/imaging.html.

To apply the MSI and MS/MSI capabilities of the stretched sample method, custom geometry files were used to automate the acquisition of MS/MS spectra from a number of stretched samples of cultured *Aplysia* neurons that were placed onto the solid metal MALDI plate, as shown for the parent mass ion of *m/z* 1540 (Fig. 6.4A). This MS/MS spectrum was taken from an automated imaging run and is labeled with *de novo* peak assignments generated by Bruker BioTools 3.0 software. Most peaks correspond to fragments of *Aplysia* pedal peptide. Loading of the results into a Mascot search engine produced a hit with a highest Mascot score of 112 for *Aplysia* pedal peptide. The quality of the MS/MS spectra automatically acquired from single cells using the stretched imaging method allows for sequencing and identification of peptides with high confidence from a sample of cultured neurons. In addition, the distributions of the parent peptide and its fragment peptides are able to be simultaneously mapped.

Reconstructed MALDI-MS/MS ion images from a stretched sample of cultured neurons are shown in Fig. 6.5. As the stretched imaging method was used to acquire MS images of the entire sample (Fig. 6.2), here selected regions were imaged to obtain MS and MS/MS ion images. Because the locations of the neurons were easily visible in optical images taken both before and after stretching, the locations of the cultured neurons in the optical images before and after stretching were first recorded. Subsequently, a geometry file containing only these cell positions was used to guide the acquisition of MS and MS/MS mode ion images only at bead locationsA similar approach can be applied for characterization/imaging of specific peptide(s) of interest after an MS imaging run of an entire sample by first manually creating a mass list of detected peptides with corresponding spatial coordinates and then optimizing the MS/MS parameters and PCIS window for the analyte(s) of interest for the subsequent MS/MS imaging scan. An advantage to only imaging from the beads that contain neurons (and not empty beads or membrane) is large reductions in image acquisition time and subsequent data. MALDI-MSI using this platform does not allow rapid transitions from MS mode to MS/MS mode. Therefore, independent scans in MS and MS/MS modes are automated in tandem thus increasing the time for complete MS imaging and analyte identification. Depending on the needs of the experiment, sample locations containing peptides of interest can be examined in the manual, semiautomatic, or automatic mode. Yet another alternative is to locate cells with the first scan in MS mode and then to perform MS/MS imaging on only the cell locations. This eliminates the necessity of running a second MS imaging experiment in MS/MS mode.

Fig. 6.5A shows a reconstructed ion image in MS mode for the parent ion of *m/z* 1540 that corresponds to pedal peptide with the sequence of PLDSVYGTHGMSGFA. Based on the quality of the MS mode peaks from the different positions of the sample-tailored geometry file, the AutoXecute feature of the Bruker FlexControl software automatically selects position/peak combinations for acquisition of MS/MS spectra occurring after the MS scan is finished. Here thresholds for MS/MS acquisition were set so that the peak intensity must be higher than 400 counts and the signal/noise greater than 10. The spatial distributions for two fragment ions corresponding to the parent ion at *m/z* 1540 are shown in Fig. 6.5B, *m/z* 419, corresponding to the amino sequence PLDS with loss of ammonia and Fig. 6.5C, *m/z* 1245, corresponding to the sequence PLDSVYGTHGMS with loss of water. Not all of the neurons in this sample satisfied the signal quality requirements to produce MS/MS spectra from the parent ion of *m/z* 1540, but the thresholds can be easily changed. Of course, some of the neurons used here did not contain appreciable amounts of pedal peptide and so were not selected for MS/MS imaging. Similarly, the fragment ion distributions for a separate unidentified parent ion mass of *m/z* 1200 are shown in Fig. 6.5E and F.. This unknown compound is difficult to fragment and MS/MS sequencing resulted in generation of only a few fragments. We have not identified this analyte although the spatial distributions of the parent and fragment ions have been obtained. Obtaining the spatial distributions of fragment ions allows detection and identification of the products of cell specific enzymatic processing that often varies spatially even among neighboring neurons.[64] The stretched imaging method is adaptable to studying neuronal network formation and repair in a range of culturing conditions and from a variety of other model organisms.

6.6 Figures

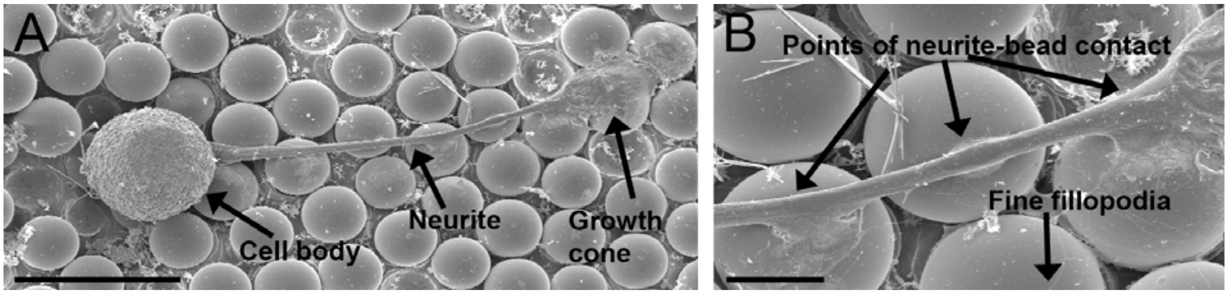

Figure 6.1. Environmental scanning electron microscopy (ESEM) images of a sample before stretching. (A) A cultured neuron is attached to beads that are embedded in a layer of Parafilm M. The neuronal process extends away from the cell body over the length of several beads. The critical point drying procedure caused some beads to be removed from the sample surface. The cell body, extending neurite, and growth cone are labeled. Scale bar is 100 µm. (B) A close up view of the center region of the left image. The neuronal process that is well attached to the beads may break apart from the cell body upon manual sample stretching, which may allow for subcellular analysis. The points of neurite-bead contact and the fine fillopodia are labeled. Scale bar is 20 µm.

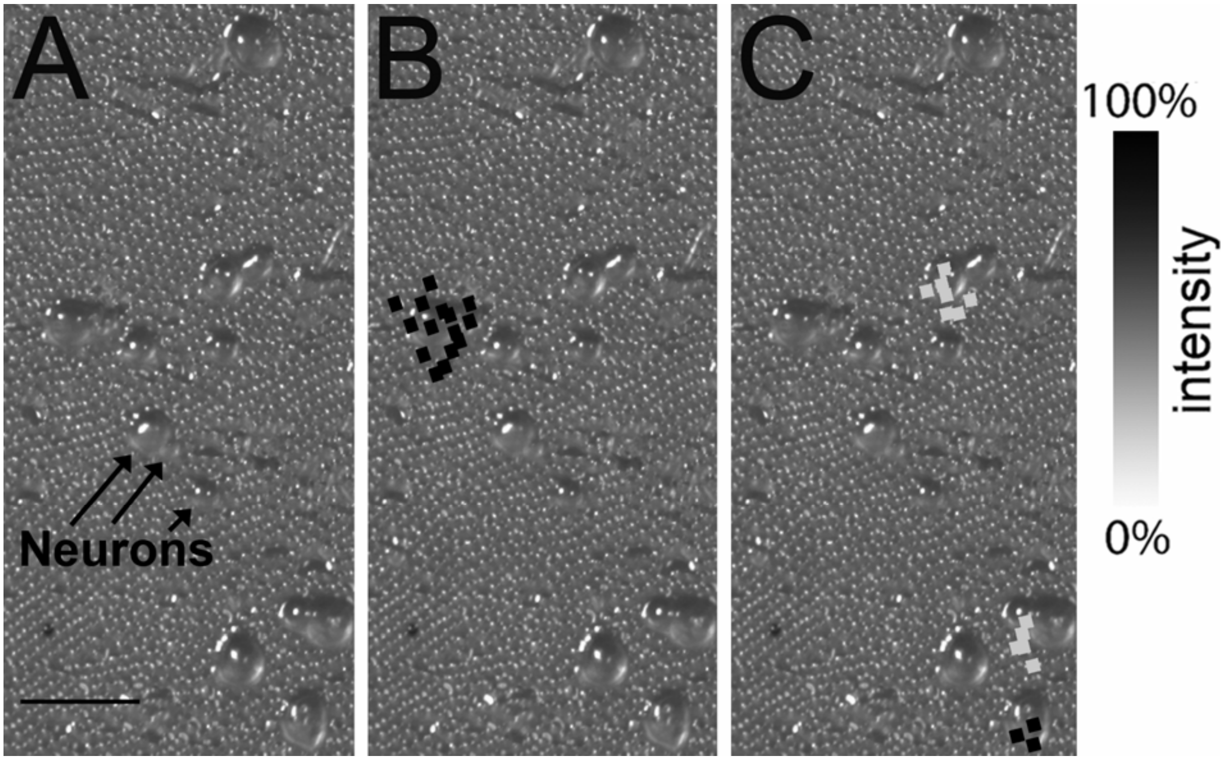

Figure 6.2. Reconstructed ion images created by the stretched imaging method from a sample of *Aplysia* cultured neurons from different CNS ganglia. About 1200 total beads were analyzed. (A) The initial sample image is an optical image showing the cultured neurons on a substrate of borosilicate glass beads embedded in a Parafilm M layer. Analyte distributions are shown in the reconstructed ion images in panels (B) *m/z* 1238 and (C) *m/z* 1540 that are assigned putative identities of FRFa peptide and pedal peptide, respectively. The intensity is scaled to the maximum intensity in each image for each analyte. The analyte distributions are confined to individual cultured neurons in many cases. Scale bar is 500 µm.

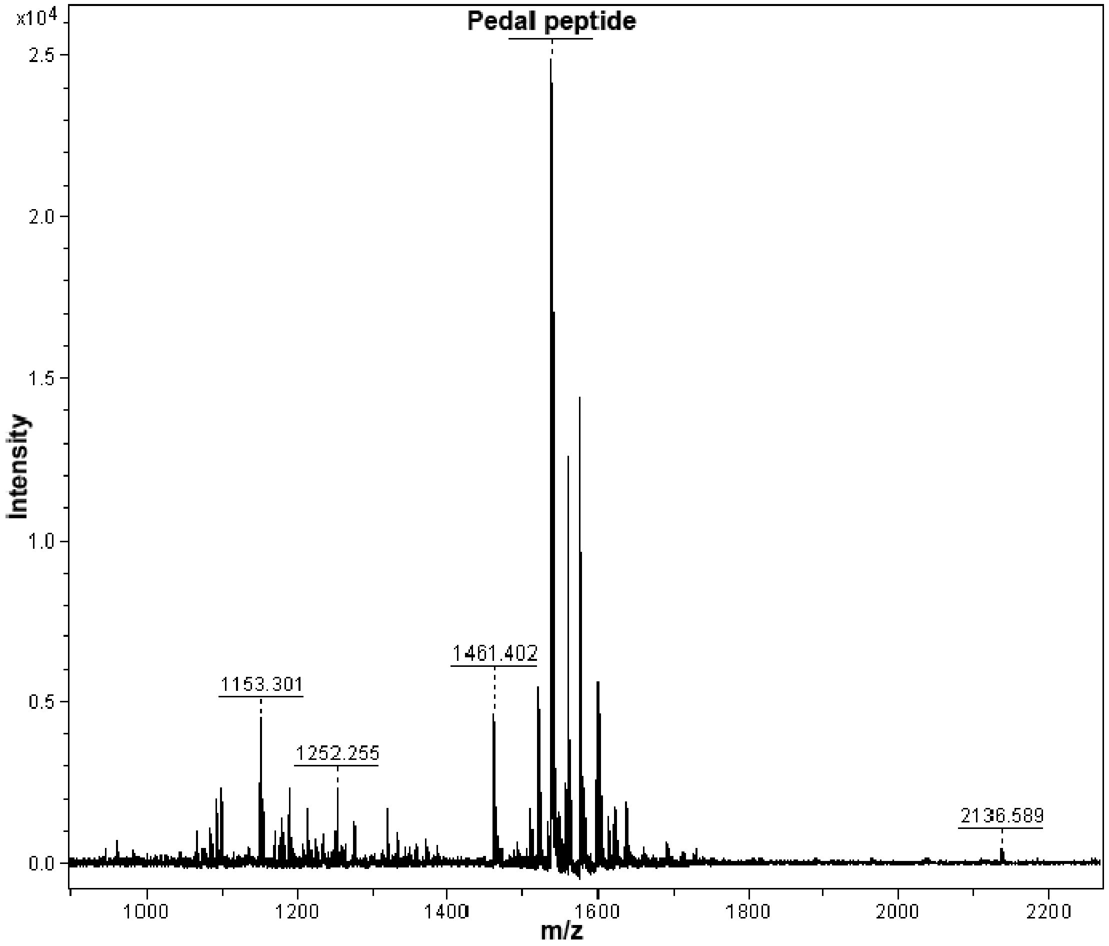

Figure 6.3. MALDI MS spectrum from a neuron cultured on the lysine-coated borosilicate beads with pedal peptide labeled along with the masses of several other intense peaks.

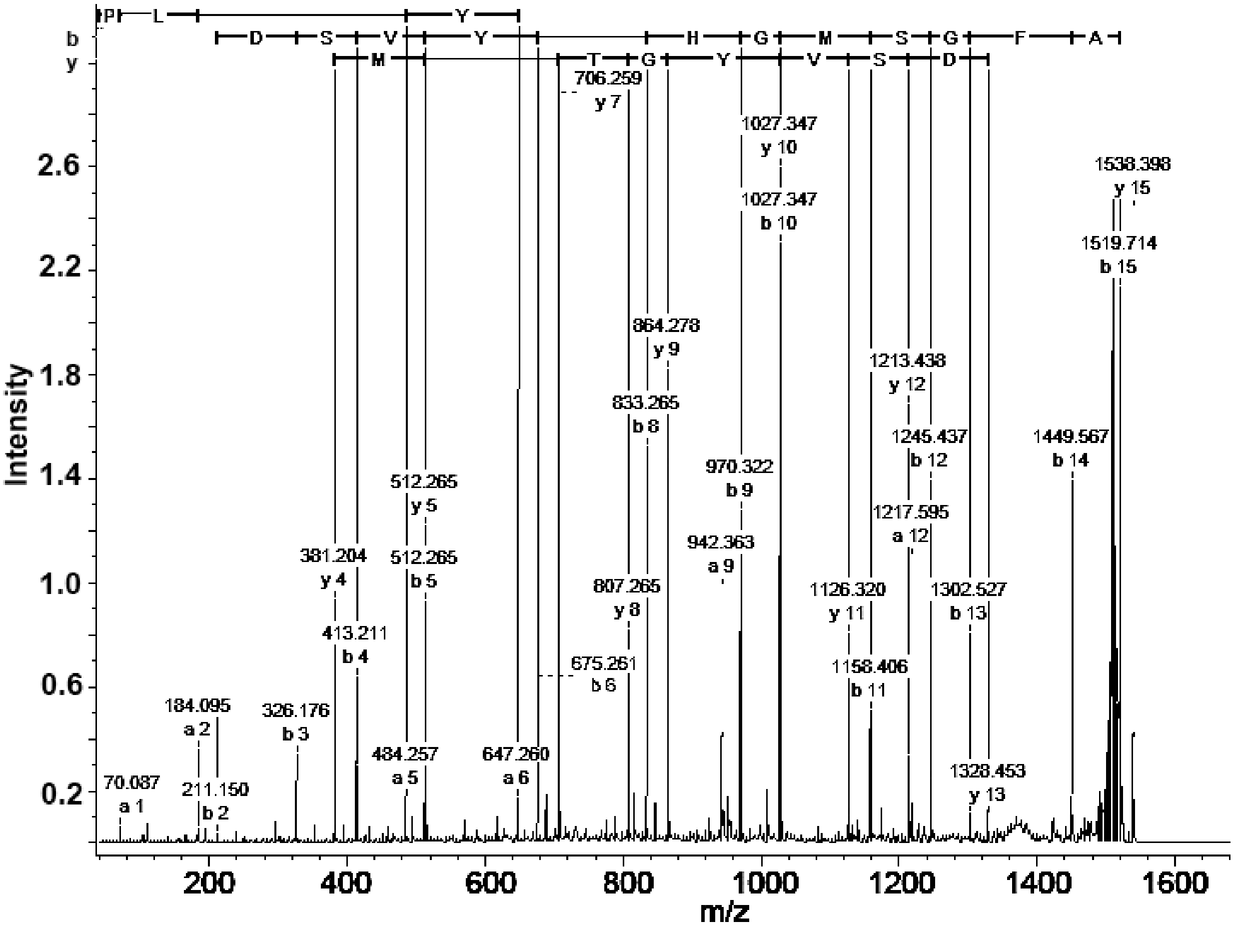

Figure 6.4. MALDI-MS produces strong neuropeptide signal in MS and MS/MS modes from cell cultures prepared using stretched imaging method. (A) Mass spectrum of the peptide profile of a selected cultured pedal neuron. Automatically generated MS/MS peak assignment for *m/z* 1540 yields the sequence that corresponds to the known amino acid sequence for *Aplysia* pedal peptide, PLDSVYGTHGMSGFA.

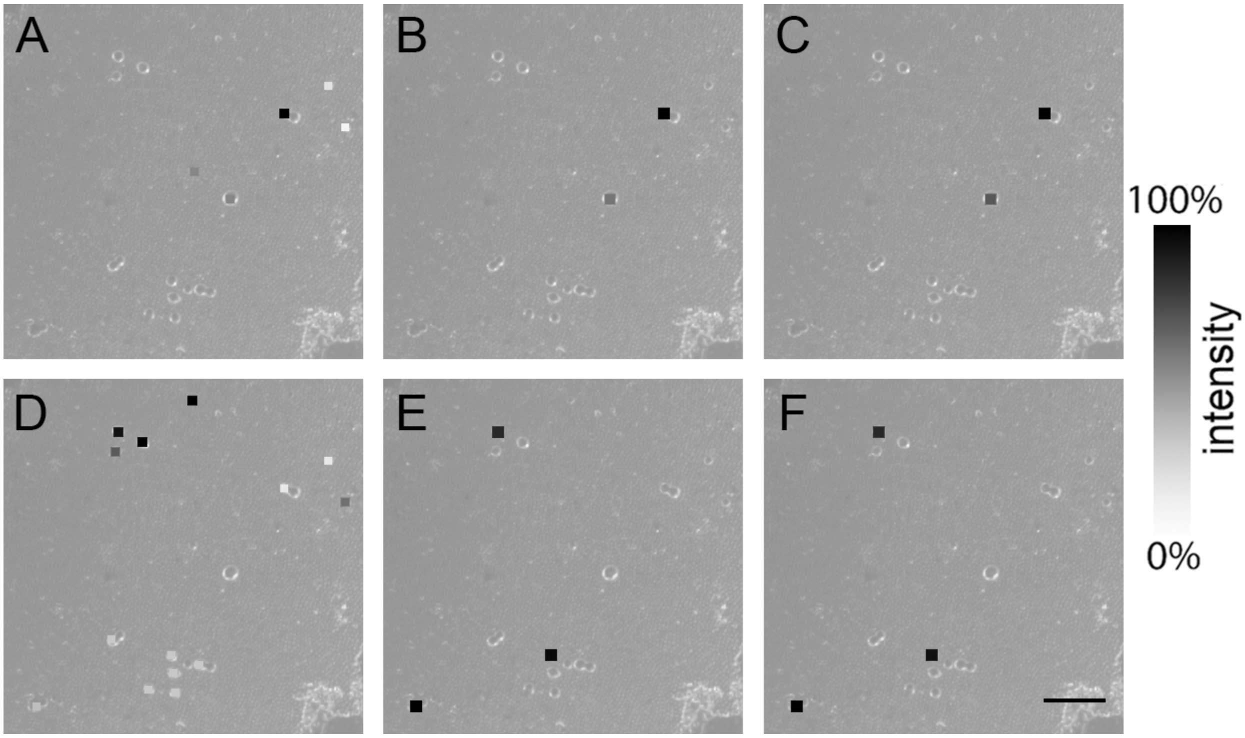

Figure 6.5. Reconstructed MS and MS/MS ion images of *m/z* 1540 and *m/z* 1200 parent ions. The background is an optical image of the sample taken before stretching where the cultured neurons are visible and labeled. (A) Reconstructed MS ion image of parent ion *m/z* 1540 that corresponds to pedal peptide. Reconstructed MS/MS ion images of pedal peptide fragments ions are shown in (B) *m/z* 419 and (C) *m/z* 1245. (D) Reconstructed MS ion image of parent ion *m/z* 1200 corresponding to a putative peptide. Reconstructed MS/MS fragment ion images are shown in (E) *m/z* 219 and (F) m/z 922. Only some neurons were selected for acquisition of MS/MS spectra because not all neurons contain the analyte of interest. Scale bar is 500 μm.

6.7 References

1. Rahman, A. The role of adenosine in alzheimer's disease. *Curr. Neuropharmacol.* **2009,** *7*, 207-216.

2. Kawane, K. and Nagata, S. Nucleases in programmed cell death. *Meth. Enzymol.* **2008,** *442*, 271-287.

3. Barar, J., Asadi, M., Mortazavi-Tabatabaei, S. A., and Omidi, Y. Ocular drug delivery; impact of in vitro cell culture models. *J. Ophthalmic Vis. Res.* **2009,** *4*, 238-252.

4. Kirkpatrick, C. J., Fuchs, S., Hermanns, M. I., Peters, K., and Unger, R. E. Cell culture models of higher complexity in tissue engineering and regenerative medicine. *Biomater.* **2007,** *28*, 5193-5198.

5. Ogilvie, M. Molecular techniques should not now replace cell culture in diagnostic virology laboratories. *Rev. Med. Virol.* **2001,** *11*, 351–354.

6. Athey, D., Shah, D. S. H., Phillips, S. R., and Lakey, J. H. A manufacturable surface-biology platform for nano applications; cell culture, analyte detection, diagnostics sensors. *Ind. Biotechnol.* **2005,** *1*, 185-189.

7. Sakudo, A., Nakamura, I., Ikuta, K., and Onodera, T. Recent developments in prion disease research: Diagnostic tools and in vitro cell culture models. *J. Vet. Med. Sci.* **2007,** *69*, 329-337.

8. Gu, Y., Wang, J., Ding, F., Hu, N., Wang, Y., and Gu, X. Neurotrophic actions of bone marrow stromal cells on primary culture of dorsal root ganglion tissues and neurons. *J. Mol. Neurosci.* **2010,** *40*, 332–341.

9. Petiot, E., Bernard-Moulin, P., Magadoux, T., Gény, C., Pinton, H., and Marc, A. In situ quantification of microcarrier animal cell cultures using near-infrared spectroscopy. *Process Biochem.* **2010,** *45*, 1427-1431.

10. Sellick, C. A., Hansen, R., Jarvis, R. M., Maqsood, A. R., Stephens, G. M., Dickson, A. J., and Goodacre, R. Rapid monitoring of recombinant antibody production by mammalian cell cultures using fourier transform infrared spectroscopy and chemometrics. *Biotechnol. Bioeng.* **2010,** *106*, 432-442.

11. Lage, H. Proteomics in cancer cell research: An analysis of therapy resistance. *Pathol. Res. Pract.* **2004,** *200*, 105-117
12. Woolley, J. F. and Al-Rubeai, M. The application of seldi-TOF mass spectrometry to mammalian cell culture. *Biotechnol. Adv.* **2009,** *27*, 177-184.

13. Zimmerman, T. A., Monroe, E. B., Tucker, K. R., Rubakhin, S. S., and Sweedler, J. V. Chapter 13: Imaging of cells and tissues with mass spectrometry: Adding chemical information to imaging. *Meth. Cell Biol.* **2008,** *89*, 361-390.

14. Francese, S., Dani, F. R., Traldi, P., Mastrobuoni, G., Pieraccini, G., and Moneti, G. MALDI mass spectrometry imaging, from its origins up to today: The state of the art. *Comb. Chem. High Throughput Screen.* **2009,** *12*, 156-174.

15. Rubakhin, S. S., Jurchen, J. C., Monroe, E. B., and Sweedler, J. V. Imaging mass spectrometry: Fundamentals and applications to drug discovery. *Drug Discov. Today* **2005,** *10*, 823-837.

16. Andersson, M., Groseclose, M. R., Deutch, A. Y., and Caprioli, R. M. Imaging mass spectrometry of proteins and peptides: 3D volume reconstruction. *Nat. Methods* **2008,** *5*, 101-108.

17. Stoeckli, M., Chaurand, P., Hallahan, D. E., and Caprioli, R. M. Imaging mass spectrometry: A new technology for the analysis of protein expression in mammalian tissues. *Nat. Med.* **2001,** *7*, 493-496.

18. Chaurand, P., Schwartz, S. A., Reyzer, M. L., and Caprioli, R. M. Imaging mass spectrometry: Principles and potentials *Toxicol. Pathol.* **2005,** *33*, 92-101.

19. Castaing, R. and Slodzian, G. Microanalyse par émission ionique secondaire. *J. Microsc.* **1962,** *1*, 395-410.

20. Nygren, H., Hagenhoff, B., Malmberg, P., Nilsson, M., and Richter, K. Bioimaging TOF-SIMS: High resolution 3D imaging of single cells. *Microsc Res Tech* **2007,** *70*, 969-974.

21. Ostrowski, S. G., Van Bell, C. T., Winograd, N., and Ewing, A. G. Mass spectrometric imaging of highly curved membranes during tetrahymena mating. *Science* **2004,** *305*, 71-73.

22. Hindie, E., Escaig, F., Coulomb, B., Lebreton, C., and Galle, P. Rapid localization of carbon 14-labeled molecules in biological samples by ion mass microscopy. *J Histochem Cytochem* **1989,** *37*, 135-138.

23. Berman, E. S. F., Fortson, S. L., and Kulp, K. S., "Preparation of single cells for imaging mass spectrometry," in *Mass spectrometry imaging: Principles and protocols*, S. S. Rubakhin and J. V. Sweedler, eds. (Springer, 2010), pp. 253-265.

24. Chandra, S. Quantitative imaging of subcellular calcium stores in mammalian llc-pk1 epithelial cells undergoing mitosis by SIMS ion microscopy. *Eur. J. Cell Biol.* **2005,** *84*, 783-797.

25. Chandra, S. and Morrison, G. H. Sample preparation of animal tissues and cell cultures for secondary ion mass spectrometry (SIMS) microscopy. *Biol. Cell.* **1992,** *74*, 31-42.

26. Chandra, S., Tjarks, W., Lorey, D. R., 2nd, and Barth, R. F. Quantitative subcellular imaging of boron compounds in individual mitotic and interphase human glioblastoma cells with imaging secondary ion mass spectrometry (SIMS). *J. Microsc.* **2008,** *229*, 92-103.

27. Chandra, S., "Quantitative imaging of chemical composition in single cells by secondary ion mass spectrometry: Cisplatin affects calcium stores in renal epithelial cells," in *Mass spectrometry imaging: Principles and protocols*, S. S. Rubakhin and J. V. Sweedler, eds. (Springer, 2010), pp. 113-130.

28. Heien, M. L., Piehowski, P. D., Winograd, N., and Ewing, A. G., "Lipid detection, identification, and imaging single cells with SIMS," in *Mass spectrometry imaging: Principles and protocols*, S. S. Rubakhin and J. V. Sweedler, eds. (Springer, 2010), pp. 85-98.

29. Ishida, Y., Madonna, A. J., Rees, J. C., Meetani, M. A., and Voorhees, K. J. Rapid analysis of intact phospholipids from whole bacterial cells by matrix-assisted laser desorption/ionization mass spectrometry combined with on-probe sample pretreatment. *Rapid Commun. Mass Spectrom.* **2002,** *16*, 1877-1882.

30. Rubakhin, S. S., Greenough, W. T., and Sweedler, J. V. Spatial profiling with MALDI MS: Distribution of neuropeptides within single neurons. *Anal. Chem.* **2003,** *75*, 5374-5380.

31. Claydon, M. A., Davey, S. N., Edwards-Jones, V., and Gordon, D. B. The rapid identification of intact microorganisms using mass spectrometry. *Nat. Biotechnol.* **1996,** *14*, 1584-1586.

32. Bergquist, J. Cells on the target matrix-assisted laser-desorption/ionization time-of-flight mass-spectrometric analysis of mammalian cells grown on the target *Chromatographia* **1999,** *49, Suppl. 1*, S41-S48.

33. Northen, T. R., Yanes, O., Northen, M. T., Marrinucci, D., Uritboonthai, W., Apon, J., Golledge, S. L., Nordström, A., and Siuzdak, G. Clathrate nanostructures for mass spectrometry. *Nature* **2007,** 1033-1036.

34. Kruse, R. A., Rubakhin, S. S., Romanova, E. V., Bohn, P. W., and Sweedler, J. V. Direct assay of Aplysia tissues and cells with laser desorption/ionization mass spectrometry on porous silicon. *J. Mass Spectrom.* **2001,** *36*, 1317-1322.

35. Shimma, S., Sugiura, Y., Hayasaka, T., Hoshikawa, Y., Nodae, T., and Setou, M. MALDI-based imaging mass spectrometry revealed abnormal distribution of

phospholipids in colon cancer liver metastasis. *J. Chromatogr. B* **2007,** *855*, 98–103.

36. Yang, H. J., Sugiura, Y., Ikegami, K., and Setou, M., "Imaging of cultured cells by mass spectrometry," in *Imaging mass spectrometry: Protocols for mass microscopy*, M. Setou, ed. (Springer, 2010), pp. 159-168.

37. Rohner, T. C., Staaba, D., and Stoeckli, M. MALDI mass spectrometric imaging of biological tissue sections. *Mech. Age. Dev.* **2005,** *126*, 177-185.

38. Klerk, L. A., Altelaar, A. F. M., Froesch, M., McDonnell, L. A., and Heeren, R. M. A. Fast and automated large-area imaging MALDI mass spectrometry in microprobe and microscope mode. *Int. J. Mass Spectrom.* **2009,** *285*, 19-25.

39. Hazama, H., Aokib, J., Nagaoa, H., Suzukia, R., Tashima, T., Fujiic, K.-I., Masudad, K., Awazua, K., Toyodab, M., and Naito, Y. Construction of a novel stigmatic MALDI imaging mass spectrometer. *Appl. Surf. Sci.* **2008,** *255*, 1257-1263.

40. Sherrod, S. D., Castellana, E. T., McLean, J. A., and Russell, D. H. Spatially dynamic laser patterning using advanced optics for imaging matrix assisted laser desorption/ionization (MALDI) mass spectrometry. *Int. J. Mass Spectrom.* **2007,** *262*, 256-262.

41. Zimmerman, T. A., Rubakhin, S. S., Romanova, E. V., Tucker, K. R., and Sweedler, J. V. MALDI mass spectrometric imaging using the stretched sample method to reveal neuropeptide distributions in Aplysia nervous tissue. *Anal. Chem.* **2009,** *81*, 9402–9409.

42. Monroe, E. B., Jurchen, J. C., Koszczuk, B. A., Losh, J. L., Rubakhin, S. S., and Sweedler, J. V. Massively parallel sample preparation for the MALDI MS analyses of tissue. *Anal. Chem.* **2006,** *78*, 6826-6832.

43. Zimmerman, T. A., Rubakhin, S. S., and Sweedler, J. V., "Mass spectrometry imaging using the stretched sample approach," in *Mass spectrometric imaging: Principles and protocols*, S. S. Rubakhin and J. V. Sweedler, eds. (Springer, 2010), pp. 465-479.

44. Hummon, A. B., Amare, A., and Sweedler, J. V. Discovering new invertebrate neuropeptides using mass spectrometry. *Mass Spectrom. Rev.* **2006,** *25*, 77–98.

45. Li, L., Moroz, T. P., Garden, R. W., Floyd, P. D., Weiss, K., and Sweedler, J. V. Mass spectrometric survey of interganglionically transported peptides in Aplysia. *Peptides* **1998,** *19*, 1425-1433.

46. Rubakhin, S. S. and Sweedler, J. V. Quantitative measurements of cell−cell signaling peptides with single-cell MALDI MS. *Anal. Chem.* **2008,** *80*, 7128–7136.

47. Zimmerman, T. A., Monroe, E. B., and Sweedler, J. V. Adapting the stretched sample method from tissue profiling to imaging. *Proteomics* **2008,** *8*, 3809-3815.

48. Rubakhin, S. S., Hatcher, N. G., Monroe, E. B., Heien, M. L., and Sweedler, J. V. Mass spectrometric imaging of the nervous system. *Curr. Pharma. Des.* **2007,** *13*, 3325-3334.

49. Schmidt, C. E. and Leach, J. B. Neural tissue engineering: Strategies for repair and regeneration. *Annu. Rev. Biomed. Eng.* **2003,** *5*, 293–347.

50. Saito, T., Hayashib, H., Kameyama, T., Hishida, M., Nagai, K., Teraoka, K., and Kato, K. Suppressed proliferation of mouse osteoblast-like cells by a rough-surfaced substrate leads to low differentiation and mineralization. *Mater. Sci. Eng. C* **2010,** *30*, 1-7.

51. Kratje, R. B., Reimann, A., Hammer, J., and Wagner, R. Cultivation of recombinant baby hamster kidney cells in a fluidized bed bioreactor system with porous borosilicate glass. *Biotechnol. Prog.* **1994,** *10*, 410–420.

52. Collazos-Castro, J. E., Cruz, A. M., Carballo-Vila, M., Lira-Cantú, M., Abad, L., Pino, Á. P. D., Fraxedas, J., Juan, A. S., Fonseca, C., Pêgo, A. P., and Casañ-Pastor, N. Neural cell growth on tio2 anatase nanostructured surfaces. *Thin Solid Films* **2009,** *518*, 160–170.

53. Wei, H., Li, H., Gao, D., and Lin, J.-M. Multi-channel microfluidic devices combined with electrospray ionization quadrupole time-of-flight mass spectrometry applied to the monitoring of glutamate release from neuronal cells. *Analytst* **2010,** *135* 2043-2050.

54. Atashi, A., Nadri, S., Hafizi, M., and Soleimani, M. Role of poly-l-lysine-coated plates and fetal calf serum concentration in sheep chondroprogenitor cell culturing. *J. Artif. Organs* **2009,** *12*, 118–122.

55. Hanson, J. N., Motola, M. J., Heien, M. L., Gillette, M., Sweedler, J. V., and Nuzzo, R. G. Textural guidance cues for controlling process outgrowth of mammalian neurons. *Lab Chip* **2009,** *9*, 122-131.

56. Zhang, J., Venkataramani, S., Xua, H., Song, Y.-K., Song, H.-K., Palmore, G. T. R., Fallonc, J., and Nurmikko, A. V. Combined topographical and chemical micropatterns for templating neuronal networks. *Biomaterials* **2006,** *27*, 5734–5739.

57. Yu, L. M. Y., Leipzig, N. D., and Shoicheta, M. S. Promoting neuron adhesion and growth. *Mater. Today* **2008,** *11*, 36-43.

58. Hatada, Y., Wu, F., Silverman, R., Schacher, S., and Goldberg, D. J. En passant synaptic varicosities form directly from growth cones by transient cessation of growth cone advance but not of actin-based motility. *J. Neurobiol.* **1999,** *41*, 242-251.

59. Monroe, E. B., Koszczuk, B. A., Losh, J. L., Jurchen, J. C., and Sweedler, J. V. Measuring salty samples without adducts with MALDI MS. *Int. J. Mass Spectrom.* **2007,** *260*, 237-242.

60. Lloyd, P. E. and Connolly, C. M. Sequence of pedal peptide: A novel neuropeptide from the central nervous system of Aplysia. *J. Neurosci.* **1989,** *9*, 312-317.

61. Chen, R., Jiang, X., Conaway, M. C. P., Mohtashemi, I., Hui, L., Viner, R., and Li, L. Mass spectral analysis of neuropeptide expression and distribution in the nervous system of the lobster homarus americanus. *J. Proteome Res.* **2010,** *9*, 818–832.

62. Drexler, D. M., Garrett, T. J., Cantone, J. L., Diters, R. W., Mitroka, J. G., Conaway, M. C. P., Adams, S. P., Yost, R. A., and Sanders, M. Utility of imaging mass spectrometry (ims) by matrix-assisted laser desorption ionization (MALDI) on an ion trap mass spectrometer in the analysis of drugs and metabolites in biological tissues. *J. Pharmacol. Toxicol. Methods* **2007,** *55*, 279-288.

63. Verhaert, P. D. E. M., Pinkse, M. W. H., Strupat, K., and Conaway, M. C. P. Imaging of similar mass neuropeptides in neuronal tissue by enhanced resolution MALDI MS with an ion trap – orbitrap hybrid instrument *Meth. Mol. Biol.* **2010,** *656*, 433-449.

64. Romanova, E. V., McKay, N., Weiss, K. R., Sweedler, J. V., and Koester, J. Autonomic control network active in Aplysia during locomotion includes neurons that express splice variants of R15-neuropeptides. *J. Neurophysiol.* **2007,** *97*, 481-491.

CHAPTER 7

CUSTOM SOFTWARE IN NEUROANALYTICAL METHOD DEVELOPMENT

7.1 Notes and Acknowledgements

During the process of learning Java programming, Michael Ewing provided some book resources.[1, 2] Learning to code in Java was made easier by the fact that I had gained some vaguely similar programming skills in MATLAB software (www.mathworks.com) while working as an undergraduate researcher with Anthony J. Myles in the Laboratory for Chemometrics at the University of Delaware. Michael Hallock, a network administrator for the School of Chemical Sciences is also acknowledged for providing information on the operation of the UIUC Neuroproteomics Center server for uploading software. This work was supported by the National Institutes of Health under Award No. DE018866, and the National Institute on Drug Abuse under Award No. DA017940 and No. DA018310 to the UIUC Neuroproteomics Center on Cell-Cell Signaling.

7.2 Abstract

It is sometimes necessary to develop custom software when studying biological samples to enable laboratory automation or data analysis. After the software creation and debugging process, a working piece of software can be adapted to mirror changes in the ongoing process of method development. After software has been optimized for one experimental protocol, it can often be adapted to new experiments. This chapter shows how custom software has evolved to meet the needs of the stretched sample method, allowing both automated imaging and image reconstruction. Subsequently, it is shown

how the custom written software is adapted to changes in the stretched imaging method or to new applications.

7.3 Introduction

Custom software is needed in cases where other software performing the necessary functions does not already exist. Custom software is cheap[3] and in-house software development is cheaper than paying an external agency to create the software.[4] Another advantage is that the researcher who creates the software understands it thoroughly and can control its output and adapt it to different applications.[5-7]

There are multiple programming platforms to choose from when developing a code, and the best suitable platform depends on the task. For instance, the Java programming language from Sun Microsystems (http://java.sun.com) is freely available and works with the freely-available java-based image analysis software, ImageJ (http://rsbweb.nih.gov/ij/). Java is also a flexible language that is desirable for the creation of adaptable software.[7] On the other hand, a commercial programming package, MATLAB (www.mathworks.com), with associated toolboxes and canned methods is useful for quick data processing. Of course, platforms can often be combined, as for example in the stretched imaging method where the mass spectral data is passed through several softwares including FlexControl, CompassXport, and Matlab for data conversion before it is able to be plotted as ion images using Java (see chapter 3 section 3.4.4). Programming skills can also often be easily transferred between several platforms.[8]

After choosing a platform for the design of custom software, the process of learning the new programming language by self teaching is utilitarian, as one learns only the skills that are necessary for each programming task. There are handbooks[1, 2, 9] available on learning Java that are useful when using this targeted learning approach. Also, the Java API (application programming interface) that is freely available on the web provides a quick reference for the programmer, showing an organized hierarchy of commands that are available in the language (http://java.sun.com/j2se/1.5.0/docs/api/).

When beginning to write a program, good programming habits[10] are also necessary to keep mind. For instance, during the debugging process, it is important to label all variables descriptively so that one can distinguish variables that are close in property. In Section A.3 of Appendix A, line 139, a variable is called "Intensity" that is used to store the maximum mass spectral intensity values in the user-specified analyte mass window. In line A.3 line 359, the variable "IntensityDummy" is used as a dummy or placeholder variable during a sorting process of intensities based the closest distances between the transformed initial bead coordinates and the stretched coordinates. In line A.3 line 363, the variable "IntensityMap" is used to store the intensity value from the spectrum taken at the nearest stretched coordinate. With three different variables related to the word intensity, labeling them all as "intensity" would cause Java to perform all operations on the same vector of values with the result of erroneous output. Descriptive naming also helps the programmer to keep track of such closely related variables. Descriptive names also allow keeping track of variables for when making future changes in the code to adapt it to new experimental protocols. Another good programming habit is to separately store working versions of a code before modifying or adapting it.

After major sections of the program are drafted, debugging is used to discover conceptual and syntax errors. Debugging is often an experimental process, usually performed by outputting the values of variables at various points along the code while running the code to give clues about how the data is being processed and to pinpoint where a bug has occurred. This can be done with the System.out.println() command as shown in section A.2 of Appendix A, line 213. This prints the value(s) of the variable for visual inspection by the programmer.

After a code works properly and achieves its designed purpose, transforming the code into a piece of software that others can easily use often requires a graphical user interface, or GUI. The GUI prompts the user to provide the inputs that the code needs to begin running and it also allows the user to easily control the values of optional parameters, as shown in the GUI for image reconstruction in Figure 7.1. For Java codes, the NetBeans software (http://www.netbeans.org) allows the creation of GUIs. Subsequently, the Java Network Launching Protocol (JNLP) syntax allows the programmer to create a web-based program, as found for example in the on-line tools of the stretched imaging method (http://neuroproteomics.scs.uiuc.edu/imaging.html). Besides a GUI, for a user to properly use the finished program, documentation and help files are necessary. An example dataset with step-by-step instructions is also helpful to new users that are learning to use the program.[11]

The next part of this chapter deals with the softwares for geometry file creation and image reconstruction that were introduced in chapter 3 of this dissertation, and covers their development and use in the stretched imaging method.

7.4 Adaptable Software for the Automated Imaging of Stretched Samples

To automate mass spectral data collection off of the individual bead locations that are stochastically assembled over the surface of a stretched sample, it was necessary to create software that generated custom geometry files that in turn controlled the locations of mass spectral acquisitions to align with the bead locations. During an experiment to test the accuracy of the newly created geometry files for bead samples, it was noticed that the accuracy of the geometry file in aligning the laser beam with the bead positions decreased with increasing distance from the origin of the geometry file coordinate system. Furthermore, this offset increased linearly with distance from the origin. This error was determined to result from the accumulation of offset from imprecision in the scaling value.

The scaling value is used to relate the scaling of the optical image in pixels (Eq. 7.1) into absolute distance in millimeters or microns (Eq. 7.2). The last equation (Eq. 7.3) uses the regular spacing between regular points in the array, called wells here, of the Bruker MTP Slide Adapter II geometry file to convert absolute distances into fractional distance coordinates used by the Bruker geometry file format.

$$\frac{1mm\_bar}{\#\,pixels} = Scaling_{\frac{mm}{pixel}} \tag{7.1}$$

$$Scaling_{\frac{mm}{pixel}} \times XYcoordinate_{pixel} = XYcoordinate_{mm} \tag{7.2}$$

$$\frac{XYcoordinate_{mm}}{4.41_{\frac{mm}{well}}} \times 0.0870_{\frac{frac.dist.}{well}} = XYcoordinate_{frac.dist} \tag{7.3}$$

The imprecision of the scaling value arises because the total number of pixels in the optical image corresponding to the length of a 1 mm calibration bar is determined by measuring this value in a fuzzy optical image. With the microscope that was used, it was not possible to focus the image enough to get a precise enough value for the length of the calibration bar in pixels. The error is further propagated in Eq. 7.3 to the final value of the XY coordinate, causing the spectra to be collected from a position that does not include the bead area.

Compare this series of equations to the series section 4.4.4 that are designed to accomplish the same goal of converting bead locations in pixel coordinates into fractional distance coordinates used by the Bruker software. The innovation of using laser melted parafilm holes as markers instead of using the calibration bar, as described in section 4.4.4, makes those equations simpler in comparison to those above by the removal of a great deal of positional error. The geometry file creation code was changed to reflect the newer series of equations found in section 4.4.4.

Logically, if the XY bead coordinates were calculated from a series of separate origins from melted markers used at positions which span the sample area, the total accuracy of the geometry file should increase. To test this idea, the Java code for geometry file creation was modified to receive the positions of four origins as inputs (Appendix A, bead geometry code, lines 47-55), and also modified to calculate the position of each bead from the nearest origin as determined from the Cartesian distance formula (Appendix A, bead geometry code, lines 121-162). Thus, a *for* loop was added to the Java program to calculate the distance from each bead to all four origins, and for calculating the bead positions from their closest origin (Appendix A, bead geometry code, lines 167-211). This creates one geometry file with bead positions calculated from four separate coordinate systems. The geometry file is required to report the positions to the Bruker instrument in one coordinate system, with one and not multiple origins, so another *for* loop was added to convert the bead positions into values corresponding to the origin of the glass slide in Bruker coordinates (Appendix A, bead geometry code, lines 158-161). Geometry files created using this altered code that was modified for use with several origins showed greatly improved positional accuracy. These examples of altering the code show how software can evolve to meet the needs of an evolving method development process.

In another example involving geometry file creation it was found that melted holes that are created by melting through the Parafilm M layer with a high repetition rate, could serve as anchor points between the stretched sample image and the Bruker instrument coordinate system.[12] This use of melted holes as anchor points is different from how the melted holes were used in the previous example, where they were used to determine scaling. If the melted markers are created in a regular array corresponding to positions in the standard Bruker Slide Adapter II geometry file, the distance in pixels between two melted markers in the stretched image can be directly anchored to the Bruker coordinate system without the need for manually selecting anchor points. The fractional distance coordinates corresponding to some of these regularly spaced anchor points are show in the code (Appendix A bead geometry code, lines 182-208).

Using the melted markers for calibrating the scaling of the two coordinate systems, in addition to their use as anchor points, created the most positionally accurate geometry files. The Java code for geometry file creation was modified to test the positional accuracy using a bead sample. In the code, the old method of scaling was replaced by the new method of dividing pixel coordinates by the spacing of the regular array of melted holes corresponding to the Bruker Slide Adapter II geometry file (Appendix A, bead geometry code, lines 158-161). It was found that geometry files showed the highest positional accuracy through combining the melted marker methods with the used of multiple origins as detailed in the previous example.

These previous two examples show how a code can evolve to test hypotheses during the course of method development. However, sometimes a conceptual leap must take place when creating a code. Case in point is the image reconstruction code. The original method of reconstructing images, which match the initial configuration of the tissue before stretching, was a vector addition method where the vector between the initial and final position of a small percentage of beads were calculated. This small percentage of manually tracked beads is called marker beads. The final positions of the rest of the beads were determined by averaging the vectors of several marker beads that were closest in proximity to the bead being predicted, higher weighting being given to closer marker bead vectors, see Figure 7.2. While this vector addition method was practical for small samples, positional accuracy worsens with larger sample areas as small changes in the weighting parameters were found to have large effects on beads that were located far from any marker bead. In fact, it was necessary to optimize the weighting parameters depending on slight variations in how the sample was manually stretched. This method was impractical and new method of image reconstruction based on the free transform was introduced (see section 3.4.5). Implementing the free transform method required an overhaul of the image reconstruction code. The code was altered to have a different set of inputs including the free transform values from the “info” palette in Photoshop (Appendix A, image reconstruction code, lines 181-195). The development of image reconstruction methods based on a free transform gave new challenges, such as when enlarging the initial sample image the beads would grow in size, making the overlay onto the stretched sample image visually difficult. Java programming was used to fashion a separate code that creates an image containing small dots at the coordinates of the initial bead locations, to be used in place of the initial sample image. The images of the initial positions can then be made transparent to aid the overlay process in Photoshop. A new section code was necessary to quantitatively test the results of the free transform method in comparison to the vector addition approach. This new section of code was associated with an in-house designed plugin to report the pixel positions of the beads as the user clicks on each bead to manually create list of true matches between the initial and stretched sample coordinates, Figure 7.3. A validation can then be performed by altering the image reconstruction code to compare each match reported by the free transform method with the set of manually generated true matches (Appendix A, image reconstruction code, lines 482-501). The new section of code also reports the rate of successful classification as a percentage (Appendix A, image reconstruction code, line 496).

In another addition to the code, it was found that the misclassification rate could be affected in cases where two of the overlaid transformed initial coordinates were assigned to the same stretched position. In these cases, the second initial bead to be assigned to a stretched position is reassigned to the nearest unassigned position, in an iterative fashion as the *for* loop progresses (Appendix A, image reconstruction code, lines 363-479). As most of the misclassifications are due to near-neighbor mismatches, this reassignment process was shown to improve the classification rate on a series of test samples.[13] Overall, the improved code enabled image reconstruction based on the free transform to be tested, and the results showed that the free transform method works sufficiently for larger area tissue samples. These examples show how software creation is very adaptable to hypothesis testing and to the needs of method development.

7.5 Adapting Existing Software to New Applications

Once a piece of software is optimized in conjunction with a particular method, it can often be extended to new applications. One such instance is the use of the geometry file creation code to create a set of three geometry files, each corresponding to a different bead color in a tricolored bead sample. As part of a recently completed project by K.R. Tuker *et al.*,[14] the three colors of beads can correspond to the location of different endopeptidase proteins that characteristically cleave peptides into fragments based on different predictable patterns. The enzyme trypsin cleaves at basic amino acid residue positions in the peptide sequence, for example. The purpose is to gain chemical information by fragmenting peptides or proteins *in situ* with several different endopeptideases, while simultaneously aligning the fragments to the genetic sequence information and also mapping their locations in the tissue through mass spectrometry imaging. The sets of fragments resulting from different endopeptideases give overlapping information that can be used to recognize the parent protein by mass matching the fragments to protein sequence information. In this proof of concept that demonstrates selective light thresholding of a sample of three different color beads, no proteolytic enzymes are used although such enzymes could be used with this approach. Selective light thresholding with the Colour Thresholding plugin in ImageJ allowed reporting of the coordinates based on bead color, see Figure 7.4. The geometry file creation code was modified to create separate geometry files for automated imaging of each set of bead colors. This example shows how a preexisting code can be altered and applied to new applications.

7.6 Conclusions

Creating custom software is an experimental process that often evolves with the changing experimental design. Custom written software is cheap[4] and often necessary in studies that try to map complex biology. Given the nature of biological samples, automation is often needed in experimental protocols to study the large number of cells that are present. This was achieved in the automated imaging method using custom designed geometry files that are generated by the Java software. Custom software may also be necessary to execute the computation required to handle the large volume of complex data created from biological studies. The image reconstruction software achieves such tailored computation, including routines for signal processing, reclassification of doubly assigned positions, and visualization of ion images from datasets of up to several tens of gigabytes in size. Custom control of computation allows the programmer to have more control over and understanding of the output, which is also useful when tailoring the software to new applications.

7.7 Figures

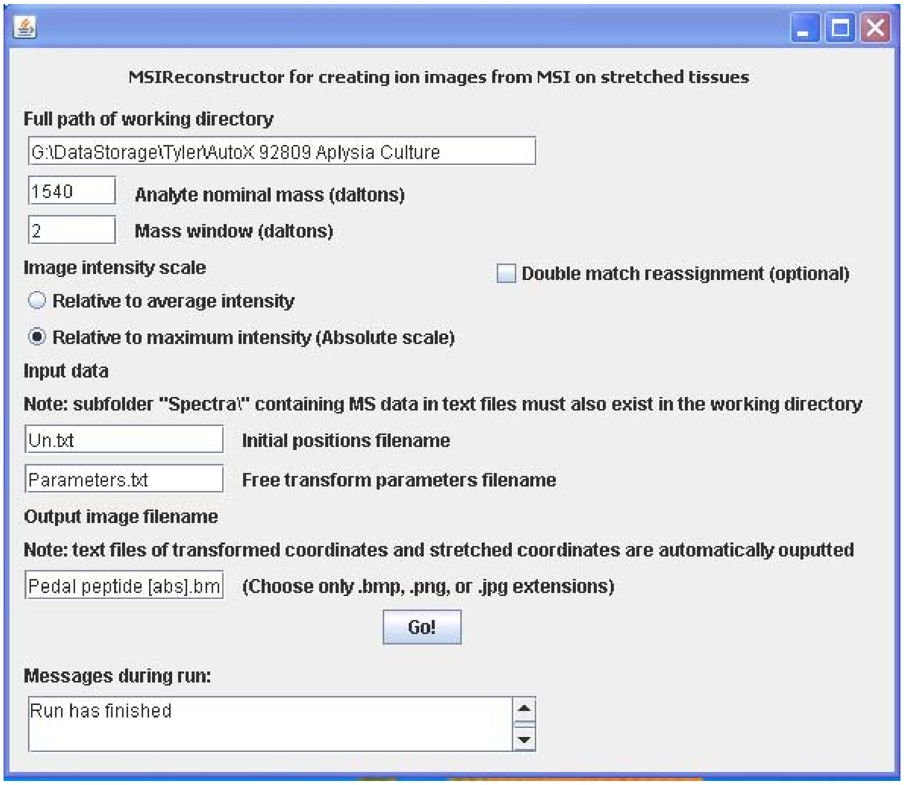

MSIReconstructor for creating ion images from MSI on stretched tissues

Full path of working directory

G:\DataStorage\Tyler\AutoX 92809 Aplysia Culture

1540 Analyte nominal mass (daltons)

2 Mass window (daltons)

Image intensity scale

☐ Double match reassignment (optional)

○ Relative to average intensity

● Relative to maximum intensity (Absolute scale)

Input data

Note: subfolder "Spectra\" containing MS data in text files must also exist in the working directory

Un.txt Initial positions filename

Parameters.txt Free transform parameters filename

Output image filename

Note: text files of transformed coordinates and stretched coordinates are automatically ouputted

Pedal peptide [abs].bm (Choose only .bmp, .png, or .jpg extensions)

Messages during run:

Run has finished

Figure 7.1. Example of a graphical user interface (GUI) developed in the used for image reconstruction in the stretched sample method. The GUI prompts the user for the required inputs, but also allows selection of optional parameters such as the choice of the intensity scale shown here. The GUI has been completed so that the mass region of 1538-1542 daltons that roughly corresponds to the mass of pedal peptide is plotted to form a reconstructed ion distribution image.

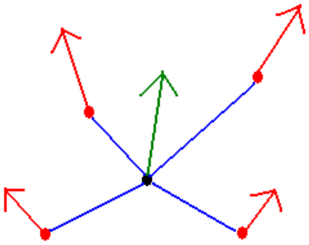

$$weight_1 = \frac{\left(\frac{1}{dist_1^m}\right)}{\frac{1}{dist_1} + \frac{1}{dist_2} + \frac{1}{dist_3} + \frac{1}{dist_4} + \ldots}, m = 2.5$$

$$\Delta y = weight_1 * dist_1 * \sin(\Theta_1) + weight_2 * dist_2 * \sin(\Theta_2) + \ldots$$

$$\Delta x = weight_1 * dist_1 * \cos(\Theta_1) + weight_2 * dist_2 * \cos(\Theta_2) + \ldots$$

Figure 7.2. Color-coded explanation of the vector addition method for image reconstruction. The vectors of travel between initial and stretched positions of the marker beads (in red) are used to predict the movement of another bead (green) based on the weighted distances from the predicted bead to the marker beads (blue). The value of *m* is produces a decay curve described by 1/(x^2.5), meaning that the bigger the distance to the marker bead the smaller the weighting value.

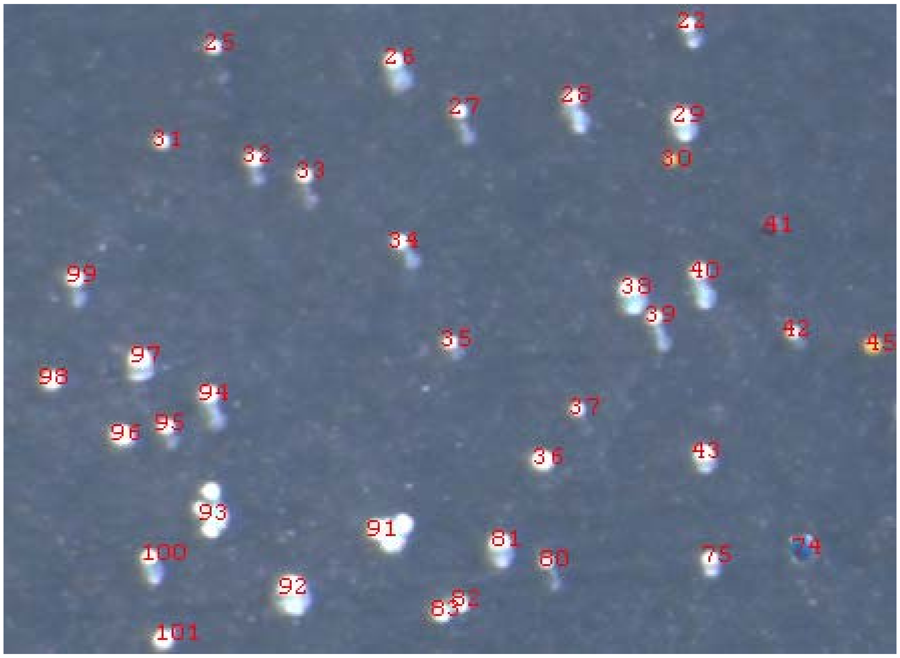

Figure 7.3. An in-house written plugin for ImageJ allows simultaneous reporting of the XY pixel coordinates upon click with the mouse while simultaneously labeling each bead in sequence with a number so that it is easier to visually keep track of which beads were clicked already. The samples used for validation are small enough to be manually validated and contain only a few hundred beads.

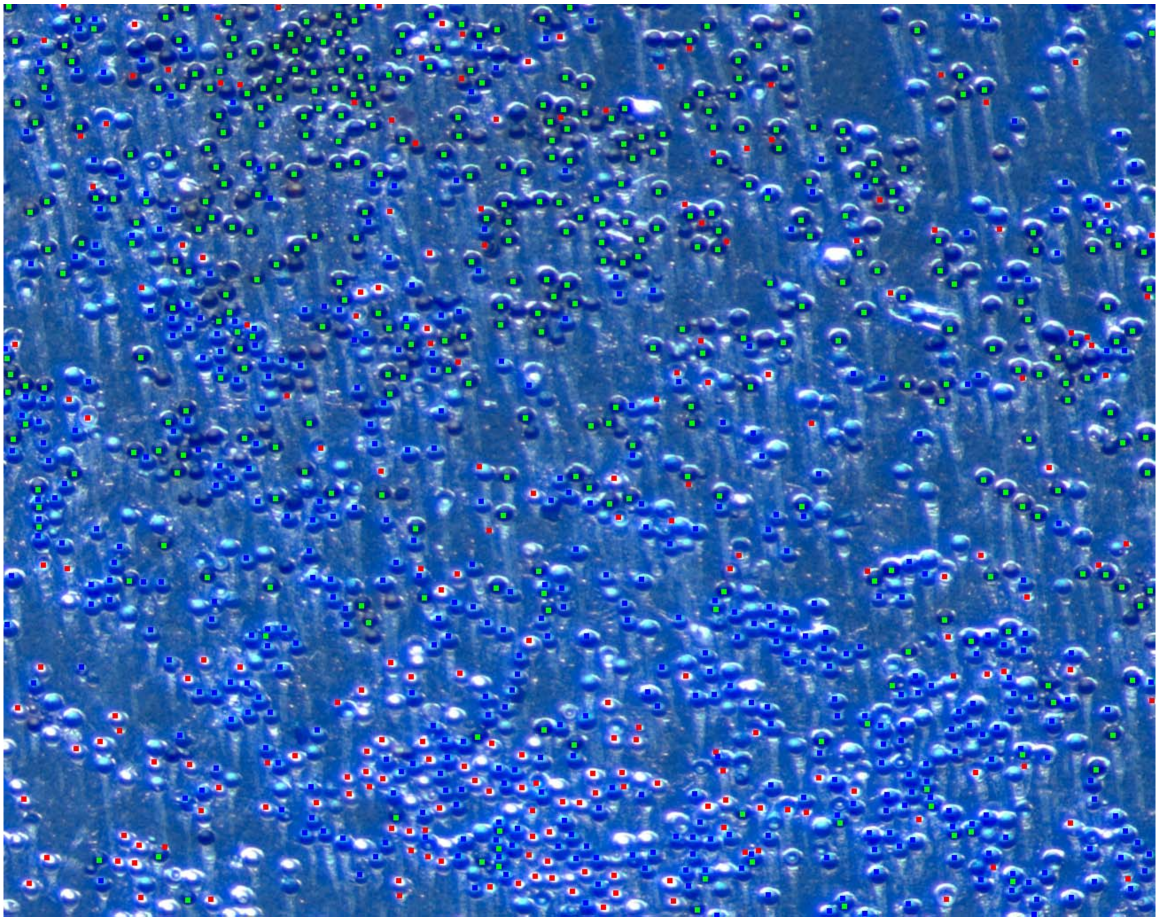

Figure 7.4. The overlaid colored dots represent positions found by selectively thresholding the image for the three different colors of beads in ImageJ with the Colour Thresholding plugin. The red dots correspond to posistions found by thresholding for clear beads, blue dots for blue beads, and green dots for black beads. An image of the dots was created from the coordinated reported by ImageJ using the in-house written PlaceDots.java code that can be found at http://neuroproteomics.scs.uiuc.edu/imaging.html. Future work could involve associating different color beads with the presence of different proteolytic enzymes to generate protein fragments from tissue for identification of proteins.

7.8 References

1. Flanagan, D., *Java in a nutshell*, 4th ed. (O'Reilly, Sebastopol, 2002).

2. Flanagan, D., *Java examples in a nutshell*, 3rd ed. (O'Reilly, Sebastopol, 2004).

3. Stamelos, I., Angelis, L., Morisio, M., Sakellaris, E., and Bleris, G. L. Estimating the development cost of custom software. *Inf. Manag.* **2004,** *40*, 729-741.

4. Wang, E. T. G., Barron, T., and Seidmann, A. Contracting structures for custom software development: The impacts of informational rents and uncertainty on internal development and outsourcing. *Manag. Sci.* **1997,** *43*, 1726-1744.

5. Alexandridis, N. A. Adaptable software and hardware: Problems and solutions. *Computer* **1986,** *19*, 29-39.

6. McKinley, P. K., Sadjadi, S. M., Kasten, E. P., and Cheng, B. H. C. Composing adaptive software. *Computer* **2004,** *37*, 56-64.

7. Fayad, M. and Cline, M. P. Aspects of software adaptability. *Commun. ACM* **1996,** *39*, 58-59.

8. Mayer, R. E., Dyck, J. L., and Vilberg, W. Learning to program and learning to think: What's the connection? *Commun. ACM* **1986,** *29*, 605-610.

9. Burd, B., *Java 2 for dummies* (Hungry Minds, New York, 2001).

10. Bentley, J. Programming pearls: Writing correct programs. *Commun. ACM* **1983,** *26*, 1040-1045.

11. Zimmerman, T. A., Rubakhin, S. S., and Sweedler, J. V., "Mass spectrometric imaging using the stretched sample method," in *Mass spectrometic imaging: History, fundamentals, and protocols*, S. S. Rubakhin and J. V. Sweedler, eds. (Springer, 2010), pp. 465-479.

12. Zimmerman, T. A., Rubakhin, S. S., Romanova, E. V., Tucker, K. R., and Sweedler, J. V. MALDI mass spectrometric imaging using the stretched sample method to reveal neuropeptide distributions in Aplysia nervous tissue,. *Anal. Chem.* **2009,** *81*, 5858–5864.

13. Zimmerman, T. A., Monroe, E. B., and Sweedler, J. V. Adapting the stretched sample method from tissue profiling to imaging. *Proteomics* **2008,** *8*, 3809–3815.

14. Tucker, K. R., Serebryannyy, L. A., Zimmerman, T. A., Rubakhin, S. S., and Sweedler, J. V. Chemically selective imaging using mass spectrometry: The modified-bead stretched sample method. **2010,** in press.

CHAPTER 8

CHARACTERIZING PEPTIDE MARKERS FOR PLANARIAN REGENERATION

8.1 Notes and Acknowledgements

I worked closely on this project with Elena Romanova and Jonathan V. Sweedler in the Sweedler lab. In Professor Neil Kelleher's lab, I worked with Ji Eun Lee on the FTMS instrument, and Leonid Zamdborg did genome searching. In Professor Phil Newmark's lab, I worked with Jim Collins who provided the animals. I additionally thank Rachel Botham, a rotation student, and Stanislav S. Rubakhin of the Sweedler lab for discussions and experimental assistance. This work was supported by Award Nos. 5P30DA018310 and DA017940 from the National Institute on Drug Abuse to the UIUC Neuroproteomics Center on Cell-Cell Signaling, from the National Institutes of Health under award R01 HD043403, and the National Science Foundation under award IOS-0744689.

8.2 Abstract

Peptide markers of anterior regeneration in *Schmidtea mediterranea* flatworms are studied. An advantage of using this model is that the planarian central nervous system and body can fully regenerate from pluripotent stem cells via cell proliferation (blastema formation), and the remodeling of pre-existing tissues to restore symmetry, proportion, and function. Here mass spectrometry is used to image and characterize spatial and temporal peptide markers throughout the regeneration process. With MALDI MS imaging, candidate marker peptides were revealed based on the spatial redistribution of

the ion signals during the anterior regeneration time course. Identity of selected marker peptides were then determined from planarian tissue extracts via nanoLC-ICR-FTMS/MS and palanrian gene database mining, which lead to discovery of two novel prohormones named here as spp-20 and spp-21. A total of 23 known, newly characterized, and putative unassigned peptides show distinct spatial and temporal redistributions with blastema development in the time course of anterior regeneration in *S. mediterranea.*

8.3 Introduction

The *Schmidtea mediterranea* freshwater planarians are flatworms from the phylum platyhelminthes that are model organisms for the study of regeneration,[1] autophaghy,[2] and stem cells.[3] These planarians contain pluripotent stem cells called neoblasts that are located throughout the body which differentiate into various cells types to restore morphologically and functionally injured tissues. As the neoblasts are located throughout the body, except for the centrally located pharynx,[4] regeneration into two or more organisms can take place after cutting an individual worm several times at any angle. Of the two strains of planaria, sexual and asexual, the asexual strain has traditionally been used to study regeneration[2] because there is less genetic variation among animals. The expressions of many genes have shown enhanced levels near the blastema when using genomic approaches such as EST (espressed sequence tag), DNA chip analyses, and in-situ hybridization.[5-8] Characterizing planarian gene function has been carried out by creating gene knockout animals using RNA interference (RNAi).[9, 10] As planaria are able to regenerate their central nervous system (CNS), several studies have focused on regeneration of the CNS.[11, 12] Regeneration of the planarian CNS has been shown to be associated with unique expression patterns of neuropeptides at the blastema,[13] and many previous studies document the correlation between neuropeptides and planarian CNS regeneration,[14-17] with another study involving regneration in hydra.[18] There are also many CNS regeneration studies in phylogenetically distant organisms.[19-21] These studies show that neuropeptides increase mitosis and may control cellular differentiation during CNS regeneration.

With the recent discovery of numerous prohormones encoding hundreds of peptides in *S. mediterranea* the study of peptide roles in regenration can be greatly facilitated.[6] Here we use mass spectrometry imaging of planarian tissue sections to study dynamic changes in localization of known and novel peptides during anterior regeneration. The ability to reveal chemical imformation and low detection limits provided by mass spectrometry (MS) are practical for measuring neuropeptides in tissue,[22-26] and providing spatial information on peptide localization.[27-30] An advantage of the MSI approach is its ability to detect multiple analytes over a mass range, and therefore preselection of an analyte of interest is not necessary. Thus, we and others use MSI as a discovery tool to map biomarker spatial distributions within tissue.[31-34] As the biggest detectable differences in planarian peptide signal detected by MALDI MS were shown to occur at 3-days after amputation,[35] experiments here are used at both 0-hr and 3-day timepoints to monitor peptides and proteins signal spatial patterns at the blastema to identify peptides markers of regeneration. Using MSI during the regeneration timecourse, we find selected ion signals enhanced near the wound site or the pharynx. To confirm the identitiy of these molecules, we performed fractionation of planarian peptide extracts by multi-stage LC folowed by tandem mass spectrometry sequncing and searching the planarian genome.[36] This proteomic level analysis identifies marker polypeptides for future functional studies.

8.3.1 Background on LC-FTMS/MS.

LC-FTMS/MS is used to obtain amino acid sequences and identify peptides and proteins located at the wound site. A separate liquid chromatography-mass spectrometry (LC/MS) analysis is done on a whole-body extract of planarians to concentrate peptides.[6, 37, 38] After purifying the peptide from the extract and detection with mass spectrometry, the peptides undergo collisionally induced dissociation (CID) to fragment the analyte where the fragments are detected by a second round of MS detection called tandem MS or MS/MS.[37] The pattern of analyte fragmentation can be used to reveal the peptide amino acid sequence and the presence of posttranslational modifications. In the mass range of neuropeptides, 500-10,000 Daltons, there are many interfering isobaric (silmilar mass) signals from complex biological matricies. Distingishing between analyte ions that are less than a dalton apart in mass can be achieved with electrospray ionization (ESI) followed by Fourier-transform ion cyclotron resonance tandem mass spectrometry (FT-ICR-MS/MS also called FTMS/MS) that provides high accuracy mass determination of the amino acid sequence through detecting the cyclotron frequence of the analyte and fragment ions in a fixed magnetic field.[38, 39] Another advantage of FTMS/MS is that the high magnetic fields allow for successful fragmentation of higher mass peptides and proteins for determination of their amino acid sequences and posttranslational modifications.[40]

8.4 Experimental

8.4.1 Mass Spectrometry Imaging (MSI).

8.4.1.1 Animals and Sample Preparation. An asexual strain *S. mediterranea* flatworm was stored at 20^{o}C in Montjuïch salts[12] solution (1.6 mmol/l NaCl, 1.0 mmol/l $CaCl_2$, 1.0 mmol/l $MgSO_4$, 0.1 mmol/l $MgCl_2$, 0.1mmol/l KCl and 1.2 mmol/l $NaHCO_3$ prepared in Milli-Q water) and were starved for 7 days to remove food signal from the analysis. The flatworms were transferred onto the surface of a solid block of agarose (Sigma-Aldrich) that is on top of a room temperature cryosectioning sample stage. The top layers of agarose were sectioned inside a Leica CM 3050 S cryostat (Leica Microsystems, Wetzlar, Germany) for making a flat surface[29] to place the planarian. The anterior parts of the planarian were amputated behind the eyes with a blade and discarded. The remaining worm bodies were either analyzed immediately or stored for 48hr or 72 hr in Montjuïch salt solution to allow the formation of a blastema and the regrowing of a new anterior portion of the body. Optical images were taken of the planarian on top of agarose using a MZ8 microscope (Leica Microsystems, Bannockburn, IL) equipped with an AxioCam MRc camera (Carl Zeiss, Göttingen, Germany) before placing some water around the base of the agarose to freeze-mount it to the sample stage and immediately storing the sample on a bed of ice. The samples were transported in ice to the -20^{o}C environment of the Leica CM 3050 S cryostat. Thin 20-µm tissue sections were cut along the longitudinal axis spanning from the wound site to the posterior end of the organism. Thin sections were transferred with an artist's brush to the conductive side of a 25 x 75 x 1.1 mm indium tin-oxide coated glass slide[41] (Delta Technologies, Stillwater, MN) and the orientation of the wound site on the glass slide was noted with a magic marker on the back of the slide. Samples were immediately sprayed with a MALDI matrix solution of 30 mg/mL 2,5-dihydroxybenzoic acid (Sigma-Aldrich, St. Louis, MO) in 75:25 methanol:water using an artist's spray brush (Thayer & Chandler, Kenosha, WI) at a distance of ~15 cm with alternating short ~2s passes with drying times of about ~10s during which only air was emitted from the artist's spray brush to speed drying of the matrix solution onto the tissue. In total, ~35 mL of the MALDI matrix solution was applied to the surface of the samples and ITO glass slide. Optical images were then taken of the sample.

8.4.1.2 MSI Data Acquisition. The thin tissue slices underwent mass spectrometry imaging imaged using a Bruker UltrafleXtreme TOF-TOF MS instrument (Bruker Daltonics, Billerica, MA). The optical images of the sample taken after matrix coating were imported into the FlexImaging 2.1 software (Bruker Daltonics) and used to specify a region for acquisition of the mass spectrometry images. All samples were imaged with a laser step size of 75 µm in a regular array pattern and each sample had about ~1000 spots in the array for an average acquisition time of ~40 min. In total, 4 thin tissue slices from 4 different worms labeled as 0-day time point were imaged immediately after amputation, with the same number of biological replicates at 3-days. In addition, one tissue slice at 2-days was imaged. Thus, nine MSI experiments were done on 9 animals.

8.4.1.3 Peak Statistics. The spectra were smoothed in FlexAnalysis (Bruker Daltonics) with Savitsky-Golay using a window of 3 m/z with 9 cycles, and baseline subtracted using the TopHat algorithm. These spectra were loaded into FlexImaging software for creation of ion images.

8.4.2 Peptide/Protein Identification.

8.4.2.1 Peptide Fractionation by microbore HPLC. 58 whole body planarians were placed in 100 µL of acidified acetone (40:6:1 acetone/water/HCl) and homogenized with a glass stir bar. Following centrifugation, the supernatant was removed and the process was repeated with the second supernatant being combined with the first. The combined supernatant was centrifuged at a relative centrifugal force of 14000 x g for 15 min at ambient temperature with a Centrifuge 5804 R (Eppendorf, Hamburg, Germany) and then dried down to under 10 µL in volume over 3 hr using a SpeedVac concentrator (Thermo Scientific, San Jose, CA). This was reconstituted in 90 µL of water containing 0.1 % formic acid and injected into a Magic 2002 analytical LC system (Michrom Bioresources Inc., Auburn, CA) equipped with a 2.1 mm inner diameter Vydac column (W. R. Grace & Co.-Conn., Columbia, MD) packed with 5µm monomeric C18 particles. The solvents A and B were 5% acetonitrile, 0.1% formic acid, 0.01 triflouroacetic acid (TFA) and 95% acetonitrile, 0.1% formic acid, 0.01 triflouroacetic acid (TFA), respectively. A five-step linear gradient over 70 min was used (0-10% B in 5 min, 10-50% B in 45 min, 50-85% in 7 min, 85-85% in 6 min, and 85-5% in 6 min) with UV detection at 215 and 280 nm. A total of 25 fractions were collected manually corresponding to the chromatographic peaks eluted.

The fractions were spotted onto an MTP 384 metal MALDI target with a matrix of 30 mg/mL of 2,5-dihydroxybenzoic acid (DHB) in 75:25 ethanol:water. MALDI mass spectra of the fractionated peptides were taken using 100 shots at 1000 Hz with a Bruker UltrafleXtreme MS instrument. Mass calibration was done with Bruker Peptide Calibration Standards II and with and insulin standard, mol. wt. 5,729.6087 Da (Sigma Aldrich). The peaks appearing on the MALDI spectra of the fractions were compared to those signals detected in the MSI experiments. Accordingly, marker peptides eluted in fractions 7, 9, 10, 14, and 15, and only these fractions were further processed for peptide sequencing.

8.4.2.2 Peptide sequencing by nanoLC–ICR-FTMS/MS. The fractions 7, 9, 10, 14, and 15 were analyzed using a custom 12 T LTQ-FT Ultra (Thermo Fisher Scientific, San Jose, CA) interfaced with a 1D NanoLC pump from Eksigent Technologies (Dublin, CA). The sample was loaded with helium bomb pressure (500 psi) to a trap column (75 µm inner diameter), 6 cm of which was fritted with LiChrosorb (EM Separations, Gibbstown, NJ) and packed with a C18 solid phase (15 µm, YMC Co., Ltd., Allentown, PA). The planarian sample was then separated on an analytical column (ProteoPep II^{TM} C18, 300 Å, 5 µm, New Objective, Woburn, MA). Data acquisition on the LTQ-FTMS consisted of a full scan event (500–2000 *m/z*, resolving power, $m/\Delta m_{50\%} = 90$ K in which $\Delta m_{50\%}$ is mass spectral peak full width at half-maximum peak height), and data-dependent CID MS/MS scans (90 K resolving power) of the five most abundant peaks from the previous full scan. MS/MS was carried out with an isolation width of 10 m/z, a minimum signal threshold of 1000 counts, a normalized collision energy of 41%, an activation Q of 0.4, and an activation time of 100 ms. Dynamic exclusion was enabled with a repeat count of 2, an exclusion duration of 180 s, and a repeat duration of 180 s.

8.4.2.3 FTMS/MS Data Analysis. Collected data files (*.raw) were analyzed using ProSightPC 2.0 (Thermo Fisher Scientific, San Jose, CA)[42] in high-throughput (HT) mode. Spectra were converted to ProSight experiments, each consisting of the monoisotopic neutral masses of one or more simultaneously fragmented (multiplexed) precursor species, and a list of monoisotopic neutral fragment masses. Conversion was carried out by the built-in signal processing functionality (cRAWler). Signal processing consisted of filtering precursor and fragment spectra by signal-to-noise ratio, summing spectra within precursor mass and retention time tolerance, and deisotoping the resulting summed spectra using the THRASH algorithm[43] to monoisotopic neutral masses.

8.4.2.4 Database Searching. The protein sequence database was generated from a six-frame translation of automatically-annotated ORFs resulting from the *de novo* sequence of the planarian genome,[36] incorporating potential N-terminal acetylation and N-terminal methionine cleavage. ProSight experiments resulting from each *.raw file were searched against a sequence database of predicted planarian proteins in Biomarker mode (nonspecific proteolysis), with a 1.1 Da precursor, and a 10 ppm fragment mass tolerance.[36] Potential hits (E-value < 10^{-4}) were processed by BLAST for structural similarity search[44] against eukaryotic sequences in the NCBI nr database and manual inspection for characteristic patterns of dibasic sites.

The complete sequence for the novel prohormone spp-21 (secreted prohormone sequence) was entered into the Neuropred application[45] (http://neuroproteomics.scs.illinois.edu/neuropred.html) to produce the predicted peptide library including masses of unmodified peptides and potential PTMs at consensus sites available. The SignalP application (http://www.cbs.dtu.dk/services/SignalP/) was used to determine the signal peptide dequences.[46]

8.5 Results and Discussion

Neuropeptides are suggested to be involved in the planarian CNS regeneration process.[14-17] We recently reported 40 prohormone genes and used several MS platforms (ESI-IT "ion trap" MS and MALDI-TOF MS) to identify 142 peptides (putative neuropeptides) from sexual and asexual strains of planarians, but do not know their functions. How can it be determined which peptides are involved? Mass spectrometry imaging (MSI) provides spatial distribution information and here it has been used at 0-hr and 3-day time points of planarian regeneration to discover how peptide signal distributions change during this period. Several are shown to be enhanced towards the blastema.

During application of the MALDI matrix in the MSI experiments, it was observed that the hydrophobic nature of the thin tissue sample causes low wettability and seemed to prevent the formation of MALDI matrix crystals on the sample surface. Initially, the MALDI matrix solution contained an equal fraction of organic:water, so a less polar matrix solution of 75:25 methanol:water was tried. This resulted in greater coverage and matrix crystallization on the tissue slice. The higher organic content also allowed the matrix solution to dry faster onto the sample surface upon spray application and so more matrix could be used in a shorter time. Using the artist's spray brush to blow a stream of air onto the sample in between successive matrix coatings also accelerated the intervening drying periods. In fact, the amount of MALDI matrix solution used here, ~35 mL of 30 mg/mL of DHB, is higher than in most MALDI-MSI studies. This larger amount was necessary to ensure sufficient coverage on the hydrophobic sample surface.

Mass spectrometry imaging provides both chemical and spatial information about thin tissue slices, and taking mass spectrometry images along a time axis adds temporal information to this. In Fig. 8.1, where the wound site is at the top of the images, the MSI ion distributions change along the time axis from 0-hr (left column), to 2-days (middle column), to 3-days (right column) after the start of the regeneration process. In Fig. 8.1D-F, the analyte at m/z 4874 is shown to localize at the wound site in Fig. 8.1F after 3-days. However, other types of changes are also seen as for instance where m/z 5117 localizes at the region of the pharynx in Fig. 8.1I, and the signal for m/z 4333 almost disappears after 3-days of regeneration in Fig. 8.1L. The biggest quantitative changes in signals in planarian regeneration are found after 3-days of regeneration and so this time point was used,[35] but the 2-day time point was also used because this is when the second phase of high mitotic activity begins.[2] Fig. 8.1 does show some intermediate changes in ion distributions at the 2-day time point between 0-hr and 3-days that correspond more closely to the distributions at the 3-day time point. In Fig. 8.1E, at 2-days the ions are seen to be located in the ventral nerve cords that are known to run bilaterally from head to tail,[47] but the distribution is confined to the rostral portion that is towards the wound site. Similarly for this mass, the distributions after 3-days are even more concentrated toward the blastema region of the tissue slice in Fig. 8.1F. In Fig. 8.1H, the distributions for *m/z* 5117 at the 2-day time point are very different and already begin to localize at the pharynx region corresponding to the circular shape seen the optical image in Fig. 8.1B,C. But by 3-days, the ion distribution is more concentrated at the region corresponding to the pharynx in Fig. 8.1I. For the signal at *m/z* 4333, the signal gradually disappears from the caudal portion of the tissue slices from 0-hr, to 2-days, to 3-days with the signal at 2-days in Fig. 8.1K at an intermediate level. The results of repeated MSI experiments at 0-hr and 3-days, N=4 in total, showed similar distributions for these masses. Experiments were not repeated at the 2-day time point. The reproducibility of the distributions is explored later in Fig. 8.3.

The mass spectrometry imaging datasets provided distribution information on many more analyte signals than those shown in Fig. 8.1. In fact, several masses were found to be redistributed towards the blastema after 3-days of regeneration: *m/z* 3507, *m/z* 3842, *m/z* 4874, *m/z* 5270, *m/z* 5365, *m/z* 5752, *m/z* 5861, *m/z* 5891, *m/z* 6674, *m/z* 7352, *m/z* 7423, *m/z* 7531, and *m/z* 7592. The signals in the MSI data were found only above 3000 Da because the mass spectrometry instrument settings were optimized for detection in this mass range, while little was seen < 3000 Da. Separate analyses could be done in the future focusing on lower masses. Because these signals are redistributed towards the blastema site, they may serve as spatial and temporal markers of the planarian regeneration process, and the next step is a characterization of these analytes with LC-FTMS/MS amino acid sequencing.

Following a first stage of LC separation on an extract of ~60 homogenized planaria, each LC fraction was analyzed by MALDI-TOF-MS for the presence of the analytes of interest that showed higher levels near the blastema site, as listed in the previous paragraph. The analyte-of-interest containing LC fractions were further analyzed by LC-FTMS/MS to produce *de novo* MS/MS amino acid sequence tags that were searched against the planarian genome. Matches to known planarian prohormones, such as the spp-15 (secreted prohormone sequence) and mpl-1 (myomodulin prohormone like) neuropeptides were found[6] as well as matches to unannotated proteins. As the planarian genome is unannotated, proteins sequences fished out with the help of MS/MS sequence tags were further analyzed for sequence similarity to known proteins deposited into the NCBI protein database (http://www.ncbi.nlm.nih.gov/protein) using BLAST.[44] As result, matches to metabolic and structural proteins and neuropeptide receptors from annotated genomes of other species have been found for the de novo sequence tags of the planarian peptides. The identifications that resulted from this process are provided in Table 8.1. Also found was a protein sequence that has no similarities among other species and had multiple dibasic amino acid sites that are characteristic of the structure of a neuropeptide prohormone. This sequence was characterized as novel planarian peptide prohormone that we named spp-20. Peptides encoded by this novel prohormone were detected at *m/z* 3000 and *m/z* 3843 (Table 8.1). Table 8.2 shows the theoretical masses of the predicted putative peptides from spp-20 based on assuming that posttranslational prohormone processing would occur at the dibasic sites in the novel sequence. Fig. 8.2 shows a structural analysis of the peptide m/z 3843 by tandem MS. A second protein sequence characteristic of a novel neuropeptide prohormone was found in the planarian genome database with a peptide sequence tag at *m/z* 1421, which we call spp-21. Table 8.3 shows the theoretical masses of the predicted putative peptides based on assuming that posttranslational prohormone processing would occur at the dibasic sites in the novel sequence. Many of these predicted peptides from the novel prohormone were seen in the imaging datasets.

Besides known or novel *S. mediterranea* peptides, Table 8.1 also includes matches of the obtained planarian sequences based on a sequence similarity to sequence tags of peptides and proteins from other species including from other planarian species. Several of these proteins are structural proteins. The *m/z* 1007.35 matches in similarity to a sequence for actins, which are structural proteins, from *A. aegypti* (mosquito). Similar as yet unidentified actins in planaria may be involved in the structural component of the regeneration process upon injury of the planaria.[48, 49] Another actin sequence from *C. gigas* (oyster) showed similarity to the sequence in Table 8.1 corresponding to *m/z* 1203.65, whereas *C. gigas* and *S. mediterranea* species are similar in that both classified as lophotrochozoa.[50] A tegumental protein from *S. japonicum*, a parasitic flatworm and relative to planarians, matches the *m/z* 1263.55 in Table 8.1. Such tegumental proteins are involved in protection of animals from damage through the epidermis and other organs. Upon injury and during growth of the blastema in the *S. mediterranea* animals studied here, tegumental proteins may be similarly involved.[51]

Besides structural proteins, several other proteins that may have different roles in cell proliferation were identified based on similarity in Table 8.1. The *m/z* 1427.61 has similarity with the 60S ribosomal subunit protein L29 from *A. flevus* (fungus), and the presence of this ribosome protein may point towards increased protein synthesis during regeneration as it does in humans[52] and mice.[53] The *m/z* 1531.81 sequence tag is similar to ornithine decarboxylase from *H. diversicolor* (sea snail) that is also a lophotrochozoan with *S. mediterranea*. Ornithine decarboxylase is an enzyme for synthesis of polyamines that are necessary for DNA repair during mitosis,[54] as could be linked with the increased mitosis in the postblastema in regenerating planaria. The *m/z* 1753.86 shows similarity to

LDL-related protein LRP6 from *D. melanogaster* (fruit fly). This protein is known to regulate cell proliferation through the Wnt signaling pathway in humans and mice.[55] The *m/z* 1966.06 has similarity with a predicted thypedin-like peptide from *S. kowalevskii* (acorn worm), and thypedin is known to cause cell proliferation in hydra.[56] The *m/z* 3694.94 is similar to β-thymosin from *S. japonicum* (parasitic flat worm), which is known to originate from the aforementioned thypedin. Most of these peptides and proteins identified based on sequence similarity have either structural functions in other species as in the case of actins and tegumental proteins, or are involved in cell proliferation as is the case for ribosomes, ornithine decarboxylase, low density lipoprotein, and thypedin. Further studies can be performed on the sequences from *S. mediterranea* that are presented in Table 8.1 to discover how or if they are involved in the planarian regeneration process.

Figure 8.3 shows ion distributions from mass spectrometry imaging data at 0-hr and 3-days of regeneration for several of the identified analytes. The left two columns show images of two different planaria tissue sections at the 0-hr time point and the right two columns show images of two different sections those a 3-days. While some similarity is observed among ion images of tissue slices taken from different animals at the same time point, reproducibility of ion distributions is difficult to achieve with these samples chiefly due to either differences in depths at which the tissue slices we taken, or from biological variation. Even though strongly reproducible images were not obtained, a general trend is seen of analytes that localize towards the blastema site after 3-days of regeneration compared to the ion images at 0-hr where more posterior signal is seen. The signal at *m/z* 822 as shown in Fig. 8.3E-H was identified at belonging to the a portion of the known prohormone spp-15[6] as corresponding to the amino acid sequence in the first row of Table 8.1. At 0-hr in Fig. 8.3E-F, this ion is localized towards the right lateral side of the tissue slice and towards posterior end. In contrast, this same ion is redistributed towards the wound site in Fig. 8.3G-H. A spatially sharp demarcation of the peptide distribution is seen in Fig. 8.3H, which may be explained by the newly formed blastema being compositionally distinct from the rest of the tissue section, which may lead to improved vaporization and extraction of the analyte. This sharp demarcation is particularly seen in the right most column of ion images, in the H and L panels. In Fig. 8.3I-L, the peptide at *m/z* 1966 has structural similarity to a larger thypedin protein sequence that contains repeating β-thymosin units and is also known to cause stem cell differentiation during foot formation in hydra and may have a similar function in planarians.[56] In the 3-day ion images in panels K-L, there is less evident agreement in terms of ion distributions among the two biological replicates, perhaps because tissue sections were taken at a different depth of the body plane. Nevertheless, there is generally more signal towards the top of both images, where blastema is located. The mass at *m/z* 3843 in Fig. 8.3Q-T corresponds to the parent ion of spp-20 predicted peptide A[138]-S[174] in Table 8.2, whose structure elucidation by tandem MS is shown in Fig. 8.2. This ion distribution is also seen to be redistributed toward the wound site. The mass at *m/z* 2019 in Fig. 8.3M-P corresponds to the predicted peptide S[104]-L[120] from the spp-21 prohormone, Table 8.3. In panels O-P, there is clear agreement of the localization of this ion towards the blastema in both images. As these peptides have been identified and are shown to be redistributed towards the wound site during planarian regeneration, future studies can focus more efficiently on functional characterization of these peptides.

Generally, more variability in ion distributions is seen in the left two columns of the tissue slices taken at 0-hr. Perhaps the regeneration process in the 3-day ion images is likely to cause increased peptide synthesis at the blastema compared to the rest of the animal thus resulting in the localizations seen in the MSI ion images.

One of the next steps in further characterizing planarian CNS regeneration is to further characterize the function of the peptides and proteins that were identified here. Knock-out studies using RNAi[57-59] can now be designed to gain insights about the two novel putative peptides that were discovered in this study. Additional studies can also be conducted on other signals in Table 8.1 that were shown from the mass spectrometry imaging data that redistribute towards the wound site.

Using mass spectrometry imaging, peptides that are markers for planarian regeneration were characterized based on changes in ion distributions during anterior regeneration. Several of these are neuropeptides, such those deriving from the two newly discovered prohormone sequences, and are likely involved in regeneration of CNS tissue at the blastema.

8.6 Figures & Tables

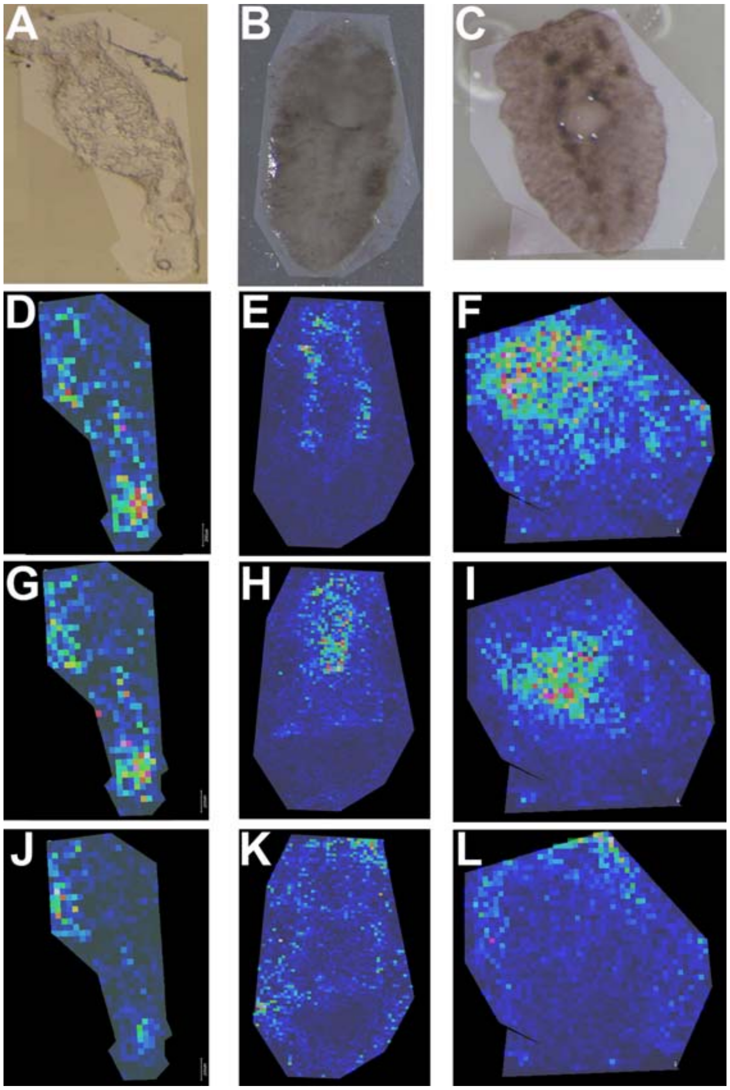

Figure 8.1. Mass spectrometry imaging of 20-μm longitudinal tissue sections of *S. mediterranea* showing different patterns of distribution changes over the time course of 3-days of regeneration. Optical images of serial tissue sections with the polygonal area of mass spectrometry image acquisition shown at (A) 0-hr, (B) 2-days, (C) and 3-days after head amputation. The wound site is at the top in all images. (D-F) MSI ion images for *m/z* 4874 showing redistribution towards the wound site after 3-days. (G-I) MSI ion images for *m/z* 5117 showing signals that are redistributed towards the pharynx region after 3-days (I). (J-L) MSI ion images of *m/z* 4333 showing little change after 3-days (L). Pixel size is 75 μm in all ion images.

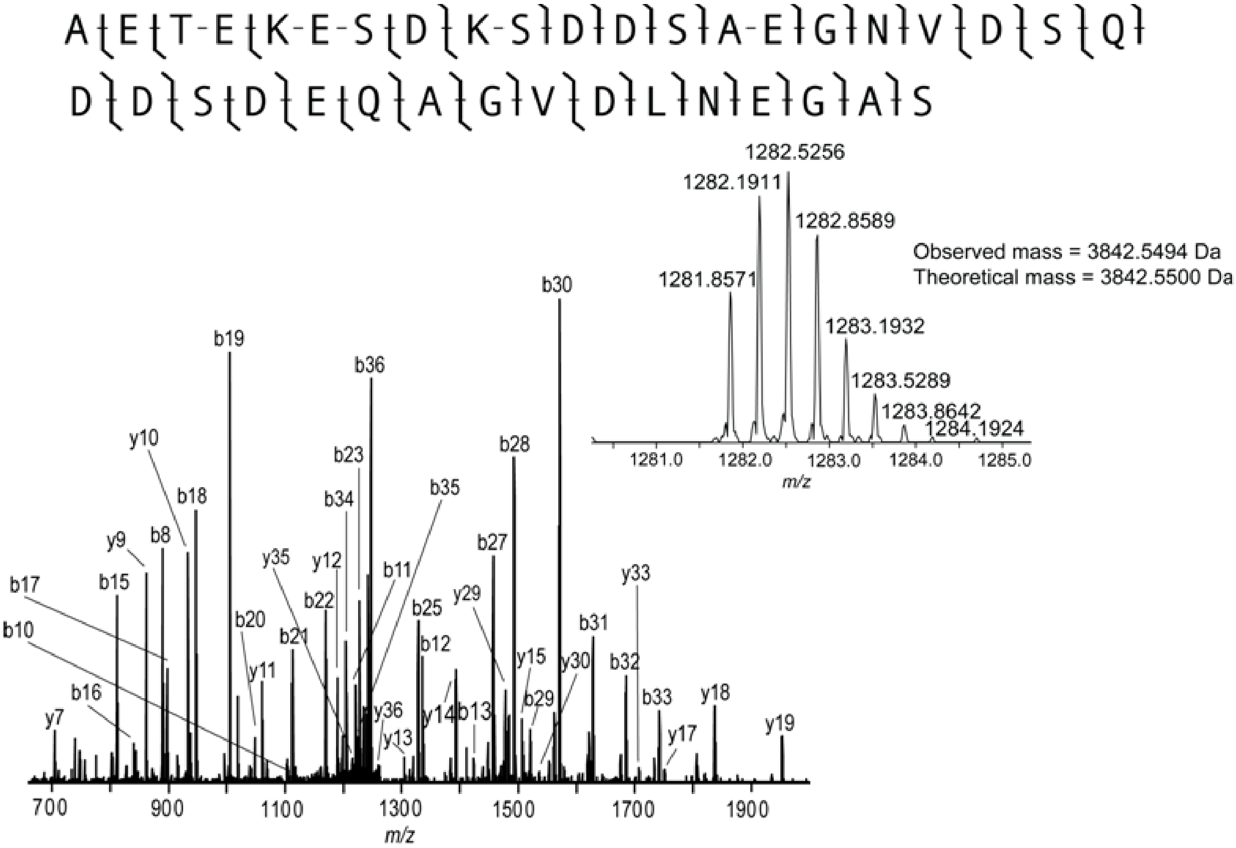

Figure 8.2 An FTMS/MS spectrum of a parent ion at *m/z* 3842 showing a sequence that corresponds to a peptide encoded by novel planarian prohormone spp-20. The sites of fragmentation with preference for placement of the positive charge are shown in the amino acid sequence at the top. The inset shows the triply charged parent ion.

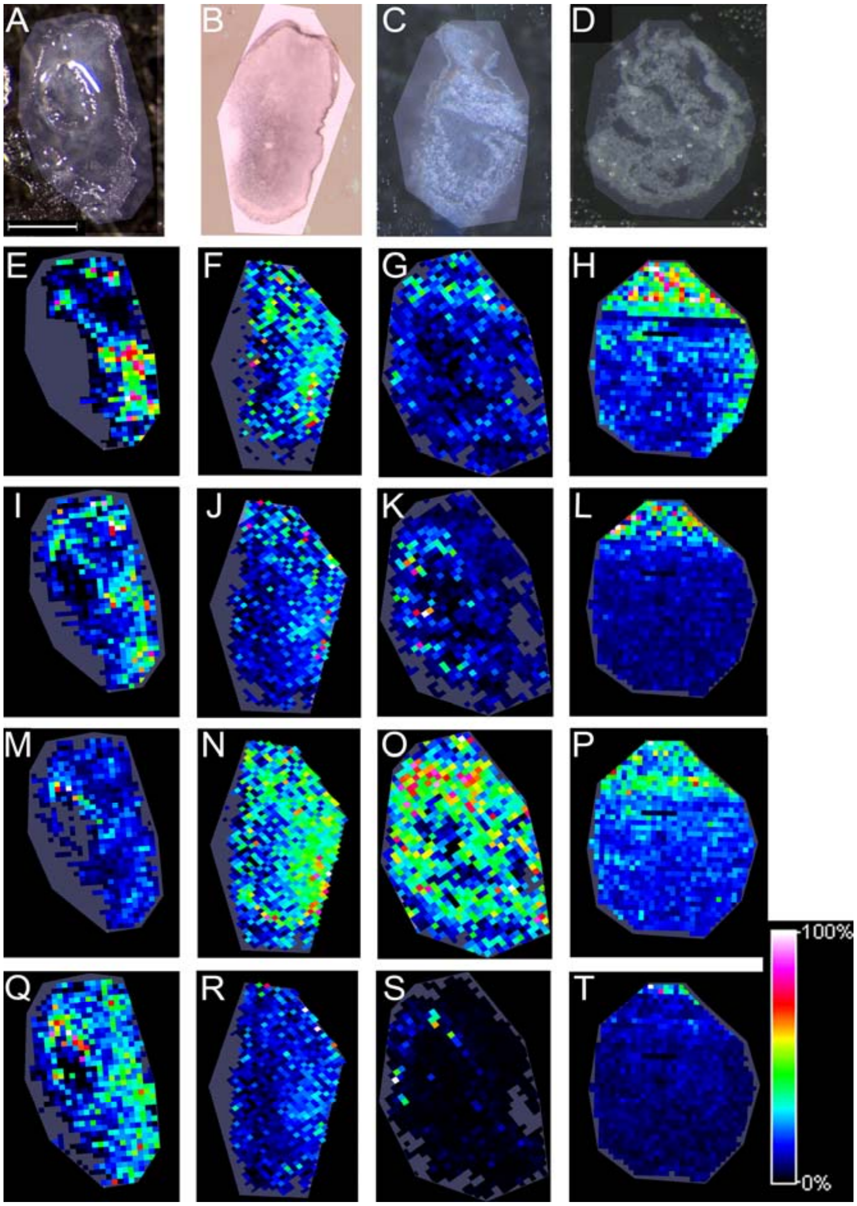

Figure 8.3. Mass spectrometry imaging of thin longitudinal tissue sections from *S. mediterranea* showing redistribution of identified analytes towards the wound site. Optical images of serial tissue sections with the polygonal area of mass spectrometry image acquisition are shown at (A, B) 0-hr and (C,D) 3-days after head amputation. The pharynx region is clearly visible in the center of the tissue slice in the left 0-hr optical image (A). The wound site is at the top in all images. (E-H) MSI ion images of *m/z* 822 of prohormone spp-15,[6] (I-L) *m/z* 1966 of β-thypedin, (M-P) *m/z* 2019 from spp-21, and (Q-T) *m/z* 3843 from prohormone spp-20, all showing obvious changes in ion distributions after 3-days of regeneration, usually tending toward the wound site.

Table 8.1. Identifications of planarian peptides. The mass columns listed as monoisotopic. The abbreviations are: spp (secreted prohormone peptide), mpl (myomodulin prohormone like), and ppp (pedal peptide prohormone like). The entries in bold face correspond to identifications of known planarian prohormones, whereas the other entires are based on the identifies of similar sequences from other species.

FTMS/MS Sequence Tag	Monoisotopic Mass	Mass Accuracy (ppm)	E-value	Sequence Name	Accession Numbers
KR.FDPIQFG.KR	**822.39**	**3.32**	**2.67E-13**	**spp-15 prohormone**	**BK007013**
HDSESFGDD	1007.35	4.73	4.46E-13	Actins	AAA62350.1
MESISHILF	1075.53	-7.5	1.69E-07	G-protein coupled receptor fragment	XP_002572360.1
KRS.TKPIDPNQYP.LVYGE	**1169.63**	**3.39**	**6.01E-05**	**spp-10 prohormone**	**BK007028**
KR.GAYYDPIGGGLL.KR	**1193.63**	**7.11**	**1.56E-05**	**ppp-1 prohormone**	**BK007041**
VAPEEHPVLLT	1203.65	0	4.10E-08	Actins	BAB84579.1
IYVCNKIYF	1218.60	-4.73	4.31E-05	PREDICTED: similar to radish CG4346-PA	XP_392825.3
KR.SSYYDPIGGGLL.KR	**1240.61**	**3.05**	**2.05E-10**	**ppp-1 prohormone**	**BK007041**
DQTHTDEKQY	1263.55	8.63	6.17E-10	Tegumental protein	AAO59421.2
KR.SYFDKIGNDLL.KR	**1283.64**	**-0.73**	**5.95E-06**	**ppp-2 prohormone**	**BK007018**
SMENRMAPSRML	**1421.67**	**5.23**	**4.59E-18**	**spp-21 prohormone**	**(not yet assigned)**
NMNDEFQFRDL	1427.61	2.22	5.70E-05	60S ribosomal subunit protein L29	XP_002372940.1
KR.IPGIGFNRNFAIY.KR	**1480.79**	**8.52**	**2.98E-05**	**spp-6 prohormone**	**GU295177**
SNKIIPNEDRSFI	1531.81	7.53	2.57E-07	Ornithine decarboxylase	ACJ63455.1

KR.TVGFGFNRNLHLY.KR	**1536.79**	**-5.32**	**1.32E-06**	**spp-7 prohormone**	**GU295178**
WFQQIFASISVNSDI	1753.86	-6.08	5.45E-07	LDL-related protein LRP6	AAF28358.1
TSPIVNEVHDFPKDKLK	1966.06	3.32	3.58E-18	Thypedin-like peptide	XP_002735323.1
IDINSNQYEEDYDPNDDHELD	**2552.00**	**-2.93**	**3.56E-08**	**mpl-1 prohormone**	**BK007017**
AETEKESDKSDDSAEGNVDSQDDSDEQA	**3000.18**	**4.5**	**4.76E-30**	**spp-20 prohormone**	**(not yet assigned)**
EEIEKGAPLKHVEVTEKVALPTKEDIEAEKQHA	3694.94	-0.22	1.34E-38	β-thymosin	CAX76731.1
AETEKESDKSDDSAEGNVDSQDDSDEQAGVDLNEGAS	**3842.55**	**-1.13**	**2.39E-48**	**spp-20 prohormone**	**(not yet assigned)**
RNEDPVGGIWPVDKCDEDTASLNYDDNVHNHYTIGSHAFVKSPNS	5069.26	-5.97	1.40E-06	PREDICTED: similar to radish CG4346-PA	XP_001631948.1
HADQTEIIDKSDAIENDSELETLTTFEENDAKNMNTKSYQELEN	5072.28	0.62	1.78E-05	PREDICTED: similar to radish CG4346-PA	XP_392825.3

Table 8.2. Predicted product peptide masses from the prohormone spp-20. The average and monoisotopic masses are presented for the predicted prohormone fragments based on assuming peptide bond cleavage at dibasic sites using the known motif model in the Neuropred application.[45] Some of these masses were observed with either the MSI or the FTMS/MS data, which are highlighted in bold italic.

Peptide	PTM applied	Predicted Aver. Mass	Predicted Mono. Mass	Peptide sequence
S21_E37	***TrimKR***	***1935.078***	***1933.943***	***SIGINNILEGQDKYNQE***
A80_D99	TrimKR	2226.027	2224.794	ADADEPEESDDDDDKDKSDD
A109_D128	TrimKR	2240.054	2238.809	AEADEPEESDDDDDKDKSDD
R79_D99	TrimKR	2382.215	2380.895	RADADEPEESDDDDDKDKSDD
K107_D128	TrimKR	2524.416	2523.006	KRAEADEPEESDDDDDKDKSDD
N177_D200	TrimKR	2751.679	2750.133	NIKRAEADEPEESDDDDDKDKSDD
N76_D99	TrimKR	2755.685	2754.073	NMKRADADEPEESDDDDDKDKSDD
A80_D104	TrimKR	2826.657	2825.081	ADADEPEESDDDDDKDKSDDKKDND
A109_D133	TrimKR	2840.684	2839.096	AEADEPEESDDDDDKDKSDDKKDND
R79_D104	TrimKR	2982.844	2981.182	RADADEPEESDDDDDKDKSDDKKDND
K107_D133	TrimKR	3125.045	3123.292	KRAEADEPEESDDDDDKDKSDDKKDND

D102_D128	TrimKR	3153.059	3151.298	DNDKRKRAEADEPEESDDDDDKDKSDD
N177_D205	TrimKR	3352.308	3350.419	NIKRAEADEPEESDDDDDKDKSDDKKDND
A138_S174	***TrimKR***	***3844.705***	***3842.553***	***AETEKESDKSDDSAEGNVDSQDDSDEQAGVDLNEGAS***
T210_S246	***TrimKR***	***3874.731***	***3872.564***	***TETEKESDKSDDSAEGNVDSQDDSDEQAGVDLNEGAS***
E40_S73	TrimKR	4048.982	4046.702	EKESNEINNPKDQIEDNSENNEENDERELEDQNS
K136_S174	TrimKR	4129.066	4126.749	KRAETEKESDKSDDSAEGNVDSQDDSDEQAGVDLNEGAS
K208_S246	***TrimKR***	***4159.093***	***4156.760***	***KRTETEKESDKSDDSAEGNVDSQDDSDEQAGVDLNEGAS***
A138_I178	TrimKR	4328.316	4325.870	AETEKESDKSDDSAEGNVDSQDDSDEQAGVDLNEGASKKNI
E40_R75	***Cleaved***	***4333.344***	***4330.89809***	***EKESNEINNPKDQIEDNSENNEENDERELEDQNSKR***
E40_M77	TrimKR	4578.640	4575.982	EKESNEINNPKDQIEDNSENNEENDERELEDQNSKRNM
K136_I178	TrimKR	4612.678	4610.066	KRAETEKESDKSDDSAEGNVDSQDDSDEQAGVDLNEGASKKNI
D131_S174	TrimKR	4757.709	4755.042	DNDKRKRAETEKESDKSDDSAEGNVDSQDDSDEQAGVDLNEGAS
D203_S246	TrimKR	4787.735	4785.053	DNDKRKRTETEKESDKSDDSAEGNVDSQDDSDEQAGVDLNEGAS
S21_S73	TrimKR	6250.406	6246.826	SIGINNILEGQDKYNQEKREKESNEINNPKDQIEDNSENNEENDERELEDQNS
S21_M77	***TrimKR***	***6780.064***	***6776.105***	***SIGINNILEGQDKYNQEKREKESNEINNPKDQIEDNSENNEENDERELEDQNSKRNM***
A138_D200	TrimKR	6834.716	6830.860	AETEKESDKSDDSAEGNVDSQDDSDEQAGVDLNEGASKKNIKRAEADEPEESDDDDDKDKSDD

Table 8.3. Predicted product peptide masses from the prohormone spp-21. The average and monoisotopic masses are presented for the predicted prohormone fragments based on assuming peptide bond cleavage at dibasic sites using the known motif model in the Neuropred application.[45] Some of these masses were observed with either the MSI or the FTMS/MS data, which are highlighted in bold italic.

Peptide	PTM applied	Predicted Aver. Mass	Predicted Mono. Mass	Peptide sequence
L30_S33	TrimKR	461.473	461.217	LNES
S109_L120	***TrimKR***	***1422.699***	***1421.663***	***SMENRMAPSRML***
S109_L120	TrimKR	1422.699	1421.663	SMENRMAPSRML
D38_V55	TrimKR	1942.073	1940.928	DNEAILYGNQQGSPHLSV
S104_L120	***TrimKR***	***2020.458***	***2019.059***	***SLIKRSMENRMAPSRML***
S104_K121	Extended	2148.632	2147.154	SLIKRSMENRMAPSRMLK
A101_L120	TrimKR	2375.898	2374.292	AKRSLIKRSMENRMAPSRML
Q224_D245	TrimKR	2477.798	2476.322	QSIADSLYRSKLEKLAELLAND
L30_V55	TrimKR	2982.266	2980.528	LNESRRKRDNEAILYGNQQGSP HLSV
S58_T93	TrimKR	4165.169	4162.701	SGRNPLESKMHSSNSQDDNNN EYAHEDSDDKYSYET
S58_L98	TrimKR	4804.023	4801.160	SGRNPLESKMHSSNSQDDNNN EYAHEDSDDKYSYETKRKLL
S180_N221	***TrimKR***	***4877.454***	***4874.405***	***SMLEDTNEPENIPYELVRVNGV PGLFFPLENPEIEKENYIIN***

F126_V177	***TrimKR***	***6216.683***	***6212.822***	***FVDDIDPITLERLRNMLENNYDSYYSDTGNQDYNDVVPYRVQEPNDDEMKPV***
R125_V177	TrimKR	6372.871	6368.923	RFVDDIDPITLERLRNMLENNYDSYYSDTGNQDYNDVVPYRVQEPNDDEMKPV

8.7 References

1. Forsthoefel, D. J. and Newmark, P. A. Emerging patterns in planarian regeneration. *Curr. Opin. Genet. Dev.* **2009,** *19*, 412–420.

2. Tettamanti, G., Saló, E., González-Estévez, C., Felix, D. A., Grimaldi, A., and Eguileor, M. d. Autophagy in invertebrates: insights into development, regeneration and body remodeling. *Curr Pharm. Des.* **2008,** *14*, 116-125.

3. Rouhana, L., Shibata, N., Nishimura, O., and Agata, K. Different requirements for conserved post-transcriptional regulators in planarian regeneration and stem cell maintenance. *Dev. Biol.* **2010,** *341* 429–443.

4. Kobayashi, C., Watanabe, K., and Agata, K. The process of pharynx regeneration in planarians. *Dev. Biol.* **1999,** *211*, 27–38.

5. Umesono, Y. and Agata, K. Evolution and regeneration of the planarian central nervous system. *Develop. Growth Differ.* **2009,** *51*, 185–195.

6. Collins, J. J., Hou, X., Romanova, E. V., Miller, C. M., Lambrus, B. G., Sweedler, J. V., and Newmark, P. A. Genome-wide analyses reveal a regulatory role for peptide hormones in planarian germline development. *PloS Biol.* **2011,** in press.

7. Nishimura, K., Kitamura, Y., Inoue, T., Umesono, Y., Sano, S., Yoshimoto, K., Inden, M., Takata, K., Taniguchi, T., Shimohama, S., and Agata, K. Reconstruction of dopaminergic neural network and locomotion function in planarian regenerates. *Dev. Neurobiol.* **2007,** *67*, 1059-1078.

8. Oviedo, N. J., Newmark, P. A., and Alvarado, A. S. Allometric scaling and proportion regulation in the freshwater planarian Schmidtea mediterranea. *Dev. Dyn.* **2003,** *226*, 326–333.

9. Pellettieri, J., Fitzgerald, P., Watanabe, S., Mancuso, J., Green, D. R., and Alvarado, A. S. Cell death and tissue remodeling in planarian regeneration. *Dev. Biol.* **2010,** *338* 76–85.

10. Guo, T., Peters, A. H. F. M., and Newmark, P. A. A bruno-like gene Is required for stem cell maintenance in planarians. *Dev. Cell* **2006,** *11*, 159–169.

11. Zhang, Y.-F., Ye, B.-P., and Wang, D.-Y. Molecular actions guiding neural regeneration in planarian. *Neurosci. Bull.* **2008,** *24*, 329-337.

12. Cebrià, F. and Newmark, P. A. Planarian homologues of netrin and netrin receptor are required for proper regeneration of the central nervous system and the maintenance of nervous system architecture. *Development* **2005,** *132*, 3691-3703.

13. Kreshchenko, N. D. Functions of flatworm neuropeptides NPF, GYIRF and FMRF in course of pharyngeal regeneration of anterior body fragments of planarian, Girardia tigrina. *Acta Biol. Hung.* **2008,** *59 Suppl.*, 199-207.

14. Bautz, A. and Schilt, J. Somatostatin-like peptide and regeneration capacities in planarians. *Gen. Comp. Endocrinol.* **1986,** *64*, 267-272.

15. Salo, E. and Baguna, J. Stimulation of cellular proliferation and differentiation in the intact and regenerating planarian Dugesia(G) tigrina by the neuropeptide substance P *J. Exp. Zool.* **1986,** *237*, 129-135.

16. Hori, I. Cytological approach to morphogenesis in the planarian blastema. II. the effect of neuropeptides. *J. Submicr. Cytol. Pathol.* **1997,** *29*, 91-97.

17. Baguna, J., Salo, E., and Romero, R. Effects of activators and antagonists of the neuropeptides substance P and substance K on cell proliferation in planarians. *Int. J. Dev. Biol.* **1989,** *33*, 261-264.

18. Schaller, H. C., Hoffmeister, S. A. H., and Dubel, S. Role of the neuropeptide head activator for growth and development in hydra and mammals. *Development* **1989,** *Supplement*, 99-107.

19. Harvey, P., Gong, B., Rossomando, A. J., and Frank, E. Topographically specific regeneration of sensory axons in the spinal cord. *Proc. Natl. Acad. Sci* **2010,** *107*, 11585-11590.

20. Philp, D. and Kleinman, H. K. Animal studies with thymosin β4, a multifunctional tissue repair and regeneration peptide. *Ann. N. Y. Acad. Sci.* **2010,** *1194*, 81-86.

21. Zhang, F., Huang, P., Yang, P., and Zhang, X. Effects of p75 neurotrophin receptor knockout on axonal regeneration in a mouse model of facial nerve injury. *Neural Regen. Res.* **2009,** *4*, 565-569.

22. Hummon, A. B., Amare, A., and Sweedler, J. V. Discovering new invertebrate neuropeptides using mass spectrometry. *Mass Spectrom. Rev.* **2006,** *25*, 77-98.

23. Hatcher, N. G., Atkins, N., Annangudi, S. P., Forbes, A. J., Kelleher, N. L., Gillette, M. U., and Sweedler, J. V. Mass spectrometry-based discovery of circadian peptides. *Proc. Natl. Acad. Sci.* **2008,** *105*, 12527-12532.

24. Brockmann, A., Annangudi, S. P., Richmond, T. A., Ament, S. A., Xie, F., Southey, B. R., Rodriguez-Zas, S. R., Robinson, G. E., and Sweedler, J. V. Quantitative peptidomics reveal brain peptide signatures of behavior. *Proc. Natl. Acad. Sci* **2009,** *106*, 2383–2388.

25. Fricker, L. D., Lim, J., Pan, H., and Che, F. Y. Peptidomics: identification and quantification of endogenous peptides in neuroendocrine tissues. *Mass Spectrom. Rev.* **2006,** *25*, 327-344.

26. Svensson, M., Sköld, K., Svenningsson, P., and Andren, P. E. Peptidomics-based discovery of novel neuropeptides. *J. Proteome Res.* **2003,** *2*, 213–219.

27. Chaurand, P., Cornett, D. S., and Caprioli, R. M. Molecular imaging of thin mammalian tissue sections by mass spectrometry. *Curr. Opin. Biotechnol.* **2006,** *17*, 431-436.

28. Rohner, T. C., Staab, D., and Stoeckli, M. MALDI mass spectrometric imaging of biological tissue sections. *Mech. Age. Dev.* **2005,** *126*, 177-185.

29. Zimmerman, T. A., Monroe, E. B., Tucker, K. R., Rubakhin, S. S., and Sweedler, J. V. Chapter 13: imaging of cells and tissues with mass spectrometry: adding chemical information to imaging. *Meth. Cell Biol.* **2008,** *89*, 361-390.

30. Hove, E. R. A. V., Smith, D. F., and Heeren, R. M. A. A concise review of mass spectrometry imaging. *J. Chromatogr. A* **2010,** *1217*, 3946-3954.

31. Seeley, E. H. and Caprioli, R. M. Imaging mass spectrometry: towards clinical diagnostics. *Proteomics Clin. Appl.* **2008,** *2* 1435–1443.

32. Debois, D., Bertrand, V., Quinton, L., DePauw-Gillet, M.-C., and DePauw, E. MALDI-in source decay applied to mass spectrometry imaging: a new tool for protein identification. *Anal. Chem.* **2010,** *82*, 4036-4045.

33. Meistermann, H., Norris, J. L., Aerni, H.-R., Cornett, D. S., Friedlein, A., Erskine, A. R., A.Augustin, Mudry, M. C. D. V., Ruepp, S., Suter, L., Langen, H., Caprioli, R. M., and Ducret, A. Biomarker discovery by imaging mass spectrometry: transthyretin is a biomarker for gentamicin-induced nephrotoxicity in rat. *Mol. Cell Proteomics* **2006,** *5*, 1876-1886.

34. Rubakhin, S. S., Jurchen, J. C., Monroe, E. B., and Sweedler, J. V. Imaging mass spectrometry: fundamentals and applications to drug discovery. *Drug Discov. Today* **2005,** *10*, 823-837.

35. Romanova, E. V., Collins, J. J., Newmark, P. A., and Sweedler, J. V., "Spatial and temporal analyses of peptides during regeneration in the planarian Schmidtea mediterranea by mass spectrometry," presented at the Society for Neuroscience, Chicago, IL, 2009.

36. Robb, S. M. C., Ross, E., and Alvarado, A. S. SmedGD: the Schmidtea mediterranea genome database. *Nucl. Acids Res.* **2007,** *36*, D599-D606.

37. Desiderio, D. M. Analysis of endogenous neuropeptides by reversed-phase high-performance chromatography and mass spectrometry. *Anal. Chim. Acta* **1997,** *352*, 85-102.

38. Pagán, O. R., Rowlands, A. L., Azam, M., Urban, K. R., Bidja, A. H., Roy, D. M., Feeney, R. B., and Afshari, L. K. Reversal of cocaine-induced planarian behavior by parthenolide and related sesquiterpene lactones. *Pharmacol Biochem Behav.* **2008,** *89*, 160-170.

39. Zhang, L.-K., Rempel, D., Pramanik, B. N., and Gross, M. L. Accurate mass measurements by Fourier transform mass spectrometry. *Mass Spectrom. Rev.* **2005,** *24*, 286-309.

40. Meng, F., Forbes, A. J., Miller, L. M., and Kelleher, N. L. Detection and localization of protein modifications by high resolution tandem mass spectrometry. *Mass Spectrom. Rev.* **2005,** *24*, 126-134.

41. Zimmerman, T. A., Rubakhin, S. S., Romanova, E. V., Tucker, K. R., and Sweedler, J. V. MALDI mass spectrometric imaging using the stretched sample method to reveal neuropeptide distributions in Aplysia nervous tissue. *Anal. Chem.* **2009,** *81*, 9402–9409.

42. Boyne, M. T., Garcia, B. A., Li, M. X., Zamdborg, L., Wenger, C. D., Babai, S., and Kelleher, N. L. Tandem mass spectrometry with ultrahigh mass accuracy clarifies peptide identification by database retrieval. *J. Proteome Res.* **2009,** *8*, 374-379.

43. Horn, D. M., Zubarev, R. A., and McLafferty, F. W. Automated reduction and interpretation of high resolution electrospray mass spectra of large molecules. *J. Am. Soc. Mass Spectrom.* **2000,** *11*, 320-332.

44. Altschul, S. F., Gish, W., Miller, W., Myers, E. W., and Lipman, D. J. Basic local alignment search tool. *J. Mol. Biol.* **1990,** *215*, 403–410.

45. Southey, B. R., Amare, A., Zimmerman, T. A., Rodriguez-Zas, S. L., and Sweedler, J. V. NeuroPred: a tool to predict cleavage sites in neuropeptide precursors and provide the masses of the resulting peptides. *Nucl. Acids Res.* **2006,** *34*, W267-W272.

46. Bendtsen, J. D., Nielsen, H., Heijne, G. V., and Brunak, S. Improved prediction of signal peptides: SignalP 3.0. *J. Mol. Biol.* **2004,** *340*, 783-795.

47. Cebrià, F. Regenerating the central nervous system: how easy for planarians! *Dev. Genes Evol.* **2007,** *217*, 733-748.

48. Pascolini, R., Rosa, I. D., Fagotti, A., Panara, F., and Gabbiani, G. The mammalian anti-α-smooth muscle actin monoclonal antibody recognizes an α-actin-like protein in planaria (Dugesia lugubris s.l.). *Differentiation* **1992,** *51*, 177-186.

49. Pascolini, R., Panara, F., Rosa, I. D., Fagotti, A., and Lorvik, S. Characterization and fine-structural localization of actin- and fibronectin-like proteins in planaria (Dugesia lugubris s.l.). *Cell Tissue Res.* **1992,** *267*, 499-506.

50. Podsiadlowski, L., Braband, A., Struck, T. H., Döhren, J. v., and Bartolomaeus, T. Phylogeny and mitochondrial gene order variation in Lophotrochozoa in the light of new mitogenomic data from Nemertea. *BMC Genomics* **2009,** *10*, 364-378.

51. Morita, M. and Best, J. B. Electron microscopic studies of planarian regeneration. *J. Exp. Zool.* **1974,** *187*, 345-374.

52. Liu, J.-J., Huang, B. H., Zhang, J., Carson, D. D., and Hooi, S. C. Repression of HIP/RPL29 expression induces differentiation in colon cancer cells. *J. Cell. Physiol.* **2006,** *207*, 287-292.

53. Kirn-Safran, C. B., Julian, J., Fongemie, J. E., Hoke, D. E., Czymmek, K. J. C., and 1, D. D. C. Changes in the cytologic distribution of heparin/heparan sulfate interacting protein/ribosomal protein L29 (HIP/RPL29) during in vivo and in vitro mouse mammary epithelial cell expression and differentiation. *Dev. Dyn.* **2002,** *223*, 70–84.

54. Pendeville, H., Carpino, N., Marine, J.-C., Takahashi, Y., Muller, M., Martial, J. A., and Cleveland, J. L. The ornithine decarboxylase gene is essential for cell survival during early murine development. *Mol. Cell. Biol.* **2001,** *21*, 6549-6558.

55. Wang, X., Adhikari, N., Li, Q., and Hall, J. L. LDL receptor-related protein LRP6 regulates proliferation and survival through the Wnt cascade in vascular smooth muscle cells. *Am. J. Physiol. Heart. Circ. Physiol.* **2004,** *287*, H2376-H2383.

56. Herrmanna, D., Hattab, M., and Hoffmeister-Ullericha, S. A. H. Thypedin, the multi copy precursor for the hydra peptide pedin, is a beta-thymosin repeat-like domain containing protein. *Mech. Dev.* **2005,** *122* 1183–1193.

57. Wang, Y., Zayas, R. M., Guo, T., and Newmark, P. A. nanos function is essential for development and regeneration of planarian germ cells. *Proc. Natl. Acad. Sci.* **2007,** *104*, 5901–5906.

58. Newmark, P. A. Opening a new can of worms: a large-scale RNAi screen in planarians. *Dev. Cell* **2005,** *8* 623-624.

59. Newmark, P. A., Reddien, P. W., Cebrià, F., and Alvarado., A. S. Ingestion of bacterially expressed double-stranded RNA inhibits gene expression in planarians. *Proc. Natl. Acad. Sci.* **2003,** *100(suppl. 1)*, 11861-11865.

CHAPTER 9

CONTRIBUTIONS TO NEUROPRED SOFTWARE FOR PREDICTING FINAL SIGNALING PEPTIDE PRODUCTS AND THEIR MASSES

9.1 Notes and Acknowledgements

Andinet Amare, Sandra L. Rodriguez-Zas, Bruce R. Southey, and Jonathan V. Sweedler were collaborators on the NeuroPred work. This work is supported by the National Institutes of Health under Award No. DE018866, and the National Institute on Drug Abuse under Award No. DA017940 and No. DA018310 to the UIUC Neuroproteomics Center on Cell-Cell Signaling. While material in this chapter was not reproduced from previous publications, the Neuropred application was published as B. R. Southey, A. Amare, T.A. Zimmerman, S.L. Rodriguez-Zas, J.V. Sweedler, Nucleic Acids Res. **34,** W267-272 (2006).

9.2 Abstract

Prohormones contain several peptides within their sequences that are released by cleavage of peptide bonds. These fragments are further modified with posttranslational modifications (PTMs) to create a final series of signaling peptide products. The structure of the final signaling peptide products can be somewhat predicted based on how enzymes reproducibly act on and modify certain peptide structures. The masses of the final predicted products can be calculated and then verified with measurements by mass spectrometry. In this chapter, a web-based software suite, including new statistical models to predict prohormone processing based on the initial genetic sequence information was enhanced with a contribution of more efficient programming. The results

of this binary logistics model, along with a contribution of consensus sequences for posttranslational modifications (PTMs), were incorporated into NeuroPred software that predicts prohormone processing. The use of NeuroPred software for new applications since its development is also reviewed.

9.3 Introduction

Neuropeptides and other signaling peptides are a diverse set of cell-to-cell signaling molecules in the nervous system and the functions of some of them have been characterized, such as regulation of homeostasis, feeding behavior, learning, memory, and circadian rhythms. Many signaling peptides transmit signals as hormones by binding to receptors to regulate these functions. To study signaling peptides, characterization of their chemical structures is done with mass spectrometry.[1, 2] Mass spectrometry allows future identification of signaling peptide locations within brain tissue and may allow detection of changes in signaling peptide levels in response to disease states or drug abuse.

The basic structure of signaling peptides is known. First, a prohormone is translated into a polypeptide from the mRNA. The prohormone is a precursor polypeptide that contains several signaling peptides and/or several copies of the same signaling peptide within its primary sequence of amino acids. Additionally, the portion of the prohormone at the N-terminus is called a signal sequence that is used as a transport marker. The signal sequence is cleaved off and the individual signaling peptides are released by enzymes called prohormone convertases, which cleave prohormones at the carbon-nitrogen peptide bond that is adjacent to amino acids with basic side chains, lysine (K) or arginine (R).[3] Cleavage breaks the bond and produces smaller peptides, which may be bioactive signaling peptide products. Cleavage sites often occur at monobasic (K or R), dibasic (KR or RR), or even tribasic motifs found within in the prohormone amino acid sequence. Specific amino acids associated with these sites are not always cleaved, and so have an associated probability (Figure 9.1). The probability of cleavage is largely determined by the properties of the amino acids that neighbor the basic site are favorable for convertase enzymes to operate at that place in the sequence. For example, presence of amino acids with bulky side chains, like proline, near the basic site tends to lower the probability of cleavage at that site. Using the identity of amino acid residues surrounding the basic site and knowledge of currently known cleaved sites, a statistical model can be built to predict the probability of cleavage for new uncharacterized basic sites.[3]

NeuroPred is freely-available online software designed to use genomic information to predict the final signaling peptide products (http://neuroproteomics.scs.uiuc.edu/NeuroPred.html).[4] The primary sequence of amino acids that is obtained from the genomic information reveals sequences containing basic sites. Based on the identity of the surrounding amino acids, the probability of enzymatic cleavage is assigned a value and predicts whether enzymatic cleavage happens. NeuroPred then calculates the theoretical masses of the final products, which can be compared to the masses obtained from mass spectrometry experiments. Mass-to-charge peaks can then be associated with a chemical identity.

The prediction of prohormone enzymatic processing to reveal the structure of final signaling peptide products is automated by the NeuroPred suite. The next section of the chapter explains how I contributed to the development of a binary logistics model to predict enzymatic cleavage of signaling peptides, which forms one model used by NeuroPred. The following section explains my contributions to NeuroPred in terms of adding the ability to determine posttranslational modifications (PTMs) of the cleaved peptides. The final section reviews how NeuroPred, in combination with mass spectrometry or genomics information, has been useful for a variety of new applications in the 3 years since its development.

9.4 Increasing the Computational Efficiency of Models to Predict Enzymatic Cleavage

A statistical method called binary logistics regression is used to predict whether a basic site is likely to be enzymatically cleaved.[5] Binary logistics regression works when an outcome to be predicted is binary, and in this case the site is either cleaved or not cleaved. In the general form of the logit function given in Eq. 1, p is the probability of cleavage and the quantity $p/(1-p)$ is the odds of cleavage. The right side of the equation is the formula for a linear line with slope and intercept, often expressed as y=mx+b, but where β_1 is the slope and β_0 is the intercept. In this case, the binary knowledge of previously characterized basic sites as to whether they are cleaved forms the left side of Eq. 9.1 and the identity of the surrounding amino acids and their distance from the basic site provides the values for X. The slope and intercept were then able to be derived for each amino acid/position combination, and Eq. 9.1 can then be applied to predict the cleavages of new and uncharacterized basic sites. A total of 18 amino acid positions surrounding each basic site were considered in the model.[6] If the summed probabilities over all positions exceed a certain threshold, cleavage of the basic site is predicted to occur.

$$\ln\left(\frac{p}{1-p}\right) = \beta_0 + \beta_1 X \tag{9.1}$$

During creation of the binary logistics model to predict enzymatic cleavages, it is important to choose the appropriate software platform. The MiniTab software package (www.minitab.com) was used to build a binary logistics regression model based on amino acid and position combinations located around basic sites. The model reported the residues surrounding the basic site within the 18 amino acid window that were the most statistically significant with respect to the likelihood of peptide bond cleavage. MiniTAB then required the user to manually update the model before it was run again in an iterative fashion. Each time the model was run, the least significant amino acid/position combination was removed and the model was run again. This manual updating process in MiniTAB proved to be tedious and time consuming. Matlab and the Statistics (www.mathworks.com) and Logit (http://www.ludgerhentschel.com/) Toolboxes can also be programmed to build such models. I recreated the model from MiniTAB using Matlab and wrote an additional routine in Matlab that automated the model updating process, allowing the iterative process to occur without requiring user input. Using the Matlab code, the results were obtained much faster than if they would have been obtained with MiniTAB. In fact, significant time was saved by using the newly created Matlab routine. The final model of the most significant amino acid/position combinations as reported by Matlab was entered into MiniTAB and applied to produce the data in Table 2 and Table 4 of Amare et al.[6] In this way, custom written software can adapt an existing process to make it more efficient. The current prediction approach in NeuroPred incorporates a variety of computational models, so that the Matlab code is no longer used.

The model described here was for predicting enzymatic cleavage at basic sites from mammalian prohormone primary sequences.[6] NeuroPred additionally combines this with similar models for predicting enzymatic cleavage from insects[7], mollusks[5], and other criteria[8, 9] and presents these models in a web-based interface, NeuroPred. Further predictive power was added by the use of advanced computational methods such as artificial neural networks, which are multi-layered perceptrons consisting of an input layer, hidden layer, and output layer. For the case of predicting neuropeptide products, the input layer consists of input nodes that each conatin pieces of information on the amino acid composition or amino acid properties (i.e. basic, acidic, hydrophobic). The output layer is a prediction of either amino acid bond cleavage or of leaving of the bond uncleaved. The intermediate hidden layer contains a number of nodes that can account for nonlinear effects, such as the presence of certain combinations of amino acids in a consensus sequence.[8] While predicting cleavage sites in neuropeptide sequences from human, mouse, rat, and cattle, it was found that artifical neural networks outperformed logistic regression models that do not account for non linear effects. The superior prediction from the artifical neural networks suggests that nonlinear effects are present like consensus sequences. Artifical neural networks were also applied to prediction of cleavage sites from insect sequences, and the superiority of prediction was not as high compared to logistic regression models perhaps due to the large genetic divergence between insect species and sequences used. In terms of prediction on insects, artifical neural networks mostly had higher sensitivity (true positives divided by total positives) and lower specificity (true negatives divided by total negatives) than logistic regression models, suggesting that either of the types of prediction models can be used depending on what needs to be optimized.[7] Another type prediction model is based on the support vector machine (SVM),[10, 11] which is related to artificial neural networks, where a multidimensional hyperplane is constructed that can separates that data into two categories (cleaved vs. not cleaved) within a hyperspace. The hyperplane, while flat in higher spatial dimensions, is not flat when plotted in lower dimensions. This nonlinearity is used to provide enhanced predictive power when separating data into two classes (cleaved vs. not cleaved). SVMs were applied to predicting cleaveage sites in neuropeptide sequences from humans and rhesus macaques, where SVMs outperformed artificial neural networks, logisitc regression models, and the known motif model (based only on the presence of basic amino acid motifs).[10]

9.5 NeuroPred and Posttranslational Modifications

The signaling peptide products that were produced from the prohormone by enzymatic cleavage are often further modified with posttranslational modifications (PTMs), where an enzyme might attach a functional group like a sulfate or acetyl group to an amino acid side chain. PTMs add to the variety of signaling molecules and regulate the activity of signaling peptides. The probability of certain PTMs occurring is sometimes indicated by the presence of a consensus sequence. An example is when a glycine residue occurs next to a C-terminal basic site that was cleaved, it is often oxidized, removed, and the C-terminus is amidated via enzymatic processes. PTMs such as the amidation just described are often required for bioactivity. Biochemically, amidation may prevent ionization of the C-terminus and create a hydrophobic peptide that can successfully interact with its receptor.[12] Another example of a consensus sequence is for N-linked glycosylation, where an enzyme covalently attaches a sugar group to the nitrogen atom on the side chain of the asparagine residue that occurs in the consensus sequence Asparagine-X-Serine, where X is any amino acid. Another part of this consensus information for N-linked glycosylation is that the consensus usually appears in regions of the signaling peptide sequence that are closer to the N-terminus. I contributed a table of other consensus sequences that were compiled through searching the scientific literature, and that were incorporated into the NeuroPred application.[4] These appear in Table 9.1 with the associated literature references tabulated at the end of this chapter. Adding the ability to NeuroPred to predict PTMs that involve addition of functional groups to signaling peptides was an important addition, as PTMs often occur on signaling peptides.

Posttranslational modifications are found among many different classes of proteins and result in changes in protein functions like activity, transport, degradation, and preservation. Only some of the many possible PTMs are found to occur on signaling peptides, the main ones being listed in Table 9.1. While the functions of many PTMs are known, the functions of some PTMs within signaling peptides are not completely characterized, such as for acetylation and O-glycosylation. The role of the rare PTM bromination is unknown, although it has been suggested that bromination prevents peptide degradation when added to an N-terminal tryptophan residue.[13]

One of the main functions of PTMs in signaling peptides is to regulate activity. Amidation is necessary for the activity of a number of signaling peptides. Similarly, the presence of pyroglutamination is necessary for the activity of several hormones, such as thyrotropin-releasing hormone (TRH), gonadotropin-releasing hormone (GnRH), and corticotropin-releasing hormone (CRH).[14] Sulfation, while known to affect signaling peptides in terms of activity, transport, and enzymatic cleavage, specifically regulates the activity of cholecystokinin that controls the speed of digestion and the sense of hunger.[15]

Another role for PTMs is in the secretion process for signaling peptides. N-linked glycosylation is used to increase the stability of secreted neuropeptides,[16] while phosphorylation is a marker for synaptic vesicle exocytosis.[17] In addition, hydroxylation of proline residues, while used to preserve collagen in connective tissue, in signaling peptides may be related to transport properties.[18] In another example, methylation of hydroxyl groups of glutamate residues is a reversible PTM used for inactivation, storage, and reactivation of anterior pituitary hormones in mammals. One example of methylation is of the prolactin signaling peptide that has a role in regulating mammalian lactation.[19]

By including the specific consensus sequences found in Table 9.1 as rules for the prediction of the location of PTMs, NeuroPred assists in the complete characterization of signaling peptides. Combining NeuroPred with mass spectrometry methods that can detect PTMs[20] will allow the locations of more PTMs to be identified so that their functions can be further explored.

9.6 Adaptability of NeuroPred to New Applications

NeuroPred is a web lauchable application with advanced options such as the prediction of posttranslational modifications.[4,1] An additional feature of NeuroPred is the calculation of masses of the predicted products. As such, NeuroPred has been used in a number of mass spectrometry studies of the nervous system. The theoretical masses calculated by NeuroPred can be compared to mass spectrometry data from the analysis of a neuronal sample to assign unknown mass-to-charge peaks with a chemical identity. NeuroPred was designed to work with several types of mass spectrometry data, including from CE-MS, which can be used to study the contents of single neurons.[21] NeuroPred as combined with either mass spectrometry or bioinformatics has been adapted to a number of new applications. The new applications that are reviewed below include studying PTMs in drug addiction, prediction of bioactive peptides in mammalian models, neuropeptide discovery in cattle and rat genomes, and characterizing protein transport processes.

Signaling peptides are involved in tolerance, withdrawal, and sensitization mechanisms that are in response to drugs of abuse. Several prohormones have been so implicated, including cocaine- and amphetamine-regulated transcript (CART) peptide in the mechanism of addiction reinforcement, and the opioid class of neuropeptides in reward effects and reward seeking behavior. Many such signaling peptides undergo common posttranslational modifications if they are located in specific brain regions, such as N-terminal acetylation of β-endorphin or differential enzymatic cleavage of the prohormone pro-opiomelanocortin (POMC) to yield different levels of endorphins.[22] When using mass spectrometry to study complex brain samples, NeuroPred can be used to predict the masses of possible signaling peptides including their posttranslational modifications. Similarly, NeuroPred in combination with mass spectrometry can be used to study signaling peptides that can act as either drugs or drug targets for the treatment of disease.[23] For example, the PTM of phosphorylation on signaling peptides may induce degradation of cancer cells. NeuroPred will have many similar future applications in studying signaling peptides involved in drug abuse or medicinal treatments.

The cleavage prediction capabilities of NeuroPred can be more broadly applied than the PTM prediction and were used to predict peptide products from not only prohormones but also from other types of bioactive peptides. NeuroPred was used for automated prediction of bioactive peptide products from very large precursor proteins in a database of bioactive peptides in metazoa. In addition to predicting signaling peptide products, the enzymatic cleavage prediction modality of NeuroPred was used to predict the sequences of other types of bioactive products in metazoa including growth factors, antimicrobial peptides, and antifreeze proteins.[24] In another study, NeuroPred was used to predict hundreds of cleavage sites in prohormones from human, cattle, rat, and mouse. After validating these results against empirically found cleavage information, it was found that the mammalian models for cleavage prediction performed well across these mammalian species.[8] The cleavage prediction modality of NeuroPred can be used by itself to predict the sequences of various kinds of bioactive peptides.

NeuroPred can also be used to discover putative signaling peptides from genomic information. NeuroPred predicted the prohormone products from a single species of cattle. Only 42 cattle prohormones had been previously validated by experiments. After using a series of bioinformatics tools, including BLAST alignment ad NeuroPred, 92 new putative prohormone sequences were identified. Among those signaling peptides that were found are relaxin that functions in the birthing process and calcitonin that regulates calcium homeostasis.[9] In another example of signaling peptide discovery, MALDI MS and FTMS mass-to-charge peaks from the analysis of rat supraoptic nucleus (SON) were mass matched to within 150 ppm Daltons to signaling peptide product masses as predicted by NeuroPred. About 40 neuropeptide products were mass matched using NeuroPred in this study of the SON, including 20 unique peptides from known prohormones.[25] Among those signaling peptides reportedly found are the enkephalins involved in nociception, interleukin with involvement in immune system function, and the growth hormone somatotrophin. More opportunities exist to employ NeuroPred in the discovery of signaling peptides.

In another new application of NeuroPred, the transport properties and cellular distribution was revealed of GFG protein, a nudix hydrolase that may be involved in hydrolyzing nucleic acids for regulation purposes. NeuroPred predicted cleavage of a monobasic arginine site with 0.99 percent probability. This cleavage event removes the mitochondrial targeting sequence (MTS) contained in the signal sequence, which would normally result in transport of the peptide to the mitochondrial matrix of the cell. Alternative splicing to create several peptide versions is likely to play a role in the observed diverse localization of the GFG protein. NeuroPred was used to indentify alternative splicing in the signal sequence as an effect on peptide transport of the GFG protein to a variety of rat tissues.[26]

9.7 Conclusions

Both in using similar approaches to those listed above, and likely in totally new areas, applications for Neuropred will continue to be reported. New data will be added as it becomes available on the peptides from specific locations, from new species or even under unusual conditions; this data, when incorporated into new models, should result in enhanced prediction performance. Efforts continue to understand signaling peptides involved in drug addition mechanisms. Also, with several ongoing genome sequencing projects, and some just recently completed,[27] the potential exists for NeuroPred to assist in the discovery of signaling peptides and other bioactive peptides from this genomic information. NeuroPred predictions can then be used, in combination with experimental verification by mass spectrometry, to assist in the complete characterization of these signaling peptides. Besides the newest applications reviewed here, NeuroPred could be conceivably used to study signaling peptides involved in specific cell-cell signaling events including homeostasis, feeding behavior, learning, memory, circadian rhythms and many other functions.

9.8 Tables and Figures

Table 9.1. Chart of posttranslational modifications (PTMs) that are found to occur on signaling peptides, along with predictive consensus sequences. Reference numbers in brackets refer to references that contain the sources of the information in this table.

Post-Translation Modification [abbrev.]	Cellular location of Modification	Enzyme	Motif	Example	Mass change (Monoisotopic)	Mass Change (Average)
N-Acetylation[28] [Ac-]	Co-translational modification Secretory granules	N-acetyltransferases	N-terminal Ser or Ala and other residues	Alpha-MSH,[29] beta-endorphin, rat growth hormones, LeuEnk	+42.0106	+42.0373
Amidation[30] [-amide]	Secretory granules	peptidylglycine a-amidating monooxygenase	C-terminal Gly	secretin, glucagons, VIP, GIP-like peptide, Vasopressin, Alpha-MSH[29]	-58.0036	-58.0366
Bromination[31] [brom]	Unknown	Unknown	Trp	Neuropeptide B[13]	+77.9105	+78.9
γ-Carboxylation[32] [GGlu]	Unknown	Vitamin K Dependent Carboxylase and others unknown	Glu-X-X-X-Glu-X-Cys (for Bone Proteins)	Conus Neuotoxins[33]	+43.98983	+44.0098
Dipeptidase[34]	Golgi	Aminopeptidase	N-terminal X-Pro and X-Ala	Substance P[34]	Depends on X	Depends on X
Disulfide bond (not supported by NeuroPred)	Rough ER	Various	Two Cys residues	Insulin, Orexin A[35]	-2.01566	-2.01588
Glycosylation N-linked[16] [gly]	ER/Golgi	Oligosaccharyl transferase (pH ~7)	NXS/T x not Proline, near N- terminal	Glycoprotein hormones, FSH, LH, choriogonadotropin, luteinizing hormone[3	+162.0528	+162.1424

				6]		
Glycosylation O-linked[37] [gly]	ER/Golgi	UDP-N-acetylgalactosamine	Ser/Thr-Pro-Pro-Pro	Proteins that are part of mucosal or the extracellular matrix fluid, Chromogranin A[37]	+162.0528	+162.1424
Hydroxylation of Proline[18]	ER	prolyl-4-hydroxylase	X-Pro-Gly/Ala	Prodermorphin[18]	+15.9949	+15.9994
Methylation of Glu[38,19] [CH$_3$]	Unknown	Various Types	Occurs on O-atom of Glu, preferentially at an N-terminal Glu in insects.	Pea-sulfakinin [38], Corticotropin[39]	+14.0157	+14.0269
Phosphorylation[17, 28]of S or T [PO$_3$H]	ER/Golgi, follows glycosylation	Casein/ Kinases	S/TXD/E/N/Q KRX-X-S and RRXS S/T(P)-X$_{1–2}$-S/T	ACTH, CLIP,[29] Chromogranin A[37]	+79.9663	+79.9799
Pyroglutamylation [14]	Secretory granules (pH 8)/ chromaffin granules	Glutaminyl cyclase	N-terminal Glu or Gln residue	Alpha-MSH[40], sulfakinin [38]	Glu: -18.0106 Gln: -17.0266	Glu: -18.02 Gln: -17.0306
Sulfation[15, 28, 41, 42] of Y [SO$_3$H]	TGN/ follows glycosylation	Tyrosylprotein sulfotransferase	D/EY and >2 acidic residues in +5 to –5 region, 1 Pro or Gly or at least two Asp Ser or Asn in –7 to +7 region, no disulfide bond or N-linked glycan within 7 aa from Y on both sides	Alpha-MSH[40], CCK, gastrin, secretogranin I &II, Leu-Enk, sulfakinin [38]	+79.9568	+80.0642

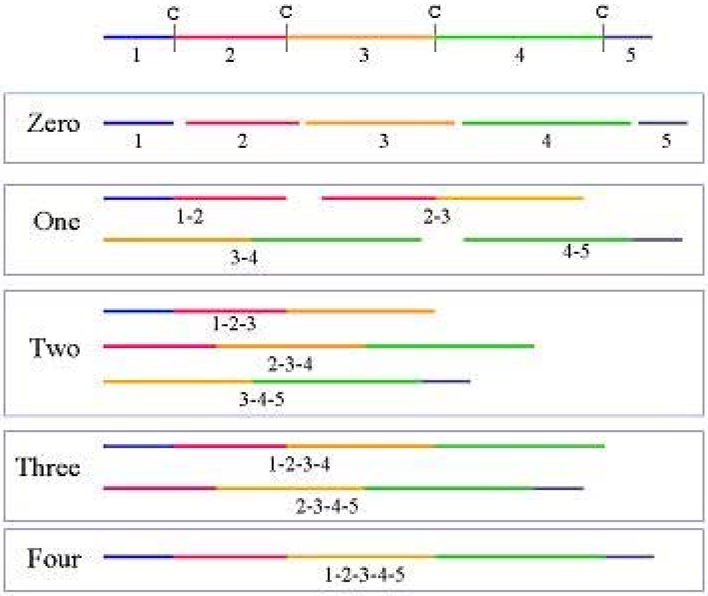

Figure 9.1. Not all basic sites are cleaved. Peptide extension by leaving basic sites as not cleaved decreases the number of possible bioactive fragment peptides. The letter C represents potential enzymatic cleavage sites along the prohormone, and the different colors and Arabic numerals represent the regions in between these cleavage sites that may become product peptides. The written numbers on the left refer to the number of potential cleavage sites that remain not cleaved. Thus, all sites in the scenario labeled zero are cleaved. Many different possibilities exist if some of the sites remain not cleaved.

9.9 References

1. Li, L. and Sweedler, J. V. Peptides in the brain: mass spectrometry–based measurement approaches and challenges. *Annu. Rev. Anal. Chem.* **2008,** *1*, 451–483.

2. Ashcroft, A. E. Protein and peptide identification: The role of mass spectrometry in proteomics *Nat. Prod. Rep.* **2003,** 202-215.

3. Duckert, P., Brunak, S., and Blom, N. Prediction of proprotein convertase cleavage sites. *Protein Eng. Des Sel.* **2004,** *17*, 107-112.

4. Southey, B. R., Amare, A., Zimmerman, T. A., Rodriguez-Zas, S. L., and Sweedler, J. V. NeuroPred: a tool to predict cleavage sites in neuropeptide precursors and provide the masses of the resulting peptides. *Nucleic Acids Res.* **2006,** *34*, W267–W272.

5. Hummon, A. B., Hummon, N. P., Corbin, R. W., Li, L., Vilim, F. S., Weiss, K. R., and Sweedler, J. V. From precursor to final peptides: A statistical sequence-based approach to predicting prohormone processing. *J. Proteome Res.* **2003,** *2*, 650–656.

6. Amare, A., Hummon, A. B., Southey, B. R., Zimmerman, T. A., Rodriguez-Zas, S. L., and Sweedler, J. V. Bridging neuropeptidomics and genomics with bioinformatics: prediction of mammalian neuropeptide prohormone processing. *J. Proteome Res.* **2006,** *5*, 1162-1167.

7. Southey, B. R., Hummon, A. B., Richmond, T. A., Sweedler, J. V., and Rodriguez-Zas, S. L. Prediction of neuropeptide cleavage sites in insects. *Bioinformatics* **2008,** *24*, 815-825.

8. Tegge, A. N., Southey, B. R., Sweedler, J. V., and Rodriguez-Zas, S. L. Comparative analysis of neuropeptide cleavage sites in human, mouse, rat, and cattle. *Mamm. Genome* **2008,** *19*, 106–120.

9. Southey, B. R., Rodriguez-Zas, S. L., and Sweedler, J. V. Characterization of the prohormone complement in cattle using genomic libraries and cleavage prediction approaches. *BMC Genomics* **2009,** *10*, 228-238.

10. Southey, B. R., Sweedler, J. V., and Rodriguez-Zas, S. L. A Python analytical pipeline to identify prohormone precursors and predict prohormone cleavage sites. *Front. Neuroinformatics* **2008,** *2*, Atricle 7.

11. Luts, J., F, O., Plasa, R. V. d., Moor, B. D., Huffela, S. V., and Suykens, J. A. K. A tutorial on support vector machine-based methods for classification problems in chemometrics. *Anal. Chim. Acta.* **2010,** *665*, 129-145.

12. Priggea, S. T., Mains, R. E., Eipper, B. A., and Amzela, L. M. New insights into copper monooxygenases and peptide amidation: structure, mechanism and function. *Cell. Mol. Life Sci.* **2000,** *57*, 1236–1259.

13. Fujii, R., Yoshida, H., Fukusumi, S., Habata, Y., Hosoya, M., Kawamata, Y., Yano, T., Hinuma, S., Kitada, C., Asami, T., Mori, M., Fujisawa, Y., and Fujino, M. Identification of a neuropeptide modified with bromine as an endogenous ligand for GPR7 and GPR8. *J. Biol. Chem.* **2002,** *277*, 34010-34016.

14. Fischer, W. H. and Spiess, J. Identification of a mammalian glutarminyl cyclase converting glutaminyl into pyroglutamyl peptides. *Proc. Natl. Acad. Sci. USA* **1987,** *84*, 3628-3632.

15. Huttner, W. B. Tyrosine sulfation and the secretory pathway. *Ann. Rev. Physiol.* **1988,** *50*, 363-376.

16. Breuer, W. and Bause, E. Oligosaccharyl transferase is a constitutive component of an oligomeric protein complex from pig liver endoplasmic reticulum. *Eur. J. Biochem.* **1995,** *228*, 689-696.

17. Knippschild, U., Gocht, A., Wolff, S., Huber, N., Lohler, J., and Stoter, M. The casein kinase 1 family: participation in multiple cellular processes in eukaryotes. *Cell. Signal.* **2005,** *17*, 675-689.

18. Seethaler, G., Caer, J. P. L., Rossier, J., and Kreil, G. Frog prodermorphin expressed in mammalian cells is partly converted to the hydroxyproline containing precursor. *Neuropeptides* **1993,** *25*, 61-64.

19. Diliberto, E. J. and Axelrod, J. Characterization and substrate specificity of a protein carboxymethylase in the pituitary gland. *Proc. Natl. Acad. Sci. USA* **1974,** *71*, 1701-1704.

20. Wiesner, J., Premsler, T., and Sickmann, A. Application of electron transfer dissociation (ETD) for the analysis of posttranslational modifications. *Proteomics* **2008,** *8*, 4466–4483.

21. Lapainis, T. and Sweedler, J. V. Contributions of capillary electrophoresis to neuroscience. *J. Chromatogr., A* **2008,** *1184*, 144–158.

22. Romanova, E. V., Hatcher, N. G., Rubakhin, S. S., and Sweedler, J. V. Characterizing intercellular signaling peptides in drug addiction. *Neuropharmacol.* **2009,** *56*, 196–204.

23. Clynen, E., Baggerman, G., Husson, S. J., Landyut, B., and Schoofs, L. Peptidomics in drug research. *Expert Opin. Drug Discov.* **2008,** *3*, 425-440.

24. Liu, F., Baggerman, G., Schoofs, L., and Wets, G. The construction of a bioactive peptide database in metazoa. *J. Proteome Res.* **2008,** *7*, 4119–4131.

25. Bora, A., Annangudi, S. P., Millet, L. J., Rubakhin, S. S., Forbes, A. J., Kelleher, N. L., Gillette, M. U., and Sweedler, J. V. Neuropeptidomics of the supraoptic rat nucleus. *J. Proteome Res.* **2008,** *7*, 4992–5003.

26. Zhang, S. C., MacDonald, K. A., Baguma-Nibasheka, M., Geldenhuys, L., Casson, A. G., and Murphy, P. R. Alternative splicing and differential subcellular localization of the rat FGF antisense gene product. *BMC Mol. Biol.* **2008,** *9*, 10-24.

27. Consortium, T. B. G. S. a. A. The genome sequence of taurine cattle: a window to ruminant biology and evolution. *Science* **2009,** *324*, 522-528.

28. Mains, R. E., Eipper, B. A., Glembotski, C. C., and Dores, R. M. Strategies for the biosynthesis of bioactive peptides. *Trends Neurosci.* **1983,** *6*, 229-235.

29. Che, F. Y., Biswas, R., and Fricker, L. D. Relative quantitation of peptides in wild-and Cpe$^{fat/fat}$ mouse pituitary using stable isotopic tags and mass spectrometry. *J. Mass Spectrom.* **2005,** *40*, 227–237.

30. Eipper, B. A., Milgram, S. L., Husten, J. E., Yun, H.-Y., and Mains, R. E. Peptidylglycine α-amidating monooxygenase: a multifunctional protein with catalytic, processing, and routing domains. *Protein Sci.* **1993,** *2*, 489-497.

31. Tanaka, H., Yoshida, T., Miyamoto, N., Motoike, T., Kurosu, H., Shibata, K., Yamanaka, A., Williams, S. C., Richardson, J. A., Tsujino, N., Garry, M. G., Lerner, M. R., King, D. S., O'Dowd, B. F., Sakurai, T., and Yanagisawa, M. Characterization of a family of endogenous neuropeptide ligands for the G-protein-coupled receptors GPR7 and GPR8. *Proc. Natl. Acad. Sci. USA* **2003,** *100*, 6251–6256.

32. Stanley, T. B., Stafford, D. W., Olivera, B. M., and Bandyopadhyay, P. K. Identifcation of a vitamin K-dependent carboxylase in the venom duct of a Conus snail. *FEBS Lett.* **1997,** *407*, 85-88.

33. Brown, M. A., Begley, G. S., Czerwiec, E., Stenberg, L. M., Jacobs, M., Kalume, D. E., Roepstorff, P., Stenflo, J., Furie, B. C., and Furie, B. Precursors of novel Gla-containing conotoxins contain a carboxy-terminal recognition site that directs γ-carboxylation. *Biochemistry* **2005,** *44*, 9150-9159.

34. Mentlein, R. Proline residues in the maturation and degradation of peptide hormones and neuropeptides. *FEBS Lett.* **1988,** *234*, 251-256.

35. Soll, R. and Beck-Sickinger, A. G. On the synthesis of orexin A: a novel one-step procedure to obtain peptides with two intramolecular disulphide bonds. *J. Peptide Sci.* **2000,** *6*, 387-397.

36. Maghuin-Rogister, G. and Hennen, G. P. Bovine luteinizing hormone: study of the primary structure around the carbohydrate attachment sites of the luteinizing hormone alpha-subunit. *Eur. J. Biochem.* **1971,** *21*, 489-497.

37. Strub, J. M., Sorokine, O., Dorsselaer, A. V., Aunis, D., and Metz-Boutigue, M. H. Phosphorylation and O-glycosylation sites of bovine chromogranin A from adrenal medullary chromaffin granules and their relationship with biological activities. *J. Biol. Chem.* **1997,** *272*, 11928–11936.

38. Predel, R., Brandt, W., Kellner, R., Rapus, J., Nachman, R. J., and Gäde, G. Post-translational modifications of the insect sulfakinins: sulfation, pyroglutamate-formation and O-methylation of glutamic acid. *Eur. J. Biochem.* **1999,** *263*, 552-560.

39. Kim, S. and Li, C. H. Enzymatic methyl esterification of specific glutamyl residue in corticotropin. *Proc. Natl. Acad. Sci. USA* **1979,** *76*, 4255-4257.

40. Bateman, A., Solomon, S., and Bennett, H. P. Post-translational modification of bovine pro-opiomelanocortin: tyrosine sulfation and pyroglutamate formation, a mass spectrometric study. *J. Biol. Chem.* **1990,** *265*, 22130-22136.

41. Hortin, G., Folz, R., Gordon, J. I., and Strauss, A. W. Characterization of sites of tyrosine sulfation in proteins and criteria for predicting their occurrence. *Biochem. Biophys. Res. Commun.* **1986,** *141*, 326-333.

42. Huttner, W. B. and Baeuerle, P. A., "Modern Cell Biology," (Liss, New York, 1988), pp. 97-140.

APPENDIX A

JAVA CODE CREATED FOR THE STRETCHED IMAGING METHOD

A.1 Notes

This appendix corresponds to and is referenced from Chapter 7 of this dissertation. Sometimes the code is indented multiple times, as when multiple *for* or *while* loops are used. Indentations help organize the code, but can cause some longer lines of code to drop onto the next line. In this case, some longer lines of code now occupy two or more lines.

A.2 Java Code for Geometry File Creation Using Melted Markers in the Parafilm

```
import java.io.*;
import java.text.*;
import java.util.regex.*;
import java.lang.Math.*;

public class BeadGeometrySlide4Scaled
{

        public static void main(String args[ ]) throws IOException
                {

                String[] filename = new String[13];
                filename[0]="071409 Str.txt";
                filename[1]=args[0];
                filename[2]=args[1];
                filename[3]=args[2];
                filename[4]=args[3];
                filename[5]=args[4];
                filename[6]=args[5];
                filename[7]=args[6];
                filename[8]=args[7];
                filename[9]=args[8];
                filename[10]=args[9];
                filename[11]=args[10];
                filename[12]=args[11];
                ReadLines(filename);
                }

static void ReadLines(String[] filename) throws IOException
                {

```

```
String OutGeoFilename = filename[12];


BufferedReader inIN = new BufferedReader(new FileReader(filename[0]));

int INlineCount = 0;

do
{
    String lineIN = inIN.readLine();
    if (lineIN == null) break;
INlineCount++;
} while (true);

double FractionalDist = Double.valueOf(filename[1]).doubleValue();
double NumPixels = Double.valueOf(filename[2]).doubleValue();
double PlateOriginXa = Double.valueOf(filename[3]).doubleValue();
double PlateOriginYa = Double.valueOf(filename[4]).doubleValue();
double PlateOriginXb = Double.valueOf(filename[5]).doubleValue();
double PlateOriginYb = Double.valueOf(filename[6]).doubleValue();
double PlateOriginXc = Double.valueOf(filename[7]).doubleValue();
double PlateOriginYc = Double.valueOf(filename[8]).doubleValue();
double PlateOriginXd = Double.valueOf(filename[9]).doubleValue();
double PlateOriginYd = Double.valueOf(filename[10]).doubleValue();

double DegRot = Math.toRadians(Double.valueOf(filename[11]).doubleValue());


int rownum = -1;

double[][] INCoord = new double[INlineCount][2];

LineNumberReader lnr = new LineNumberReader(new FileReader(filename[0]));
lnr.setLineNumber(1);
StreamTokenizer stok = new StreamTokenizer(lnr);
stok.parseNumbers();
stok.eolIsSignificant(true);
stok.nextToken();

        while (stok.ttype != StreamTokenizer.TT_EOF)
        {
            double x=0;
            double y=0;

            while (stok.ttype != StreamTokenizer.TT_EOF)
            {

                for (int colnum=1; colnum<=3; colnum++)
                {
                        if (colnum==1) {x=stok.nval;
                                }

                        if (colnum==2) {y=stok.nval;
                                }

                        if (colnum==3)
```

```
{stok.nextToken();
                                        rownum++;
                                        break;}

                                stok.nextToken();
                        }

                    double[] Coord = new double[2];

                    Coord[0]=x;
                    Coord[1]=y;

                    for (int col=0; col<=1; col++)
                    {
                    INCoord[rownum][col] = Coord[col];
                    }


                    if (stok.ttype == StreamTokenizer.TT_EOF) {break;}

                    }

                if (stok.ttype == StreamTokenizer.TT_EOF) {break;}

                }


        double[][] OutCoordTemp = new double[INCoord.length][2];


        double PlateOriginX = 0;
        double PlateOriginY = 0;

        for (int i = 0; i <= INCoord.length-1; i++)
        {
            Double DistA =  Math.sqrt( Math.pow((INCoord[i][0] - PlateOriginXa), 2) +
Math.pow((PlateOriginYa - INCoord[i][1]), 2) );
            Double DistB =  Math.sqrt( Math.pow((INCoord[i][0] - PlateOriginXb), 2) +
Math.pow((PlateOriginYb - INCoord[i][1]), 2) );
            Double DistC =  Math.sqrt( Math.pow((INCoord[i][0] - PlateOriginXc), 2) +
Math.pow((PlateOriginYc - INCoord[i][1]), 2) );
            Double DistD =  Math.sqrt( Math.pow((INCoord[i][0] - PlateOriginXd), 2)
+ Math.pow((PlateOriginYd - INCoord[i][1]), 2) );


            if (DistA <= DistB && DistA <= DistC && DistA <= DistD)
            {
            PlateOriginX = PlateOriginXa;
            PlateOriginY = PlateOriginYa;
            }

            if (DistB <= DistA && DistB <= DistC && DistB <= DistD)
            {
            PlateOriginX = PlateOriginXb;
            PlateOriginY = PlateOriginYb;
            }
```

```


            if (DistC <= DistA && DistC <= DistB && DistC <= DistD)
            {
            PlateOriginX = PlateOriginXc;
            PlateOriginY = PlateOriginYc;
            }

            if (DistD <= DistA && DistD <= DistB && DistD <= DistC)
            {
            PlateOriginX = PlateOriginXd;
            PlateOriginY = PlateOriginYd;
            }

            OutCoordTemp[i][0] = (INCoord[i][0] - PlateOriginX) *
FractionalDist/NumPixels;
            OutCoordTemp[i][1] = (PlateOriginY - INCoord[i][1]) *
FractionalDist/NumPixels;
        }


        double[][] OutCoord = new double[OutCoordTemp.length][2];

        for (int i = 0; i <= INCoord.length-1; i++)
        {

            Double DistA =  Math.sqrt( Math.pow((INCoord[i][0] - PlateOriginXa), 2) +
Math.pow((PlateOriginYa - INCoord[i][1]), 2) );
            Double DistB =  Math.sqrt( Math.pow((INCoord[i][0] - PlateOriginXb), 2) +
Math.pow((PlateOriginYb - INCoord[i][1]), 2) );
            Double DistC =  Math.sqrt( Math.pow((INCoord[i][0] - PlateOriginXc), 2) +
Math.pow((PlateOriginYc - INCoord[i][1]), 2) );
            Double DistD =  Math.sqrt( Math.pow((INCoord[i][0] - PlateOriginXd), 2)
+ Math.pow((PlateOriginYd - INCoord[i][1]), 2) );

            if (DistA < DistB && DistA < DistC && DistA <= DistD)
            {
            OutCoord[i][0] = OutCoordTemp[i][0]*Math.cos(DegRot) +
OutCoordTemp[i][1]*Math.sin(DegRot) -0.391304;
            OutCoord[i][1] = -1*OutCoordTemp[i][0]*Math.sin(DegRot) +
OutCoordTemp[i][1]*Math.cos(DegRot) + 0.304348;
            }

            if (DistB < DistA &&  DistB < DistC && DistB <= DistD)
            {
            OutCoord[i][0] = OutCoordTemp[i][0]*Math.cos(DegRot) +
OutCoordTemp[i][1]*Math.sin(DegRot) -0.304348;
            OutCoord[i][1] = -1*OutCoordTemp[i][0]*Math.sin(DegRot) +
OutCoordTemp[i][1]*Math.cos(DegRot) + 0.130435;
            }

            if (DistC < DistA &&  DistC < DistB && DistC <= DistD)
            {
            OutCoord[i][0] = OutCoordTemp[i][0]*Math.cos(DegRot) +
OutCoordTemp[i][1]*Math.sin(DegRot) -0.217391;
            OutCoord[i][1] = -1*OutCoordTemp[i][0]*Math.sin(DegRot) +
```

```
OutCoordTemp[i][1]*Math.cos(DegRot) + 0.391304;
                        }

                        if (DistD <= DistA && DistD <= DistB && DistD <= DistC)
                        {
                        OutCoord[i][0] = OutCoordTemp[i][0]*Math.cos(DegRot) +
OutCoordTemp[i][1]*Math.sin(DegRot) - 0.478261;
                        OutCoord[i][1] = -1*OutCoordTemp[i][0]*Math.sin(DegRot) +
OutCoordTemp[i][1]*Math.cos(DegRot) + 0.391304;
                        }

                }

                System.out.println(OutCoordTemp[0][0]);
                System.out.println(OutCoordTemp[0][1]);


                BufferedWriter outFile = new BufferedWriter(new FileWriter(OutGeoFilename));
                PrintWriter out = new PrintWriter(outFile);

                out.println("<!-- $Revision: 1.5 $-->");

                out.println("<PlateType>");

                out.println("       <GlobalParameters PlateTypeName=\"MTP Slide Adapter II\"
ProbeType=\"MTP\"");
                out.println("                       RowsNumber=\"100\" ChipNumber=\"1\"
ChipsInRow=\"1\"");
                out.println("                       X_ChipOffsetSize=\"0\" Y_ChipOffsetSize=\"0\"");
                out.println("                       HasDirectLabels=\"false\"
HasColRowLabels=\"true\"");
                out.println("                       HasNearNeighbourCalibrants=\"false\"");
                out.println("                       ProbeDiameterX=\"103.5\" SampleDiameter=\"2\"");
                out.println("                       SamplePixelRadius=\"5\" ZoomFactor=\"1\"");
                out.println("                       FirstCalibrant=\"TPX1\" SecondCalibrant=\"TPX2\"
ThirdCalibrant=\"TPX3\"");
                out.println("                       />");

                out.print("        <MappingParameters mox=\"56.239998\" moy=\"42.635009\"
sinphi=\"0.000000\" cosphi=\"1.000000\"");
                out.println(" alpha=\"51.750000\" beta=\"51.750000\" tansigma=\"0.000000\"/>");

                out.print("        <PlateSpots PositionNumber=\"");
                out.print(INCoord.length);
                out.println("\">");

                String a = "                    <PlateSpot PositionIndex=\"";
                String b = "\" PositionName=\"";
                String c = "\" UnitCoord_X=\"";
                String d = "\" UnitCoord_Y=\"";
                String e = "\"/>";

                DecimalFormat df = new DecimalFormat("#.######");

                for (int i=0; i <= INCoord.length-1; i++)
                {
```

```
            out.print(a);
            out.print(i);
            out.print(b);
            out.print("x_" + (int)INCoord[i][0] + "y_" + (int)INCoord[i][1]);
            out.print(c);
            out.print(df.format(OutCoord[i][0]));
            out.print(d);
            out.print(df.format(OutCoord[i][1]));
            out.println(e);
        }

        out.println("      </PlateSpots>");

        out.println("      <AutoTeachSpots>");
        out.println("            <PlateSpot PositionIndex=\"0\" PositionName=\"TPX1\"
UnitCoord_X=\"-0.729469\" UnitCoord_Y=\"0.550725\"/>");
        out.println("            <PlateSpot PositionIndex=\"1\" PositionName=\"TPX2\"
UnitCoord_X=\"0.729469\" UnitCoord_Y=\"0.550725\"/>");
        out.println("            <PlateSpot PositionIndex=\"2\" PositionName=\"TPX3\"
UnitCoord_X=\"0.729469\" UnitCoord_Y=\"0.057971\"/>");
        out.println("            <PlateSpot PositionIndex=\"3\" PositionName=\"TPX4\"
UnitCoord_X=\"-0.729469\" UnitCoord_Y=\"0.057971\"/>");
        out.println("            <PlateSpot PositionIndex=\"4\" PositionName=\"TPY1\"
UnitCoord_X=\"-0.729469\" UnitCoord_Y=\"-0.057971\"/>");
        out.println("            <PlateSpot PositionIndex=\"5\" PositionName=\"TPY2\"
UnitCoord_X=\"0.729469\" UnitCoord_Y=\"-0.057971\"/>");
        out.println("            <PlateSpot PositionIndex=\"6\" PositionName=\"TPY3\"
UnitCoord_X=\"-0.729469\" UnitCoord_Y=\"-0.550725\"/>");
        out.println("            <PlateSpot PositionIndex=\"7\" PositionName=\"TPY4\"
UnitCoord_X=\"0.729469\" UnitCoord_Y=\"-0.550725\"/>");
        out.println("      </AutoTeachSpots>");

        out.println("</PlateType>");

        out.close();

        }

}
```

A.3 Java Code for Image Reconstruction

```
import java.io.*;
import javax.imageio.*;
import java.awt.image.*;
import java.awt.*;
import java.lang.*;
import java.lang.Math.*;
import java.util.*;
import java.util.Arrays.*;


public class ImageTransformMassForward
```

```
{

    public static void main(String args[ ]) throws IOException
        {

        String[] filename = new String[7];
        filename[0]="Original.txt";
        filename[1]=args[0];
        filename[2]=args[1];
        filename[3]="Parameters.txt";
        filename[4]=args[2];
        filename[5]=args[3];
        filename[6]=args[4];
        ReadLines(filename);
        }

static void ReadLines(String[] filename) throws IOException
        {


        BufferedReader inO = new BufferedReader(new FileReader(filename[0]));

        int Validate = Integer.valueOf(filename[1]).intValue();
        int Double = Integer.valueOf(filename[2]).intValue();

        int MassCenter = Integer.valueOf(filename[4]).intValue();
        int MassWindow = Integer.valueOf(filename[5]).intValue();
        int MassLow = MassCenter - MassWindow;
        int MassHigh = MassCenter + MassWindow;

        if (!(filename[6].toLowerCase().endsWith(".bmp")) &&
!(filename[6].toLowerCase().endsWith(".png"))
            && !(filename[6].toLowerCase().endsWith(".jpg")))
            {System.out.println("Error: output image can only end in .jpg, .png, or
.bmp");}


        int OlineCount = 0;

        do
        {
           String lineO = inO.readLine();
            if (lineO == null) break;
        OlineCount++;
        } while (true);



        String userDir = System.getProperty("user.dir") + "\\mzXML";

        File dir = new File(userDir);

        String[] childrenTemp = dir.list();

        String[] children = new String[childrenTemp.length];

```

```
        for (int i = 0; i <= childrenTemp.length-1; i++)
        {
            children[i] = "mzXML\\" + childrenTemp[i];
        }


        double[] Intensity = new double[children.length];


        String[] SplitName = new String[5];


        double[][] SCoordUncentered = new double[children.length][2];

        for (int i = 0; i <= children.length-1; i ++)
        {
            SplitName = children[i].split("_");

            SCoordUncentered[i][0] = Integer.valueOf(SplitName[2].substring(0,
SplitName[2].length()-1)).intValue();
            SCoordUncentered[i][1] = Integer.valueOf(SplitName[3].substring(0,
SplitName[3].length()-4)).intValue();
        }

        int SlineCount = children.length;



        int Rownum = -1;

        for (int i = 0; i <= children.length-1; i++)
        {

        LineNumberReader lnr = new LineNumberReader(new FileReader(children[i]));
        lnr.setLineNumber(1);
        StreamTokenizer stokCurrentData = new StreamTokenizer(lnr);
        stokCurrentData.parseNumbers();
        stokCurrentData.eolIsSignificant(true);
        stokCurrentData.nextToken();

            while (stokCurrentData.ttype != StreamTokenizer.TT_EOF)
            {
                double intensMax = 0;

                while (stokCurrentData.ttype != StreamTokenizer.TT_EOF)
                {
                    double mz = 0;

                    for (int colnum=1; colnum<=3; colnum++)
                        {
                        if (colnum==1) {mz=stokCurrentData.nval;
                                }

                        if (colnum==2) {
                        if (mz >= MassLow && mz <= MassHigh)
                            {
```

```
                    if (stokCurrentData.nval > intensMax)
                    {
                    intensMax = stokCurrentData.nval;
                    }
                    }
                    }

                if (colnum==3) {stokCurrentData.nextToken();
                            Rownum++;
                            break;}

                    stokCurrentData.nextToken();
                }
        }

    Intensity[i] = intensMax;

    if (stokCurrentData.ttype == StreamTokenizer.TT_EOF) {break;}

    }

}


double[][] OCoordUncentered = new double [OlineCount][2];

BufferedReader Par = new BufferedReader(new FileReader(filename[3]));
StreamTokenizer stokPar = new StreamTokenizer(Par);
stokPar.eolIsSignificant(true);
stokPar.nextToken();

Double[] par = new Double[15];
int a = 0;

Rownum = 0;

        while (stokPar.ttype != StreamTokenizer.TT_EOF)
        {
            for (int colnum=1; colnum<=3; colnum++)
            {
                if (colnum==1) {a=1;
                        }

                if (colnum==2) {par[Rownum]=stokPar.nval;
                        }

                if (colnum==3) {Rownum++;
                        stokPar.nextToken();
                        break;
                        }

                stokPar.nextToken();
            }


        }
```

```

        Double XCenStretched = par[0];
        Double YCenStretched = par[1];
        Double XCenTransformed = par[2];
        Double YCenTransformed = par[3];
        Double XCenOriginal = par [4];
        Double YCenOriginal = par [5];
        Double DeltaADeg = Math.toRadians(par[6]);
        Double WOriginal = par[7];
        Double HOriginal = par[8];
        Double WTransformed = par[9];
        Double HTransformed = par [10];
        Double XCenAloneStretched = par [11];
        Double YCenAloneStretched = par [12];
        Double XCenAloneOriginal = par [13];
        Double YCenAloneOriginal = par [14];

        Double deltaXcen = XCenTransformed - XCenOriginal;
        Double deltaYcen = YCenTransformed - YCenOriginal;

        int rownum = -1;


        LineNumberReader lnrO = new LineNumberReader(new
FileReader(filename[0]));
        lnrO.setLineNumber(1);
        StreamTokenizer stokO = new StreamTokenizer(lnrO);
        stokO.parseNumbers();
        stokO.eolIsSignificant(true);
        stokO.nextToken();

        StreamTokenizer stok = new StreamTokenizer(lnrO);



                while (stokO.ttype != StreamTokenizer.TT_EOF)
                {
                    double xS=0;
                    double xO=0;
                    double yS=0;
                    double yO=0;

                    while (stokO.ttype != StreamTokenizer.TT_EOF)
                    {
                        for (int colnum=1; colnum<=3; colnum++)
                            {
                                if (colnum==1) {xO=stokO.nval;}

                                if (colnum==2) {yO=stokO.nval;}

                                if (colnum==3)
                                    {stokO.nextToken();
                                        rownum++;
                                        break;}

                                stokO.nextToken();
```

```
                            }


                    double[] Coord = new double[2];

                    Coord[0]=xO;
                    Coord[1]=yO;

                    if (rownum <= OlineCount-1)
                    {
                        for (int coll=0; coll<=1; coll++)
                        {
                        OCoordUncentered[rownum][coll]= Coord[coll];
                        }
                    }

                    if (stokO.ttype == StreamTokenizer.TT_EOF) {break;}

                    }


                if (stokO.ttype == StreamTokenizer.TT_EOF) {break;}

                }


    double[][] SCoord = new double [SlineCount][2];
    double[][] OCoord = new double [OlineCount][2];

    for (int i = 0; i <= SCoord.length-1; i++)
    {
        SCoord[i][0] = SCoordUncentered[i][0] + (XCenStretched - XCenAloneStretched);
        SCoord[i][1] = SCoordUncentered[i][1] + (YCenStretched - YCenAloneStretched);
    }

    for (int i = 0; i <= OCoord.length-1; i++)
    {
        OCoord[i][0] = OCoordUncentered[i][0] + (XCenOriginal - XCenAloneOriginal);
        OCoord[i][1] = OCoordUncentered[i][1] + (YCenOriginal - YCenAloneOriginal);
    }



    double[][] TCoord = new double[OCoord.length][2];
    double[][] Dummy1 = new double[OCoord.length][2];
    double[][] Dummy2 = new double[OCoord.length][2];
    double[][] Dummy3 = new double[OCoord.length][2];

    for (int i = 0; i <= OCoord.length-1; i++)
    {
        Dummy1[i][0] = OCoord[i][0] + deltaXcen;
        Dummy1[i][1] = OCoord[i][1] + deltaYcen;

        Dummy2[i][0] = -1*(XCenTransformed - ((Dummy1[i][0] -
XCenTransformed)*Math.cos(DeltaADeg) - (Dummy1[i][1] -
YCenTransformed)*Math.sin(DeltaADeg) + XCenTransformed));
```

```
        Dummy2[i][1] = -1*(YCenTransformed - ((Dummy1[i][1] -
YCenTransformed)*Math.cos(DeltaADeg) + (Dummy1[i][0] -
XCenTransformed)*Math.sin(DeltaADeg) + YCenTransformed));

        Dummy3[i][0] = (Dummy2[i][0]*Math.cos(DeltaADeg) +
Dummy2[i][1]*Math.sin(DeltaADeg)) * WTransformed/WOriginal;
        Dummy3[i][1] = (Dummy2[i][1]*Math.cos(DeltaADeg) -
Dummy2[i][0]*Math.sin(DeltaADeg)) * HTransformed/HOriginal;

        TCoord[i][0] = Dummy3[i][0]*Math.cos(DeltaADeg) -
Dummy3[i][1]*Math.sin(DeltaADeg) + XCenTransformed;
        TCoord[i][1] = Dummy3[i][0]*Math.sin(DeltaADeg) +
Dummy3[i][1]*Math.cos(DeltaADeg) + YCenTransformed;
    }



    double TMatchCoord[][] = new double[TCoord.length][2];
    double[] IntensityMap = new double[TCoord.length];

    for (int i = 0; i <= OCoord.length-1; i++)
        {
        double Dist[] = new double[SCoord.length];

        double TCoordDummy[][] = new double[TCoord.length][2];
            for (int j = 0; j <= TCoord.length-1; j++)
            {
            TCoordDummy[j] = TCoord[j];
            }


        double IntensityDummy[] = new double[SCoord.length];
            for (int j = 0; j <= SCoord.length-1; j++)
            {
            IntensityDummy[j] = Intensity[j];
            }


        for (int l = 0; l <= SCoord.length-1; l++)
            {
            Dist[l] = Math.sqrt(Math.pow(TCoordDummy[i][0] - SCoord[l][0], 2) +
Math.pow(TCoordDummy[i][1] - SCoord[l][1], 2));
            }


        for (int lastPlace = Dist.length-1; lastPlace > 0; lastPlace--)
            {
        int maxLoc = 0;

                for (int k = 0; k <= lastPlace; k++)
                {
                if (Dist[k] > Dist[maxLoc])
                {
                    maxLoc = k;
                }
                }
```

```

            double Temp = Dist[maxLoc];
            Dist[maxLoc] = Dist[lastPlace];
            Dist[lastPlace] = Temp;

            double Temp2 = IntensityDummy[maxLoc];
            IntensityDummy[maxLoc] = IntensityDummy[lastPlace];
            IntensityDummy[lastPlace] = Temp2;
            }

        IntensityMap[i] = IntensityDummy[0];




            if (Double == 1)
            {
                int DoubleInd = 0;
                int DoubleCount = 0;
                double DoubleTCoord[][] = new double[2][2];

                for (int e = 0; e <= i-1; e++)
                {
                    if (TMatchCoord[i][0] == TMatchCoord[e][0] &&
TMatchCoord[i][1] == TMatchCoord[e][1])
                    {
                    DoubleCount++;
                    DoubleInd=e;
                    DoubleTCoord[1] = TMatchCoord[e];
                    }
                }


                DoubleTCoord[0] = TMatchCoord[i];

                if (DoubleCount > 0)
                {

                double DistTCoord[] = new double[TCoord.length-1];
                double DistTCoordO[] = new double[2];


                double TCoordMinus1[][] = new double[TCoord.length-1][5];
                    int RemoveInd = 0;

                for (int z = 0; z <= TCoord.length-1; z++)
                {
                    if (TCoord[z] == TCoordDummy[0])
                        {
                        RemoveInd = z;
                        break;
                        }
                }

                for (int b = 0; b <= RemoveInd-1; b++)
                        {
```

```
                        TCoordMinus1[b] = TCoord[b];
                        }

                for (int c = RemoveInd+1; c <= TCoordMinus1.length-1; c++)
                        {
                        TCoordMinus1[c] = TCoord[c];
                        }

                    for (int f = 0; f <= TCoord.length-2; f++)
                    {
                    DistTCoord[f] = Math.sqrt(Math.pow(TCoordMinus1[f][0]
- TMatchCoord[i][0], 2) + Math.pow(TCoordMinus1[f][1] - TMatchCoord[i][1], 2));
                    }

            for (int lastPlace = DistTCoord.length-1; lastPlace > 0; lastPlace--)
                    {
                        int maxLoc = 0;

                        for (int k = 0; k <= lastPlace; k++)
                        {
                        if (DistTCoord[k] > DistTCoord[maxLoc])
                        {
                            maxLoc = k;
                        }
                        }

                    double Temp = DistTCoord[maxLoc];
                    DistTCoord[maxLoc] = DistTCoord[lastPlace];
                    DistTCoord[lastPlace] = Temp;

                    double Temp1[] = TCoordMinus1[maxLoc];
                    TCoordMinus1[maxLoc] = TCoordMinus1[lastPlace];
                    TCoordMinus1[lastPlace] = Temp1;
                    }

                    double TCoordClosest[] = new double[2];

                    for (int h = 0; h <=1; h++)
                    {
                    TCoordClosest[h] = TCoordMinus1[0][h];
                    }

                    double IntensitySub = 0;

                    for (int y = 0; y <= TMatchCoord.length-1; y++)
                    {
                        if (TCoordClosest[0] == TMatchCoord[y][0] &&
TCoordClosest[1] == TMatchCoord[y][1])
                        {
                            IntensitySub = IntensityMap[y];
                        }
                    }



                    DistTCoordO[0] = Math.sqrt(Math.pow(OCoord[i][0] -
```

```
TCoordClosest[0], 2) + Math.pow(OCoord[i][1] - TCoordClosest[1], 2));
                    DistTCoordO[1] =
Math.sqrt(Math.pow(OCoord[DoubleInd][0] - TCoordClosest[0], 2) +
Math.pow(OCoord[DoubleInd][1] - TCoordClosest[1], 2));

                    if (DistTCoordO[0] < DistTCoordO[1])
                    {
                    TMatchCoord[i] = TCoordClosest;
                    IntensityMap[i] = IntensitySub;
                    }

                    if (DistTCoordO[1] < DistTCoordO[0])
                    {
                    TMatchCoord[DoubleInd] = TCoordClosest;
                    IntensityMap[DoubleInd] = IntensitySub;
                    }
                }
            }

        }


        if (Validate == 1)
        {
        double PointCount = TCoord.length;
        double CorrectPointCount = 0;


        for (int j = 0; j <= TCoord.length-1; j++)
                {
        if (TMatchCoord[j][0] == TCoord[j][0] && TMatchCoord[j][1] == TCoord[j][1])
                {
                    CorrectPointCount++;
                }
                }

            double ClassificationRate = (CorrectPointCount/PointCount) * 100;

            System.out.println("CorrectPointCount " + CorrectPointCount);
            System.out.println("PointCount " + PointCount);
            System.out.println("ClassificationRate " + ClassificationRate);
        }


        double MaxX = 0;
        double MaxY = 0;

        for (int i = 0; i <= OCoord.length-1; i++)
        {
            if (OCoordUncentered[i][0] > MaxX)
            {
                MaxX = OCoordUncentered[i][0];
            }

            if (OCoordUncentered[i][1] > MaxY)
            {
```

```
                MaxY = OCoordUncentered[i][1];
            }
        }

        int width = (int)MaxX;
        int height = (int)MaxY;


        BufferedImage image = new BufferedImage(width + 10, height + 10,
BufferedImage.TYPE_INT_RGB);

        String format = "JPG";

        if (filename[6].toLowerCase().endsWith(".png"))
                        {format = "PNG";}

        if (filename[6].toLowerCase().endsWith(".bmp"))
                        {format = "BMP";}

        double MaxIntensity = 0;
        double IntensitySum = 0;

        double MaxInd = 0;


        for (int i = 0; i <= IntensityMap.length-1; i++)
        {
            if (IntensityMap[i] > MaxIntensity)
            {
                MaxIntensity = IntensityMap[i];
                MaxInd = i;
            }

            IntensitySum += IntensityMap[i];
        }

        double IntensityAvg = IntensitySum / IntensityMap.length;

        System.out.println(Arrays.toString(IntensityMap));
        System.out.println(MaxInd);

        String[] SplitTemp = filename[6].split("\\.");

        String OutImageName = SplitTemp[0] + "_mz" + MassCenter + "+-" +
MassWindow + "_Imax" + (int)MaxIntensity + "." + SplitTemp[1];

        double colorValue = 0;


        for (int i = 0; i <= IntensityMap.length-1; i++)
        {

        colorValue = IntensityMap[i] / MaxIntensity;

            if (colorValue > 1)
            {
```

```
				colorValue = 1;
			}

			if (IntensityMap[i] < 10)
			{
				colorValue = 0;
			}

			Graphics graphics = image.getGraphics();
			Color color = new Color((int)(colorValue * 255), (int)(colorValue * 255),
(int)(colorValue * 255));
			graphics.setColor(color);
			graphics.fillRect((int)OCoordUncentered[i][0] -7,
(int)OCoordUncentered[i][1] - 7, 14, 14);
		}

		ImageIO.write(image, format, new File(OutImageName));


	}

}
```

CURRICULUM VITAE

TYLER A. ZIMMERMAN

SKILLS

- Mass spectrometry imaging and image analysis, mass spectrometry instrumentation (MALDI-TOF), cryosectioning, bioinformatics, software development, method development, chemometrics

VITAL STATISTICS

- Born: January 16, 1983 in Doylestown, PA

EDUCATION

Ph.D. in Analytical Chemistry, University of Illinois at Urbana-Champaign, IL (October 2010)

- Neurochemistry, Sampling, Method development, Mass spectrometry, Bioinformatics
- Research Advisor: Professor Jonathan V. Sweedler

B.S. in Chemistry, ACS certified, University of Delaware, Newark, DE (May 2005)

- Chemometrics, Pattern Recognition
- Research Advisor: Professor Steven D. Brown

SOFTWARE

- MATLAB (PLS Toolbox, Statistics Toolbox, Bioinformatics Toolbox), UNIX, Java, Netbeans, GUI design, Visual Basic, Photoshop, ImageJ, Mascot, LabVIEW, Bruker Daltonics, mzXML, EMBOSS, PAUP*, MrBayes, Biology Workbench, HTML, EndNote, Microsoft Office

LANGUAGES

- Intermediate Spanish and French, elementary German

RESEARCH EXPERIENCE

Graduate Research Assistant, Beckman Institute, University of Illinois, Urbana, IL (November 2005-Present)

- Developed the stretched imaging method to image neuropeptide distributions in thin tissue sections
- Coded Java software for automation of experiments
- Other lab duties: set up a server, networking and installation of printers, external/internal hard drives, lab data backup, computer troubleshooting

Hourly Researcher, University of Illinois, Urbana, IL (June-August 2005)

- Collaborated on the development of NeuroPred software, a tool to predict final prohormone products

Undergraduate Researcher, University of Delaware, Newark, DE (April 2004 - May 2005)

- Explored the chemometrics of classification transfer between near-infrared spectrometers

WORK EXPERIENCE

Teaching Assistant, University of Illinois, Urbana, IL (2005-2006)

- Instructed 250 total students for recitation and laboratory sections of general chemistry courses

Science Educator, Da Vinci Science Center, Bethlehem, PA (2003-2004)

- Guide for exhibits on forensics and magnetism

ACTIVITIES

- Sing tenor in the most selective vocal ensemble, University of Illinois Chorale, Urbana, IL (2009-present)
- Volunteer work, ACORN organization, New Orleans, LA (2009)
- Dance competition chair, quoted in American Dancer Magazine, Dancing Illini, Urbana, IL (2008-present)
- Sing tenor with solo roles, The CHORALE, Champaign, IL (2008-present)
- Sing tenor, Unitarian Universalist Church Choir, Urbana, IL (2008-present)
- Co-founder and treasurer, Illini Classical Guitar Club, Urbana, IL (2008-2009)
- Head of Inventory, University of Illinois Sailing Club, Urbana, IL (2007-2009)
- Active participant, Swing Dance Society, Urbana, IL (2007-2008)
- Violin section, Illini String Orchestra, Urbana, IL (2007)
- Illinois Leadership I-program on Integrity, Urbana, IL (2007)
- Sing tenor, University of Illinois Oratorio Society, Urbana, IL (2005, 2007-2008)
- Violin lessons, School of Music, University of Illinois, Urbana, IL (2005-present)
- Violin co-section leader, Newark Symphony Orchestra, Newark, DE (2001-2005)

AFFILIATIONS

- Student member of the American Society for Mass Spectrometry (2008-present)

AWARDS

- Postdoctoral fellowship, Belgian federal subsidy for research (2010)
- Hypercube Scholar Award (2005)
- Howard Hughes Medical Institute Research Scholarship (2005)
- University of Delaware Undergraduate Summer Research Fellowship (2004)

PUBLICATIONS

- Zimmerman, T. A.; Romanova, E. V.; Lee, J. E.; Zamdborg, L.; Collins, J. J.; Kelleher, N. L.; Newmark, P.A.; Sweedler, J. V. “Characterizing peptide markers for planarian regeneration.” 2010, in preparation.

- Zimmerman, T. A.; Rubakhin, S. S.; Sweedler J. V. “MALDI mass spectrometric imaging of neuronal cell cultures using the stretched sample method.” 2010, submitted.

- Tucker, K. R.; Serebryannyy, L. A.; Zimmerman, T. A.; Rubakhin, S. S.; Sweedler, J. V. “Chemically selective imaging using mass spectrometry: the modified-bead stretched sample method.” 2010, submitted.

- Zimmerman, T. A.; Rubakhin, S. S.; Sweedler J. V. “Mass spectrometry imaging using the stretched sample approach.” Meth. Mol. Biol., 2010, 656, 465-479.

- Zimmerman, T. A.; Rubakhin, S. S.; Romanova, E. V.; Tucker, K. R.; Sweedler, J. V. “MALDI Mass spectrometric imaging using the stretched sample method to reveal neuropeptide distributions in Aplysia nervous tissue.” Anal. Chem., 2009, 81, 9402-9409.

- Zimmerman, T. A.; Monroe, E. B.; Sweedler, J. V. “Adapting the stretch sample method from tissue profiling to imaging.” Proteomics, 2008, 8, 3908-3915.

- Zimmerman, T. A.; Monroe, E. B.; Tucker, K. R.; Rubakhin, S. S.; Sweedler, J. V. “Chapter 13: Imaging of cells and tissues with mass spectrometry: adding chemical information to imaging.” Meth. Cell Biol., 2008, 89, 361-390.

- Southey, B. R.; Amare, A.; Zimmerman, T. A.; Rodriguez-Zas, S. L.; Sweedler, J. V. “NeuroPred: a tool to predict cleavage sites in neuropeptide precursors and provide the masses of the resulting peptides.” Nucleic Acids Res., 2006, 34, W267-W272.

- Amare, A.; Hummon, A. B.; Southey, B.; Zimmerman, T. A.; Rodriguez-Zas, S. L.; Sweedler, J. V. “Bridging neuropeptideomics and genomics with bioinformatics: prediction of mammalian neuropeptide prohormone processing.” J. Proteome Res., 2006, 5, 1162-1167.

- Myles, A. J.; Zimmerman, T. A.; Brown, S. D. “Transfer of multivariate classification models between laboratory and process near-infrared spectrometers for the discrimination of green Arabica and Robusta coffee beans.” Appl. Spectrosc., 2006, 60, 1198-1203.

PRESENTATIONS

- Zimmerman, T. A.; Rubakhin, S. S.; Sweedler, J. V. “Mass spectrometric imaging of neuronal cell cultures using the stretched sample method.” Poster presentation at the ASMS conference on Mass Spectrometry, Salt Lake City, UT, May 2010.

- Zimmerman, T. A.; Rubakhin, S. S.; Romanova, E. V.; Tucker, K. R.; Sweedler, J. V. “Enhanced sample preparation for the mass spectrometric imaging of neuropeptides from cultured neurons.” Poster presentation at the PittCon Conference and Expo, Orlando, FL, March 2010.

- Zimmerman, T. A.; Rubakhin, S. S.; Romanova, E. V.; Tucker, K. R.; Sweedler, J. V. “MALDI Mass spectrometric imaging using the stretched sample method to reveal neuropeptide distributions in Aplysia nervous tissue.” Poster presentation at the Turkey Run Analytical Chemistry Conference, Marshall, IN, October 2009.

- Zimmerman, T. A.; Rubakhin, S. S.; Romanova, E. V.; Sweedler, J. V. “MALDI mass spectrometric using the stretched sample method to reveal detailed neuropeptide distributions in Aplysia nervous tissue.” Poster presentation at the Beckman Institute Imaging Initiative Workshop, Urbana, IL, October 2009.

- Zimmerman, T. A.; Rubakhin, S. S.; Romanova, E. V.; Sweedler, J. V. “MALDI mass spectrometric imaging of nervous tissue using the stretched sample method.” Poster presentation at the ASMS conference on Mass Spectrometry, Philadelphia, PA, June 2009.

- Zimmerman, T. A.; Monroe, E. B.; Tucker, K. R.; Sweedler, J. V. “Traditional and stretched sample imaging of the *Aplysia* abdominal ganglion.” Poster presentation at the Turkey Run Analytical Chemistry Conference, Marshall, IN, October 2008.

- Zimmerman, T. A.; Monroe, E. B.; Sweedler, J. V. “Adapting the stretched sample method from tissue profiling to imaging.” Poster presentation at the ASMS conference on Mass Spectrometry, Denver, CO, June 2008.

- Zimmerman, T. A. “Accelerator mass spectrometry: measuring rare isotopes in biomedicine.” Literature seminar at the Department of Chemistry, University of Illinois, Urbana, IL, November 2006.